COMPREHENSIVE CHEMICAL KINETICS

EDITED BY

C. H. BAMFORD M.A., Sc.D., F.R.S., C. F. H. TIPPER Ph.D., D.Sc.

and R. G. COMPTON M.A., D.Phil.

VOLUME 21

REACTIONS OF SOLIDS WITH GASES

ELSEVIER

COMPREHENSIVE CHEMICAL KINETICS

COMPREHENSIVE

Section 1. THE PRACTICE AND THEORY OF KINETICS (3 volumes)

Section 2. HOMOGENEOUS DECOMPOSITION AND ISOMERISATION REACTIONS (2 volumes)

Section 3. INORGANIC REACTIONS (2 volumes)

Section 4. ORGANIC REACTIONS (6 volumes)

Section 5. POLYMERISATION REACTIONS (3 volumes)

Section 6. OXIDATION AND COMBUSTION REACTIONS (2 volumes)

Section 7. SELECTED ELEMENTARY REACTIONS (1 volume)

Section 8. HETEROGENEOUS REACTIONS (4 volumes)

Section 9. KINETICS AND CHEMICAL TECHNOLOGY (1 volume)

Section 10. MODERN METHODS, THEORY, AND DATA

CHEMICAL KINETICS

EDITED BY

C.H. BAMFORD

M.A., Ph.D., Sc.D. (Cantab.), F.R.I.C., F.R.S.
Formerly Campbell-Brown Professor of Industrial Chemistry,
University of Liverpool

The late C.F.H. TIPPER

Ph.D. (Bristol), D.Sc. (Edinburgh)
Senior Lecturer in Physical Chemistry,
University of Liverpool

AND

R.G. COMPTON

M.A., D.Phil. (Oxon.)
Lecturer in Physical Chemistry,
University of Liverpool

VOLUME 21

REACTIONS OF SOLIDS
WITH GASES

ELSEVIER
AMSTERDAM—OXFORD—NEW YORK—TOKYO
1984

ELSEVIER SCIENCE PUBLISHERS B.V.
Molenwerf 1,
P.O. Box 211, 1000 AE Amsterdam, The Netherlands

Distributors for the United States and Canada

ELSEVIER SCIENCE PUBLISHING COMPANY INC.
52 Vanderbilt Avenue
New York, N.Y. 10017

Library of Congress Card Number: 68-29646

ISBN 0-444-41631-5 (Series)
ISBN 0-444-42288-9 (Vol. 21)

with 55 illustrations and 10 tables

Printed in The Netherlands

COMPREHENSIVE CHEMICAL KINETICS

ADVISORY BOARD

Volumes in the Series

Section 1. THE PRACTICE AND THEORY OF KINETICS

Volume 1 The Practice of Kinetics
Volume 2 The Theory of Kinetics
Volume 3 The Formation and Decay of Excited Species

Section 2. HOMOGENEOUS DECOMPOSITION AND ISOMERISATION REACTIONS (2 volumes)

Volume 4 Decomposition of Inorganic and Organometallic Compounds
Volume 5 Decomposition and Isomerisation of Organic Compounds

Section 3. INORGANIC REACTIONS (2 volumes)

Volume 6 Reactions of Non-metallic Inorganic Compounds
Volume 7 Reactions of Metallic Salts and Complexes, and Organometallic Compounds

Section 4. ORGANIC REACTIONS (6 volumes)

Volume 8 Proton Transfer
Volume 9 Addition and Elimination Reactions of Aliphatic Compounds
Volume 10 Ester Formation and Hydrolysis and Related Reactions
Volume 12 Electrophilic Substitution at a Saturated Carbon Atom
Volume 13 Reactions of Aromatic Compounds

Section 5. POLYMERISATION REACTIONS (3 volumes)

Volume 14 Degradation of Polymers
Volume 14A Free-radical Polymerisation
Volume 15 Non-radical Polymerisation

Section 6. OXIDATION AND COMBUSTION REACTIONS (2 volumes)

Volume 16 Liquid-phase Oxidation
Volume 17 Gas-phase Combustion

Section 7. SELECTED ELEMENTARY REACTIONS (1 volume)

Volume 18 Selected Elementary Reactions

Section 8. HETEROGENEOUS REACTIONS (4 volumes)

Volume 19 Simple Processes at the Gas—Solid Interface
Volume 20 Complex Catalytic Processes
Volume 21 Reactions of Solids with Gases
Volume 22 Reactions in the Solid State

Section 9. KINETICS AND CHEMICAL TECHNOLOGY (1 volume)

Volume 23 Kinetics and Chemical Technology

Section 10. MODERN METHODS, THEORY, AND DATA (1 volume)

Volume 24 Modern Methods in Kinetics

Contributors to Volume 21

D. BRENNAN	Donnan Laboratories, The University, Liverpool, Gt. Britain
A.T. FROMHOLD, Jr.	Department of Physics, Auburn University, Auburn, AL 36849, U.S.A.
R.G. FROMHOLD	Department of Physics, Auburn University, Auburn, AL 36849, U.S.A.
L.G. HARRISON	Department of Chemistry, University of British Columbia, Vancouver, B.C., Canada
Y. KOGA	Department of Chemistry, University of British Columbia, Vancouver, B.C., Canada

Preface

Section 8, which comprises the four volumes 19—22, deals with reactions which occur at gas—solid and solid—solid interfaces other than the degradation of solid polymers which has already been reviewed in Volume 14A. Reactions at the liquid—solid interface are not considered, but those involving electrochemical processes will be covered in subsequent volumes. With respect to chemical processes at gas—solid interfaces, it has been necessary to discuss surface structure and adsorption as a lead-in to the consideration of the kinetics and mechanisms of catalytic reactions.

Volume 21 is concerned with the reactions of solids with gases. Chapter 1 describes the reaction of gaseous oxygen with metal surfaces to form oxide layers, whilst the reaction of hydrogen, halogens and other gases with solids is dealt with in Chapter 2. The process of heterogeneous atomisation is a crucial step in the reaction of simple gases with solid surfaces and this, together with the reverse process of recombination, is examined in detail in Chapter 3.

The editors thank Professor D.A. King for invaluable advice.

Liverpool
April 1984

C.H. Bamford
The late C.F.H. Tipper
R.G. Compton

This Page Intentionally Left Blank

Contents

Chapter 2 (Y. Koga and L.G. Harrison)

Chapter 3 (D. Brennan)

This Page Intentionally Left Blank

Chapter 1

An Overview of Metal Oxidation Theory

ALBERT. T. FROMHOLD, Jr. and REGINA G. FROMHOLD

1. An introduction to the fundamental concepts

1.1 STAGES OF OXIDE FORMATION

As is the case for most natural phenomena, oxide films often have a rapid initiation, a vigorous youthful growth period, a fruitful middle age, a declining later period and, finally, destruction. In this vein, we can list at least ten overlapping stages which may characterize an oxide film at one time or another during its lifetime.

(1) Oxygen molecule impingement from the gas (or solution) phase onto the metal surface.

(2) Physical adsorption of the impinging oxygen molecules onto the metal surface.

(3) Dissociation of the physically adsorbed oxygen molecules with attendant chemical bond modifications.

(4) Chemisorption of the resultant oxygen atoms with the formation of two-dimensional configurations on the parent metal surface.

(5) Place exchange of the atoms in the parent metal surface with the oxygen atoms to form a monolayer of oxide.

(6) Transport of metal atoms or oxygen atoms through the oxide so formed in order that chemical reaction between metal and oxygen can continue.

(7) Various stages of three-dimensional oxide growth under electric-field-controlled conditions.

(8) Recrystallization of the oxide into new structural or stoichiometric phases.

(9) Breakdown of the coherent oxide layer by cracking and spalling, with partial or full loss of its protective character.

(10) Plastic flow and sintering of the oxide to recover, in part, some of its protective character.

Figure 1 indicates the very early stages. Van der Waal forces between the impinging oxygen molecules and the atoms in the parent metal surface cause a number of the molecules to stick to the surface. In this way, the oxygen molecules become physically adsorbed onto the metal surface. The van der Waal force is dipolar in nature. It involves induced and fluctuating electric charge dipoles. Such a force is relatively weak and the associated potential energy of binding is small, being typically less than 10 kJ mole $^{-1}$ [1]. (Because one electron-volt, abbreviated 1 eV, equals

References pp. 116—117

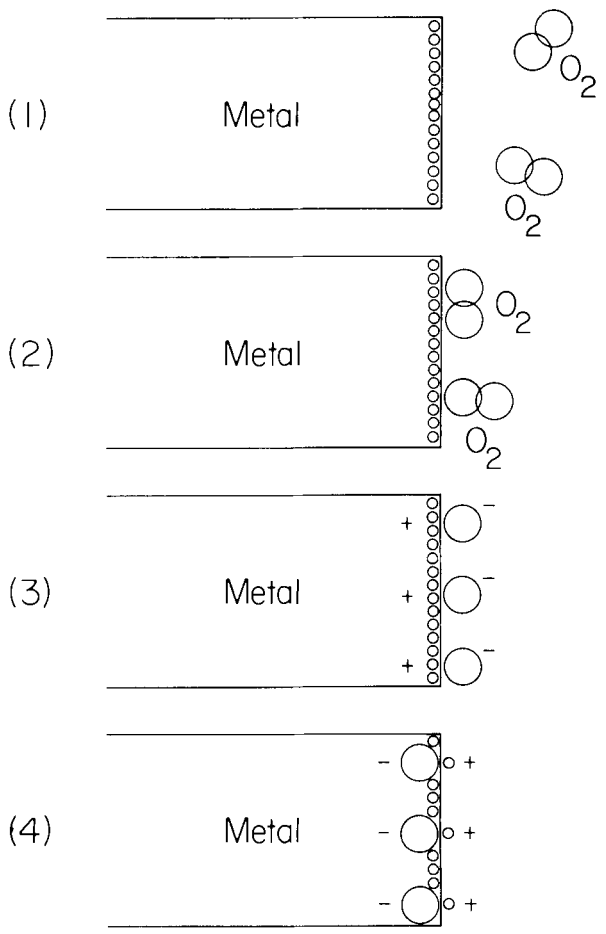

Fig. 1. Initial stages of metal oxidation. (1) Oxygen impingement; (2) Physical adsorption; (3) Oxygen dissociation and chemisorption; (4) Place exchange.

96.4 kJ mole^{-1}, 1 kJ mole^{-1} is equivalent to only 0.01036 eV molecule^{-1}). An energy state with a much greater binding energy can be attained if the oxygen molecule dissociates and subsequently bonds chemically to the metal atoms. This chemisorption bond is typically of the order of 40—120 kJ mole^{-1} (0.4—1.3 eV per chemisorbed atom) but sometimes [2, 3] as high as 600 kJ mole^{-1} (6.5 eV per chemisorbed atom). The formation of two-dimensional configurations of bonded oxygen atoms on metal surfaces has been confirmed [4] in a number of cases by low energy electron diffraction (LEED) (see Vol. 19, Chap. 1). The chemisorption process constitutes, in the chemical sense, an oxidation of some of the parent metal atoms. At this point, the first oxide molecules can be considered to have been formed. The lowest energy configuration will usually

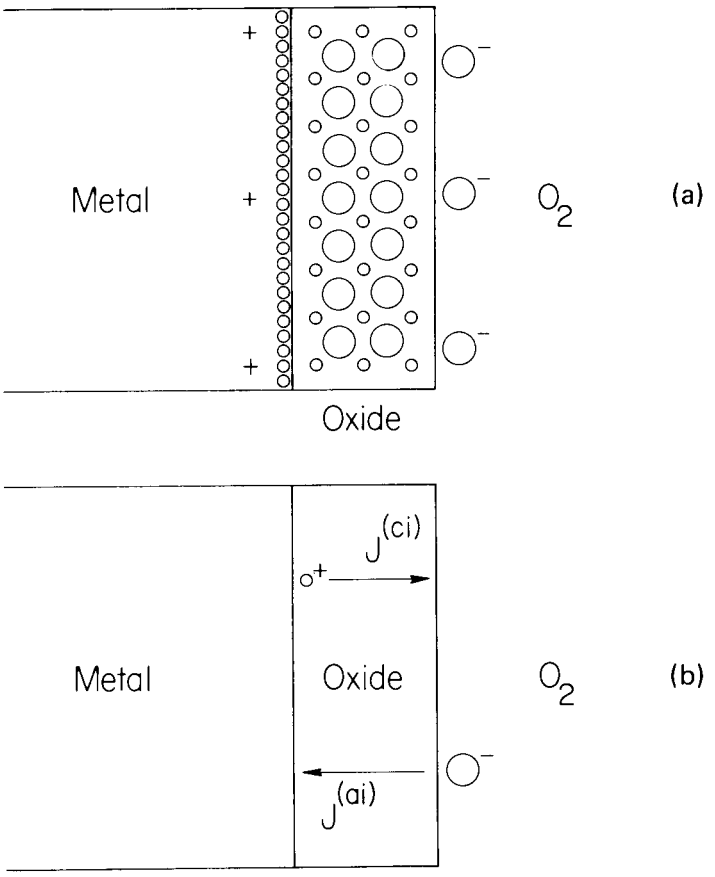

Fig. 2. Field-controlled oxide growth. (a) Surface and interfacial charges; (b) Cation interstitial (ci) and anion interstitial (ai) currents.

require some reorientation of the bonded metal-to-oxygen atoms. This may even involve the switching of places between the metal and oxygen atoms, so that the oxygen becomes imbedded in the metal surface, while the metal atoms move outward from the parent metal towards the gaseous atmosphere. This is referred to as *place exchange.* As noted at the bottom of Fig. 1, it constitutes a reversal in the direction of the electric dipole created previously by the charge exchange between the metal and oxygen. (We are tacitly assuming the metal—oxygen bond to be at least partially ionic). That is, the negative charge located to the right of the positive charge in step 3 of Fig. 1 is located to the left of the same positive charge in step 4 of Fig. 1.

Figure 2 indicates the growth of the oxide once the initial monolayer or two have been formed by the place-exchange mechanism. The oxide separates the parent metal from the oxygen, so that transport of metal

atoms or oxygen atoms is necessary for the chemical reation of metal oxidation to continue. The transport of metal or oxygen can occur by a number of different mechanisms. One category of transport involves the sequential motion of an extra atom (or actually its charged equivalent, viz. a cation or an anion) by means of a hopping motion from one microscopic potential energy minimum in the oxide layer to another potential minimum, until finally it traverses the entire thickness of the oxide layer. This is termed *interstitial transport.* An analog of this mechanism involves the motion of a vacant atom position (viz. the absence of a cation or an anion on a normal lattice site) from point to point in the oxide. This is termed *vacancy transport.* This vacancy motion is accomplished by the successive jumping of ions on normal lattice sites into the vacancy when the vacancy becomes a nearest neighbor. It can be perceived that vacancy motion involves the sequential motion of a great many different ions. In a one-dimensional representation, the vacancy motion through an oxide film of thickness L serves to transport N ions each a distance d in the opposite direction, where $Nd = L$ is the thickness of the oxide layer. Therefore the motion of the vacancy through the oxide layer has the average effect of transporting one ion entirely through the oxide in the opposite direction. Such motion of extra ions (interstitial transport) or missing ions (vacancy transport) as described above is well characterized by diffusion theory [5]. The essentials will be presented subsequently in Sect. 1.10 of this review.

Another category of transport involving analogous considerations to that of vacancy motion is that of non-simultaneous place exchange [6]. In that mechanism, the cation—anion pairs along a chain extending through the oxide switch places in sequence, so the net effect is the transport of one metal ion from the parent metal interface to the gaseous oxygen phase and the simultaneous transport of one oxygen ion from the oxygen phase to the metal surface. Both categories of transport, namely individual vacancy or interstitial transport and non-simultaneous place exchange, lead to the same hopping transport equation [5, 6]. However, the microscopic parameter values, such as the activation energy and the hopping distance, are characteristic of the particular mechanism. In this review, we do not limit our considerations to one or another of these transport mechanisms. To keep our presentation concrete, we will use the terminology of hopping transport with the qualification that the same equations can apply equally well to either transport mechanism.

Both categories of transport discussed above involve the motion of *defects* relative to an otherwise ordered array of ions, so the transport is referred to as *defect transport.* The concentrations of such defects (as contrasted with the total atom concentrations within the oxide lattice) are the important quantities for mass transport, charge transport, and space—charge effects, so it is the *species defect concentration* which appears in the diffusion equation. Likewise, the diffusion coefficients

and mobilities *of the defects* are the parameters which appear in the diffusion equation.

Figure 2 indicates that an electric field exists in the oxide layer during the three-dimensional growth phase, due to the positive and negative charges at the oxide interfaces. The lower part of the figure indicates the transport currents. For example, cation interstitial motion would lead to a particle current $J^{(ci)}$ of cation interstitials from the metal to the oxygen, whereas anion interstitial motion would lead to a particle current $J^{(ai)}$ of anion interstitials from the oxygen to the metal. Similarly, one can visualize a cation vacancy current $J^{(cv)}$ from the oxide—oxygen interface to the metal—oxide interface, or an anion vacancy current $J^{(av)}$ from the metal—oxide interface to the oxide—oxygen interface.

An important question we address is the following: What causes transport to take place through the oxide so that the chemical reaction of oxidation can proceed? (If that chemical reaction halted, the oxide film could no longer increase in thickness). There are different answers to the question depending upon the discipline invoked and the level of explanation required. Thermodynamically, it is the free energy release upon chemical reaction which provides the driving force for transport leading to oxide growth. Figure 3 illustrates a typical chemical barrier picture for an activated process in which a net free energy change, ΔU_{oxide}, per molecule takes place when the molecule is formed from its constituent atoms, the sign of the free energy change being in the direction to favor formation of a stable compound. Considered from a physical viewpoint, however, the driving forces for particle transport are the concentration gradients and the electric fields which are created in the oxide film. This is described in greater detail in the following sections.

1.2 INTERFACIAL REACTIONS AND CONCENTRATION DIFFERENCES

Figure 4 illustrates the equilibrium conditions at the two interfaces of the oxide. Since the system is asymmetrical with respect to the two oxide interfaces, there is no reason to expect that the equilibrium concentrations of the defect species at the two interfaces will be the same. In fact, there is every reason to expect that the defect concentration for a given species will differ greatly at the two oxide interfaces. Consider, for example, the cation interstitials as one of the defect species. Because the parent metal constitutes a good source of metal atoms for entry into the oxide at the metal—oxide interface, the concentration of the cation interstitials should be relatively high at that interface. On the other hand, at the oxide—oxygen interface, the cation interstitials are absorbed in the chemical reaction of oxide formation. That is, the ready supply of oxygen from the gaseous phase at the oxide—oxygen interface means that the rate-limiting step for the oxide formation reaction at that interface will more than likely be the supply of cation species and so any cation interstitials which

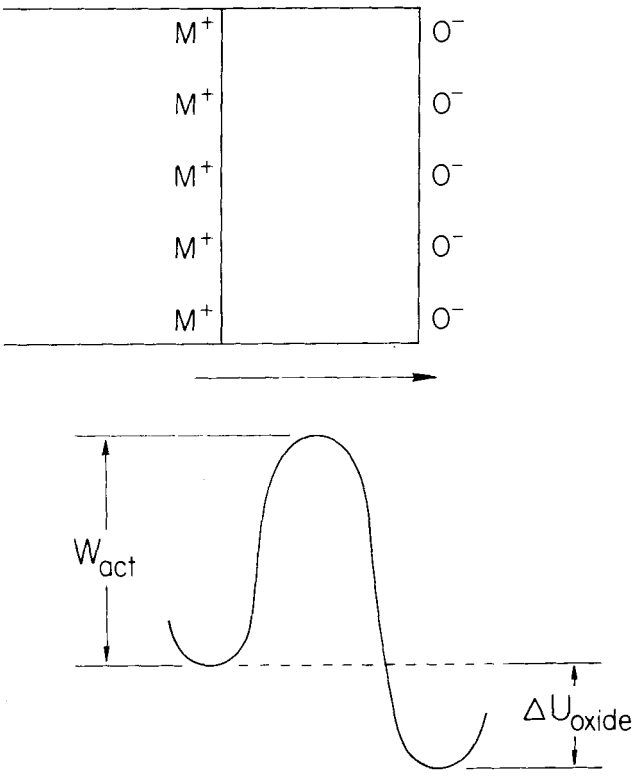

Fig. 3. Thermodynamic model of oxide layer as a reaction activation barrier, with free energy release ΔU_{oxide} following upon reaction.

happen to be at that interface will be rapidly consumed in the oxidation reaction. Thus we expect the concentration of cation interstitials to be relatively quite low at the oxide—oxygen interface. The differences in the cation interstitial concentration at the two oxide interfaces means that a concentration gradient of cation interstitials exists across the oxide and such a concentration gradient can lead to a particle current of cation interstitials through the oxide.

Even considering that the reactions at the interfaces may have proceeded to equilibrium, there is nevertheless a vast difference in the numbers of a given type of defect species which exist in the oxide at the two interfaces; this difference then constitutes an effective driving force for transport of the defect species through the oxide layer. The concentration difference of a given species can be considered in terms of a difference in the chemical potential of that species across the oxide and it is this difference in chemical potential which may be considered to lead to a transport of that species through the oxide layer. The chemical and electrochemical

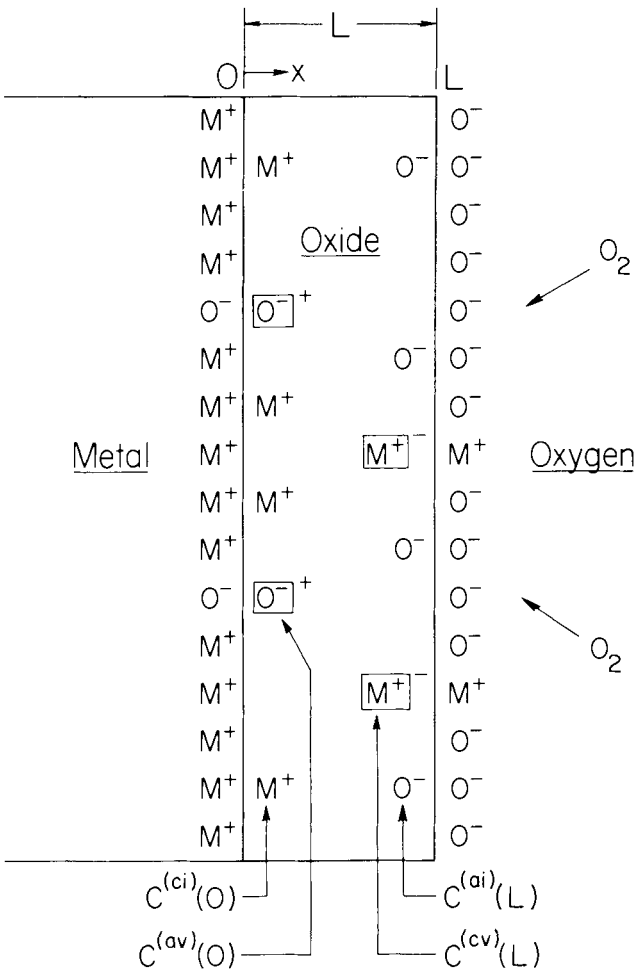

Fig. 4. Bulk ionic defect concentrations at the oxide interfaces associated with equilibrium interfacial reactions. [At the metal—oxide interface, there are cation interstitital (ci) and anion vacancy (av) species, while at the oxide—oxygen interface, there are anion interstitial (ai) and cation vacancy (cv) species].

potentials of the defect species will be considered in more detail in Sect. 1.10 of this review and a more quantitative analysis of the particle current produced by a concentration gradient will be given in Sect. 1.11. The major point, however, is that from the microscopic viewpoint, the interfacial reactions are all-important.

Note in Fig. 4 that there are four primary ionic defect species which we must consider, namely cation interstitials, cation vacancies, anion interstitials, and anion vacancies (denoted by the superscripts ci, cv, ai and av, respectively). In the case of non-simultaneous place exchange, referred to

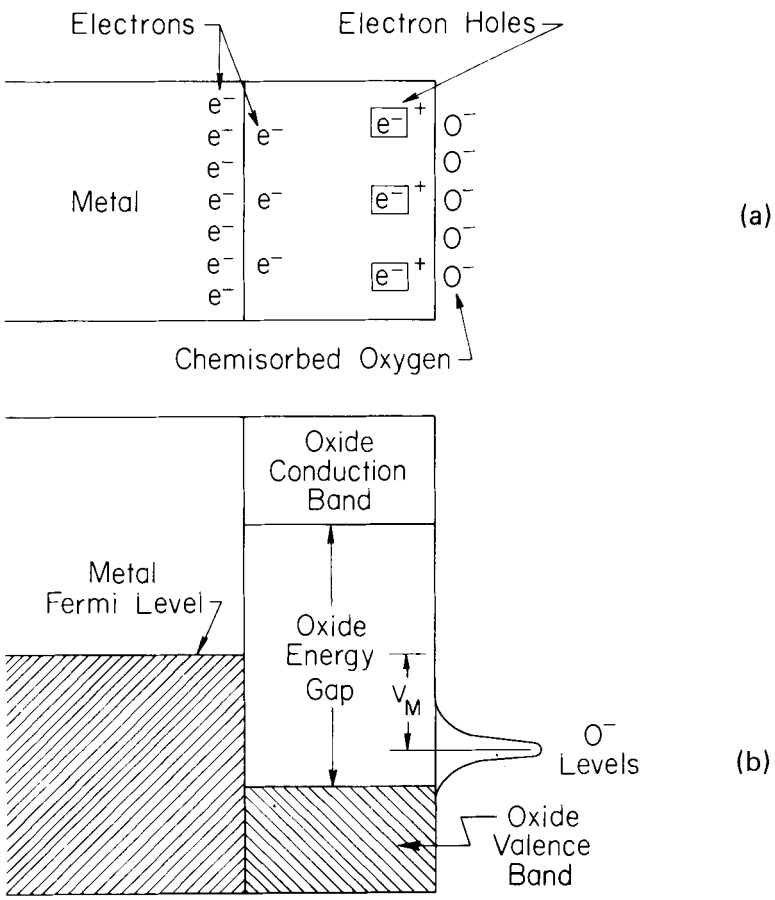

Fig. 5. (a) Bulk electronic concentration at the metal—oxide interface and electron-hole concentration at the oxide—oxygen interface associated with equilibrium interfacial reactions. (b) Electronic energy-level diagram illustrating the dielectric (or semiconducting) nature of the oxide, with the possibility of electron transport (e.g. by tunneling or thermal emission) from the metal to fill O^- levels at the oxide—oxygen interface to create a potential difference, V_M, across the oxide.

as *hopon transport* [7], there are two primary defect species to consider, namely cat-ons and an-ons. Each of these defect species is charged, so electric fields in the oxide must be carefully considered.

1.3 ROLE OF ELECTRONS AND ELECTRON HOLES

Not only must we consider the *ionic* defects produced by the interfacial reactions, but equally important in a description of metal oxidation are the *electronic* defects produced by the interfacial reactions. This is illustrated schematically in Fig. 5. The parent metal constitutes a ready source

of electrons, so the electron concentration in the oxide at the metal—oxide interface should be relatively high. On the other hand, the neutral oxygen molecules which decompose into oxygen atoms require electrons in order to become O^- ions; such electrons must come immediately from the oxide. This can happen in two ways: either there are excess electrons in the oxide which have entered from the parent metal, or else an electron is taken from the neutral oxide, thus creating an electron hole in the oxide. (An electron hole is an electron vacancy). Such an electron hole, constituting as it does the absence of an electron from an otherwise charge-neutral molecule of oxide, has an effective positive charge. The upper part of Fig. 5 illustrates both the negatively charged excess electrons which have entered the oxide at the metal—oxide interface and the positively charged electron holes which have been created in the oxide at the oxide—oxygen interface.

Any electrons which reach the oxide—oxygen interface will be quickly utilized in the formation of O^- ions, and similarly, any positive holes which manage to reach the metal—oxide interface will be quickly annihilated by electrons from the parent metal. The asymmetrical surface reactions thus lead us to expect widely different electron concentrations in the oxide at the two interfaces of the oxide. This difference in electron concentration is equivalent to a difference in the chemical potential for the electronic species at the two interfaces. As in the case of the ionic defect species, such differences in concentration (and chemical potential) can be expected to produce particle currents of the defect species in question. If the primary electronic defects are excess electrons, then we can expect an electron particle current from metal to oxygen; if the primary electron defects are the positive holes, then we can expect a positive-hole particle current from oxygen to metal. Of course, an intermediate situation is also possible in which electrons flow from the metal towards the oxygen while simultaneously a positive-hole current flows from the oxygen towards the metal, with recombination [8] (partial or total) occurring within the oxide film.

The lower part of Fig. 5 shows a typical energy level diagram for electrons in the metal—oxide—oxygen system. The electronic levels are filled to the Fermi level in the metal, whereas the adsorbed oxygen at the opposite interface provides acceptor levels for the electrons. Assuming the oxide to be a typical insulator, or at least a wide-band-gap semiconductor, then we have a situation of an essentially filled oxide valence band with an essentially empty oxide conduction band, the valence and conduction bands being separated by an energy gap in which there are no electronic states. If this is the case, then electron transport from metal to oxygen requires either thermal excitation of electrons from the Fermi level of the metal into the conduction band of the oxide, or else quantum tunneling of electrons from the Fermi level of the metal through the energy barrier due to the energy gap in the oxide. (There are, of course, analogous mechanisms [9] for electron holes).

References pp. 116—117

There are other cases of electron motion which must also be considered, as for example, when the oxide is an impurity semiconductor. In that case, any electrons which enter the oxide may be able to migrate through it with relative ease. The question hinges on how easily the electrons can enter and exit from the oxide at the oxide interfaces. One possibility is the thermal excitation of electrons into the oxide from the metal interface, but that in itself may prove to be rate limiting.

If thermal excitation of electrons from the metal into the oxide occurs, but the oxide is not a good electronic conductor, transport through the oxide may prove to be a very important factor for the rate. If the oxide is thin, then there may be very little electron scattering due to collisions with lattice vibrations (electron—phonon interaction), impurities, or other types of lattice defects. In this case, the electrons can be thermally excited across the entire barrier represented by the oxide without scattering in the conduction band of the oxide. On the other hand, in thick oxides, such scattering mechanisms can be expected to attenuate the electronic current. This leads to a hopping picture for transport, very similar to the case of the motion of ionic defects through the oxide film. Our subsequent treatment of charged particle hopping and diffusion will thus be equally applicable to both ionic and electronic motion.

In all cases of electron transport, whether it be hopping, thermal emission, or quantum tunneling, the effect of the electric field in the oxide film is extremely important. In fact, the electric field effect on ion motion is the primary reason the electronic species must be considered at all in most real metal oxidation reactions. This can be understood better when we discuss the *coupled-currents approach* [10, 11] in Sect. 1.15.

1.4 CHARGE CONSERVATION

We have already pointed out the importance of charged particle transport in metal oxidation. Charge separation involves electrical forces and electrical energies. To cite examples, a charged capacitor represents stored energy, while a bolt of lightning manifests energy "on the move". Both involve two types of electric charge. The two types could have been named "tweedledum" and "tweedledee", but instead, they were termed "positive" and "negative" after the suggestion of the eclectic American publisher-inventor-scientist-statesman Benjamin Franklin following his observations on static electricity [12] in 1748. Franklin suggested that "electrical fire" is present in all matter and that an excess of the normal amount appears as a "positive" charge, while less than the normal amount appears as a "negative" charge. He demonstrated the repulsion of similarly charged objects and the attraction of oppositely charged objects and he demonstrated the mutual-cancellation effects of stored quantities of positive and negative charge. In his famous "silk kite" experiments in 1752, Franklin drew "electric fire" from the clouds in the sky and performed with it the same electric experiments (such as charging his glass

of spirits) which he had previously carried out with static electricity produced by rubbing a glass tube. He thereby demonstrated the "sameness of the electric matter with that of lightning". The later hypothesis of Symmer in 1759 that electricity consists of "positive and negative fluids" was subscribed to by the French experimental physicist Charles-Augustin de Coulomb (1785) and the French mathematical physicist Simeon-Denis Poisson (1812).

Experiments show that the two types of electric charge come in elementary quantized units of precisely the same magnitude. Neither type is, under *ordinary* circumstances, created or destroyed; apparent charge "creation" by the frictional rubbing of two dissimilar charge neutral materials together only separates charges which already exist. Similarly, a battery does not "create" charge; it likewise only separates the two types of intermingled charge. Under *extraordinary* conditions, however, charge *can* be created. The simultaneous annihilation of two gamma rays having a total energy equal to or exceeding the basic minimum value of 0.511 MeV can lead to the production of two particles of equal mass which carry elementary units of charge, one particle carrying a single unit of one type and the other particle carrying a single unit of the other type. In light of this experimentally observed phenomenon, the earlier suggestion of Franklin to label the two types as "positive" and "negative" seems remarkably precocious: The created charges, being equal in magnitude but considered to have opposite signs, add to zero. Due to the convention adopted for the terminology, the total charge produced in a "pair creation" event is thus zero. The particles so created are called the "electron" and the "positron"; the particles we refer to as the electron carries the unit of negative charge, while the particle we call the positron carries the positive unit of charge. The charge q_e of the electron can thus be written as $q_e = -e$ and the charge q_p of the positron can be written as $q_p = +e$, with e denoting the magnitude of the elemental electric charge unit which in SI units is 1.6022×10^{-19} coulombs.

The inverse process to "pair creation", namely, "pair annihilation", is also experimentally observed. In this event, an electron and a positron mutually annihilate with the simultaneous creation of two gamma rays. Because gamma rays, being electromagnetic waves similar to light but of much higher energy, are uncharged and have zero rest mass, we say that both the charges and the rest masses of the electron and the positron have been "annihilated" with the consequent production of energy in the form of gamma rays. Mass has been converted into energy, but no net difference in the total charge in the universe takes place due to our convention of calling charge of one type positive and charge of the other type negative. That is, the annihilated charges are equal in magnitude but are opposite in sign. Thus our convention in using Franklin's terminology leads us to say that charge is always "conserved"; that is, no "net" charge is ever created or destroyed, even though the amount of charge of either sign in the

universe can change in pair production and in pair annihilation experiments. The meaning of this conservation law is that the two types of charge are always created locally in equal amounts and the two types of charge are always destroyed locally in equal amounts.

Insofar as we know today, all stable distributions of electric charge are made up in units of e. Electric charge distributions thus exhibit a "graininess" and quantities of electric charge can come only in packages containing integral units of e. For this reason, it is sometimes said that charge is "quantized".

One other example of the production of equal units of charge of opposite type is afforded by the process of neutron decay. The neutron is an unstable neutral particle which decays with a half-life of approximately 15 min into a proton having charge $+e$ and an electron having charge $-e$. It is interesting that, even though the charges on the electron and the proton created in the neutron decay event are equal in magnitude, the two masses differ by a factor of almost 2000 ($m_e = 9.1096 \times 10^{-31}$ kg; $m_p = 1.6726 \times 10^{-27}$ kg; $m_p/m_e = 1836$). The neutron mass ($m_n = 1.6749 \times 10^{-27}$ kg) exceeds the sum of the electron and proton masses ($m_e + m_p = 1.6735 \times 10^{-27}$ kg), the difference, Δm, being carried off as the energy $(\Delta m)c^2$ of a particle called the "neutrino", which is created in the neutron decay event, where c represents the speed of light.

The electron and the proton are stable particles known as "leptons". Stable means they do not decay spontaneously into any other type of particle. The hydrogen atom in its ground state and in its various excited states represents different spatial configurations of the electron–proton pair. The unstable configurations of the excited states decay with various half-lives into the stable configuration of the ground state with the simultaneous emission of energy in the form of a quantum of electromagnetic radiation known as the "photon". Visible light, for example, is a stream of photons having wavelengths λ in the range 4000—7000 Å, which corresponds to energies $\mathscr{E} = h\nu = hc/\lambda$ in the range 3.1—1.8 eV. (Planck's constant, h, has the value 6.6262×10^{-34} J s and the speed of light, c, has the value 2.997925×10^{8} m s^{-1}). Gamma rays are likewise quanta of electromagnetic radiation but, typically, the energy is in the range of millions of electron volts. Whereas electromagnetic radiation in the form of light is produced in electron transitions between quantized energy levels in the atom, electromagnetic radiation in the form of gamma rays is produced in so-called "nuclear" reactions.

The relatively heavy proton in the hydrogen atom is called the "nucleus" of the hydrogen atom. Atoms other than hydrogen are composed of a relatively heavy dense positively charged core, similarly known as the nucleus, with a surrounding cloud of electrons equal in number to the number of elemental positive charges carried by the nucleus. The mass of the nucleus for all atoms other than hydrogen exceeds by a factor of approximately two the mass of Z protons, where $+Ze$ is the charge of the

nucleus. For this reason, the nucleus is viewed in an oversimplified way as a dense collection of neutrons and protons held together by the so-called "nuclear" forces.

Although we normally find that e is the smallest unit of charge, elementary particle physicists have constructed theories based on hypothetical particles called "quarks", which are considered to carry charges having values of $2/3$, and $-1/3$ of the basic unit e. Such speculation was prompted by the continuing effort to simplify our understanding by finding some way to build all of the observed particles out of a fewer number of more elemental units. Not only have quarks been hypothesized, but, in addition, very elegant and extremely expensive experiments have been undertaken to confirm the existence of such particles. Thus the quest for the ultimate explanation of nature's mysteries continues.

To reiterate and summarize ideas presented above, frictional rubbing does not produce charge of *either* type; nevertheless, it does lead to a *separation* of charges already existing in the form of atomic "nuclei" and "outer shell" electrons. In rubbing a glass rod with silk, electrons stripped from the outer shells of the otherwise neutral atoms in the glass rod are transferred from the glass rod to the silk. The silk thus becomes negatively charged while the glass rod is left with an equivalent amount of positive charge. Alternately, rubbing a hard rubber rod on cat fur leads to a charge separation in which the rod becomes negatively charged while the fur is left positively charged.

No charge is created in a lightning bolt. Charge separation between the earth and the cloud moisture sets up the conditions required for an electric discharge through the air separating the two; the associated ionization of the intervening air molecules in the discharge is itself a charge separation process, and the rearrangement and recombination of the electrons within the atoms and molecules during the discharge leads to the flash of light which we interpret as the lightning. The accompanying thunder reaching us subsequent to the flash is the sound wave generated at the time of the flash by the compressions and rarefactions of the air which are associated with the air density changes accompanying the discharge.

A charge separation can be essentially static in time or it can alter rapidly with time. The charge separation produced by frictional rubbing can be observed experimentally for many minutes afterwards in a room where the ambient atmosphere is "dry"; however, if the atmosphere is humid, the water vapor molecules can act as "return carriers" for the charge which quickly will undo the charge separation initially produced by the frictional rubbing. Similarly, a capacitor charged by means of a battery and then left under open-circuit conditions may maintain the charge separation for long periods of time; on the other hand, charge leakage paths can lead to a rapid deterioration of the charged state of the capacitor. A good conductor placed across the two metal "plates" of the capacitor leads to a rapid flow of charge. Charge flow is referred to as

"electric current". Currents in adjacent conductors lead to magnetic forces between the conductors. Such magnetic forces are useful in defining the SI unit of electric current, namely the "ampere". (The ampere is defined as the current required in each of two long parallel conductors separated by a distance of one meter to produce a force per unit length on each conductor of 2×10^{-7} N m^{-1}). The direction of the current is chosen by convention to be antiparallel to the direction of electron flow, or if the current is due to a positive charge flow, then the direction of the current is parallel to that direction. The SI unit of charge, namely the "coulomb", is defined to be that charge which passes in one second through the cross-sectional area of a wire carrying an electric current of one ampere. One coulomb of charge represents an incredibly large number (approximately 6.2414×10^{18}) of elemental charges e. As one can readily appreciate, this number is not easily obtained by merely assigning a graduate student the seemingly straightforward task of separating and counting one-by-one until this number of charges have been grouped together. The largeness of the number becomes more understandable if one writes it out with all of its zeros, namely, 6,241,400,000,000,000,000. From another viewpoint, if pebbles on the beach were selected until this number had been accumulated, with each selected pebble equal in size or exceeding a cube 1 mm on the edge, there would be enough pebbles to cover a road 10 m in width to a depth of 1 cm for a distance exceeding 62,414,000 km (38,782,000 miles). The distance is equivalent to 1560 circumferences of the earth, 81 round trips to the moon, or 40% of the distance from the earth to the sun.

In addition to the coulomb, another common unit for electric charge is the "Faraday", named after the great British physicist Michael Faraday. The Faraday is based on Avogadro's number, $N_{\mathrm{A\,vog}} = 6.0222 \times 10^{23}$. If a graduate student were assigned the task of counting the number of atoms in 12 g of the pure carbon 12 isotope in order to obtain a value for $N_{\mathrm{A\,vog}}$, it could perhaps take too long. If one atom were separated each second and counted as it was placed on the mass balance, the procedure would take 6.0222×10^{23} seconds, or equivalently, 1.9083×10^{16} years. If the student were to be awarded his degree in a length of time shorter than his expected lifespan, then the experiment would need to be conducted in a space ship traveling relative to the earth with a speed which differed from the speed of light by less than one part in 10^{29} in order for the relativistic time dilation [13] to make it possible for the student to live that long. It takes an Avogadro's number of elemental electric charges to make one Faraday of electricity. One Faraday is equivalent to approximately 96,500 coulombs. Because of the enormous number of charges associated with most macroscopic charge distributions and charge currents, the discreteness of the charge does not usually lead to any observable effects. The discreteness of the charge can nevertheless be observed with the proper experiment, as for example, in the Millikan oil drop experiment used to measure the value of the elemental charge, e. In this experiment, the

Nobel-prize-winning American physicist Robert Andrews Millikan counterbalanced the gravitational force on an oil droplet by an upward electric force due to an applied electric field acting on isolated charges on the droplet. As commonly observed today in the student laboratory, the droplet can be observed through a telescope to reverse its downward fall as the electric force is increased sufficiently to overcome the force of gravity.

The magnetic effects of a charge current are closely related to the electrical effects of a static charge distribution. This can be better appreciated by considering two reference frames having a relative velocity with respect to one another. What appears to be a charge current of a given value to one observer can be observed merely to be a static charge distribution to another observer in relative motion such that he keeps abreast of the moving charge. Thus, what is charge and what is current is more or less relative to the observer. Since electric charge produces electrical forces, whereas electrical currents produce magnetic forces, we must conclude that which force seems to be entirely electric in nature and which force appears to be partly magnetic is a function of the observer. Einstein's theory of special relativity enables us to transform electric and magnetic forces between different inertial reference frames [14]. In his famous 1905 paper on special relativity, Einstein bases his logic on the fact that it is immaterial whether a magnet is moving towards the plane of a circular loop of wire or whether the wire loop is moving towards the magnet; in either event, a voltage is generated around the loop. The voltage depends only upon the *relative* motion of the magnet and the loop. Uniform motion is always relative; it is never absolute.

1.5 ELECTRIC FORCES

Electric forces between electric charges are very important for transport in metal oxidation. Two charges of the same type experience a repulsive force; two charges of opposite type experience an attractive force. Experiments published by Coulomb in the year 1785 showed that the larger the electric charge, the larger the force; quantitatively, the force was found to be proportional to the product of the two charge values. Coulomb also found experimentally that the greater the separation distance between the two charges, the smaller the force. The surprising feature is that there is any force at all if the charges are separated, since to explain this fact, one must postulate some mechanism for the force to act through the intervening distance. The modern way of viewing that is to say that the free space which surrounds any charge is modified by the presence of the charge; the modification is such that another charge, separated in distance from the first charge, senses the modification in the free space at its location and thus experiences a force due to the first charge. This is the "electric field" concept; every charge makes a contribution to the field and

it is the field due to all other surrounding charges which acts on any specific charge. In many respects, this concept is quite strange; however, it is found to be useful in describing not only electric and magnetic forces, but also gravitational forces. Quantitatively, both the electrical and the gravitational forces between two particles are found to be inversely proportional to the square of the separation distance. Since the surfaces mapping out constant distances from a given point charge are concentric spheres, and in addition the area of each sphere increases as the square of its radius, the notion of directed straight line rays emanating radially outward from the point charge towards infinity is suggested. This idea underlies the famous "lines of force" concept introduced by Faraday. The lines so visualized do not terminate except on other charges, so any fictitious closed surface surrounding a charged object can be deformed arbitrarily without changing the number of such lines which pierce the surface. This visual aid likewise constitutes a basis for Carl Friedrich Gauss' law of electricity, which proves so useful for obtaining the electric field in some charge distribution problems having special symmetries.

The experimental observations of Coulomb on electric forces are summarized in the "Coulomb force law"

$$F \propto \frac{q_1 q_2}{r^2} \tag{1}$$

where F is the force directed along the line of centers between the charges, q_1 and q_2 are the values of the two charges, and r is the center-to-center distance of separation between the two charges. In the conventional wisdom of the SI system of units, the proportionality constant is chosen to be $(4\pi\epsilon)^{-1}$, where ϵ is called the "dielectric constant" for the medium in which the charges are imbedded. Free space is denoted by ϵ_0; any other medium can be represented in terms of κ, referred to as the "relative dielectric constant" and defined as the ratio ϵ/ϵ_0. From Coulomb's experiments, two coulombs of charge separated by a distance of 1 m in free space experience a force of approximately 8.988×10^9 N. Thus, in free space, the Coulomb law can be written as

$$\mathrm{F} = (q_1 q_2 / 4\pi\epsilon_0 r^2)\,\hat{\mathrm{r}} \tag{2}$$

where $\epsilon_0 = 8.854 \times 10^{-12}$ $\mathrm{C^2\ N^{-1}\ m^{-2}}$, where C, N and m are the standard abbreviations for the coulomb of charge, the newton of force, and the meter of distance. The unit vector $\hat{\mathrm{r}}$ represents the direction of the line of centers between the two charges, which is the direction of the force. The choice of the forward or reverse direction along the line of centers depends upon the physical situation, as detailed below. Because charges are named "positive" and "negative", $q_1 q_2$ is a positive quantity for like charges but a negative quantity for unlike charges. This leads to a negative sign for $q_1 q_2 / 4\pi\epsilon_0 r^2$ when the force is attractive, but a positive sign when

the force is repulsive. The actual direction of this force parallel to $\hat{\mathbf{r}}$ is dependent upon which of the two charges one is considering. The two forces satisfy Newton's third law of motion that for every force exerted by body A on body B, there is an equal magnitude but oppositely directed force exerted by body B on body A. The fact that an attractive or a repulsive force exists *between* the two charges means that the force on charge 2 is equal in magnitude but *opposite* in direction to the force on charge 1. This can lead to some confusion in the sign for the vector components of the Coulomb force. That is, the force is given a sign by the product of the two charges, independent of which charge is being considered and independent of the usual signs associated with vector components of the force relative to the chosen coordinate system. The easiest way to avoid confusion is to use common sense: sketch the vector force on the charge in question using the Coulomb force law and *then* resolve this directed vector into components in the coordinate system chosen for the problem to find the signs for the vector components. The components so obtained will have signs depending upon which one of the two charges is under consideration.

The Coulomb force relation [eqn. (2)] indicates that the electric force is a vector quantity, namely a quantity having both magnitude and direction. Experiment proves that Coulomb forces indeed add like vectors. For example, if two Coulomb forces $\mathbf{F}_1$ and $\mathbf{F}_2$ act on a so-called "test" charge q' introduced as a probe, the resultant Coulomb force $\mathbf{F}'$ on q' is given by the vector sum of $\mathbf{F}_1$ and $\mathbf{F}_2$. If $\mathbf{F}_1$ has x, y, and z components F_{1x}, F_{1y}, and F_{1z}, respectively, and $\mathbf{F}_2$ has x, y, and z components F_{2x}, F_{2y}, and F_{2z}, respectively, then $\mathbf{F}'$ has x, y, and z components $F_{1x} + F_{2x}$, $F_{1y} + F_{2y}$, and $F_{1z} + F_{2z}$, respectively. Namely, whenever

$$\mathbf{F}_1 = \hat{\mathbf{x}}F_{1x} + \hat{\mathbf{y}}F_{1y} + \hat{\mathbf{z}}F_{1z} \tag{3}$$

and

$$\mathbf{F}_2 = \hat{\mathbf{x}}F_{2x} + \hat{\mathbf{y}}F_{2y} + \hat{\mathbf{z}}F_{2z} \tag{4}$$

then

$$\mathbf{F}_1 + \mathbf{F}_2 = \hat{\mathbf{x}}(F_{1x} + F_{2x}) + \hat{\mathbf{y}}(F_{1y} + F_{2y}) + \hat{\mathbf{z}}(F_{1z} + F_{2z}) \tag{5}$$

with $\hat{\mathbf{x}}$, $\hat{\mathbf{y}}$ and $\hat{\mathbf{z}}$ designating unit vectors along the x, y, and z directions, respectively.

1.6 ELECTRIC FIELDS

The consideration of electric force as a vector quantity leads to the concept of the "electric field". The electric field is the quantity of most concern to us in metal oxidation. The electric field $\mathbf{E}$ at a point $\mathbf{r}$ in space is defined to be the force per unit charge acting on a positive test charge q' *located at the point* $\mathbf{r}$, *namely*

$$\mathbf{E}(\mathbf{r}) = \frac{\mathbf{F}'}{q'} \tag{6}$$

From this point of view, every surrounding charge makes some contribution to the electric field at position r. Charges thus create electric fields; the net electric field at a point in space determines the direction and magnitude of the force on some test charge placed at the point to function as a probe. The convention of labeling charges "positive" and "negative" now proves quite useful: Consistent with eqn. (6), we can write

$$\mathbf{F}' = q'\mathbf{E}$$

so the electric force direction is automatically reversed as required by Coulomb's law if a positive test charge is replaced by a negative test charge.

1.7 ELECTRICAL ENERGY

Work is defined in physics as the product of the value of the force exerted on a body with the distance the body moves parallel to the force. This is equivalent to the product of the value of a vector displacement with the force component parallel to the displacement. Whenever the force component F_R parallel to some displacement R is constant, then the work W done by the force is given by

$$W = F_R R \tag{7}$$

This simple form applies, in general, only over very short distances for the case where F_R is the Coulomb force between two charges, because F_R itself changes whenever the separation distance r is changed. If the changes in R are confined to small increments ΔR, however, then it is a good approximation to write

$$\Delta W = F_R \Delta R \tag{8}$$

Using the differential calculus and vector notation, this can be written in a terse, but elegant and exact form

$$\mathrm{d}W = \mathbf{F} \cdot \mathrm{d}\mathbf{R} \tag{9}$$

That is, the differential work $\mathrm{d}W$ done by a force $\mathbf{F}$ during the differential vector displacement $\mathrm{d}\mathbf{R}$ is the scalar ("dot") product of the force vector with the differential displacement vector. For those who may be unfamiliar with the vector notation, the centered dot indicates the operation of multiplying the magnitude of the vector to the left of the dot with the magnitude of the vector to the right of the dot, and then multiplying this result by the cosine of the angle between the two vectors. This operation, which is termed the "scalar" or "dot" product in vector analysis, is mathematically equivalent to multiplying the magnitude of one of the vectors by the projection of the other vector along a line parallel to the first vector. This general form is required, for example, to obtain the work done by a force not directed parallel to the displacement.

The work done by a force does not come to us as a free gift; it must come from somewhere, because from the first law of thermodynamics we know that energy must be conserved. Thus any force must be produced by some agent, or we can say that it has a "source". Energy expended by the force comes at the expense of the "source". This energy may be recoverable. If reversing the displacement leads to a recovery of the expended energy, we say that the force is "conservative". The recoverable work associated with the force in the above relation (9) can then be considered to represent "stored" or "potential" energy. The energy stored in a capacitor is one example of electrical potential energy. In contrast, the energy expended in a bolt of lightning is not recoverable in the main; it largely represents heat, which we know from the entropy principle of thermodynamics to be the antithesis of a totally recoverable potential energy.

1.8 PLANAR CHARGE DISTRIBUTIONS

Sometimes it happens that an electrical field is constant over a region of space or within a thin planar oxide layer. (When we say constant, we imply that the vector force acting on a test charge is fixed in magnitude and also fixed in direction, independent of the location of the test charge). In the interior region of a parallel plate capacitor having a small plate separation distance d relative to the short dimension of the plates, for example, it is an excellent approximation to say that the electric field E is directed perpendicular to the plates and that it has a fixed value in the region between the plates. The direction of the field can be inferred by contemplating the force on a test charge close to a very large plane covered with a uniform density of electric charge. Each charge in the plane exerts individually its force on the test charge but, considering the mutual cancellation of the effects of these various forces parallel to the plane, with no such cancellation occurring perpendicular to the plane, we reach the conclusion that the net force (and hence the net electric field) is directed perpendicular to the plane. The direction of the field is determined by the direction of the force on a *positive* test charge. This direction will be *outward* from a plane of *positive* charge, but will be directed *towards* a plane of negative charge. Since a positive test charge to the right of a plane of positive charge will experience a force to the right, whereas the same positive test charge placed to the left of the plane of positive charge will experience a force to the left, we conclude that the vector direction of the field produced by a plane of charge differs by 180° on the two sides of a plane of charge, although the field magnitude will be the same on the two sides of the plane.

Even though the direction of the field produced by a plane of charge was not so difficult to deduce above, the *magnitude* of the field and its dependence on the separation distance between the test charge and the

plane cannot be obtained so easily from intuition. It can be shown by means of integral calculus that, in fact, the field **E** is independent of position of the test charge with respect to the source charge density plane [15]. The value of the field [16] is found to depend upon the charge density, σ, per unit area in the plane such that

$$E = \sigma/2\epsilon_0$$

in free space (in the SI system of units). For a parallel-plane capacitor geometry, we must consider the net field to be produced by *two* charge planes, one positive and one negative, since the plates carry equal magnitude charge densities which are opposite in sign. The magnitudes of each of these field contributions are the same. From the above discussion of the field direction, we readily see that the fields produced by the two charge planes are oppositely directed for all positions to the left of both plates and to the right of both plates, but the two fields are in the same direction for all positions between the two planes. Thus the two fields add to zero outside of the capacitor, but add to give a net field of

$$\mathbf{E} = (\sigma/\epsilon_0)\,\hat{\mathrm{n}} \tag{10}$$

within the capacitor, where $\hat{\mathrm{n}}$ is a unit vector perpendicular to the plates.

The magnitude of the work, W, done by an externally applied force in overcoming the force $q\mathbf{E}$ due to the internal electric field **E** in the parallel-plate capacitor, while moving a charge q from one plate to the other along a line *within* the capacitor perpendicular to the plates is given by

$$|W| = |qEd| \tag{11}$$

The sign associated with the work depends upon several factors, such as the physical situation considered, the conventions adopted for sign of work done and energy stored, and whether we are talking about work done by the external force effecting the transfer or whether we are talking about work done by or against the internal electric field. It is best obtained by applying common sense to any specific case in question. For example, if a negative charge is transferred *from* the positively charged plate *towards* the negatively charged plane, the positive plate exerts an attractive force on the negative charge while the negative plate simultaneously exerts a repulsive force on the negative charge. Both forces thus act to retard motion of the negative charge from the positive plate to the negative plate (see Fig. 6). The external "source" which exerts the force to transfer the charge must therefore *expend* energy in effecting the charge transfer. The energy of the source is decreased as a consequence, while simultaneously the charge gains potential energy. The potential energy thereby stored in the capacitor by the charge transfer is recoverable. The applied force in this imaginary experiment is parallel to the displacement, so the work done is given by

$$W_{\text{source}} = F_{\text{applied}}\, d \tag{12}$$

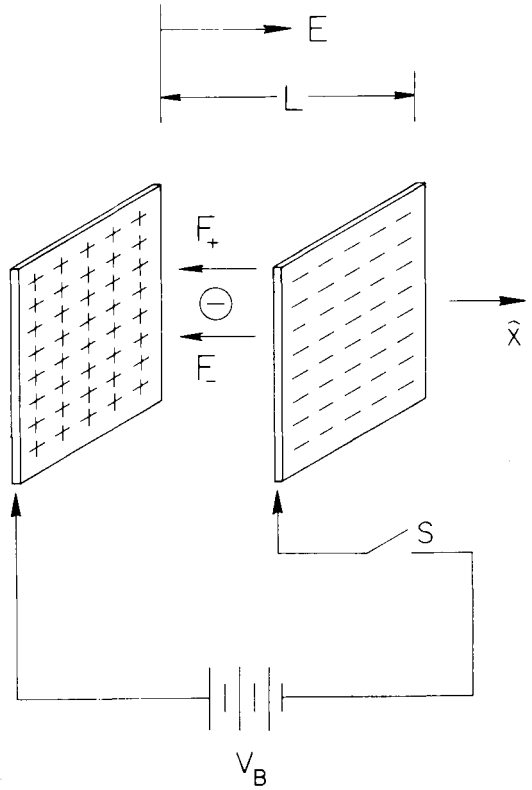

Fig. 6. Net electric field produced by a plane of positive charge to the left and a plane of negative charge to the right, as in the case of a parallel-plate capacitor which is charged to a voltage V_B.

The electric force opposing the transfer is directed oppositely, namely,

$$\mathbf{F}_{elec} = -\mathbf{F}_{applied} \tag{13}$$

If we speak of work done by the internal field created by the electric charges on the plates, then

$$W_{internal} = F_{elec}\, d = -W_{source} \tag{14}$$

However, the stored electrical energy, U, is equal to the work done by the source

$$U = W_{source} \tag{15}$$

Therefore

$$U = W_{source} = F_{applied}\, d = -F_{elec}\, d = -qEd \tag{16}$$

1.9 ELECTROSTATIC POTENTIALS AND VOLTAGES

The electric potential, V, is defined as the potential energy per unit positive test charge. Thus, for the case of a planar charge distribution,

$$V = \frac{U}{q} = -Ed \tag{17}$$

(The electrostatic potential is the electric potential under time-independent, viz. static, conditions. For our present consideration of metal oxidation, the two terms are interchangeable).

In a more general situation where the electric field is position-dependent, the differential change in electric potential dV over a differential vector distance $\mathbf{dr}$ is given by

$$dV = -\mathbf{E} \cdot d\mathbf{r} \tag{18}$$

The reason for the negative sign is the same as that previously discussed, namely that the externally applied force acting to store the potential energy must overcome the internal electric force $q\mathbf{E}$ resisting the transfer. The differential change in potential energy dU due to motion of a charge q through the differential vector distance dr is thus

$$dU = qdV = -q\mathbf{E} \cdot d\mathbf{r} \tag{19}$$

If q experiences an internal electrical retarding force during the displacement dr, then $dU > 0$ and energy is stored by the motion. On the other hand, if q experiences an aiding internal electrical force during the displacement dr, then $dU < 0$ and the potential energy is reduced. While a capacitor is charging, $dU > 0$, whereas during a capacitor discharge, $dU < 0$. During capacitor discharge, the recoverable energy, U, is accompanied by a positive work dW_{world} done on the external world. If

$$dW_{\text{world}} = -dU \tag{20}$$

we say that the process is "reversible". On the other hand, the potential energy, U, may be partially or totally lost, in which case the process is said to be "irreversible". For example, dielectric breakdown of a capacitor due to arcing at high voltage usually leads to a loss in energy; heat is generated and irreversible damage is done to the capacitor. Shorting a capacitor with an external conductor is another example of "lost" energy. From a practical viewpoint, however, heat may not always be considered by everyone to be a waste in energy, since resistance heating can be a useful means of preserving our lives on a frigidly cold day. The stored energy, U, can be slowly drained by ohmic heating of an external conductor to produce over a period of time an amount of heat $Q = U$.

The voltage is a quantity closely related to the quantity defined above as the electric (or electrostatic) potential V. Strictly speaking, the voltage is a *difference* in electrostatic potential, but it is often taken as simply the

magnitude of the electrostatic potential difference.When sign is important, we designate it by the "polarity" of the charged capacitor, namely by designating which plate carries the positive charge and which plate carries the negative charge. Depending upon the coordinate system utilized for the electric potential, the voltage can be equal to the electric potential difference between the plates or else equal to the negative of the electric potential difference between the plates. Again, we recommend that whenever so many quantities, signs, and conventions are involved, one should rely heavily on common sense to deduce the direction of the force and whether the stored energy is decreasing or increasing, and whether work is being done *by* or *on* some external "source".

One important point should be clarified, namely that the charging of a capacitor leads to the same increase in the potential energy even if the charge is transferred through an *external* circuit instead of directly through the internal region of the capacitor where the electric field exists. The reason for this is simple if one considers the capacitor as a conservative system, since it is a fundamental principle that the net change in the potential energy when a body is transferred from point 1 to any point 2 in a conservative system is strictly independent of the actual path employed in moving the body from point 1 to point 2. (If this were not the case, a perpetual motion machine capable of yielding useful work with no energy input could be designed which operated on the principle of moving the body from point 1 to point 2 along one path requiring a relatively low energy input and returning from point 2 to point 1 along another path yielding a larger energy output, and repeating this motion in a cyclic manner).

The differential capacitance, C_{diff}, of a capacitor is defined as the magnitude of the differential charge transfer, dQ, from one plate to the other divided by the change, dV, in electric potential produced by this transfer, namely

$$C_{\text{diff}} = |dQ/dV| \tag{21}$$

or equivalently

$$|dQ| = C_{\text{diff}}|dV| \tag{22}$$

Consider a case in which the field is uniform within the capacitor, as it is in the example of a parallel-plate capacitor discussed above. In that example

$$E = \frac{\sigma}{\epsilon_0}$$

with $\sigma = Q/A$, where A is the area of one side of one of the two capacitor plates. Because

$$V = -Ed = \frac{-\sigma d}{\epsilon_0} \tag{23}$$

for this case

$$\Delta V = \frac{-d}{\epsilon_0} \Delta\sigma = \frac{-d}{\epsilon_0 A} \Delta Q \tag{24}$$

so that

$$C_{\text{diff}} = \epsilon_0 \frac{A}{d} \tag{25}$$

The differential capacitance is then a constant, independent of charge on the capacitor and independent of the voltage. In this example, the total charge and the total voltage are related by

$$|Q| = C_{\text{diff}} |V| \tag{26}$$

Often, the total capacitance is defined to be $|Q/V|$, which in the present example has the same value as the differential capacitance. This is true even for geometries other than planar parallel plates, as for example, in cases of capacitors having concentric cylindrical plates or concentric spherical plates. It is only in the realm of space charge where we must be concerned with differences between the total capacitance and the differential capacitance. The space charge situation will be discussed later.

If the electric potential is V, then the transfer of an additional differential charge dQ through this potential difference gives a differential change in the potential energy

$$dU = V\,dQ = \left(\frac{Q}{C}\right) dQ \tag{27}$$

in accordance with eqn. (17). The integration from an initial charge $Q_i = 0$ to a final charge $Q_f = Q$ gives the total energy stored in the capacitor

$$U = \frac{Q^2}{2C} \tag{28}$$

Since $Q = CV$ in accordance with eqn. (26), this energy can also be written as

$$U = \frac{CV^2}{2} \tag{29}$$

If, instead of free space there is a material having dielectric constant ϵ separating the plates, the field is given by σ/ϵ instead of σ/ϵ_0. Because $\epsilon > \epsilon_0$, the capacitance is correspondingly larger. In this case, more charge can be stored at a given voltage and a given charge produces a lower voltage.

Suppose that a capacitor is charged by a battery to a voltage V_B, the

source disconnected, and then some of the charge Q is permitted to leak into the material separating the two plates. This would constitute a "space charge" in the dielectric. As a consequence, what will happen to the voltage? It is intuitively clear that the field will then be lower over some region near the leakage plate within the capacitor; as a consequence of this, the value of V_B will be lowered. (As an extreme example, if all charge on one of the plates leaked entirely through the plate separation distance, d, the charge on each plate would then be zero and so the voltage across the capacitor would be zero).

On the other hand, if the battery remains connected across the capacitor while charge leaks into the medium, the charge on the plate will be partly replenished by the battery in order to restore the voltage across the capacitor to the battery potential and maintain it at that value. Since there is now more total charge stored in the capacitor than before the leakage into the dielectric material occurred, we see that the total capacitance has been increased. (Think of $Q = CV$ as defining the magnitude of the capacitance C; that is $C = |Q/V|$, so any increase in charge Q at fixed V indicates an increase in C. Similarly, any decrease in V at fixed Q likewise denotes an increase in C).

If we accept the fact that the electric field **E** produced by an infinite plane of charge of density σ has a fixed value independent of distance away from the plane, in accordance with eqn. (10) we can easily understand intuitively how the electric potential varies with position in the medium for various physical charge distributions within the medium. The basic idea is to consider distributed charge to be localized on closely spaced planes throughout the medium. Consider, once again, the example of a parallel plate capacitor. If the charge Q were entirely on the plate itself, with the charge $-Q$ entirely on the opposite plate, then according to eqn. (23), the value of V increases linearly with separation distance between the plates. Because $dV = -E_x\, dx$ for a displacement dx, then for the case in which E_x is a constant

$$V = -Ex \tag{30}$$

The electric potential is thus a *linear* function of position within the region between the two plates.

As the next example, consider two planes of charge having densities σ_0 and σ_1, respectively, with the test charge being to the right of both planes. Then the fields produced individually by these charge distributions are given by $\sigma_0/2\epsilon$ and $\sigma_1/2\epsilon$, so the total (or "net") field will be $(\sigma_0 + \sigma_1)/2\epsilon$, independent of the distances to the test charge located to the right of the planes.

If we have a whole series of planes having charges $\sigma_0, \sigma_1, \sigma_2, \ldots, \sigma_{j-1}$ to the left of the test charge, then the net field at the test charge *due to these planes of charge* will be given by

$$E_{\text{left}} = (\sigma_0/2\epsilon) + (\sigma_1/2\epsilon) + (\sigma_2/2\epsilon) + \ldots + (\sigma_{j-1}/2\epsilon) \tag{31}$$

References pp. 116—117

or, equivalently,

$$E_{\text{left}} = \sum_{i=0}^{j-1} \frac{\sigma_i}{2\epsilon} \qquad (j = 0, 1, 2, 3, \ldots) \tag{32}$$

If, in addition to the planes of charge to the left, there are also planes of charge to the right of the test charge, then the contribution of these planes to the total electric field must also be taken into account. Labeling the planes to the right of the test charge as $j, j + 1. j + 2, \ldots, N$, there will be the additional contribution

$$E_{\text{right}} = -\sum_{i=j}^{N} \frac{\sigma_i}{2\epsilon} \tag{33}$$

[The minus sign arises because the charge planes are to the right instead of to the left of the test charge: see the discussion leading to eqn. (10)]. If, in addition, we have the special situation in which the *total* charge of all the planes adds to zero

$$0 = \sum_{i=0}^{N} \sigma_i \tag{34}$$

then we have the equality

$$-\sum_{i=j}^{N} \sigma_i = +\sum_{i=0}^{j-1} \sigma_i \tag{35}$$

In this case, it follows that

$$E_{\text{right}} = E_{\text{left}} \tag{36}$$

Added to these fields, of course, would be any *externally applied field*, E_0, due to charge distributions other than the planes of space charge presently considered. Using the convention of labeling the *total* electric field existing in the region between charge planes $j - 1$ and j as E_j, then we can write

$$E_j - E_0 = E_{\text{left}} + E_{\text{right}} = 2E_{\text{left}} = \sum_{i=0}^{j-1} \frac{\sigma_i}{\epsilon} \tag{37}$$

As the test charge is moved between charge planes $j - 1$ and j located at the positions x_{j-1} and x_j, the electric potential V changes by $-E_j(x_j - x_{j-1})$ where $x_j - x_{j-1} = d_j$ the separation distance between the two charge planes in question. Thus

$$V_j = V_{j-1} - E_j(x_j - x_{j-1}) \quad (j = 1, 2, \ldots, N) \tag{38}$$

It can be noted from this relation that V_1 depends upon V_0 and E_1, where it is acceptable as a convention to choose V_0 to have the value zero. Then it can be noted that V_2 depends upon V_1 and E_2, and thus it can be written in terms of E_2 and E_1. Continuing with V_3, V_4, V_5, and so on, we see that the potential V_k can be written as

$$V_k - V_0 = -\sum_{j=1}^{k} E_j (x_j - x_{j-1}) \quad (k = 1, 2, 3, \ldots, N) \tag{39}$$

Because E_j itself is increasing with position x_j, V_k increases as a higher power in x_k than is the case for a single charge plane. This can be noted also from the result obtained by substituting eqn. (37) for E_j in terms of the charge density into the last equation above to obtain

$$\begin{aligned} V_k - V_0 &= -E_0 x_k - \sum_{j=1}^{k} (E_j - E_0)(x_j - x_{j-1}) \\ &= -E_0 x_k - \sum_{j=1}^{k} (x_j - x_{j-1}) \sum_{i=0}^{j-1} \frac{\sigma_i}{\epsilon} \quad (k = 1, 2, 3, \ldots, N) \end{aligned} \tag{40}$$

In continuum notation, this relation would constitute one form of *Poisson's equation of electrostatics.* The continuum forms of $E(x)$ and $V(x)$ are valid if the charge density planes are so close together that over small regions of space the charge density can be viewed as a continuous function $\rho(x)$ of position x. [The local space charge density $\rho(x)$ has units of Coulombs m^{-3}]. In such cases, the sums in eqns. (37) and (40) for $E(x)$ and $V(x)$ can be approximated by integrals to give

$$E(x) = E(0) + (1/\epsilon) \int_0^x \rho(x')\, dx' \quad (0 \leqslant x \leqslant L) \tag{41}$$

and

$$V(x) = V(0) - E(0)x - (1/\epsilon) \int_0^x dx' \int_0^{x'} \rho(x'')\, dx'' \quad (0 \leqslant x \leqslant L) \tag{42}$$

This latter relation constitutes the integral form of *Poisson's equation of electrostatics.*

To return to our discrete notation for the moment, the increase in V between plane k and plane $k + 1$ is determined not only by the charge density of plane k, but also by all other planes of charge density preceding the plane labeled k. This directly reflects the fact that the electric field itself involves all charge density planes, as can be noted from eqn. (37), and not merely the nearby charge plane. That is, the electric field and the electric potential are not merely functions of the *local* charge density, but instead, are functions of cumulative charge densities over other regions of space. This contrasts sharply with the usual quantities considered in

equilibrium and non-equilibrium thermodynamics which are assumed to be local functions of the other intensive thermodynamic variables. For example, the chemical potential at a given point in a non-homogeneous thermodynamic system depends only on the chemical composition in the neighborhood of that point: it does not depend upon the composition of the system in regions far removed from the point in question. Similarly, the fluxes as usually introduced into non-equilibrium thermodynamics are presumed to be linear functions of the gradients of the local electrochemical potential. This presumption may be acceptable if the gradients in question are not too steep, but even then, the computation of the electrical portion of the electrochemical potential involves much more than a consideration of the local composition and the local charge density, as indicated above.

This is not at all meant to imply that electric fields and electrostatic potentials cannot be incorporated correctly into thermodynamics; instead, it is meant to be a warning that thermodynamics itself is incomplete in the sense that it cannot generally be used to evaluate the electric field [17]. In addition, the electric potential is sometimes miscontrued to be a local driving force in thermodynamics (as for example, in the monolayer region of solid surfaces), whereas in actuality it is the *gradient* (i.e. the rate of change) of the electric potential which yields the local driving force called the electric field.

1.10 CONCENTRATION AND ELECTROCHEMICAL POTENTIAL GRADIENTS AS DRIVING FORCES FOR PARTICLE CURRENTS AND OXIDE GROWTH

Figure 7 illustrates in a schematic way the concentration profiles for the charged interstitial defect ionic species within the oxide. The concentration profiles simply illustrate the distribution of each charged species within the oxide layer. The value of the bulk defect concentration is plotted as a function of position. The reason the concentration varies with position can be understood as follows. Because the equilibrium kinetic processes involving a given defect species (such as cation interstitials) are different at the two interfaces of the oxide layer, the bulk concentrations of that defect species near the two interfaces will adjust to different values. Each defect species will thus have a larger concentration near one interface than near the other. The random movement of all of the defects of a given species within the oxide layer then leads, on the average, to a greater number of defects which wander away from the higher concentration region than the number which wander into that region. Likewise, a greater number of defects wander into a low concentration region than wander away from the region. Thus, we have a net transport rate of a given type of defect from the higher concentration regions into the lower concentration regions. This rate of transport can be expressed in terms of a particle current density, J, viz. the number of such defects crossing unit

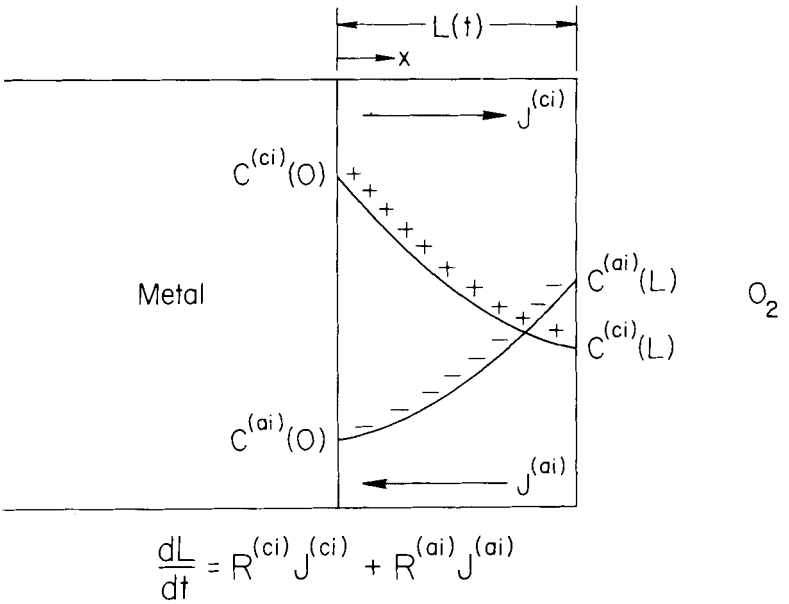

Fig. 7. Schematic representation of charged cation interstitial (ci) and anion interstitial (ai) bulk concentration profiles within the oxide, leading to defect currents of cation and anion interstitials and subsequent chemical reaction leading to a continual increase in oxide layer thickness, L, with time, t.

area in unit time. Superscripts can be used to designate the type of defect; we use (ci) for cation interstitial, (ai) for anion interstitial, (cv) for cation vacancy, and (av) for anion vacancy.

As an example, it is conceivable that in some metal—oxide systems, the cation interstitials entering the oxide at the metal—oxide interface ($x = 0$) rise to appreciable bulk concentration values $C^{(ci)}(0)$. These defects can then migrate through the oxide layer. Chemical reaction of any such interstitials which happen to reach the oxide—oxygen interface ($x = L$) will serve to deplete the number at that interface. Thus the bulk concentration $C^{(ci)}(L)$ will be much lower than the number $C^{(ci)}(0)$. The net flow of the cation interstitials from $x = 0$ to $x = L$ can be expressed as a particle current density $J^{(ci)}$. This particle current density proceeding from the source interface ($x = 0$) to the sink interface ($x = L$) can be essentially uniform (i.e. $J^{(ci)}$ independent of position x) if there is no build-up or depletion of the bulk density $C^{(ci)}$ between source and sink. On the other hand, any build-up or depletion of the bulk density $C^{(ci)}(x)$ at a position x within the layer will require the current to decrease or increase, respectively, at that position x in order to supply or take away, as the case may be, the requisite number of such defects.

The total number of defects emerging from the source interface is thus partitioned in such a way as to equal the sum of the number reaching the

sink and the number required to satisfy the total build-up of particle density throughout the oxide layer. The counting process can be done locally by choosing any small volume element within the oxide and requiring that the number ΔN_{into} of defects flowing into the volume element minus the number ΔN_{out} flowing out in any given time increment, Δt, must equal the increase ΔN_{within} in the number of such defects within the volume element over the time interval, namely

$$\Delta N_{\text{into}} - \Delta N_{\text{out}} = \Delta N_{\text{within}} \tag{43}$$

In more sophisticated mathematics, this can be expressed as

$$(J_{\text{into}} - J_{\text{out}})A(\Delta t) = A(\Delta x)(\Delta C) \tag{44}$$

where A is the cross-sectional area perpendicular to the flow direction and Δx is the distance separating the points where J_{into} and J_{out} are evaluated. If Δx is small, the difference $(J_{\text{out}} - J_{\text{into}})$ can be designated as ΔJ, so the preceding relation can be written in the form

$$-\frac{\Delta J}{\Delta x} = \frac{\Delta C}{\Delta t} \tag{45}$$

In terms of differential calculus, this becomes

$$\frac{\partial J}{\partial x} = -\frac{\partial C}{\partial t} \tag{46}$$

This relation is called the one-dimensional *equation of continuity.* In general, the dependent variables J and C can be functions of both position x and time t. In the special case where the concentration C at a position x is not changing its value with time t, $\partial C/\partial t = 0$ and it follows that J is independent of position x. Indeed, it is usually an excellent approximation in metal oxidation to assume that J is independent of position in the region between source and sink. This is termed the *steady-state approximation.*

If the particle current $J^{(ci)}$ of cation interstitials is flowing from the metal—oxide interface to the oxide—oxygen interface at time t, and if the area of the parent metal surface is A, then a number $J^{(ci)}A\,\Delta t$ of cation interstitials is transported in the time increment Δt. If the volume of new oxide formed per transported cation interstitial is designated as $R^{(ci)}$, then a total quantity of new oxide $R^{(ci)}(J^{(ci)}A\,\Delta t)$ is formed during the time interval Δt. The increase ΔL in oxide thickness is given by the ratio of this volume to the area A. Thus

$$\Delta L = R^{(ci)}J^{(ci)}\Delta t \tag{47}$$

In terms of differential calculus, we can write this as a *growth rate equation* for motion of cation interstitials

$$\frac{dL}{dt} = R^{(ci)}J^{(ci)} \tag{48}$$

Similarly, a flow of anion interstitials from the oxide—oxygen interface to the metal—oxide interface can lead to new oxide growth. We can write

$$\frac{dL}{dt} = R^{(ai)}J^{(ai)} \tag{49}$$

for the oxide growth rate produced by the anion interstitial current, assuming we are careful in the choice of signs so that the right-hand side will be positive when oxygen is moving towards the metal.

Cation vacancy and anion vacancy currents can similarly lead to oxide growth. To generalize, we can state that the total oxide growth rate will be the algebraic sum of all such contributions. Mathematically, this can be written as

$$\frac{dL}{dt} = \sum_{s=1}^{l} R^{(s)}J^{(s)} \tag{50}$$

where the index s ranges over all mobile ionic defect species in the oxide layer. The number of such mobile ionic species is designated by the symbol l. Included in this number are not only the simple ionic defects such as interstitials and vacancies of the cation species and the interstitials and vacancies of the anion species, but also more complex defect species such as the an-ons and cat-ons involved in non-simultaneous place exchange [6].

From our previous discussion of the net transport of defects of a given species from high concentration regions to low concentration regions by random motion, it is evident that the difference in bulk defect concentrations between the source and the sink interfaces constitutes a type of *potential* for the movement of defects. This potential acts to create a driving force proportional to the potential difference per unit distance for the motion of defects across the oxide layer.

The chemical potential difference for species s across the oxide layer can be written as

$$\begin{aligned} u^{(s)}(L) - u^{(s)}(0) &= k_B T \ln[C^{(s)}(L)] - k_B T \ln[C^{(s)}(0)] \\ &= k_B T \ln[C^{(s)}(L)/C^{(s)}(0)] \end{aligned} \tag{51}$$

(A variable activity coefficient, ζ, should be added as a multiplier of the bulk concentration, C, if the defect concentrations are so large that there is an interaction between defects). The chemical potential at an arbitrary position x within the layer (refered to the chemical potential at $x = 0$) can similarly be written as

$$u^{(s)}(x) - u^{(s)}(0) = k_B T \ln[C^{(s)}(x)] - k_B T \ln[C^{(s)}(0)] \tag{52}$$

Phenomenologically, the greater the difference in chemical potential per unit distance across a given region, the greater will be the particle

currents from the region of higher to the region of lower chemical potential. Thus, $-\Delta u/\Delta x$ represents a driving force $F^{(s)}$ for the motion of the defect species across the incremental distance Δx. (The sign is essential if the direction of flow is to be from a region of higher to a region of lower chemical potential, rather than the converse). In terms of the calculus, the force per particle acting on a defect of the species labeled s is given by

$$F^{(s)} = \frac{-\mathrm{d}u^{(s)}}{\mathrm{d}x} \tag{53}$$

Substituting the preceding relation for $u^{(s)}(x)$ into this relation gives

$$F^{(s)} = \frac{-[k_B T/C^{(s)}(x)]\,\mathrm{d}C^{(s)}(x)}{\mathrm{d}x} \tag{54}$$

Each particle of defect species s will respond to this force, but the degree of response will be dependent upon the species in question and the diffusion medium. The proportionality factor is termed the mobility coefficient, $B^{(s)}$, of the species in question. The current, $J^{(s)}$, produced by a given force, $F^{(s)}$, per defect particles will be larger for a greater number of particles per unit volume, since then more particles are set into motion by the force. Thus, from a phenomenological standpoint, it is reasonable to write

$$J^{(s)} = B^{(s)}F^{(s)}C^{(s)} \tag{55}$$

Substituting eqn. (54) for $F^{(s)}$ then gives

$$J^{(s)} = \frac{-k_B T B^{(s)}\,\mathrm{d}C^{(s)}}{\mathrm{d}x} \tag{56}$$

for the current produced by the chemical potential (or concentration) gradient.

Analogously, a current can be produced by an electrical potential difference. If the electric potential is denoted by V, then the electric field E (viz. the force per unit charge) is given by $E = -\mathrm{d}V/\mathrm{d}x$. This follows from an energy consideration: $[q^{(s)}V(x) - q^{(s)}V(0)]$ is the electrostatic energy (relative to the point $x = 0$) of a charge $q^{(s)}$ located at point x. The force on the charge $q^{(s)}$ which tends to move it from a region of higher to a region of lower electric potential is determined by the energy difference per unit distance. Thus

$$F^{(s)} = \frac{-\mathrm{d}[q^{(s)}V(x)]}{\mathrm{d}x} = \frac{-q^{(s)}\mathrm{d}V(x)}{\mathrm{d}x} = q^{(s)}E \tag{57}$$

where

$$E = \frac{-\mathrm{d}V}{\mathrm{d}x} \tag{58}$$

is termed the "electric field" (see Sect. 1.6). If the concentration of such charges is given by $C^{(s)}$, then the particle current due to the electrical potential difference is

$$J^{(s)} = B^{(s)} q^{(s)} E C^{(s)} \tag{59}$$

If there are both chemical potential and electrical potential differences, then the net principle current is given by the sum of the two currents. Then we may write

$$\begin{aligned} J^{(s)} &= -k_B T B^{(s)} \, dC^{(s)}/dx + B^{(s)} q^{(s)} E C^{(s)} \\ &= B^{(s)} \left[-k_B T \, (dC^{(s)}/dx) - q^{(s)} C^{(s)} \, (dV/dx)\right] \\ &= -B^{(s)} C^{(s)} \, d[k_B T \ln C^{(s)} + q^{(s)} V]/dx \\ &= -B^{(s)} C^{(s)} \, d\tilde{u}^{(s)}/dx \end{aligned} \tag{60}$$

where

$$\tilde{u}^{(s)} = u^{(s)}(0) + k_B T \ln[C^{(s)}] + q^{(s)} V \tag{61}$$

is termed the *electrochemical potential* of species s. The arbitrary constant $u^{(s)}(0)$ added to the right-hand side in eqn. (61) is, in a sense, superfluous because it does not enter into the equations directly preceding it, but it was added in order to allow some flexibility in the choice of the reference state for concentration and electric potential. Note that the electrochemical potential basically is the sum of the chemical potential $[k_B T \ln C^{(s)}]$ and the electrical potential energy $q^{(s)} V$. The electrochemical potential has the units of energy per particle. The mobility coefficient $B^{(s)}$ is often replaced by the parameter $\mu^{(s)}$ defined by

$$\mu^{(s)} = q^{(s)} B^{(s)} \tag{62}$$

which is called the *electrical mobility* of species s. In terms of $\mu^{(s)}$, we see that the current produced by the electrical potential difference is $\mu^{(s)} E C^{(s)}$ and the current produced by the chemical potential difference is $-(k_B T \mu^{(s)}/q^{(s)}) \, dC^{(s)}/dx$. Often the ratio $(k_B T \mu^{(s)}/q^{(s)})$ is indicated by the symbol $D^{(s)}$, viz.

$$D^{(s)} = k_B T \, \mu^{(s)}/q^{(s)} \tag{63}$$

so the chemical potential difference produces the current $-D^{(s)} dC^{(s)}/dx$. The total current given by eqn. (60) can then be written in the form

$$J^{(s)} = -D^{(s)} dC^{(s)}/dx + \mu^{(s)} E C^{(s)} \tag{64}$$

It is evident from the last equation that the effects of the gradient and the electric field can be either additive or subtractive, because each term on the right-hand side can be of either sign. In fact, a flow of charged particles produced by a chemical potential difference across a diffusion medium can lead to charge flow and the creation of an electric potential which effectively cancels the effects of the chemical potential difference

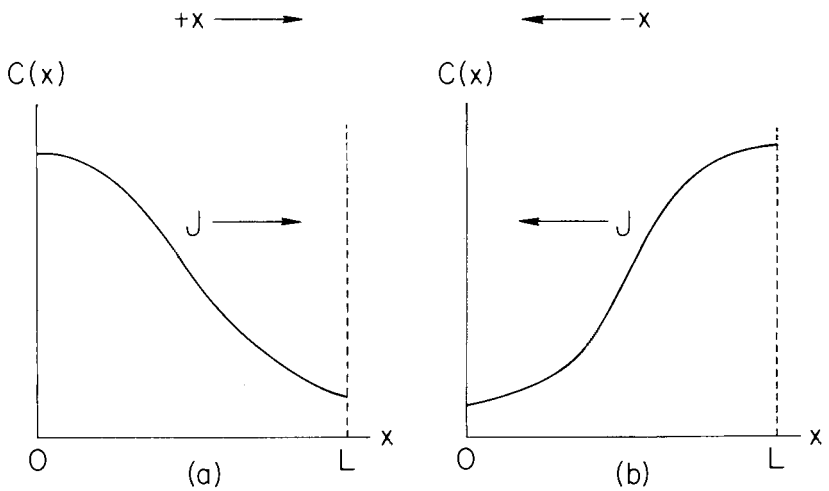

Fig. 8. Schematic diagrams of concentration profiles and the associated particle currents. (a) Cation interstitials or anion vacancies $[(dC/dx) < 0]$ and positively directed particle currents $(J > 0)$. (b) Cation vacancies or anion interstitials $[(dC/dx) > 0]$ and negatively directed particle currents $(J < 0)$.

insofar as the flow of particles is concerned. The gradient can be either negative in sign, as can be noted (from the slope of the curve) to be the case indicated in Fig. 8(a), or positive in sign, as can be noted (from the slope of the curve) to be the case indicated in Fig. 8(b). Negative gradients lead to particle currents in the positive x direction, in accordance with eqn. (56). On the other hand, positive gradients lead to particle currents in the negative x direction, which also is in accord with eqn. (56). Gradients of any of the ionic species tend to give charge transport leading to the same electrical polarity, as indicated by the sketches shown in Fig. 9(a)—(d). That is, cation interstitials [Fig. 9(a)] and anion vacancies [Fig. 9(d)] have their source interfaces at the metal—oxide interface ($x = 0$) and thus have negative gradients (i.e. negative slopes for concentration profile curves), as noted in Fig. 8(a). Both carry positive charge from the metal—oxide interface to the oxide—oxygen interface, leaving behind the equivalent amount of negative charge. On the other hand, anion interstitials [Fig. 9(b)] and cation vacancies [Fig. 9(c)] have their source interfaces at the oxide—oxygen interface ($x = L$) and thus have positive gradients [Fig. 8(b)]. Both carry negative charge from the oxide—oxygen interface to the metal—oxide interface, leaving behind the equivalent amount of positive charge. Thus the electric polarity created is independent of the nature of the ionic defect species carrying the charge and independent of the sign of the charge carried by the ionic defect [*cf.* Figs. 9(a)—(d)].

From another viewpoint, a negative surface charge at the metal—oxide

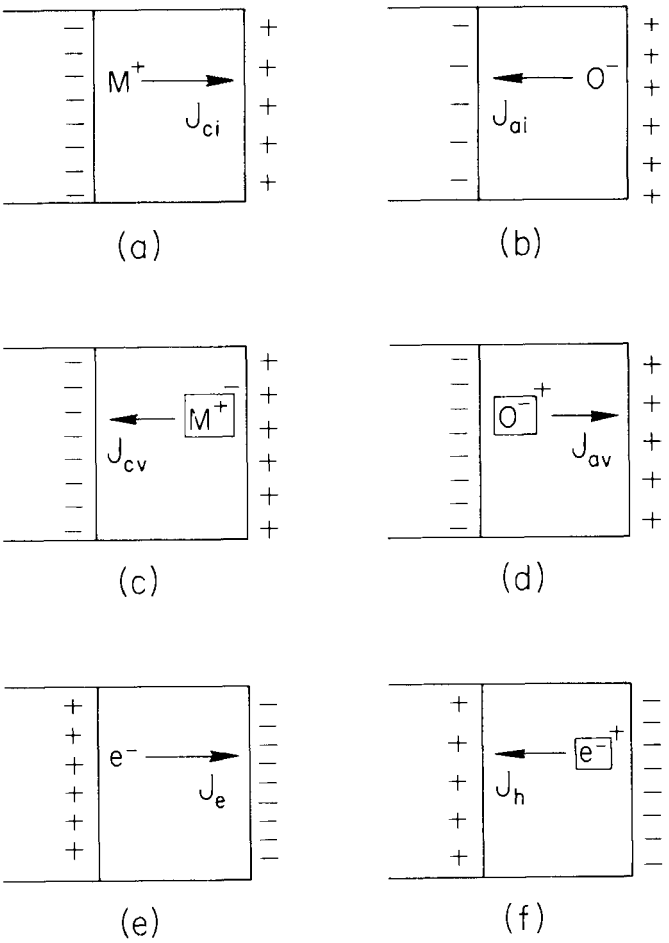

Fig. 9. Electric field polarities produced by the easy diffusion of various charged defect species. (a) Cation interstitials; (b) anion interstitials; (c) cation vacancies; (d) anion vacancies; (e) electrons; (f) electron holes. Note from (a)—(d) that easy diffusion of any of the ionic species produces the same electrical polarity, whereas (e) and (f) show that easy diffusion of either of the electronic species leads to the opposite polarity.

interface attracts, and the positive surface charge at the oxide—oxygen interface repels, the positively charged cation interstitials [Fig. 9(a)]; thus both of the interfacial surface-charge densities tend to retard the flow of cation interstitials in the forward direction, which is induced by the action of the chemical potential gradient of the cation interstitial species. Similarly, the negative surface charge at $x = 0$ retards and the positive charge at $x = L$ attracts the negatively charged anion interstitials [Fig. 9(b)]; thus both interfacial surface-charge densities tend to retard

the flow of anion interstitials in the negative direction, which is induced by the action of the chemical potential gradient of the anion interstitial species. The cation vacancy, being effectively a negatively charged defect species since it constitutes the absence of a positively charged cation from an otherwise charge-neutral matrix, acts in the same way as the negatively charged anion interstitial, since both species have the same charge sign and both have positive chemical potential gradients. That is, the negative surface charge at $x = 0$ retards the transport of both negative species in the negative direction by electrostatic repulsion and the positive charge at $x = L$ retards the transport of both negative species in the negative direction by electrostatic attraction. The anion vacancy acts analogously to the cation interstitial; both are effectively positively charged and have negative gradients, so transport of both positively charged species in the positive direction by the gradients is retarded by the electrostatic attraction of the negative surface charge at $x = 0$ and also retarded by the electrostatic repulsion of the positive surface charge at $x = \mathrm{L}$.

The electric polarity produced by the flow of *electrons* under the expected gradient (metal as electron source; oxygen as electron sink) is *opposite in sign* to that produced by ion flow. This can be noted by referring to Fig. 9(e). Moreover, the polarity produced by electron-hole flow from the oxide—oxygen interface to the metal—oxide interface [see Fig. 9(f)] is the same as that produced by electron flow from the metal to the oxygen. It can therefore be concluded that chemical potential differences producing electronic transport of either type tend to produce a given electrical polarity, whereas chemical potential differences producing ionic transport of any type tend to produce the opposite polarity. This conclusion turns out to have extremely important ramifications in metal oxidation theory, as will be discussed in some detail in Sect. 1.15 describing the coupled currents approach.

1.11 MICROSCOPIC HOPPING TRANSPORT

A microscopic view leads to great insight into the problem of charge transport in solids. Consider the hopping of particles (viz. the mobile defects) over a potential energy barrier, as illustrated in Fig. 10(a). If local thermodynamic equilibrium prevails between the defects and the phonon spectrum of the oxide diffusion medium, any defect will have the Boltzmann probability [proportional to $\exp(-\mathscr{E}/k_{\mathrm{B}}T)$] of having an energy $\mathscr{E}$ after any dynamic interaction with the lattice ions when the temperature is T. The Boltzmann constant, k_{B}, has the value $1.3806 \times 10^{-23}\,\mathrm{J\,K^{-1}}$; the energy $k_{\mathrm{B}}T$ is sometimes referred to as the thermal energy. To cross from one side of the potential energy barrier to the other, the particle must generally have an energy $\mathscr{E}$ at least equal to the maximum potential energy $U_{\max} \equiv W$ of the barrier $U(x)$. This is the classical view for particles. Quantum tunneling [18] permits some

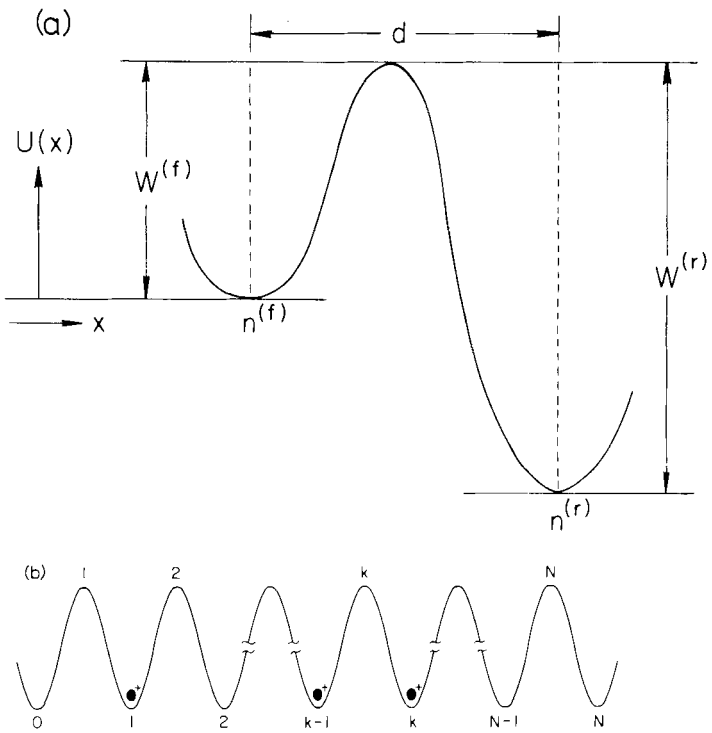

Fig. 10. (a) Energy barrier for hopping transport illustrating activation energy $W^{(f)}$ for forward motion and activation energy $W^{(r)}$ for reverse motion. (b) Series of energy barriers which must be crossed in sequence as the carrier proceeds from one interface of the oxide film to the other interface.

relaxation of this rule by invoking the wave-like properties of matter, but for relatively large particles such as ions, which are thousands of times heavier than the more wave-like electrons, quantum tunneling usually provides negligible deviations from the predictions of the classical picture. The frequency of dynamical interaction between the defect and the lattice depends on the spectrum of phonon frequencies in the solid. (Phonon frequencies are the frequencies of the normal vibrational modes of the interacting ions making up the oxide lattice, the interaction being due to the chemical bonding forces existing between the ions). A complete treatment of the interactions between the mobile defect species and the lattice would be quite complicated, especially since there is a temperature dependence of the normal mode occupation numbers for the elemental quanta of energy associated with the phonons. In the spirit of the Einstein model for the specific heat of a solid, however, the problem is simplified considerably by selecting a single frequency ν to characterize the dynamical interaction of the mobile defect with the lattice. The frequency

ν is chosen to be of the order of 10^{13}—10^{14} s^{-1}, representative of typical values for phonon frequencies. The quantity ν is often referred to as the *attempt frequency* because this is the number of times per second that the defect interchanges energy with the lattice, which in turn determines the number of possible times the particle might gain an energy in excess of the barrier maximum so that barrier crossing becomes possible. The product of the attempt frequency ν with the total probability $P(U_{max}^{(f)})$ of having an energy associated with the forward component of the momentum which exceeds the barrier maximum $U_{max}^{(f)}$ in the forward direction then gives the crossing rate. If there are $n^{(f)}$ such particles per unit area attempting to hop forward in this way, then the forward particle current density will be given by

$$J^{(f)} = n^{(f)} \nu P(U_{max}^{(f)}) \tag{65}$$

Let us now attempt to evaluate $P(U_{max}^{(f)})$ in a simplistic way. The Boltzmann factor, $\exp(-\mathscr{E}/k_B T)$, determines the relative probability of the particle being transferred to some allowed energy state $\mathscr{E}$ following a random interaction with the lattice vibrations. If we make the somewhat naïve assumption that the density of such allowed energy levels to which the particle may be transferred is constant, independent of the value of the energy, then it follows that the probability that after lattice interaction the particle will have an energy in the differential energy interval $d\mathscr{E}$ at energy $\mathscr{E}$ is given by

$$p(\mathscr{E})\, d\mathscr{E} = \Gamma \exp(-\mathscr{E}/k_B T)\, d\mathscr{E} \tag{66}$$

where the constant Γ is determined by requiring that the total probability be unity that the particle have some energy in the interval $(0 \leqslant \mathscr{E} \leqslant \infty)$, viz.

$$1 = \int_0^\infty p(\mathscr{E})\, d\mathscr{E} = \Gamma \int_0^\infty \exp(-\mathscr{E}/k_B T)\, d\mathscr{E} \tag{67}$$

The value of the last integral is readily shown to be $k_B T$, so that

$$\Gamma = \frac{1}{k_B T} \tag{68}$$

The total probability, P_{tot}, that the particle will be excited to a total energy exceeding the value $U_{max}^{(f)}$ is then given by

$$P_{tot} = \int_{U_{max}^{(f)}}^\infty p(\mathscr{E})\, d\mathscr{E} = \Gamma \int_{U_{max}^{(f)}}^\infty \exp(-\mathscr{E}/k_B T)\, d\mathscr{E} \tag{69}$$

The value of the last integral is readily shown to be $k_B T \exp[-U_{max}^{(f)}/k_B T]$ so that

$$P_{tot} = \exp[-U_{max}^{(f)}/k_B T] \tag{70}$$

If all the energy given to the particle were associated with the forward component of the momentum, then P_{tot} could be substituted for $P(U^{(f)}_{max})$ in eqn. (65). For a three-dimensional system, however, there are also transverse momentum components p_y and p_z in addition to the forward component p_x, since

$$\mathscr{E} = \frac{p_x^2 + p_y^2 + p_z^2}{2m}$$

with m representing the mass of the particle. Thus $p_x^2/2m$ will be less than $\mathscr{E}$, so that in general

$$P(U^{(f)}_{max}) < P_{tot} \tag{71}$$

Furthermore, the assumption of a uniform density of states, although not too unpalatable from a classical viewpoint where any kinetic energy is possible, may not be allowable. In fact, from the standard approach of considering the quantum eigenstates for a particle in a box, we know it is not correct. The merit of the above simplistic approach, however, is that the errors due to the various assumptions tend to cancel. One factor is that the density of final states for a given x component of momentum p_x and a given energy $\mathscr{E}$ is indeed independent of both p_x and $\mathscr{E}$, assuming a particle-in-a-box model [18] and it is the x component of momentum yielding the energy $p_x^2/2m$ which is critical for surmounting the barrier in the forward direction. Furthermore, the barrier height for forward motion turns out to be a parameter which must generally be deduced from experimental measurements of the temperature dependence of the particle current, so it is a phenomenological constant in the theory. Taking into consideration also our approximation of representing the lattice phonon spectrum by a single phenomenological frequency ν, it is acceptable for our present purposes to utilize P_{tot} for $P(U^{(f)}_{max})$ in eqn. (65). Thus, we obtain the particle current density in one direction over a given barrier to be

$$J^{(f)} = n^{(f)}\nu \exp(-U^{(f)}_{max}/k_B T) \tag{72}$$

Many such barriers must be crossed before a given defect traverses the oxide film, as indicated in Fig. 10(b). Each defect moves randomly, so it can hop in the reverse direction as well as in the forward direction. The net motion is determined by the difference between the number of forward hops and the number of reverse hops. There are two aspects of this to be considered. First, a difference between the maximum barrier heights in the two directions can lead to a greater number of hops in one direction as opposed to the number in the other direction. [See, for example, Fig. 10(a) depicting a single barrier with the potential minima at different depths on either side of the maximum]. Considering $W^{(f)}$ to be the maximum height in the barrier as viewed in the forward direction for defects in the one potential energy minimum and $W^{(r)}$ to be the

maximum height in the barrier in the reverse direction for the defects in the adjacent potential energy minimum, then if the same value holds for the area density in the two adjacent potential minima, the net particle current over the barrier will be given by

$$J^{(\mathrm{net})} = n\nu\,[\exp(-W^{(\mathrm{f})}/k_{\mathrm{B}}T) - \exp(-W^{(\mathrm{r})}/k_{\mathrm{B}}T)] \tag{73}$$

One might inquire into the reasons why the barriers may be of different height in the forward and reverse directions. A more accurate picture of the motion of the defect through the diffusion medium would necessarily include a statistical distribution of barrier heights and potential energy minima, so there would naturally be differences on a local basis. Even if all barriers were of the same height, any internal macroscopic electric field would give rise to potential energy differences between different spatial points within the oxide and these differences would lead to different heights in the barriers as viewed from the forward and reverse directions. This matter will be treated quantitatively later in this section.

The second aspect of this problem is that the area densities may be different on the two sides of a given barrier. This difference in the area densities would lead to a difference in the forward and reverse components of the hopping current, even if the height of the barrier were the same as viewed from the forward and reverse directions. For example, if the barrier heights are $W^{(\mathrm{f})}$ and $W^{(\mathrm{r})}$ as viewed from the two directions, respectively, and the area density for forward hopping is denoted by $n^{(\mathrm{f})}$ and the area density for reverse hopping is denoted by $n^{(\mathrm{r})}$, then the net current density over the barrier would be given by

$$J_{\mathrm{net}} = n^{(\mathrm{f})}\nu \exp(-W^{(\mathrm{f})}/k_{\mathrm{B}}T) - n^{(\mathrm{r})}\nu \exp(-W^{(\mathrm{r})}/k_{\mathrm{B}}T) \tag{74}$$

One could ask why the area densities may be different on the two sides of the barrier. This is due to the innate asymmetry in the metal—oxide—oxygen structure. One interface of the oxide may constitute the sink for defects whereas the other interface constitutes the source of the defects. The attendant concentration difference across the oxide layer leads to local concentration differences across the individual barriers. In other words, the area density differences are simply a manifestation of the concentration gradient which exists in the oxide for a given type of defect species.

It is informative to examine the limiting cases of the above expressions for the current over a specific local barrier. The thermal equilibrium limit is reached whenever the current J is chosen to be zero. We note that this requires forward and reverse components of the hopping current to be equal in magnitude. From eqn. (74), we obtain

$$n^{(\mathrm{f})}\nu \exp(-W^{(\mathrm{f})}/k_{\mathrm{B}}T) = n^{(\mathrm{r})}\nu \exp(-W^{(\mathrm{r})}/k_{\mathrm{B}}T) \tag{75}$$

or, equivalently

$$n^{(r)} = n^{(f)} \exp[-(W^{(f)} - W^{(r)})/k_B T] \tag{76}$$

This relates the area densities on the two sides of the barrier for this situation of a zero net current. We can conclude that even moderate differences between the forward and reverse barrier heights lead to very large differences in the area densities, due to the exponential relationship on the difference in barrier heights. On the other hand, eqn. (75) shows that whenever the forward and reverse barrier heights are equal, the area densities on the two sides of the barrier must be equal if the current is to be zero.

If the fixed defect concentrations at the oxide interfaces consistent with the interfacial kinetic reactions are incompatible with the series of local relationships between area densities given by the above thermal equilibrium relation, then the current cannot be zero. There are two limiting cases for this non-equilibrium situation and these are characterized by the relative magnitudes of the three terms in eqn. (74), namely, J_{net}, $n^{(f)}\nu \exp(-W^{(f)}/k_B T)$, and $n^{(r)}\nu \exp(-W^{(r)}/k_B T)$. Consider, first of all, the situation in which one of the two terms containing $n^{(f)}$ or $n^{(r)}$ is much larger than the other. Then, in eqn. (74), the smaller one can be neglected relative to the larger and we obtain one of the following approximations for the current.

$$J \simeq n^{(f)}\nu \exp(-W^{(f)}/k_B T) \tag{77}$$

$$J \simeq -n^{(r)}\nu \exp(-W^{(r)}/k_B T) \tag{78}$$

In the first case, the current is in the positive direction, whereas in the second case, it is in the reverse direction. We designate these, respectively, as the large forward current and the large reverse current cases, respectively, since the current is almost equal in magnitude to one of the two terms on the right-hand side of eqn. (74) and is far larger in magnitude than the other of the two terms on the right-hand side of eqn. (74).

Next, consider the situation in which both of the terms on the right-hand side of eqn. (74) are much larger in magnitude than their difference. Since the difference between the two is the particle current itself, we designate this as the *small current limit.* Although not quite the same as the equilibrium case of eqn. (75), nevertheless the relationship between the area densities will not deviate markedly from those predicted by the equilibrium expression given in eqn. (75). If, in this small current limit, we further restrict our consideration to barriers of equal height as viewed from the forward and reverse directions, then the area densities on the two sides of the barrier will be almost equal, viz. $n^{(r)} \simeq n^{(f)}$.

Let us next consider the situation in which the barrier is of the same height as viewed in the forward and reverse directions, $W^{(r)} = W^{(f)} = W$, where we can now drop the superscript on W designating the forward or

reverse direction. The hopping current given by eqn. (74) then becomes

$$J = [n^{(f)} - n^{(r)}]\, \nu \exp(-W/k_B T) \tag{79}$$

We see that the net current is directly proportional to the difference in the area densities on the two sides of the barrier.

In terms of an equivalent bulk concentration of defects, C, we can write, from conservation of the number of particles, the relation

$$(\text{Unit area})n = (\text{Unit area})\,(2a)C \tag{80}$$

That is, the number, n, per unit area in a given potential energy minimum is equal to the product of the distance, $2a$, across the potential minimum with the area (to give the volume) and that times the bulk concentration of defects (in units of number of defects per unit volume). Dividing through by (Unit area) in eqn. (80) gives

$$n = 2aC \tag{81}$$

whereas n is a *discrete variable*, having different values from potential minimum to potential minimum, the bulk concentration can be viewed in general as a *continuum variable* because it is usually considered to be an average over distances that are large compared with the distance separating individual potential minima.

In terms of the bulk defect concentration, the hopping current for equal barrier heights in the forward and reverse directions [see eqn. (79)] takes the form

$$\begin{aligned} J &= 2a[C^{(f)} - C^{(r)}]\, \nu \exp(-W/k_B T) \\ &= -[(C^{(r)} - C^{(f)})/2a]\; (4a^2\, \nu) \exp(-W/k_B T) \end{aligned} \tag{82}$$

However, the difference $(C^{(r)} - C^{(f)})$ is the *increase* in concentration over the distance $2a$ across the potential barrier. This, in terms of differential calculus, is the *concentration gradient.* Thus

$$J = -D\frac{dC}{dx} \tag{83}$$

and we have a microscopic derivation of Fick's first law of diffusion. This derivation simultaneously gives an evaluation of the *diffusion coefficient* D

$$D = 4a^2 \nu \exp(-W/k_B T) \tag{84}$$

as obtained from comparison of eqns. (82) and (83). We note that the units appropriate for D are (area/time). This limiting case is called the *pure diffusion limit*, since the assumption of equal forward and reverse barrier heights precludes, in general, the presence of an electric field with an attendant field-produced component of the particle current.

If the only difference between the forward and reverse barrier heights is the potential energy difference associated with the presence of an electric field, then it is possible to examine the field-dependence of the hopping current in various limits without too much difficulty. By referring back to Sect. 1.7, we see that the electrostatic potential energy difference associated with a uniform electric field acting over a distance a is given by $-qEa$, where q is the charge of the mobile defect for which we are calculating the potential energy difference. The negative sign means that the potential energy is lower at greater distances when the force qE on the defect is in the positive direction. We then have the relations

$$W^{(f)} = W - qEa \tag{85}$$

and

$$W^{(r)} = W + qEa \tag{86}$$

where W is the barrier height (as viewed from either direction) in zero field. Since, mathematically

$$\exp(y + z) = \exp(y)\exp(z) \tag{87}$$

the expression given by eqn. (74) for the current for this situation can be written in the form

$$J = \nu \exp(-W/k_B T)\,[n^{(f)} \exp(qEa/k_B T) - n^{(r)} \exp(-qEa/k_B T)] \tag{88}$$

We can have the equilibrium case of zero current, in which case we find from this expression that

$$n^{(r)} = n^{(f)} \exp(2qEa/k_B T) \tag{89}$$

For the non-equilibrium situation, $J \neq 0$, we have the large and the small current possibilities. By analogy with eqns. (77) and (78), we obtain for large forward and reverse currents, respectively

$$J \simeq n^{(f)} \nu \exp(-W/k_B T) \exp(qEa/k_B T) \tag{90}$$

and

$$J \simeq -n^{(r)} \nu \exp(-W/k_B T) \exp(-qEa/k_B T) \tag{91}$$

where, in the first case, the electric force $qE > 0$ and, in the second case, the electric force $qE < 0$. For the other limiting situation of small current, the two terms do not differ greatly in value, so that the current, determined by the *difference* between the two, is small relative to either one.

Let us now examine the limiting case of eqn. (88) in which the electric field is not too large. If the criterion

$$|qEa| \lesssim k_B T \tag{92}$$

is met, then it is useful to expand the exponentials containing the field in accordance with the small argument relation

$$\exp(\delta) \simeq 1 + \delta + \tfrac{1}{2}\delta^2 + \ldots \tag{93}$$

Deciding on how many terms to keep is sometimes a difficult problem. If we keep only the first term (namely unity) in the expansion for each of the three exponentials, then we regain the pure diffusion limit given by eqn. (83). Keeping, in addition, the next term in the first two exponentials leads to

$$\begin{aligned} J &= \nu \exp(-W/k_B T)\,[n^{(f)} \exp(qEa/k_B T) - n^{(r)} \exp(-qEa/k_B T)] \\ &\simeq \nu \exp(-W/k_B T)\,[n^{(f)}\,\{1 + (qEa/k_B T)\} \\ &\quad - n^{(r)}\{1 - (qEa/k_B T)\}] \\ &\simeq \nu \exp(-W/k_B T)\,[(n^{(f)} - n^{(r)}) + (qEa/k_B T)\,(n^{(f)} + n^{(r)})] \\ &\simeq 4a^2 \nu \exp(-W/k_B T)\,[\{-(n^{(r)} - n^{(f)})/2a\}/2a \\ &\quad + (qE/k_B T)\tfrac{1}{2}(n^{(f)} + n^{(r)})/2a] \end{aligned} \tag{94}$$

Note that we now have two terms, one corresponding to the gradient-produced pure diffusion current and the second involving the first power of the electric field. The term linear in the electric field can be interpreted more readily by noting that

$$\tfrac{1}{2}[n^{(f)} + n^{(r)}] = n_{avg} \tag{95}$$

where n_{avg} is the *average* area density for the two potential minima on either side of the barrier. Utilizing eqn. (82) for the gradient and also employing the continuum notation $C = n_{avg}/2a$, in accordance with eqn. (81), this expression can be written in the form

$$J = -D(\mathrm{d}C/\mathrm{d}x) + \mu EC \tag{96}$$

where

$$D = 4a^2 \nu \exp(-W/k_B T) \tag{97}$$

and

$$\mu = \frac{qD}{k_B T} \tag{98}$$

Equation (96) is known as the *linear diffusion equation* since the lowest-order field dependence is linear. Thus we have a microscopic derivation of the *Einstein relation*, eqn. (98). This relation is normally derived from quite different considerations based on setting the current equal to zero in the linear diffusion equation and comparing the concentration profile $C(x)$ with that predicted by equilibrium thermodynamics.

It is interesting that we have derived the well-known linear diffusion

equation by considering the hopping current over a single energy barrier. There are, in general, many such barriers across the diffusion medium, as indicated by Fig. 10(b). The linear diffusion equation then applies locally throughout the oxide layer. If the current varies from position to position, then there is a change in the local defect concentration in accordance with eqn. (46). The content of Fick's second law of diffusion is that a change in current with position leads to a build-up of the concentration whenever J decreases with position x, but leads to a depletion in the concentration, C, whenever J increases with position x. Mathematically

$$\frac{\partial C(x,t)}{\partial t} = \frac{-\partial J(x,t)}{\partial x} \tag{99}$$

as given by the equation of continuity [eqn. (46)]. If the concentration at a given position is not changing with time, then the current does not vary with position. Then we have what is known as the *steady-state condition* [19].

Because the mobile defects are charged, there can be a variation in the electric field from place to place within the oxide layer in accordance with Poisson's equation. From eqn. (41)

$$\frac{dE}{dx} = \frac{\rho(x)}{\epsilon} \tag{100}$$

or, equivalently

$$E(x) - E(0) = (1/\epsilon) \int_0^x \rho(x) dx \tag{101}$$

Therefore

$$E(x_2) - E(x_1) = (1/\epsilon) \int_{x_1}^{x_2} \rho(x) dx \tag{102}$$

The content of this expression is that the fields differ at any two arbitrary positions x_1 and x_2 by an amount depending upon the net space charge located between the two points.

If, at places within the oxide layer, the electric field is too large for the exponential expansion utilized above in deriving the linear diffusion equation to be a valid approximation, then the more exact hopping current expression given by eqn. (88) should be utilized instead. Numerical computations are usually easier to carry out in any electric field limit by using the exact microscopic hopping expression (88).

Let us now refer back to Fig. 10(b) to set up a formal indexing system for the system of potential energy maxima and potential energy minima. Then the equations for transport across the series of potential energy barriers can be identified for individual barriers, and the relationship between the equations can be examined. It is clear that the area densities effective for forward hopping over one barrier will be the same area

densities effective for reverse hopping over the preceding barrier, so we expect there to be some coupling between the difference equations for the barrier hopping currents. In Fig. 10(b), an index, k, labels the potential energy barrier in question. The potential energy minimum which *follows* a given potential energy barrier is labeled by the same index. The area density, n, associated with a given potential energy minimum labeled k is given the subscript k of that potential energy minimum, viz. n_k. Thus n_k is the effective area density for reverse hopping over the barrier labeled k, whereas n_{k-1} is the effective area density for forward hopping over the barrier labeled k. Since n_{k-1} can differ from n_k, the number of forward hops over barrier k can be expected in general to differ from the number of reverse hops over barrier k, viz.

$$J_k^{(\mathrm{net})} = n_{k-1}\,\nu \exp(-W_k^{(\mathrm{f})}/k_\mathrm{B}T) - n_k \nu \exp(-W_k^{(\mathrm{r})}/k_\mathrm{B}T) \tag{103}$$

As mentioned above, the forward barrier maximum $W_k^{(\mathrm{f})}$ may be the same as the reverse barrier maximum $W_k^{(\mathrm{r})}$, although this is not necessarily the case. Electrostatic potential energy differences associated with a macroscopic electric field within the oxide lead to a raising of the barriers for hopping in one direction and a lowering of the barriers for hopping in the opposite direction. Quantitatively, the electrostatic potential energy difference over a local distance a is given by the product of electric field E and microscopic distance a in accordance with eqn. (19)

$$\Delta W = -qEa \tag{104}$$

The potential energy minimum labeled k is lowered with respect to the barrier labeled k by an amount $-qE_k a$, assuming a to represent the distance separating the potential energy barrier labeled k from the potential energy minimum labeled k. Similarly, the potential energy maximum labeled k, is lowered by a similar amount relative to the potential energy minimum labeled $k-1$. To view the matter conversely, a lowering of the potential energy minimum labeled k by an amount $|\Delta W|$ relative to the barrier labeled k is equivalent, insofar as the hopping current is concerned, to a raising of the potential energy barrier labeled k relative to the potential energy minimum labeled k. Thus a field which lowers barrier k relative to the minimum labeled $k-1$ simultaneously raises barrier k relative to the minimum labeled k. Hopping in the forward direction is increased whereas hopping in the reverse direction is decreased. The net current J_k over barrier k is thus given by

$$\begin{aligned} J_k &= \nu \exp(-W/k_\mathrm{B}T)\,[n_{k-1}\exp(qE_k a/k_B T) \\ &\quad - n_k \exp(-qE_k a/k_\mathrm{B}T)] \\ &= (D/4a^2)\,[n_{k-1}\exp(qE_k a/k_\mathrm{B}T) - n_k \exp(-qE_k a/k_\mathrm{B}T)] \\ &\quad (k = 1, 2, 3, \ldots, N) \end{aligned} \tag{105}$$

In terms of this discrete notation, the equation of continuity given by eqn. (44) takes the form

$$\Delta n_k = (J_k - J_{k+1})\Delta t \tag{106}$$

Let us now examine the local variation of the electric field, E_k, produced by the charged defects within the oxide layer in accordance with Poisson's equation [see eqn. (40)]. The electric field at the potential barrier maximum labeled $k + 1$ is related to the electric field at the potential barrier maximum labeled k, the difference between the fields being due to the intervening space charge located in the potential minimum labeled k. From eqn. (102)

$$\begin{aligned} E(x_{k+1}) &= E(x_k) + (1/\epsilon) \int_{x_k}^{x_k+2a} \rho(x)\,\mathrm{d}x \\ &\simeq E(x_k) + (1/\epsilon)\,\rho(x_k)\,(2a) \end{aligned} \tag{107}$$

Equivalently, in discrete notation

$$E_{k+1} = E_k + (1/\epsilon) \sum_s q^{(s)} n_k^{(s)} \tag{108}$$

The sum over the species index s gives the additive effects of all charged species in the oxide. Later, we will examine the effects of space charge on the particle current by using models yielding easy insight into the essence of this problem. Before doing this, however, it is informative to examine the particle currents through oxides due to the diffusion of uncharged particles and then to examine the currents through oxides due to the diffusion of charged particles in surface-charge fields only.

If transport takes place by the diffusion of uncharged atoms, eqn. (96) tells us that

$$J = -D \frac{\mathrm{d}C}{\mathrm{d}x} \tag{109}$$

or, equivalently

$$J\,\mathrm{d}x = -D\,\mathrm{d}C \tag{110}$$

Integrating both sides of this expression

$$\int_0^x J\,\mathrm{d}x = -\int_{C(0)}^{C(x)} D\,\mathrm{d}C \tag{111}$$

In the steady-state limit, J is independent of x. In accordance with eqn. (97), D is likewise a constant. Thus we can write

$$J \int_0^x \mathrm{d}x = -D \int_{C(0)}^{C(x)} \mathrm{d}C \tag{112}$$

which gives

$$Jx = -D[C(x) - C(0)] \tag{113}$$

Solving for $C(x)$ gives the concentration profile

$$C(x) = C(0) - (J/D)x \tag{114}$$

Evaluating the concentrations at $x = L$ gives

$$C(L) = C(0) - (J/D)L \tag{115}$$

Solving for the current J gives

$$J = D[C(0) - C(L)]/L \tag{116}$$

Substituting this result into the concentration profile given by eqn. (114) gives

$$C(x) = C(0) - [C(0) - C(L)]x/L \tag{117}$$

Our conclusions thus are that whenever the boundary concentrations $C(0)$ and $C(L)$ are fixed in value by the interfacial reactions, the current is inversely proportional to L and the concentration is a linear function of the position x within the oxide. Considering x/L to be a dimensionless *normalized* position within the oxide, we can conclude further that the defect concentration is a linear function of this normalized position. It requires only a few more easy steps (cf. Sect. 1.13) to show that the corresponding oxide layer thickness would increase as the square root of the time under these conditions.

Let us now examine the microscopic hopping current in the presence of surface-charge fields only. That is to say, we ignore the effects of the space charge of the mobile species. We choose to utilize the exact microscopic hopping expression given by eqn. (105) without making any approximations based on the magnitude of the electric field. Thus our results will be generally applicable to all electric field limits, extending from zero electric field to very high electric fields. In addition, we carry out the development without resorting to the use of calculus. The difference equation approach which is utilized is easy to follow by anyone who is acquainted with elementary geometric series. Although the analogous non-steady-state problem [20] can be treated without too much difficulty, it is sufficient for present purposes to confine our attention to the steady-state limit. In this limit, the defect concentrations are not changing with time within the oxide layer, so the particle currents are uniform within the layer. That is

$$J_{k+1} = J_k \qquad (k = 1, 2, 3, \ldots, N-1) \tag{118}$$

The microscopic hopping expression for J_k given by eqn. (105) can be written in the form

$$J_k = \nu \exp(-W/k_B T)\,[n_{k-1}\,\zeta^{1/2} - n_k\,\zeta^{-1/2}] \tag{119}$$

where the quantity ζ is defined by

$$\zeta = \exp(2qEa/k_B T) \tag{120}$$

This quantity is independent of the index k because, for the present development, we are ignoring any effects of the space charge. [From eqn. (37), we see that $E_k = E_0$ for all values of k when the space charge is negligible]. Equation (119) above likewise yields J_{k+1} merely by replacing k by $k+1$ in the three places where it occurs. Thus substituting eqn. (119) into the steady-state relation given by eqn. (118) yields

$$n_k \zeta^{1/2} - n_{k+1} \zeta^{-1/2} = n_{k-1} \zeta^{1/2} - n_k \zeta^{-1/2} \tag{121}$$

This expression is easily arranged to give

$$(n_{k+1} - n_k)\zeta^{-1/2} = (n_k - n_{k-1})\zeta^{1/2} \quad (k = 1, 2, 3, \ldots, N-1) \tag{122}$$

Let us now define the difference quantities

$$\psi_k = n_k - n_{k-1} \qquad (k = 1, 2, 3, \ldots, N) \tag{123}$$

so that eqn. (122) takes the form

$$\psi_{k+1} \zeta^{-1/2} = \psi_k \zeta^{1/2} \qquad (k = 1, 2, 3, \ldots, N-1) \tag{124}$$

or, equivalently

$$\psi_{k+1} = \psi_k \zeta \qquad (k = 1, 2, 3, \ldots, N-1) \tag{125}$$

Thus we can write the series of equations

$$\begin{aligned}
\psi_2 &= \psi_1 \zeta \\
\psi_3 &= \psi_2 \zeta = (\psi_1 \zeta)\zeta = \psi_1 \zeta^2 \\
\psi_4 &= \psi_3 \zeta = (\psi_1 \zeta^2)\zeta = \psi_1 \zeta^3 \\
\psi_5 &= \psi_4 \zeta = (\psi_1 \zeta^3)\zeta = \psi_1 \zeta^4 \\
&\vdots \\
\psi_N &= \psi_{N-1} \zeta = (\psi_1 \zeta^{N-2})\zeta = \psi_1 \zeta^{N-1}
\end{aligned} \tag{126}$$

Utilizing now the defining relation $\psi_k = n_k - n_{k-1}$, we can write

$$n_k = n_{k-1} + \psi_k \qquad (k = 1, 2, 3, \ldots, N) \tag{127}$$

Utilizing this relation recursively, we obtain

$$\begin{aligned} n_k &= n_{k-1} + \psi_k \\ &= (n_{k-2} + \psi_{k-1}) + \psi_k = n_{k-2} + \psi_{k-1} + \psi_k \\ &= (n_{k-3} + \psi_{k-2}) + \psi_{k-1} + \psi_k \\ &\quad \vdots \\ &= n_0 + \psi_1 + \psi_2 + \psi_3 + \ldots + \psi_k \qquad (k = 1, 2, 3, \ldots, N) \end{aligned} \tag{128}$$

Substituting the above evaluation of the various ψ_j then gives

$$\begin{aligned} n_k &= n_0 + \psi_1 + \psi_1\zeta + \psi_1\zeta^2 + \psi_1\zeta^3 + \ldots + \psi_1\zeta^{k-1} \\ &= n_0 + \psi_1 [1 + \zeta + \zeta^2 + \zeta^3 + \ldots + \zeta^{k-1}] \\ &= n_0 + \psi_1 \sum_{j=0}^{k-1} \zeta^j \qquad (k = 1, 2, 3, \ldots, N) \end{aligned} \tag{129}$$

The sum is a geometric series and its value can be obtained from standard handbook formulas

$$\sum_{j=0}^{k-1} \zeta^j = \frac{1-\zeta^k}{1-\zeta} \tag{130}$$

In this way we obtain

$$n_k = n_0 + \psi_1(1-\zeta^k)/(1-\zeta) \qquad (k = 1, 2, 3, \ldots, N) \tag{131}$$

The as yet undetermined parameter ψ_1 follows from an evaluation of this result for $k = N$

$$n_N = n_0 + \psi_1(1-\zeta^N)/(1-\zeta) \tag{132}$$

since n_0 and n_N are presumed to be fixed quantities characteristic of the interfacial reactions. Solving for ψ_1 gives

$$\psi_1 = \frac{(n_N - n_0)(1-\zeta)}{1-\zeta^N} \tag{133}$$

Substituting this result into eqn. (131) gives the area density profile

$$n_k = n_0 + \frac{(n_N - n_0)(1-\zeta^k)}{1-\zeta^N} \qquad (k = 1, 2, 3, \ldots, N) \tag{134}$$

We note that this expression for n_k gives the correct boundary values n_0 and n_N in the limits $k = 0$ and $k = N$, respectively.

The current follows from eqn. (119), viz.

$$J_k = \nu \exp(-W/k_B T)\,[n_{k-1}\zeta^{1/2} - n_k\zeta^{-1/2}] \tag{135}$$

Using eqn. (134) for n_k gives

$$n_{k-1}\zeta^{1/2} = n_0\zeta^{1/2} + [(n_N - n_0)\zeta^{1/2}\ (1-\zeta^{k-1})/(1-\zeta^N)] \tag{136}$$

and

$$n_k\zeta^{-1/2} = n_0\zeta^{-1/2} + [(n_N - n_0)\zeta^{-1/2}\ (1-\zeta^{k})/(1-\zeta^N)] \tag{137}$$

Thus

$$\begin{aligned} J_k &= \nu\ \exp(-W/k_B T)\ [n_0(\zeta^{1/2} - \zeta^{-1/2}) \\ &\quad + [(n_N - n_0)/(1-\zeta^N)]\ [\zeta^{1/2}(1-\zeta^{k-1}) - \zeta^{-1/2}(1-\zeta^k)]] \end{aligned} \tag{138}$$

and so

$$\begin{aligned} J_k &= \nu\ \exp(-W/k_B T)\ (\zeta^{1/2} - \zeta^{-1/2})\ [n_0 + (n_N - n_0)/(1-\zeta^N)] \\ &= \nu\ \exp(-W/k_B T)\ (\zeta^{1/2} - \zeta^{-1/2})\ (n_0 - n_0\zeta^N \\ &\quad + n_N - n_0)/(1-\zeta^N) \\ &= \nu\ \exp(-W/k_B T)\ (\zeta^{1/2} - \zeta^{-1/2})\ (n_N - n_0\zeta^N)/(1-\zeta^N) \end{aligned} \tag{139}$$

Note that the right-hand side of this equation is independent of k, showing the homogeneous-field characteristic that

$$J_1 = J_2 = J_3 = \ldots = J_N \tag{140}$$

so we can designate the homogeneous-field current simply as J.

Utilizing the definition $\zeta = \exp(2qEa/k_B T)$ then gives

$$\begin{aligned} J &= \nu\ \exp(-W/k_B T)\ [\exp(qEa/k_B T) - \exp(-qEa/k_B T] \\ &\quad \times\ [n_N - n_0\ \exp(2qENa/k_B T)]/[1 - \exp(2qENa/k_B T)] \end{aligned} \tag{141}$$

The quantity $2Na$ is the thickness, L, of the oxide layer. Also, the factor involving the difference in the exponentials can be expressed as twice the hyperbolic sine function. We therefore obtain

$$\begin{aligned} J &= 2\nu\ \exp(-W/k_B T)\ \sinh\ (qEa/k_B T) \\ &\quad \times\ [n_N - n_0\ \exp(qEL/k_B T)]/[1 - \exp(qEL/k_B T)] \end{aligned} \tag{142}$$

as the final expression for the current in the discrete notation. In terms of the continuum notation, $n_N = 2aC(L)$ and $n_0 = 2aC(0)$, so that

$$\begin{aligned} J &= (D/a)\sinh(qEa/k_B T) \\ &\quad \times\ [C(L) - C(0)\exp(qEL/k_B T)]/[1 - \exp(qEL/k_B T)] \end{aligned} \tag{143}$$

References pp. 116—117

In the intermediate-field limit, viz. $|qEa/k_B T| < 1$, we can make the approximation $\sinh(qEa/k_B T) \simeq qEa/k_B T$, and the current reduces to

$$J \simeq \mu E[C(L) - C(0)\exp(qEL/k_B T)]/[1 - \exp(qEL/k_B T)] \tag{144}$$

where $\mu = qD/k_B T$ in accordance with eqn. (98).

We now convert the area density expression for the profile into the analogous bulk concentration defect profile by means of the relation $n = 2aC$, where the position x of the potential minimum labeled k is given by $x_k = 2ak$.

Substituting these relations, plus the definition

$$\zeta = \exp\left(\frac{2qEa}{k_B T}\right)$$

into eqn. (134) for the profile gives

$$C(x) = C(0) + [C(L) - C(0)]\ [1 - \exp(qEx/k_B T)]/ \\ [1 - \exp(qEL/k_B T)] \tag{145}$$

This exponential relation is appropriate for the intermediate-field limit corresponding to the current given by eqn. (144), as well as for the high-field limit since it does not further reduce whenever $|qEa/k_B T| \ll 1$.

In the limit of a negligibly small field, the exponentials in eqns. (144) and (145) can be expanded in accordance with eqn. (93) in which $\exp(\delta) \simeq 1 + \delta$. The current given by eqn. (144) then reduces in lowest order to

$$J \simeq \mu E[C(L) - C(0)]/(-qEL/k_B T) \\ = D[C(0) - C(L)]/L \tag{146}$$

and the concentration profile given by eqn. (145) reduces in lowest order to

$$C(x) \simeq C(0) + [C(L) - C(0)]\ [(-qEx/k_B T)/(-qEL/k_B T)] \\ = C(0) + [C(L) - C(0)]\ (x/L) \tag{147}$$

Note that these results [eqns. (146) and (147)] for the current and the profile agree with those which we deduced earlier [see eqns. (116) and (117)] for the case of transport by uncharged particles.
particles.

Let us now ask how the currents are modified by the effects of space charge. Space charge is present whenever growth occurs by the diffusion of charged defect species.

1.12 EFFECTS OF SPACE CHARGE ON THE CURRENTS

The contribution of the space charge to the electric field is given by eqn. (41) in Sect. 1.9. Equations for the currents were then developed for the case where such space charge had a negligible effect on transport relative to the surface-charge field. Now we examine, in as simple a manner as possible, the effects of space charge on the particle currents. Since the particle currents determine the oxidation rate, this will, in turn, lead to an understanding of the effects of space charge on the oxidation rate.

For the ultimate in simplicity, let us consider the effects of a uniform density of immobile (trapped) space charge on the transport of a mobile charged species of sufficiently low concentration that it does not contribute appreciably to the total space charge. This oversimplified version of the generally much more complicated space charge problem gives us an easy insight into the effects of space charge. Figure 11 indicates schematically the uniform trapped space charge density ρ_0, which may be of either sign, the surface-charge density τ_0 at the metal—oxide interface, which may also be of either sign, a surface-charge density τ_L at the oxide—oxygen interface sufficient to yield overall charge neutrality for the entire system, and the charge Ze of the mobile carrier under consideration. From eqn. (10), we know that the surface-charge field can be obtained from τ_0, namely

$$E(0) = \frac{\tau_0}{\epsilon} \tag{148}$$

Note that the surface-charge field $E(0)$ has the same sign as the surface-charge density τ_0. The field $E(x)$ at position x in the oxide for the present case of a uniform space charge density follows readily from eqn. (41), viz.

$$\begin{aligned} E(x) &= E(0) + (1/\epsilon)\int_0^x \rho(x)\,\mathrm{d}x \\ &= E(0) + (\rho_0/\epsilon)x \end{aligned} \tag{149}$$

The electrostatic potential then follows from eqn. (42)

$$V(x) = -\int_0^x E(x)\,\mathrm{d}x = -E(0)x - (\rho_0/2\epsilon)x^2 \tag{150}$$

with $V(0)$ chosen to be zero. Evaluating this result at $x = L$ gives

$$V(L) = -E(0)\,L - (\rho_0/2\epsilon)L^2 \tag{151}$$

We restrict our consideration in the present example to a fixed voltage across the oxide film, so that $V(L)$ is a constant. (This would be the case, for example, if a battery producing a fixed voltage, V_B, was used to drive current through the sample). The critical point is then to notice in the above equation how the magnitude of the surface-charge field, $E(0)$,

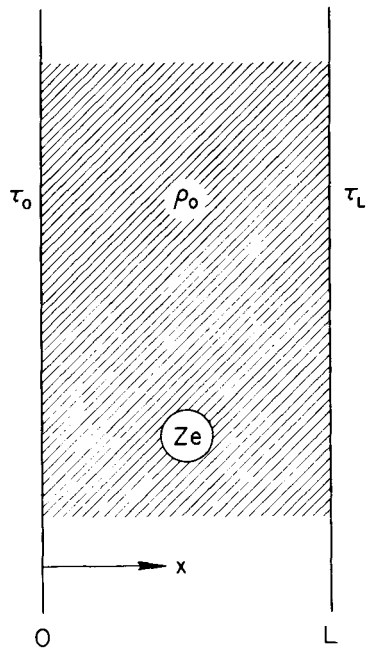

Fig. 11. Diagram illustrating a density, ρ_0, of trapped space charge in the oxide layer, a surface charge, τ_0, at the metal—oxide interface, and an interfacial charge τ_L at the oxide-oxygen interface, with a carrier of charge Ze being driven through the oxide under the combined action of the surface-charge and space-charge electric fields and the concentration gradient.

varies with the level of trapped space charge, ρ_0, at any given thickness, L. It can be seen from the last equation that this variation will depend upon the relative signs of $E(0)$ and ρ_0. Whenever $E(0)$ and ρ_0 are of the same sign, $|E(0)|$ decreases with increasing values of $|\rho_0|$, but whenever $E(0)$ and ρ_0 are of opposite sign, $|E(0)|$ *increases* with increasing values of $|\rho_0|$. Thus the development subdivides into these two possibilities. Consider, for example, the four situations illustrated in Fig. 12. In (a) and (b), $E(0)$ and ρ_0 are of the same sign, so $|E(0)|$ decreases with increasing $|\rho_0|$. That is, the greater the space charge, the *smaller* the magnitude of the surface-charge field. In (c) and (d) in this figure, however, $E(0)$ and ρ_0 are of opposite sign, so $|E(0)|$ increases with increasing $|\rho_0|$. That is, the greater the space charge, the *larger* the magnitude of the surface-charge field.

Next, we must ask what effects the respective variations in the surface-charge field will have on the particle currents originating near that interface in the two cases. This question does not have a straightforward answer in general because the various expressions for the particle current can be quite complicated, involving concentration gradients in addition to

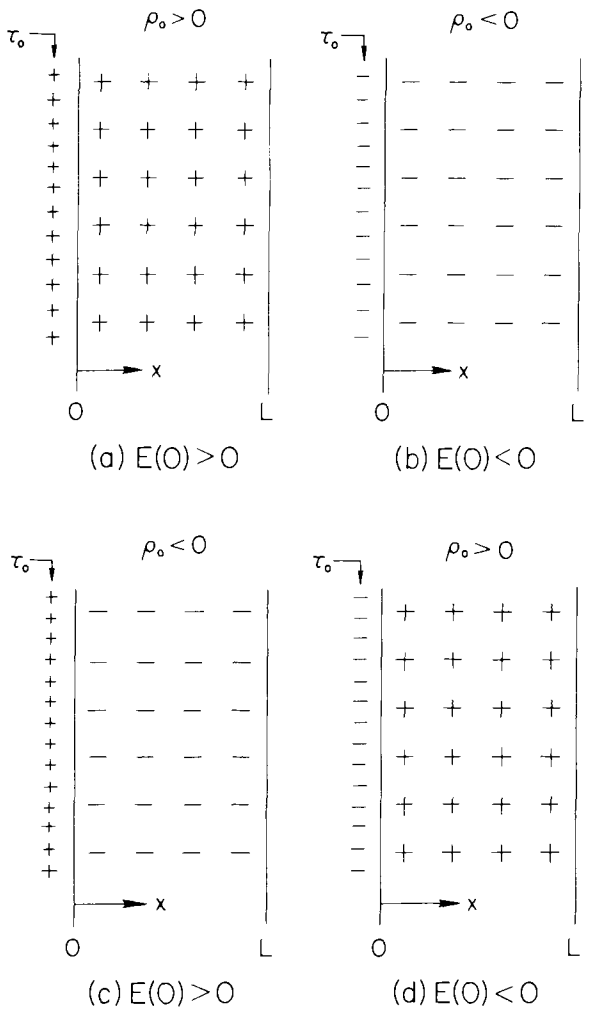

Fig. 12. Diagram illustrating various sign combinations for the surface-charge at the metal—oxide interface and the space charge, ρ_0, within the oxide layer. Diagrams (a)—(d) illustrate field-driven carrier motion for the following cases. (a) Mobile carrier is cation interstitial (or anion vacancy); trapped space charge positive in sign. (b) Mobile carrier is electron; trapped space charge negative in sign. (c) Mobile carrier is cation interstitial (or anion vacancy); trapped space charge is negative in sign. (d) Mobile carrier is electron; trapped space charge is positive in sign.

electric fields. The rearrangement of the concentration profile in the presence of the space-charge field will affect both the local concentration and the local concentration gradient, so both driving forces for the current are changed locally throughout the oxide film. Furthermore, all changes occur in such a way as to maintain a current which is essentially

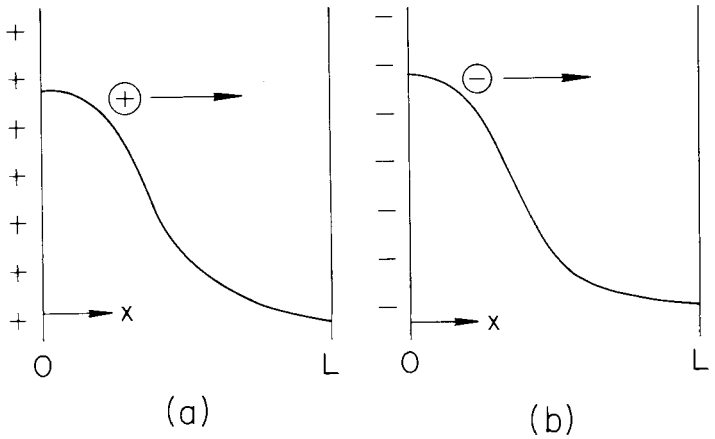

Fig. 13. Possible sign combinations involving the sign of the surface charge at the metal—oxide interface and the sign of the charge of the field-driven mobile species originating at the metal—oxide interface, together with schematic diagrams of the concentration profiles for the mobile species. (a) Field-driven cation interstitial (or anion vacancy) transport; (b) Field-driven electron transport.

steady-state, viz. independent of position within the oxide film. It can be argued intuitively and subsequently verified analytically for special cases, however, that in the region of oxide near $x = 0$ where the only contribution to the field can be considered to be the surface charge at the metal—oxide interface (see Fig. 12), any increase in the field magnitude can be expected to increase the field-driven particle current originating at that interface and, correspondingly, any decrease in the field magnitude can be expected to decrease the field-driven particle current originating at that interface. Consider the situations depicted in Fig. 13 for the possible signs of the surface-charge field and the signs for the charge of the field-driven mobile species originating at the metal—oxide interface, together with schematic illustrations of the concentration profiles for that mobile species. Case (a) is for the positive carrier situation of cation interstitial (or anion vacancy) transport. Case (b) is for the situation of electron transport. In both cases, the carrier has the same sign as the surface-charge field. It is noteworthy that we have chosen to examine the local region where the concentration of mobile defects is expected to be the highest, because intuitively we know that is where the predominant modification in the current will take place when the field is changed. (If one does not like to rely this heavily on intuition, then one can turn to exact numerical and analytical treatments [10] which lead to the same conclusions).

Let us now consider the particle current in the high-field limit for the cases depicted in Fig. 13. Equation (90) is applicable to each of these cases, so that it is possible to examine the predicted effects of the immobile (trapped) space charge on these particle currents. Utilizing our previous conclusion that space charge having the same sign as the surface-charge

field (and thus the same sign as the charge of the field-driven species) decreases the magnitude of the field, we must conclude from the field dependence of the current given by eqn. (90) that space charge having the same sign as the charge of the field-driven mobile carrier will decrease the transport rate. On the other hand, utilizing our second previous conclusion that space charge having the opposite sign as the surface-charge field (and thus opposite to the sign of the charge of the field-driven carrier) increases the magnitude of the field, we must conclude from the field-dependence of the current given by eqn. (90) that space charge having the opposite sign to that of the field-driven mobile carrier will increase the transport rate.

The present qualitative deductions can be supplemented by a more quantitative treatment which has been presented in the literature [21]. One can refer to that development for the predicted functional dependences of the current on space-charge density.

One may question why we have chosen to focus attention so strongly on field-driven carriers, for concentration gradients likewise drive carriers through the oxide film. In oxidation rate calculations, of course, we are primarily concerned with the rate-limiting species, since we think of those species as determining the oxidation rate. Nevertheless, we must similarly be concerned with the particle currents of the non-rate-limiting mobile species, since the coupled-currents condition (see Sect. 1.15) shows that such currents influence, in a very important way, the voltage which will be established across the oxide film. The space charge also modifies the transport rate of the non-rate-limiting species and this often leads to a further adjustment in the voltage across the oxide during thermal oxidation. The non-rate-limiting species will also be field-driven in a certain sense, but the direction of the motion imposed by the field is opposite to that expected in the case of a rate-limiting species. For non-rate-limiting species, the concentration gradient and the electric field act in opposition, so the concentration gradient must be considered more carefully than in the case of a rate-limiting species for which the electric field and concentration gradient act in the same direction. In fact, whenever a non-rate-limiting species is near equilibrium, the concentration gradient and the electric field act in quite a delicate balance to give a net current which is almost zero, so that in this situation the effect of the concentration gradient cannot be neglected, even in an intuitive consideration of the effects of space charge. On the other hand, there is no such delicate balance in the case of a rate-limiting species, so the effect of the electric field can be considered somewhat independently of the effect of the concentration gradient. Even in such cases, however, it must be recognized that this can be done only for intuitive purposes or for approximate calculations and cannot be done when rigorous developments are to be carried out.

In the near equilibrium situation, two distinct limiting cases must

actually be considered, namely, the case in which the outer boundary concentration is not fixed in value and the case in which the outer boundary concentration is indeed fixed in value. The first includes the case of a true equilibrium, where the species concentration can rise to larger values in some regions of the oxide film than the value at the source interface, in which case our study of the variation of the electric field at the oxide interface which is the source of the mobile species in question becomes inadequate. In the alternate case of a fixed lower outer boundary concentration and a voltage having a value near that required for a so-called "virtual current equilibrium" situation [22, 23] consistent with those boundary conditions, the space-charge modification in the current should be correctly predicted by the above development provided the voltage is fixed by some external source. On the other hand, if the voltage is allowed to readjust itself, any space-charge field which induces a change in the current can produce charge transport which in turn modifies the surface-charge field in such a way that the current is again reduced to a nearly zero value. No conclusions are possible in that case.

The matter becomes even more involved in the case of thermal oxidation where the transport of rate-limiting and non-rate-limiting species are "coupled" through a common surface-charge field [10, 11]. Then space charge initiates changes in the currents of both species; this in turn leads to charge transport which modifies the surface-charge field to again balance the net charge transport to zero. Since the mobile species (ionic and electronic) are oppositely charged, a space charge (whatever its sign) will tend to increase the current of one of the mobile species but will tend to decrease the current of the other mobile species. The overall voltage (the so-called "kinetic potential" [22]) can adjust to a new value as a consequence of balancing these two space-charge-modified currents, so the present development becomes inapplicable. We would think intuitively, and it is borne out by exact numerical calculations [24], that it is the space-charge modification for the rate-limiting species which is the most important for determining the space-charge modification in the thermal oxidation rate.

The case of anodic oxidation [25] under constant voltage conditions is, in principle, much more simple than thermal oxidation since only a single mobile species is required to be transported through the growing oxide. In that case, the present intuitive development is immediately applicable. To summarize, our present intuitive development is most obviously applicable to the strongly field-driven case of a rate-limiting mobile species, because for that case the mobile species concentration will have its largest value near the interface where it originates.

The reason that our development so far has been restricted to cases of cation interstitial (or anion vacancy) and electron transport, as illustrated in Fig. 13, is that these are the species which have their sources at the metal—oxide interface. To consider the other possibilities of cation

vacancy (or anion interstitial) and electron-hole transport, we must examine the behaviour of the electric field near the oxide—oxygen interface located at $x = L$. There are two ways of doing this, an indirect method and a direct method. The indirect method involves a change in coordinate system such that the oxide—oxygen interface becomes located at $x = 0$, and the positive x-direction becomes the direction from the oxide—oxygen interface to the metal—oxide interface. Under these transformations, the source interface is again located at $x = 0$, so once again it is the behaviour of the surface-charge field, $E(0)$, with space-charge concentration which is relevant in determining the space-charge modification of the rate of current transport. Sketch (a) in Fig. 13 then becomes applicable to field-driven positive electron-hole transport, and sketch (b) in that figure can represent either field-driven cation vacancy or field-driven anion interstitial transport. Similarly, sketches (a) and (c) in Fig. 12 become applicable for positive electron-hole transport, whereas sketches (b) and (d) in that figure become applicable to cation vacancy and anion interstitial transport. The conclusions regarding the effects of space charge on the currents follow in an analogous way.

The general convention of choosing the coordinate system such that $x = 0$ is the origin of the mobile species, with the direction of motion of that species to produce oxide growth chosen to be the positive x direction, has been utilized throughout our developments for anodic oxidation [25]. It is also the convention utilized earlier in a paper [21] devoted to giving easy insight into space charge effects. On the other hand, that convention is not used in general for our thermal oxidation developments [10, 11]. For thermal oxidation we must consider the transport of more than one species at any given time through the oxide layer, so it is simpler always to consider the metal—oxide interface to be located at $x = 0$, with the positive direction in the oxide being chosen from metal interface to oxygen interface. Using this coordinate system, we now deduce the effects of space charge on cation vacancy motion, anion interstitial motion, and positive electron-hole motion anew. This is what we earlier referred to as the direct method.

Figure 11 again indicates schematically the mobile carriers of charge Ze in the oxide, but the carriers now under consideration (i.e. cation vacancies, anion interstitials, or electron holes) migrate in the negative x direction, viz. they are travelling from the oxide—oxygen interface to the metal—oxide interface. Again, the trapped space-charge density is considered to be much larger than the mobile carrier density in order to produce a readily tractable problem in the mathematical sense, with the solution yielding easy insight into the effects of space charge on the rate of transport of the presently considered mobile species. The surface-charge density, τ_0, at the metal—oxide interface (see Fig. 11) determines the surface-charge field, $E(0)$, in accordance with eqn. (148) already presented at the beginning of this section. The electric field, $E(x)$, within

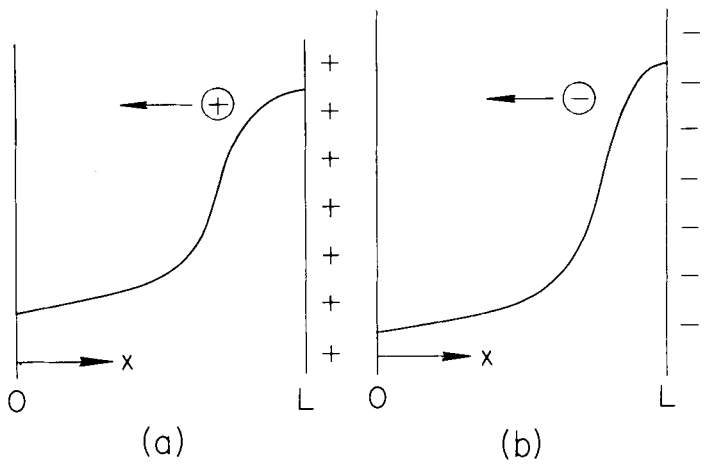

Fig. 14. Possible sign combinations involving the sign of the interfacial charge at the oxide—oxygen interface and the sign of the charge of the field-driven mobile species originating at the oxide—oxygen interface, together with schematic diagrams of the concentraion profiles for the mobile species. (a) Field-driven positive-hole transport; (b) field-driven anion interstitial (or cation vacancy) transport.

the oxide is given by eqn. (149) and the electrostatic potential within the oxide is given by eqn. (150). The expression for the total potential, $V(L)$, across the film is given by eqn. (151) and, as in the previously considered situations, we restrict our consideration to fixed voltages across the oxide so that $V(L)$ is a constant.

The first point of departure of the present development from the previous development is that we must consider the effect of the electric field in the region of the oxide near the oxide—oxygen interface instead of near the metal—oxide interface. As indicated in Fig. 14, the higher concentrations of the mobile cation vacancies, anion interstitials, and electron holes will be at the oxide—oxygen interface, so intuitively we know that the predominant effects of any space-charge modifications in the electric field will occur at that interface. The appropriate high-field expression for the current for this situation is given by eqn. (91), which involves the electric field $E(L)$ at the oxide—oxygen interface. Thus, we must examine the dependence of the field $E(L)$ on the space-charge density in order to delineate the effects of space charge on the particle currents originating at $x = L$. Evaluating eqn. (149) for $E(x)$ at $x = L$ gives

$$E(L) = E(0) + (\rho_0/\epsilon)L \tag{152}$$

Solving for $E(0)$ and substituting into eqn. (151) previously derived for $V(L)$ yields

$$V(L) = -E(L)L + (\rho_0/2\epsilon)L^2 \tag{153}$$

For fixed $V(L)$, this relation requires the field $E(L)$ to increase its magnitude as the space-charge density, ρ_0, increases in magnitude if $E(L)$ and ρ_0 are of the same sign. Alternatively, $|E(L)|$ must decrease with increasing $|\rho_0|$ if $E(L)$ and ρ_0 are of opposite sign. This dependence of $|E(L)|$ on $|\rho_0|$ is inverse to the dependence of $|E(0)|$ on $|\rho_0|$ already determined. The two possibilities for the cases at hand lead to a subdivision of our treatment in accordance with the four situations sketched in Fig. 15.

In Fig. 15 (a) and (b), the surface-charge density τ_L at the oxide—oxygen interface and the space-charge density ρ_0 are of the same sign, whereas in sketches (c) and (d) the quantities τ_L and ρ_0 are of opposite sign. The sign of τ_L determines which carrier is being field-driven near the oxide—oxygen interface, because it is the repulsive Coulomb force of τ_L on the carrier charge Ze which forces the carrier to move towards the metal—oxide interface. Sketches (a) and (c) thus represent the two possibilities of field-driven electron-hole transport, whereas sketches (b) and (d) represent the two possibilities of field-driven cation vacancy (or anion interstitial) transport. Let us next examine the relationship between the sign of τ_L and the sign of the electric field $E(x)$ near $x = L$. This we shall do in two ways. First we argue that the force $ZeE(x)$ on the carrier must be in the negative x direction if it is to travel towards the metal—oxide interface, so $E(x)$ evaluated near $x = L$ must be opposite in sign to the carrier charge Ze. For the two cases of positive electron-hole motion depicted in sketches (a) and (c) in Fig. 15, $E(L)$ must thus be negative, which is opposite in sign to the interfacial charge density τ_L noted in these sketches. Similarly, for the two cases of motion of negatively charged carriers depicted in sketches (b) and (d) in Fig. 15, $E(L)$ must be positive to yield a negatively directed force $ZeE(L)$ on the carriers, so that $E(L)$ must be positive in sign. A comparison of this deduction with the interfacial charge densities τ_L noted in these two sketches shows opposite signs for $E(L)$ and τ_L. Thus, in all four cases, $E(L)$ must be opposite in sign to τ_L. A second approach leading to this same conclusion is based on the more mathematical consideration of overall charge neutrality of the system. That is

$$\tau_0 + \tau_L + \int_0^L \rho(x)\mathrm{d}x = 0 \tag{154}$$

which for $\rho(x) = \rho_0$ gives

$$\tau_0 + \tau_L + \rho_0 L = 0 \tag{155}$$

Dividing through by the dielectric constant, ϵ, gives

$$\frac{\tau_0}{\epsilon} + \frac{\tau_L}{\epsilon} + \frac{\rho_0 L}{\epsilon} = 0 \tag{156}$$

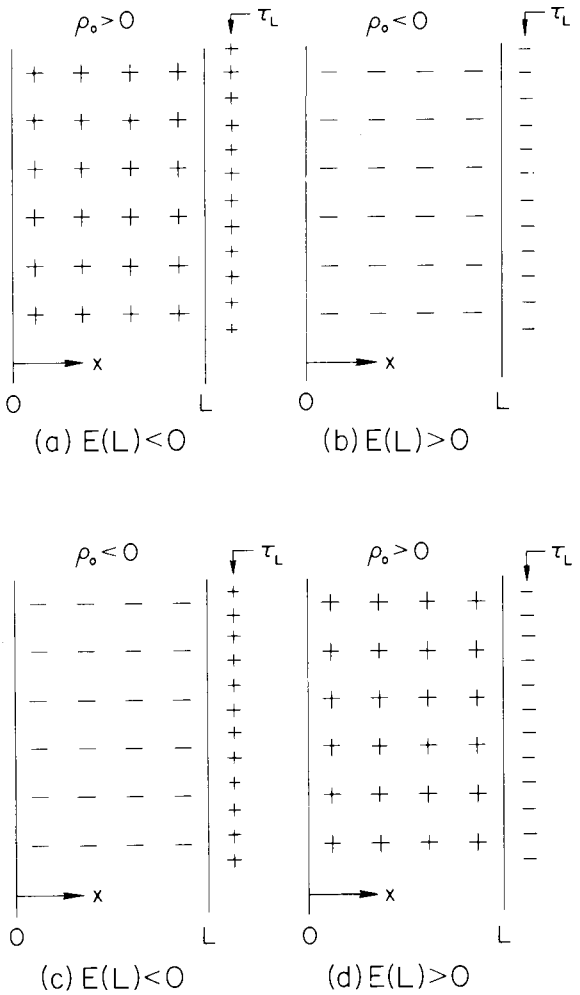

Fig. 15. Diagram illustrating various sign combinations for the surface-charge at the oxide—oxygen interface and the space charge, ρ_0, within the oxide layer. Diagrams (a)—(d) illustrate field-driven carrier motion for the following cases. (a) Mobile carrier is electron hole; trapped space charge positive in sign. (b) Mobile carrier is cation vacancy (or anion interstitial); trapped space charge negative in sign. (c) Mobile carrier is electron hole; trapped space charge negative in sign. (d) Mobile carrier is cation vacancy (or anion interstitial); trapped space charge positive in sign.

which can be written as

$$\frac{\tau_0}{\epsilon} + \frac{\rho_0 L}{\epsilon} = \frac{-\tau_L}{\epsilon} \tag{157}$$

However, the left-hand side must be equal to $E(L)$, according to eqns. (148) and (152), so that

$$E(L) = \frac{-\tau_L}{\epsilon} \tag{158}$$

The conclusion is again reached that the electric field $E(x)$ near the oxide—oxygen interface is opposite in sign to the interfacial charge density τ_L at that interface.

Now let us put together the deductions so far reached. (a) The mobile carrier has the same sign as τ_L, which is of opposite sign to $E(L)$. Thus the carrier charge Ze and the field $E(L)$ are opposite in sign. (b) The magnitude of $E(L)$ increases with increasing values of $|\rho_0|$ whenever $E(L)$ and ρ_0 are of the same sign, but decreases with increasing values of $|\rho_0|$ whenever $|E(L)|$ and ρ_0 are of opposite sign. We can therefore conclude the following: the magnitude of $E(L)$ increases with increasing values of $|\rho_0|$ whenever the space-charge density ρ_0 is opposite in sign to the sign of the mobile carrier charge Ze and, conversely, the magnitude of $E(L)$ decreases with increasing values of $|\rho_0|$ whenever the space-charge density has the same sign as the sign of the mobile carrier charge Ze. Next, referring to the high-field particle current expression [eqn. (91)] appropriate for this situation and keeping in mind that the argument of the exponential is positive since $ZeE(L)$ is negative, we conclude that the magnitude of the particle current increases with increasing $|E(L)|$ and thus with increasing $|\rho_0|$, whenever the space-charge density is opposite in sign to the sign of the mobile charge carrier. The particle current is therefore enhanced by space charge having the opposite sign to the sign of the charge of the mobile species. Conversely, the particle current given by eqn. (91) decreases in magnitude whenever $|E(L)|$ decreases, which in turn is produced by increasing values of $|\rho_0|$ whenever the space-charge density ρ_0 has the same sign as the sign of the mobile charge carrier. The particle current is therefore *retarded* by space charge having the same sign as the sign of the charge of the mobile species. These conclusions regarding space-charge enhancement and space-charge retardation of the particle currents originating at the oxide—oxygen interface are identical to the conclusions which we reached previously regarding the particle currents originating at the metal—oxide interface. Our conclusions regarding the effects of space charge on the currents of positive holes, cation vacancies, and anion interstitials just obtained by our so-called "direct" method are in agreement with corresponding conclusions deduced by means of the "indirect" method based on a coordinate-system transformation. Our earlier remarks as to focusing our attention on situations of predominantly field-driven transport in order to reach firm conclusions without undue consideration of the parallel driving forces due to concentration gradients are again *apropos*.

References pp. 116—117

In summary, we have carried out an in-depth consideration of a very simple limiting case for the effects of space charge on particle currents in order to gain insight into the effects of space charge on the rates of transport of mobile species. Attention is restricted to the various situations of mobile species transport under constant-voltage conditions assuming the mobile species concentrations to be much smaller than a uniform concentration of immobile trapped charge. The qualitative conclusions reached by the analysis of this model have been summarized in two rules for space-charge effects. These rules apply, respectively, to cases where the space-charge density is either of the same sign as the sign of the mobile carrier, or is of opposite sign to the sign of the charge of the mobile carrier. An immediate extension of these qualitative rules to situations in which the large background space charge is non-uniform and/or is due to mobile instead of immobile species is possible, but we do not go into further detail concerning this matter at the present time. For the case of a linear variation of the space-charge density of a mobile species, the reader is referred to the discussion published earlier [26] where an averaging technique is used to draw analogous conclusions to those reached above.

This concludes the section on the effects of space charge on the currents. Our review of some of the various theories for metal oxidation begins with the next section, where the simplest model involving transport of only uncharged particles is presented. The so-called "single-current theories" are reviewed in the section following. Emphasis in that section is placed on anodic oxidation under constant voltage and under constant current conditions, since anodic oxidation represents a realistic situation for one-carrier transport. That section is followed by one on the "coupled-currents" approach to the theory of thermal oxidation. A particular example of the coupled-currents approach is then developed in some detail, namely, the situation of growth of thick oxide films by diffusing charged species under conditions of local space-charge neutrality. That will conclude our introduction to the fundamental concepts of metal-oxidation theory.

1.13 GROWTH BY UNCHARGED PARTICLE TRANSPORT

If transport of the mobile species occurs by uncharged metal or oxygen atoms, or by uncharged O_2 molecules as has been speculated to be the case for silicon oxidation, then the problem becomes relatively simple from a theoretical viewpoint. Electric-field effects then need not be considered, since the concentration gradient would provide the only driving force for transport and the particle current of the mobile species would be given by eqn. (116). Substituting eqn. (116) into the growth-rate expression [eqn. (50)] thus gives

$$\frac{dL}{dt} = \sum_{s=1}^{l} R_s J_s = \sum_{s=1}^{l} \frac{R_s D_s [C_s(0) - C_s(L)]}{L} \tag{159}$$

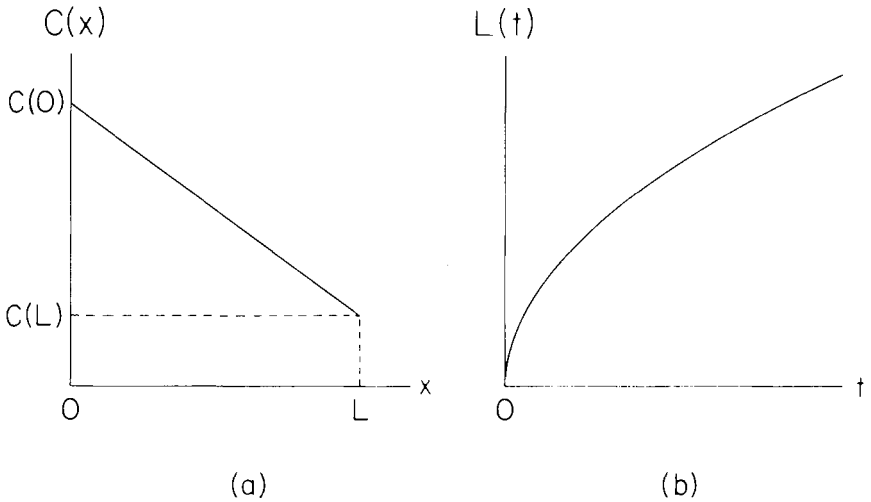

Fig. 16. Concentration profile and growth kinetics for the case of the diffusion of uncharged defects. (a) Linear concentration profile; (b) parabolic growth kinetics.

where R_s represents the volume of new oxide formed when one mobile defect of species s is transported through the growing oxide film. The sum reduces to a single term if only one species is mobile. The boundary concentrations $C_s(0)$ and $C_s(L)$ of the mobile species labeled s are considered to be constants which are fixed by the interfacial reactions. Denoting the sum by $\mathscr{D}_0$, where

$$\mathscr{D}_0 = \sum_{s=1}^{l} R_s D_s [C_s(0) - C_s(L)] \tag{160}$$

we thus obtain

$$\frac{dL(t)}{dt} = \frac{\mathscr{D}_0}{L(t)} \tag{161}$$

where $\mathscr{D}_0$ is a constant which is independent of the oxide film thickness. Integrating this growth-rate equation gives

$$L(t)^2 - L(0)^2 = 2\mathscr{D}_0 t \tag{162}$$

where $L(0)$ is the oxide film thickness at time $t = 0$. This result is denoted as the *parabolic growth law for uncharged particles.* This type of growth behaviour is illustrated by Fig. 16(b).

The concentration profiles of the diffusing species are likewise especially simple for growth by uncharged particle transport. Equation (117) shows that the mobile species concentrations are linear functions of position. This is illustrated in Fig. 16(a).

As appealing as the simplicity of the theory of oxide growth by the

diffusion of uncharged particles may be, it is unlikely to be the natural mode of growth for very many oxides. Even in the case of silicon oxidation, there is experimental evidence that the carrier is a charged oxygen molecule O_2^- instead of merely uncharged oxygen atoms or uncharged molecules [27].

The linear concentration profile for the steady-state growth of oxides by the diffusion of uncharged particles may not be strictly applicable to some cases, namely, those in which growth is so extremely rapid that non-steady-state effects [19] may be significant. It should be pointed out that the experimental observation of a linear concentration profile is in itself insufficient to conclude that growth is occurring by the steady-state diffusion of uncharged particles, since in the case of thick-film growth by the diffusion of a monovalent ionic species under local space-charge-neutrality conditions (see Sect. 1.16), a linear dependence of the mobile species concentrations on position is similarly predicted for the interior region of the oxide film [28, 29].

1.14 SINGLE CURRENT THEORIES

1.14.1 Cabrera—Mott approach to thermal oxidation

Suppose that some ionic species i is strongly rate-limiting and that the rapid flow of an electronic species produces a constant voltage V_B across the oxide, independent of oxide thickness L. Furthermore, assume the electric field in the oxide to be due primarily to surface charge, such that space-charge effects are negligible. Then the electric field, $E(x)$, in the oxide can be written as a constant E_0

$$E(x) = E_0 = \frac{V_B}{L} \tag{163}$$

If this field provides a driving force much greater than the driving force of the concentration gradient of the ionic species and if the behaviour of the ionic species is ohmic in this field, then the ionic current can be written as

$$J_i = \mu_i C_i E_0 \tag{164}$$

where μ_i is the mobility of the ionic species. The product of the particle current density with the charge $Z_i e$ per ion gives the charge density current $\mathscr{J}_i$, as

$$\mathscr{J}_i = Z_i e J_i = Z_i e \mu_i C_i E_0 = \sigma_i E_0 \tag{165}$$

where

$$\sigma_i = Z_i e \mu_i C_i \tag{166}$$

is designated the *ionic conductivity*. The particle current must be position-independent, in accordance with the criterion for steady-state growth [see

eqn. (118)]. This, in turn, requires, for the present case, that $C_i(x) = C_i(0)$ throughout the oxide layer. Thus we obtain

$$J_i = \mu_i C_i(0) E_0 = \frac{\mu_i C_i(0) V_B}{L} \tag{167}$$

This leads to a growth rate

$$\frac{dL(t)}{dt} = R_i J_i = \frac{R_i \mu_i C_i(0) V_B}{L(t)} \tag{168}$$

Employing now the assumption made by Cabrera and Mott [30] of a constant voltage V_B, the growth rate can be written as

$$\frac{dL(t)}{dt} = \frac{\mathscr{D}_{CM}}{L(t)} \tag{169}$$

where the value of the rate constant $\mathscr{D}_{CM}$ for this limit of purely ohmic growth is

$$\mathscr{D}_{CM} = R_i \mu_i C_i(0) V_B \tag{170}$$

Integration of this growth-rate expression then yields the parabolic growth law

$$L(t)^2 - L(0)^2 = 2\mathscr{D}_{CM} t \tag{171}$$

This is designated as a "single current" oxide growth theory, since it does not explicitly include the transport current of the non-rate-limiting species. Equation (170) is essentially the result given by eqn. (14) in the Cabrera–Mott review [30]. That the sole effect of the non-rate-limiting species is to produce a relatively large voltage across the oxide layer, which moreover is a constant independent of the oxide film thickness, indeed involves major assumptions. Furthermore, that this voltage provides the major driving force for an ohmic transport of ions constitutes an additional major assumption, since the effect of the ionic concentration gradient is thereby ignored. The validity of this host of assumptions can be tested by the "coupled-currents approach" to metal oxidation which is summarized in Sect. 1.15. The coupled-currents development of the presently considered problem has been carried out analytically [31] and it was found to lead to what we refer to as the *thin-film parabolic growth law* [31]. The coupled-currents approach has, in fact, been used for a rigorous analysis of a number of specific single-current theories [32–34], including the more familiar "high-field Mott–Cabrera theory" [30, 35, 36] and it has been successful in providing insight into several criteria which must be met for the various single-current theories to yield reasonably accurate kinetics in certain limiting film-thickness regions of oxide growth [37–41].

1.14.2 Anodic oxidation under constant voltage conditions

The case of anodic oxidation is almost the antithesis of the case discussed in Sect. 1.13 for which growth of the oxide was presumed to be due predominantly to the diffusion of uncharged atoms or molecules. In anodic oxidation, it is the electric field, without question, which plays the dominant role with the concentration gradient producing secondary, albeit important, effects.

Although most treatments of anodic oxidation begin directly with some limiting form of the very-high-field hopping equation [see eqns. (90) and (91)], this is an entirely unnecessary restriction which can prove to be a poor approximation to the true state of affairs in some cases. In all cases, it limits the developments to the early region of growth before the thickness begins to level off at an asymptotic value consistent with the applied voltage.

The effects of space charge will be discussed briefly. Good developments of this topic are rather scarce.

The basic starting point for consideration of the particle current over each barrier in anodic oxides is eqn. (103). This general form for barriers of various height (see Fig. 3 in an earlier review [25]) is usually approximated by eqn. (105), which is the form resulting when the energy barriers in zero field are of a uniform height. This expression, though not actually an integrated form for the current, is an excellent one to use if one is carrying out numerical calculations with a microcomputer. It must, however, be supplemented with the discrete form of Poisson's equation [eqn. (37)] in order to include the space-charge variation of the electric field with position within the oxide. Because concentration gradient effects are already built into the expression, the analysis is exact once realistic boundary conditions have been imposed on the area defect densities of the mobile species at the oxide film interfaces. Such numerical calculations have been carried out and presented in the literature [25, 42]. Significant effects on the kinetics were noted to be introduced by the concentration gradient and the space-charge contribution to the electric field. In particular, the concentration profiles for the mobile species are modified greatly and the currents (and thus growth rates) can be retarded significantly by the space charge. The concentration gradient was noted to produce a limited amount of growth in the absence of an applied voltage and, even in cases of small opposing voltage, some growth was produced by the concentration gradient. The behavior of the system in the low-voltage domain is quite interesting due to the competing effects of the electric field and the concentration gradient. The reader is referred to the literature [25, 42] for more details.

In the higher voltage domain, the concentration-gradient effects are less pronounced due to the large effect of the electric field. In this case, the very-high-field forms of the hopping transport equation can be used with

impunity [see eqns. (90) and (91)]. The concentration of the diffusing species still varies strongly with position within the anodic oxide because of the space-charge variation of the electric field given by Poisson's equation. Numerical calculations have been carried out in this domain using the integrated form of these equations [see refs. 25 and 43]. The concentration profiles in the very-high-field limit are profoundly altered from the homogeneous-field case by the space charge and the particle currents and attendant growth rates are severely retarded by the effects of the space charge. The space-charge retardation of the growth rate under constant voltage conditions follows qualitatively the behavior which is predicted by the simple model developed by physical insight in Sect. 1.12. Although quantitative results can also be deduced by means of the oversimplified model, it is better to refer to the exact calculations [43] based on more realistic space-charge distributions whenever quantitative information is required.

1.14.3 Anodic oxidation under constant current conditions

If the particle current driven through the anodic oxide is fixed by the external circuitry, then the voltage developed across the oxide will change as the oxide film increases in thickness. This can be most easily understood by referring to various limiting cases, such as the very-high-field current expressions [eqns. (90) and (91)]. It can be noted from eqn. (90), for example, that a fixed current requires a fixed value of the surface-charge field $E(0)$, independent of the oxide film thickness $L(t)$. However, the simple model developed in Sect. 1.12 shows that in such a situation the magnitude of the potential will increase markedly with the oxide thickness. The increase in voltage can be attributed to the two aspects of the electric field, namely, the surface-charge contribution, $-E(0)L$, and the space-charge contribution. By following the signs of the contributions carefully, one can deduce that with space charge the voltage increases even more rapidly than in the homogeneous-field case whenever the space charge has the same sign as the sign of the charge of the mobile species. This is certainly the case whenever the space charge is due to the mobile carriers themselves. However, to obtain the exact functional form of the increase is not so straightforward as in the case of the oversimplified model developed in Sect. 1.12. Therefore, numerical calculations have been carried out for the more realistic case in both the low-field domain [42] and in the very-high-field [43] domain. The results for constant current growth show good qualitative agreement with the predictions of the easy insight model developed in Sect. 1.12. The interested reader is referred to the literature [25, 42, 43] for more details.

1.15 COUPLED-CURRENTS APPROACH TO THERMAL OXIDATION

If we inquire as to the differences between thermal and anodic oxidation, we can list some which are a matter of degree and others which are

a matter of basic phenomena. For example, the electric fields can, in principle, be made arbitrarily large in anodic oxidation because we impose external voltages across the growing oxide by means of batteries or power supplies, external circuitry, electrodes, and ionic conducting solutions. Although the higher fields may necessitate using a transport equation which includes the effects of very-high-field thermally activated hopping [see eqn. (105)] and in addition may bring about in a practical sense the production of very thick oxides, nevertheless this is more or less merely a matter of degree. On the other hand, the fact that no such external circuitry to provide a charge path exists in the case of ordinary thermal oxidation means that some electronic species must be simultaneously transported through the growing oxide in order for ionic transport to continue, and this is a matter of basic phenomenon. The theory of thermal oxidation is thus vastly more complicated in principle than the theory of anodic oxidation. In essence, the difference in the theory is that for anodic oxidation we specify at the outset whether the external circuit requires the oxide to grow under constant voltage, constant current, or some similarly prescribed condition. This in turn serves as a type of boundary condition, or compatibility relation, which must be satisfied by the oxide-producing ionic current and the attendant electric fields. Thus the simultaneous difference equations for hopping of the mobile charged species over the sequence of energy barriers must be solved simultaneously, subject to the constraint imposed by the external circuitry.

On the other hand, neither the voltage nor the currents of the ionic and electronic species are specified at the outset in the problem of thermal oxidation. These quantities are obtained as a consequence of solving the system of transport equations and a fundamental electric-field relation in a self-consistent manner. There is an individual tendency for each ionic species and each electronic species to attain a state of equilibrium with respect to flow across the asymmetrical system comprised of metal—oxide—oxygen. Any electric field created by charge flow of any one of the r charged species immediately exerts a force on all of the other charged species, so the currents of the various mobile charged species become coupled through the electric field. The complete set of non-steady-state equations [19] describing the motion of the charged species and the electric fields so created were at one time programmed for numerical computation [44] and actual calculations were carried out. The results indicated that, under ordinary conditions, the electric field is very rapidly adjusted by charge flow to a value which, at any given oxide thickness, is just sufficient to produce a net charge current which is nearly zero. This supplies a fundamental basis for the "coupled-currents" approach to thermal oxidation theory [10, 11]. For the case of growth by only two charged species, which must then, of necessity, be one ionic species and one electronic species, the requirement of a net zero charge transport can be attained in general only if the magnitudes of the charge currents of

the two oppositely charged species are essentially equal to one another as the oxide film steadily increases in thickness. The voltage at each given thickness must therefore be consistent with this requirement as well as with the requirements imposed by Poisson's equation. The electrostatic potential so calculated, which is sometimes referred to [22] as the "kinetic potential" to emphasize its role in equalizing the charge current magnitudes, actually represents a dynamic "built-in" voltage across the growing oxide. This contrasts sharply with the case of anodic oxide growth, which occurs under some arbitrary, but nevertheless specified, program of voltage and/or current determined by the external circuitry.

We can think of the coupled-currents approach to metal oxidation in terms of the following logical sequence.

(a) If electrons move through the oxide more easily than ions, they will establish an electric field which will retard further electron transport but which will aid ion transport.

(b) If ions move through the oxide more easily than electrons, they will establish an electric field which will retard further ion transport but which will aid electron transport.

(c) In either of the above two cases, the electric field which is established will have the polarity to retard transport of the more mobile species and enhance transport of the less mobile species.

(d) The field increases in magnitude until the charge current of the less mobile species reaches the same magnitude as the charge current of the more mobile species.

(e) Because the currents are also of opposite sign, the net charge current will then be zero.

(f) A net charge current that is zero leads to no net charge transport, which in turn means than the electric field is not changing. This stationary electric field which balances the net charge current to zero is the field which exists in the oxide layer during oxide growth. Mathematically it is determined from the coupled-currents condition [45]

$$\sum_{s=1}^{r} Z_s e J_s = 0 \tag{172}$$

(g) The corresponding electrostatic potential within the oxide layer can be obtained from an integration of the electric field within the oxide.

(h) The oxide growth rate, dL/dt, at thickness L is obtained by substituting the electric field derived from the coupled-currents condition into the ionic current J_i

$$\frac{dL}{dt} = RJ_i \tag{173}$$

where R is the volume of new oxide formed for each ion which is transported through the oxide layer. If more than one ionic species is mobile,

the total growth rate is given by the sum of the individual growth rates $R_i J_i$.

(i) The various coupled-currents models for oxide film growth differ from one another by specific choices for the ionic current relation and the electronic current relation. The coupled-currents condition is, in all cases, imposed to find the electric field versus oxide film thickness and this electric field is then used to obtain the ionic current as a function of oxide film thickness. An integration of the growth rate expression involving this ionic current then gives the oxide film thickness, $L(t)$, versus time, t.

(j) Simultaneously, the voltage across the oxide (designated the kinetic potential) can be obtained by evaluating the electrostatic potential (as obtained above) at the position $x = L(t)$.

(k) The techniques required to carry out the above "coupled-currents prescription" can be either analytical or numerical, depending upon personal preference and the complexity of the relations chosen for the particle currents.

(l) All ionic current expressions needed for the various "coupled-currents models" can be derived from the fundamental hopping transport difference equations. Limiting cases follow from assuming very large and very small space-charge concentrations.

(m) Other simplifications in the hopping-current transport equations follow if one can assume the very-high-field limit, the linear diffusion current limit, or the zero-field limit.

(n) The possible electronic current relations include the various hopping current transport equations mentioned above and, in addition, include electron tunneling as well as the various types of thermal electron emission.

(o) The various oxide thickness domains prove to be quite important, since transitions between various rate-limiting mechanisms occur during growth, even in the limit where growth occurs throughout in accordance with a given coupled-currents model [10].

As one example of a coupled-currents theory, the growth of very thick oxide films under local space-charge neutrality conditions will be considered in detail in the following section.

1.16 THE THICK-FILM PARABOLIC GROWTH LAW

Consider the limit of thick oxides and moderate values of the electric field where both ion transport and electron transport take place in accordance with the linear diffusion equation [see eqn. (96)]. In essence, this means that we are assuming that the inequality

$$|ZeEa/k_B T| \lesssim 1/2 \tag{174}$$

holds, which can be interpreted to mean that the energy the charged defect will receive from the electric field in moving a distance equal to that between adjacent potential energy minima will be smaller than the

thermal energy $k_B T$; [see eqn. (19)]. For the present development, we restrict our consideration to cases involving a single ionic current and a single electronic current. The particle defect currents can then be expressed as

$$J_1 = -D_1 \frac{dC_1}{dx} + \mu_1 E C_1 \qquad \text{(ions)} \tag{175}$$

and

$$J_2 = -D_2 \frac{dC_2}{dx} + \mu_2 E C_2 \qquad \text{(electrons)} \tag{176}$$

The coupled-currents condition [eqn. (172)] for this case can be written as

$$Z_1 e J_1 + Z_2 e J_2 = 0 \tag{177}$$

Substituting the ionic current (species 1) and the electronic current (species 2) given by eqn. (96) into the coupled-currents condition gives the relation

$$-Z_1 e D_1 \frac{dC_1}{dx} + Z_1 e \mu_1 E C_1 - Z_2 e D_2 \frac{dC_2}{dx} + Z_2 e \mu_2 E C_2 = 0 \tag{178}$$

and so

$$E = \frac{Z_1 e D_1 (dC_1/dx) + Z_2 e D_2 (dC_2/dx)}{Z_1 e \mu_1 C_1 + Z_2 e \mu_2 C_2} \tag{179}$$

If local space-charge neutrality can be assumed, which has been justified by extensive numerical calculations [46] for the present case, then we can write

$$Z_1 e C_1 + Z_2 e C_2 = 0 \tag{180}$$

It should be emphasized that the local space-charge neutrality assumption [28, 29] employed here restricts our development to the case of very thick oxide layers (e.g. $L \gtrsim 10{,}000$ Å, but this value depends greatly upon the actual values of the mobile charged defect densities at the oxide film interfaces). If the oxide layer is thin enough, there will be very little space charge, so the alternate assumption of a uniform electric field throughout the oxide film will be a far more realistic approximation. This latter has been designated [31, 47] the "homogeneous-field approximation", and it leads to the "thin-film parabolic growth law" in the case of ionic and electronic diffusion which are in accord with eqn. (96) given above. The thin-film parabolic growth law [31, 48] is quite different, both fundamentally and in predicted values for the rate coefficient, from the so-called *thick-film parabolic growth law* [28, 29] developed in the present section on the basis of the assumption of local space-charge neutrality. In

the transition thickness region between very thin and very thick oxides, very large deviations from local space-charge neutrality are encountered [24, 49], which, in turn, lead to large deviations from kinetics obeying either parabolic growth law.

Equation (180) for local space-charge neutrality requires that the oppositely charged mobile defect species concentrations have a very special relationship. Solving for C_2 gives

$$C_2 = -(Z_1 e/Z_2 e)C_1 = -(Z_1/Z_2)C_1 \tag{181}$$

Substituting this relation into eqn. (179) for the electric field gives

$$\begin{aligned} E &= \frac{Z_1 D_1 (\mathrm{d}C_1/\mathrm{d}x) + Z_2 D_2 (-Z_1/Z_2)(\mathrm{d}C_1/\mathrm{d}x)}{Z_1 \mu_1 C_1 + Z_2 \mu_2 (-Z_1/Z_2) C_1} \\ &= \frac{Z_1 (\mathrm{d}C_1/\mathrm{d}x)(D_1 - D_2)}{Z_1 C_1 (\mu_1 - \mu_2)} \\ &= [(D_1 - D_2)/(\mu_1 - \mu_2)]\,(1/C_1)\,(\mathrm{d}C_1/\mathrm{d}x) \end{aligned} \tag{182}$$

Note from this expression that, in general, $E \neq 0$, even though we have assumed local space-charge neutrality. In addition, this expression indicates that E can vary with position x. These results do, indeed, require some departure from a strict local space-charge neutrality condition. That is, the development is not rigorously internally self-consistent. Exact numerical solutions show, however, that space-charge modifications in the electric field produced by only slight deviations from local space-charge neutrality are entirely sufficient to give the local electric-field values and the attendant position-dependence of the electric field predicted by eqn. (182). Thus our present approach is quite legitimate. Substituting eqn. (182) for the electric field into eqn. (175) for the ionic particle current gives

$$\begin{aligned} J_1 &= -D_1 \mathrm{d}C_1/\mathrm{d}x + \mu_1 C_1 [(D_1 - D_2)/(\mu_1 - \mu_2)](1/C_1)\mathrm{d}C_1/\mathrm{d}x \\ &= (\mathrm{d}C_1/\mathrm{d}x)\,[-D_1(\mu_1 - \mu_2) + \mu_1(D_1 - D_2)]/(\mu_1 - \mu_2) \\ &= [(D_1\mu_2 - \mu_1 D_2)/(\mu_1 - \mu_2)]\,\mathrm{d}C_1/\mathrm{d}x \\ &= -\beta \mathrm{d}C_1/\mathrm{d}x \end{aligned} \tag{183}$$

where

$$\beta = \frac{\mu_1 D_2 - \mu_2 D_1}{\mu_1 - \mu_2} \tag{184}$$

Note the similarity of the result given by eqn. (183) to the expression for uncharged particle transport

$$J = -D \frac{\mathrm{d}C}{\mathrm{d}x} \tag{185}$$

as given by eqn. (109) in Sect. 1.11. However, in the presently considered special case of local space-charge neutrality, the effective diffusion coefficient is β, which is an *ambipolar diffusion coefficient* [28] with a value which is dependent upon the values of the diffusion coefficients (and corresponding mobilities) for both the ionic and the electronic species.

Since local space-charge neutrality does not hold at the oxide interfaces, the above expression for the current is restricted to the interior zone [28] where local space charge neutrality has been found [46] to be a good approximation. This is illustrated for the case of cation vacancy (or anion interstitial) and electron-hole diffusion by Fig. 17. Thus, the domain of validity is not $0 \leqslant x \leqslant L$ but instead is $\delta^* \leqslant x \leqslant L^*$, where δ^* indicates that edge of the local space-charge-neutral zone nearer to the metal interface and L^* indicates that edge of the local space-charge-neutral zone nearer to the oxygen interface. The region $0 \leqslant x \leqslant \delta^*$ has been designated zone 1 [28]. The local space-charge-neutrality zone extending from δ^* to L^* has been designated zone 2. The region $L^* \leqslant x \leqslant L$ has been designated zone 3. Thus zones 1 and 3 do not satisfy the condition of local space-charge neutrality, but zone 2 does. The ionic current expression given by eqn. (183) is, of course, restricted to zone 2. Integrating that relation from δ^* to position x within zone 2, assuming the steady-state condition of a current independent of position within the oxide, gives

$$J_1 (x - \delta^*) = -\beta[C_1(x) - C_1(\delta^*)] \tag{186}$$

Evaluation of this result at $x = L^*$ gives

$$J_1 (L^* - \delta^*) = -\beta[C_1(L^*) - C_1(\delta^*)] \tag{187}$$

or, equivalently

$$J_1 = \frac{\beta[C_1(\delta^*) - C_1(L^*)]}{(L^* - \delta^*)} \tag{188}$$

To evaluate $C_1(\delta^*)$ and $C_1(L^*)$, we introduce what has been designated [28, 29] the *interfacial zone equilibrium approximation: the concentration profiles of all charged defect species within the two interfacial regions* $(0 \leqslant x \leqslant \delta^*)$ *and* $(L^* \leqslant x \leqslant L)$ *adjoining the interior zone* $(\delta^* \leqslant x \leqslant L^*)$ *of local space-charge neutrality can be approximated by their thermal equilibrium counterparts.* One condition required for this approximation to be valid is that the space-charge-neutral zone $(\delta^* \leqslant x \leqslant L^*)$ be sufficiently thick so that transport through this central zone will be the rate-limiting factor for oxide film growth. In this limit, $L^* - \delta^* \simeq L$.

An important consequence of the zone equilibrium approximation is that the quantities $C_1(\delta^*)$ and $C_1(L^*)$ appearing in the above expressions can be viewed as constants independent of oxide film thickness L. In this limit

$$\frac{dL}{dt} = R_1 J_1 \simeq \frac{R_1 \beta[C_1(\delta^*) - C_1(L^*)]}{L} = \frac{\mathscr{D}_\Omega}{L} \tag{189}$$

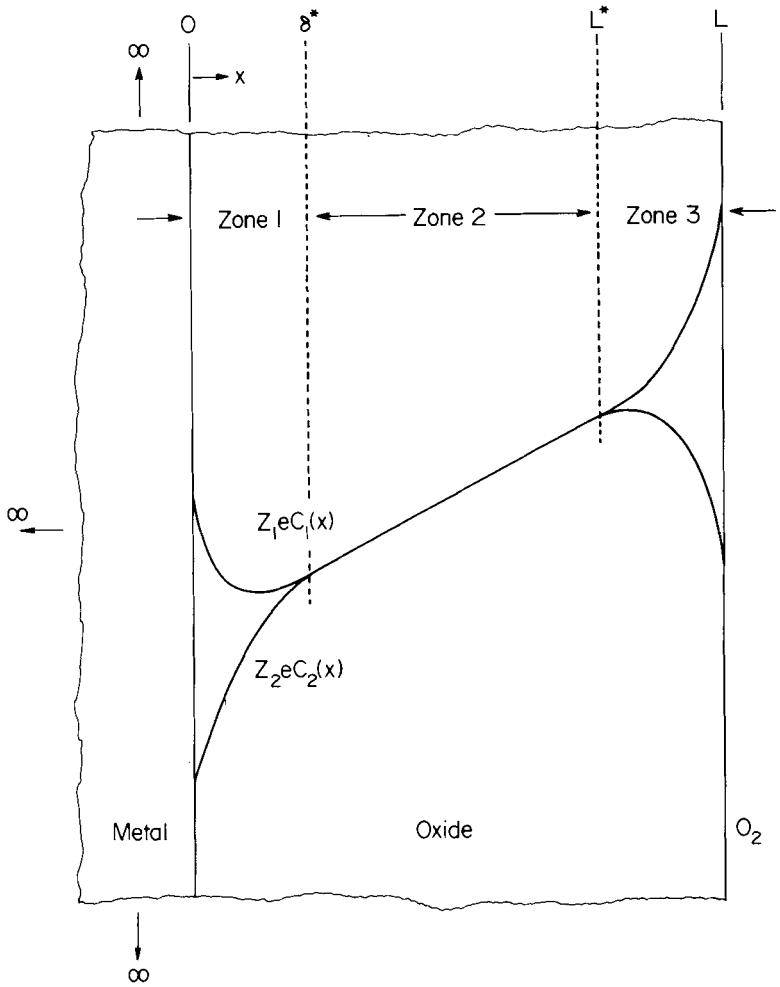

Fig. 17. Schematic diagram of monovalent cation vacancy (or monovalent anion interstitial) and electron hole profiles for thick-film oxide growth by diffusion of these two oppositely charged diffusing species. Note the locally non-space-charge neutral interfacial regions (zones 1 and 3) adjoining the parent metal and the gaseous oxygen, respectively, and the central region (zone 2) where local space-charge neutrality is a good approximation.

where

$$\mathscr{D}_{\Omega} = R_1 [(\mu_1 D_2 - \mu_2 D_1)/(\mu_1 - \mu_2)] \; [C_1(\delta^*) - C_1(L^*)] \qquad (190)$$

Therefore, we obtain from the integration of eqn. (188) the *thick-film parabolic growth law*

$$L(t)^2 - L(0)^2 = 2\mathscr{D}_{\Omega} t \qquad (191)$$

To evaluate the rate coefficient $\mathscr{D}_\Omega$ in terms of the interfacial defect concentrations, it is thus necessary to evaluate $C_1(\delta^*)$ and $C_1(L^*)$, utilizing one aspect of the interfacial zone equilibrium approximation. At thermal equilibrium

$$C(x) = C(0)\exp[-U(x)/k_B T] \tag{192}$$

where $U(x)$ is the energy as a function of position x, and $U(0) = 0$. In our case, the energy is due to the electrostatic potential

$$U(x) = ZeV(x) \tag{193}$$

where Ze is the charge per particle of the species in question. Quite generally, if one considers two points x and x' in a region where the concentration profile of a species labeled s has an equilibrium behaviour, then the defect densities of species s at the two points x and x' are related exponentially to the difference in defect energies at the two points, namely

$$C_s(x) = C_s(x')\exp\{-[U_s(x) - U_s(x')]/k_B T\} \tag{194}$$

Substituting $U_s = Z_s eV$ gives

$$C_s(x) = C_s(x')\exp\{-Z_s e[V(x) - V(x')]/k_B T\} \tag{195}$$

In order to apply this expression to zone 1, let $x = \delta^*$ and $x' = 0$. Conventionally, $V(0) = 0$ so that we obtain

$$C_s(\delta^*) = C_s(0)\exp[-Z_s eV(\delta^*)/k_B T] \tag{196}$$

To apply eqn. (195) to zone 3, let $x = L^*$ and $x' = L$, so that we obtain

$$C_s(L^*) = C_s(L)\exp\{-Z_s e[V(L^*) - V(L)]/k_B T\} \tag{197}$$

These values for $C_s(\delta^*)$ and $C_s(L^*)$ are likewise appropriate at the respective edges of zone 2, since defect concentrations are continuous functions of position within the oxide layer. The subscript s can have the value 1 or 2 in the above relations, corresponding respectively to the ionic or electronic species concentrations. Substituting eqn. (196) for $C_s(\delta^*)$ into the local space-charge neutrality relation [eqn. (180)] gives

$$Z_1 eC_1(0)\exp[-Z_1 eV(\delta^*)/k_B T] + Z_2 eC_2(0)\exp[-Z_2 eV(\delta^*)/k_B T] = 0 \tag{198}$$

Equivalently

$$Z_2 eC_2(0)\exp[(Z_1 - Z_2)eV(\delta^*)/k_B T] = -Z_1 eC_1(0) \tag{199}$$

so that

$$V(\delta^*) = [k_B T/(Z_1 e - Z_2 e)]\ln[-Z_1 eC_1(0)/Z_2 eC_2(0)] \tag{200}$$

This is a major result, representing as it does the *potential difference across zone 1.* This result in turn leads to

$$\exp[-Z_s eV(\delta^*)/k_B T] = \exp\{-[Z_s/(Z_1 - Z_2)]\ln[-Z_1 C_1(0)/Z_2 C_2(0)]\} \tag{201}$$

which, when substituted into eqn. (196) for $C_s(\delta^*)$, gives

$$C_s(\delta^*) = C_s(0)\,[-Z_1C_1(0)/Z_2C_2(0)]^{-Z_s/(Z_1-Z_2)} \qquad (s = 1, 2) \tag{202}$$

This provides the important evaluation of $C_1(\delta^*)$ and $C_2(\delta^*)$ needed for the rate coefficient $\mathscr{D}_\Omega$.

Next we substitute eqn. (197) into the local space-charge neutrality relation [eqn. (180)] to obtain

$$Z_1eC_1(L)\exp\{-Z_1e[V(L^*)-V(L)]/k_BT\} + Z_2eC_2(L)\exp\{-Z_2e[V(L^*)-V(L)]/k_BT\} = 0 \tag{203}$$

The important quantity $[V(L)-V(L^*)]$ constitutes the *potential difference across zone 3.* By rewriting this result in the form

$$Z_2eC_2(L)\exp\{-(Z_1-Z_2)e[V(L)-V(L^*)]/k_BT\} = -Z_1eC_1(L) \tag{204}$$

we can readily solve for this potential difference. It is noted to be given by

$$V(L)-V(L^*) = [-k_BT/(Z_1e-Z_2e)]\ln[-Z_1eC_1(L)/Z_2eC_2(L)] \tag{205}$$

This potential difference across zone 3 enables us to evaluate the boundary concentrations $C_s(L^*)$ for the two species by means of eqn. (197). This gives

$$C_s(L^*) = C_s(L)[-Z_1C_1(L)/Z_2C_2(L)]^{-Z_s/(Z_1-Z_2)} \qquad (s = 1, 2) \tag{206}$$

Thus we obtain the important evaluation of $C_1(L^*)$ and $C_2(L^*)$.

Next, we substitute the expressions given by eqns. (202) and (206) into eqn. (190) for the thick-film parabolic rate constant to obtain

$$\mathscr{D}_\Omega = R_1[(\mu_1D_2-\mu_2D_1)/(\mu_1-\mu_2)] \times \{C_1(0)\,[-Z_1C_1(0)/Z_2C_2(0)]^{-Z_1/(Z_1-Z_2)} - C_1(L)\,[-Z_1C_1(L)/Z_2C_2(L)]^{-Z_1/(Z_1-Z_2)}\} \tag{207}$$

This result can be compared to the rate coefficient

$$\mathscr{D}_0 = R_1D_1[C_1(0)-C_1(L)] \tag{208}$$

for oxide growth by ionic diffusion in zero field [cf. eqn. (160)].

Next, let us examine the total "built-in" voltage developed across the oxide. Formally, we can write the total potential across the oxide as the sum of the potentials developed across the three zones

$$V(L) = V(\delta^*) + [V(L^*)-V(\delta^*)] + [V(L)-V(L^*)] \tag{209}$$

The potentials $V(\delta^*)$ and $[V(L) - V(L^*)]$ have already been evaluated [eqns. (200) and (205)], so it is now only necessary to evaluate the potential $[V(L^*) - V(\delta^*)]$ across zone 2. Substituting the electric field expression given by eqn. (182) into the general expression given by eqn. (18) for the electrostatic potential gives

$$\begin{aligned} V(x) - V(\delta^*) &= -\int_{\delta^*}^{x} E(x)\mathrm{d}x \\ &= -[(D_1 - D_2)/(\mu_1 - \mu_2)] \int_{\delta^*}^{x} (1/C_1)\,(\mathrm{d}C_1/\mathrm{d}x)\mathrm{d}x \\ &= -[(D_1 - D_2)/(\mu_1 - \mu_2)] \int_{C_1(\delta^*)}^{C_1(x)} (1/C_1)\mathrm{d}C_1 \\ &= -[(D_1 - D_2)/(\mu_1 - \mu_2)] \ln[C_1(x)/C_1(\delta^*)] \end{aligned} \quad (210)$$

Evaluating this result at $x = L^*$ gives

$$V(L^*) - V(\delta^*) = -[(D_1 - D_2)/(\mu_1 - \mu_2)] \ln[C_1(L^*)/C_1(\delta^*)] \quad (211)$$

But we have evaluations of $C_1(\delta^*)$ and $C_1(L^*)$ in terms of the interfacial densities. Thus, substituting eqns. (202) and (206) into eqn. (211) gives us, after some algebraic rearrangement, the final expression for the potential difference across zone 2, viz.

$$\begin{aligned} V(L^*) - V(\delta^*) = &-[(D_1 - D_2)/(\mu_1 - \mu_2)] \\ &\times \{[Z_2/(Z_1 - Z_2)] \ln[C_1(0)/C_1(L)] \\ &- [Z_1/(Z_1 - Z_2)] \ln[C_2(0)/C_2(L)]\} \end{aligned} \quad (212)$$

This result can be noted to depend upon the mobilities of both species and the boundary concentrations of these species at the interfaces of the oxide film. In contrast, the potential differences across zones 1 and 3 do not involve the mobilities, which is in accordance with the interfacial zone equilibrium approximation.

This completes our development of the thick-film parabolic growth law. This particular theory has been presented in some detail because it is an extremely important domain of metal oxidation. In addition, it provides an excellent example of the way the coupled-currents approach [10, 11] can be used to obtain oxide growth kinetics and built-in voltages in thermal oxidation.

2. Multilayer oxides

2.1. BACKGROUND

Section 1 of this review represented a detailed consideration of the various theoretical aspects of single-layer oxide growth. It is now our

intention to consider the additional features of the theory when the oxide forms simultaneously in two or more layers. It is well known that copper oxide can be found in two forms [50], namely octagonal cubic red cuprous oxide, Cu_2O, and tetragonal cubic black hygroscopic cupric oxide, CuO, and evidence has been presented [51] for still other stoichiometries. Iron oxide can be found in three forms, namely black ferrous oxide, FeO, known as wüstite, the cubic black iron oxide, Fe_3O_4, known as magnetite, and the hexagonal reddish-black hexagonal ferric oxide, Fe_2O_3, known as hematite [50]. Cobalt oxide can be found in the form of the greenish-brown cubic cobaltous oxide, CoO, the black cubic oxide Co_3O_4, and the blackish-gray cobaltic oxide, Co_2O_3. Many other metals, such as chromium, also form a series of oxides [50].

Let us consider any given oxide in symbolic form Me_pO_q, where Me represents the metal species, O the oxygen species, p the number of metal atoms in a molecule of the oxide, and q the number of oxygen atoms in a molecule of the oxide. When two or more stoichiometric forms of the oxide can be found, as in the cases mentioned, it is useful to index the forms with the subscript i, such that the molecule $Me_{p_i}O_{q_i}$ consists of p_i metal atoms and q_i oxygen atoms. Thus for wüstite, $p_i = 1$ and $q_i = 1$, whereas for magnetite, $p_i = 3$ and $q_i = 4$. The ratio p_i/q_i can be expected to be greater for an oxide formed under metal-rich oxygen-deficit conditions than it would be for an oxide formed under metal-deficit and oxygen-rich conditions. In the case of a parent metal surface overlaid with a protective growing oxide film, the ambient conditions at the metal—oxide interface favor the formation of a metal-rich oxygen-deficit oxide whereas the ambient conditions at the oxide—oxygen interface favor the formation of an oxygen-rich metal-deficit oxide [52]. In accordance with these expectations, experimental measurements [52] have shown in a number of cases that oxide overlayers of different stoichiometries exist simultaneously during growth of the oxide. For example, cobalt [53], iron [54], and copper [55] have been found to form multilayer oxides [56, 57]. Also, the solution of oxygen into the parent metal substrate in zircaloy-4 leads to an alpha phase metal layer having different physical properties which is sandwiched between the outer protective oxide and the inner bulk beta phase of the metal [58, 59]. Our development [60] of the theory of multilayer oxide growth holds for any arbitrary number of layers. We thus represent the number of such layers in a multilayer oxide by the integer N. Figure 18 illustrates the layered oxides and the notation employed. The oxide layer thicknesses are labeled $L_1, L_2, \ldots, L_N$, starting with the innermost layer (layer 1) adjacent to the parent metal and continuing to the outermost layer (layer N) in contact with the oxygen (or similar reactive anion species). The treatment of multilayer oxide formation becomes especially simple in the case of duplex oxide layers [61, 62], namely for $N = 2$. Note from Fig. 18 that position x in the oxide (having total thickness L) is measured from the parent metal

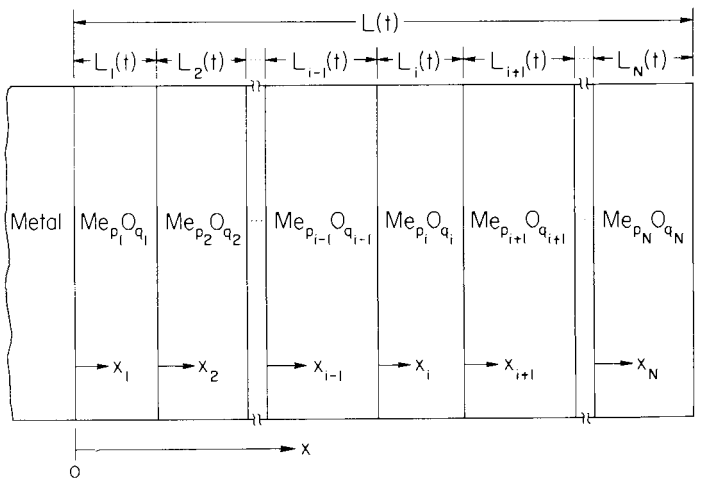

Fig. 18. Multilayered oxides of different stoichiometry growing on a parent metal.

surface. The quantity x_i represents the position in oxide layer i (having thickness L_i) as measured from the phase boundary separating layers $i-1$ and i.

It is interesting to note that the coordinate system utilized throughout this work (and also throughout the majority of the literature on metal oxidation [10]) is not strictly stationary relative to a laboratory coordinate system. The origin $x = 0$ is always chosen to be at the phase boundary separating the parent metal from the first oxide layer and this phase boundary moves (relative to the center of mass of the parent metal) as layers of the parent metal are consumed in the metal oxidation reaction. Similarly, $x_i = 0$ always occurs at the phase boundary separating layer $i-1$ from layer i.

Our development subdivides into four parts, corresponding, respectively, to growth due to cation interstitial (ci) and electron motion, cation vacancy (cv) and electron-hole motion, anion interstitial (ai) and electron-hole motion, or lastly, anion vacancy (av) and electron motion. The symbols (ci), (cv), (ai), and (av) are utilized as superscripts to distinguish the various parameters in the theory. The symbol e^- is used to designate electrons as a defect species in the oxide, each particle of such defect species having the charge $-e$, where $e = |e|$. The symbol h^+ is used to designate electron holes as a defect species in the oxide, each particle of such defect species having the charge e.

Each of the four cases delineated [(ci), (cv), (ai), and (av)] is developed individually in such a way that it is self-contained. Each theoretical development is preceded by a formulation of the relevant equations for the defect solid-state reactions [63, 64] occurring at the phase boundaries separating the oxides. That is, balanced chemical equations involving

reactants and products are formed, including both ionic and electronic defect species. Finally, the kinetic equations developed in some detail are cast into a compact matrix form and a tabular comparison of the results for the various cases is made.

2.2 THE CASE OF OXIDE GROWTH BY DIFFUSION OF CATION INTERSTITIALS AND ELECTRONS

Cation interstitials and electrons can enter oxide layer 1 at the metal interface (see Fig. 18). The cation interstitials and electrons then migrate through layers $1, 2, \ldots, i-1, i, i+1, \ldots, N$ towards the oxygen interface, being consumed bit by bit in the chemical reactions at the phase boundaries. The transport of cation interstitials takes place through layer i by means of the cation interstitial particle current $J_i^{\{ci)}$ produced by the gradient of cation interstitials in layer i and the electric field $E(x_i)$ in layer i (see Fig. 19). The gradient exists because the cation interstitial concentrations near the interfaces ($x_i = 0$ and $x_i = L_i$) of layer i are different, being determined by the different conditions at the two interfaces. That is, the conditions at $x_i = 0$ involve contact between layers $i-1$ and i, whereas the conditions at $x_i = L_i$ involve contact between layers i and $i+1$. Those cation interstitials moving through layer i will be available for chemical reaction with the oxygen-richer layer $i+1$ to form more oxide of layer i (see Fig. 19). Thus, at $x_i = L_i$, we have the balanced chemical reaction

$$n_i \, \mathrm{Me}^{Z_i} + n_i Z_i \, \mathrm{e}^- + q_i \, \mathrm{Me}_{p_{i+1}} \mathrm{O}_{q_{i+1}} \longleftarrow\!\!\!\!\!\!\rightarrow q_{i+1} \, \mathrm{Me}_{p_i} \mathrm{O}_{q_i}$$
$$(i = 1, 2, 3, \ldots, N-1) \tag{213}$$

where

$$n_i = p_i q_{i+1} - p_{i+1} q_i \tag{214}$$

That is, n_i cations of Me, each of charge $Z_i e$, react with $n_i Z_i$ electrons e^- and q_i molecules of layer $i+1$ to form q_{i+1} new molecules for increasing the thickness of layer i. Thus a cation interstitial current through layer i can lead to decomposition of layer $i+1$, with the attendant growth of layer i. Layer i therefore grows at the expense of layer $i+1$.

The electrons required for the reaction given by eqn. (213) must be provided by an electron current through layer i. In addition, this electron current must be sufficient for the corresponding reactions to take place in layers $i+1, i+2, \ldots$. Since a charge equivalent number, relative to the charge transported by the mobile reacting cation interstitials, is required for each of these reactions, the imposition of the coupled-currents condition [45] which is employed to deduce the rate constant for single-phase growth assures the correct electron current through layer i. In this way, an amount of electronic charge equivalent to the cation interstitial charge current continuously utilized for the growth of layers $i, i+1, \ldots, N$ is assured.

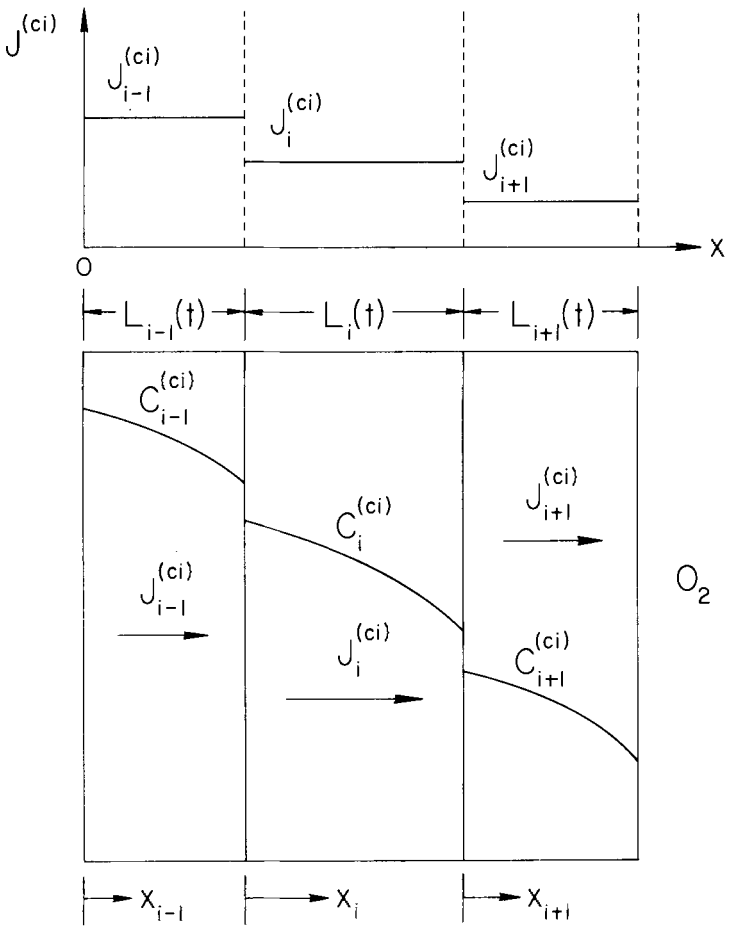

Fig. 19. One of the interior oxide layers labeled i in a sandwich array of multilayered oxides growing by cation interstitial (ci) diffusion illustrated with the relative magnitudes of the positively directed particle currents through layer i and the adjacent layers $i-1$ and $i+1$.

If the volume of one molecule of $Me_{p_i}O_{q_i}$ is denoted by R_i, then the amount of oxide $R_i^{(ci)}$ which can be formed by one cation interstitial is R_i/p_i, namely

$$R_i^{(ci)} = R_i/p_i \qquad (i = 1, 2, 3, \ldots, N) \tag{215}$$

In all cases, R represents oxide volume, with superscript denoting the species and subscript denoting the layer. Figure 19 indicates the cation interstitial currents through the layers. Because all cation interstitials originate at the metal interface, the cation interstitial currents decrease from layer to layer, as noted in Fig. 19. The difference current $J_i^{(ci)} - J_{i+1}^{(ci)}$, for example, serves to increase the thickness of layer i.

This gives one contribution to the growth kinetics of layer i (with $i = 1, 2, 3, \ldots, N-1$), namely, $R_i^{(ci)}\ (J_i^{(ci)} - J_{i+1}^{(ci)})$. If gaseous oxygen were readily available at the interfaces of layer i, then this would usually represent the only contribution to the growth kinetics of layer i. However, our intent is to develop the growth kinetics for a multilayer oxide, assuming the various layers i to be impermeable to oxygen. In this case, the basic principle which holds is that all layers not in direct contact with gaseous oxygen can grow only by decomposition of the adjoining oxygen-richer layer. First, let us consider the growth of any *interior* layer L_i ($i \neq 1$, $i \neq N$). Because the layers are successively more oxygen-rich as one proceeds in the order $1, 2, \ldots, i-1, i, i+1, \ldots, N$ from metal to oxygen, layer i can grow only if a portion of layer $i+1$ simultaneously decomposes by solid-state reaction to provide the necessary oxygen, in accordance with the solid-state defect reaction equation given by (213). However, in providing the necessary oxygen to react with the difference current $J_i^{(ci)} - J_{i+1}^{(ci)}$ at $x_i = L_i$, the cations simultaneously freed by the decomposition of layer $i+1$ become immediately available for growth of layer i. This leads to an additional equivalent cation current for growth of layer i given by

$$J_i^{(Met)} = (1/R_{i+1}^{(ci)})\,(dL_{i+1}/dt)_- \qquad (i = 1, 2, 3, \ldots, N-1) \tag{216}$$

where subscript "minus" denotes decomposition rate as opposed to growth rate. The superscript (Met) denotes that the equivalent current is due to ions of the *metal* species. Similarly, the superscript (Oxy) denotes the *oxygen* species. In this formulation, the decomposition rates $(dL_{i+1}/dt)_-$ are considered to be *positive* in sign if decomposition is indeed occurring.

The growth of layer $i-1$, on the other hand, will require an analogous decomposition of layer i by solid-state reaction at the interface $x_i = 0$. This will lead to a negative contribution to the growth kinetics of layer i. Thus, from the time-dependence of the cation interstitial balance at the interfaces we can write the net growth rate of any inner layer i as

$$\frac{dL_i}{dt} = \left(\frac{dL_i}{dt}\right)_+ - \left(\frac{dL_i}{dt}\right)_- \qquad (i = 2, 3, 4, \ldots, N-1) \tag{217}$$

where

$$\left(\frac{dL_i}{dt}\right)_+ = R_i^{(ci)}\,[(J_i^{(ci)} - J_{i+1}^{(ci)}) + J_i^{(Met)}] \qquad (i = 1, 2, 3, \ldots, N-1) \tag{218}$$

with $J_i^{(Met)}$ given by eqn. (216).

In addition to the cation interstitial current balance at the interface $x_i = L_i$, we must also consider the oxygen balance. In the present case, there can be no oxygen transport through any individual layer. Therefore

the oxygen consumed at the interface $x_i = L_i$ by the growth rate $(dL_i/dt)_+$ of layer i must be derived entirely from the equivalent oxygen current $(1/R_{i+1}^{(Oxy)})\ (dL_{i+1}/dt)_-$, $(i = 1, 2, 3, \ldots, N-1)$ obtained from the decomposition of layer $i+1$ at that interface. The volume of oxide $R_i^{(Oxy)}$ associated with each oxygen atom in the layer i is given by

$$R_i^{(Oxy)} = \frac{R_i}{q_i} \qquad (i = 1, 2, 3, \ldots, N) \tag{219}$$

Consideration of the oxygen balance at the phase boundary between layers i and $i+1$ thus leads to an alternate expression for the formation rate of layer i at the interface $x_i = L_i$

$$(dL_i/dt)_+ = R_i^{(Oxy)}[(1/R_{i+1}^{(Oxy)})\ (dL_{i+1}/dt)_-]$$
$$(i = 1, 2, 3, \ldots, N-1) \tag{220}$$

It is convenient to convert from $R_i^{(Oxy)}$ to $R_i^{(ci)}$. Since a molecule $Me_{p_i}O_{q_i}$ of volume R_i consists of p_i cations and q_i anions

$$R_i = p_i R_i^{(ci)} = q_i R_i^{(Oxy)} \qquad (i = 1, 2, 3, \ldots, N) \tag{221}$$

Substituting this relation into eqn. (220) and equating the result to the corresponding rate $(dL_i/dt)_+$ obtained from the cation balance [eqn. (218)] utilizing eqn. (216) gives

$$(dL_i/dt)_+ = [(p_i/q_i)R_i^{(ci)}]\ [(q_{i+1}/p_{i+1})\ (1/R_{i+1}^{(ci)})]\ (dL_{i+1}/dt)_-$$
$$= R_i^{(ci)}\ (J_i^{(ci)} - J_{i+1}^{(ci)}) + (R_i^{(ci)}/R_{i+1}^{(ci)})\ (dL_{i+1}/dt)_-$$
$$(i = 1, 2, 3, \ldots, N-1) \tag{222}$$

Solving this equation for the decomposition rate of layer $i+1$ yields

$$(dL_{i+1}/dt)_- = \beta_{i+1} R_i^{(ci)}\ (J_i^{(ci)} - J_{i+1}^{(ci)})$$
$$(i = 1, 2, 3, \ldots, N-1) \tag{223}$$

where

$$1/\beta_{i+1} = [(p_i/q_i)\ (q_{i+1}/p_{i+1}) - 1]\ (R_i^{(ci)}/R_{i+1}^{(ci)})$$
$$(i = 1, 2, 3, \ldots, N-1) \tag{224}$$

This result, evaluated for layer i as well as layer $i+1$, can in turn be used in eqns. (216)—(218) to evaluate the net growth rate of any inner layer i.

$$\frac{dL_i}{dt} = A_{i,i-1}J_{i-1}^{(ci)} + A_{ii}J_i^{(ci)} + A_{i,i+1}J_{i+1}^{(ci)}$$
$$(i = 2, 3, 4, \ldots, N-1) \tag{225}$$

where, for any specific value of i

$$A_{i,i-1} = -\beta_i R_{i-1}^{(ci)} = -\lambda_i R_i^{(ci)} \tag{226}$$

$$A_{ii} = R_i^{(ci)} + (R_i^{(ci)}/R_{i+1}^{(ci)})\,\beta_{i+1} R_i^{(ci)} + \beta_i R_{i-1}^{(ci)}$$

$$= R_i^{(ci)} (1 + \lambda_i + \lambda_{i+1}) \tag{227}$$

$$A_{i,i+1} = -R_i^{(ci)} - (R_i^{(ci)}/R_{i+1}^{(ci)})\,\beta_{i+1} R_i^{(ci)}$$

$$= -R_i^{(ci)} (1 + \lambda_{i+1}) \tag{228}$$

with the required parameters λ_i and λ_{i+1} for a specific value of i determined from the relation

$$\lambda_i = [(q_i/p_i)\,(p_{i-1}/q_{i-1}) - 1]^{-1} \qquad (i = 2, 3, \ldots, N) \tag{229}$$

Because the layers become successively more rich in oxygen as the oxygen interface is approached, the ratio q_i/p_i increases with increasing i. Thus $(q_{i+1}/p_{i+1})/(q_i/p_i)$ is greater than one, so that $\lambda_i > 0$. The coefficients $A_{i,i-1}$ and $A_{i,i+1}$ are thus negative for layer i, whereas A_{ii} is positive. (It is interesting to note that $A_{i,i-1} + A_{ii} + A_{i,i+1} = 0$.) The growth rate of layer i thus has positive and negative contributions. The positive contribution is produced by $J_i^{(ci)}$ and the negative contributions are produced by $J_{i+1}^{(ci)}$ (constituting a loss of particles into layer $i+1$ which would otherwise be utilized in the growth of layer i in single-phase growth) and by $J_{i-1}^{(ci)}$ (which will usually lead to some decomposition of layer i to increase the thickness of layer $i-1$ in addition to being the source of the particle current $J_i^{(ci)}$ into layer i).

It is of interest to determine λ_i for some specific stoichiometric oxides. For example, if layer $i+1$ is CuO and layer i is Cu_2O, then $\lambda_{i+1} = 1$. If layer $i+1$ is Co_2O_3 and layer i is Co_3O_4, then $\lambda_{i+1} = [(3/2)\,(3/4) - 1]^{-1} = 8$. If layer $i+1$ is Fe_3O_4 and layer i is FeO, then $\lambda_{i+1} = [(4/3) - 1]^{-1} = 3$. The coefficients $A_{i,i-1}$, A_{ii}, and $A_{i,i+1}$ can thus be expected to have values in the range of 1 to 10 times the value of $R_i^{(ci)}$. Clearly, the λ_i can be expressed in terms of the valences Z_i as well as the stoichiometry q_i/p_i, since molecular charge neutrality requires that

$$Z_i^{(ci)} e p_i + Z_i^{(Oxy)} e q_i = 0 \tag{230}$$

where Z_i is defined to include sign as well as magnitude for the charge $Z_i e$ per ion of a given type in layer i. This relation can be utilized in eqn. (229) to obtain

$$\lambda_{i+1} = [(Z_{i+1}^{(ci)}/Z_{i+1}^{(Oxy)})\,(Z_i^{(Oxy)}/Z_i^{(ci)}) - 1]^{-1} \tag{231}$$

Thus far, our development has been for any inner layer i of the multilayer oxide. It is now required to examine separately the growth of the two layers L_1 and L_N which are in contact, respectively, with the parent metal and the gaseous oxygen. The growth of L_1 proceeds in exactly the

same way as any inner layer i except for the fact that there is no decomposition required for growth of any underlying oxide. Therefore

$$\left(\frac{dL_1}{dt}\right) = \left(\frac{dL_1}{dt}\right)_+ \tag{232}$$

since $(dL_1/dt)_- = 0$. The cation and anion balances at $x_1 = L_1$ obey the same conditions as were developed above, namely, those given by eqns. (216) and (220). Thus

$$\frac{dL_1}{dt} = R_1^{(ci)}(J_1^{(ci)} - J_2^{(ci)}) + \left(\frac{R_1^{(ci)}}{R_2^{(ci)}}\right)\beta_2 R_1^{(ci)}(J_1^{(ci)} - J_2^{(ci)}) \tag{233}$$

or, equivalently

$$\frac{dL_1}{dt} = A_{11}J_1^{(ci)} + A_{12}J_2^{(ci)} \tag{234}$$

where

$$A_{11} = R_1^{(ci)} + \left(\frac{R_1^{(ci)}}{R_2^{(ci)}}\right)\beta_2 R_1^{(ci)} = R_1^{(ci)}(1 + \lambda_2) \tag{235}$$

and

$$A_{12} = -R_1^{(ci)}(1 + \lambda_2) \tag{236}$$

with

$$\lambda_2 = \left[\left(\frac{q_2}{p_2}\right)\left(\frac{p_1}{q_1}\right) - 1\right]^{-1} \tag{237}$$

Consider now the layer L_N in direct contact with the gaseous oxygen. The chemical reaction for this layer can be written as

$$p_N\ \mathrm{Me}^{Z_N} + p_N Z_N\ \mathrm{e}^- + \tfrac{1}{2} q_N\ \mathrm{O}_2 \longleftrightarrow \mathrm{Me}_{p_N}\mathrm{O}_{q_N} \tag{238}$$

The $p_N Z_N$ electrons required for this reaction are provided by the electron current through layer N, which again is in accord with the coupled-currents condition for single-phase growth. This layer will have a decomposition rate as required for the formation of the new oxide in layer $N-1$, so in this respect it does not differ from the inner layers. However, this layer is not required to carry an additional cation interstitial current which subsequently flows into an adjacent layer, so in this respect it differs from the remaining layers. On the other hand, some oxides are volatile, or else they may decompose due to the presence of some agent in the ambient gas phase. In such cases, there is a loss which can be described in terms of the equivalent current $J_{N+1}^{(ci)}$ of cation interstitials required to

supply this loss of oxide. For fixed ambient conditions, this quantity will generally be constant in time, which in turn can exert a marked effect on the last stages of the kinetics of growth. In fact, when the film becomes sufficiently thick that the overall formation rate has decreased essentially to this loss rate, the overall thickness of the multilayer oxide will no longer change with time. In yet another respect, the formulation for the kinetics of layer N will differ from the kinetics for the inner layers; namely, no decomposition of an adjacent layer is required to supply the oxygen for growth. Instead, the oxygen supply from the ambient gas phase in presumed adequate to maintain an absorbed layer [65] on the surface of the oxide. This permits the formation rate of layer N to be controlled by the cation interstitial current $J_N^{(ci)}$. Thus, we may write

$$\frac{dL_N}{dt} = R_N^{(ci)} \left(J_N^{(ci)} - J_{N+1}^{(ci)}\right) - \left(\frac{dL_N}{dt}\right)_- \tag{239}$$

where

$$J_{N+1}^{(ci)} = \left(\frac{1}{R_N^{(ci)}}\right)\left(\frac{dL_N}{dt}\right)_{evap} \tag{240}$$

and $(dL_N/dt)_-$ arises from the decomposition rate of layer N to form layer $N-1$. This rate, which is given by our previously deduced expression (223) with $i = N-1$, when substituted into eqn. (239) leads to the following expression for the growth rate of layer N.

$$\begin{aligned}\frac{dL_N}{dt} &= R_N^{(ci)} \left(J_N^{(ci)} - J_{N+1}^{(ci)}\right) - \beta_N R_{N-1}^{(ci)} \left(J_{N-1}^{(ci)} - J_N^{(ci)}\right) \\ &= -\beta_N R_{N-1}^{(ci)} J_{N-1}^{(ci)} + \left(R_N^{(ci)} + \beta_N R_{N-1}^{(ci)}\right) J_N^{(ci)} - R_N^{(ci)} J_{N+1}^{(ci)} \\ &= A_{N,N-1} J_{N-1}^{(ci)} + A_{NN} J_N^{(ci)} + A_{N,N+1} J_{N+1}^{(ci)}\end{aligned} \tag{241}$$

where, for a specific value of N

$$A_{N,N-1} = -\beta_N R_{N-1}^{(ci)} = -\lambda_N R_N^{(ci)} \tag{242}$$

$$A_{NN} = R_N^{(ci)} + \beta_N R_{N-1}^{(ci)} = R_N^{(ci)} + \lambda_N R_N^{(ci)} = (1+\lambda_N) R_N^{(ci)} \tag{243}$$

$$A_{N,N+1} = -R_N^{(ci)} \tag{244}$$

with the required λ_N determined from the relation

$$\lambda_N = \beta_N R_{N-1}^{(ci)} / R_N^{(ci)} = \left[\left(p_{N-1}/q_{N-1}\right)\left(q_N/p_N\right) - 1\right]^{-1} \tag{245}$$

The parameter β_N, in accordance with the definition of eqn. (224), is given by

$$\beta_N = \frac{\lambda_N R_N^{(ci)}}{R_{N-1}^{(ci)}} \tag{246}$$

Also, it should be remembered that $J_{N+1}^{(ci)}$ is not a true cation interstitial current but, instead, is the equivalent current due to oxide evaporation as defined by eqn. (240).

In summary, the growth equations for the N layers can be written in the form

$$\frac{dL_i}{dt} = A_{i,i-1} J_{i-1}^{(ci)} + A_{ii} J_i^{(ci)} + A_{i,i+1} J_{i+1}^{(ci)}$$

$$(i = 1, 2, 3, \ldots, N) \tag{247}$$

where for any specific value of i

$$A_{i,i-1} = -\lambda_i R_i^{(ci)} \tag{248}$$

$$A_{ii} = (1 + \lambda_i + \lambda_{i+1}) R_i^{(ci)} \tag{249}$$

$$A_{i,i+1} = -(1 + \lambda_{i+1}) R_i^{(ci)} \tag{250}$$

with the λ_i and λ_{i+1} determined from

$$\lambda_j = [(q_j/p_j)(p_{j-1}/q_{j-1}) - 1]^{-1} \qquad (j = 2, 3, 4, \ldots, N) \tag{251}$$

and

$$\lambda_j = 0 \qquad (j = 1, N+1) \tag{252}$$

and with

$$J_0^{(ci)} = 0 \tag{253}$$

and

$$J_{N+1}^{(ci)} = (1/R_N^{(ci)})(dL_N/dt)_{evap} \tag{254}$$

(The choice $J_0^{(ci)} = 0$ is equivalent to assuming no continuous oxygen solution into the parent metal). Assuming known values for the parameters p_i, q_i, and $R_i^{(ci)}$, and also assuming that the evaporation rate is known or can be evaluated from experimental data, we thus have a set of N equations for the rates of growth dL_i/dt of the N layers. This formalism is quite general so far, since no assumption (beyond that of cation diffusion) has been made concerning the model for growth of any specific layer. The formalism can thus be used with any theory for single phase growth. Each cation interstitial current $J_i^{(ci)}$ $(i = 1, 2, 3, \ldots, N)$ can therefore be evaluated by using the rate coefficient appropriate for single-phase growth of that layer and the use of the set of such currents $J_i^{(ci)}$ in the formulation [see, for example, eqn. (247)] enables one to solve the linked equations for multilayer growth.

2.3 THE CASE OF OXIDE GROWTH BY DIFFUSION OF CATION VACANCIES AND ELECTRON HOLES

Cation vacancies and electron holes can be created in layer N at the oxygen interface (see Fig. 18). This occurs when oxygen at the surface utilizes metal ions from the oxide lattice of layer N to form new oxide molecules, in accordance with the reaction

$$\tfrac{1}{2} q_N \, O_2 \longleftrightarrow Me_{p_N} O_{q_N} + p_N Z_N \, h^+ + p_N \, V_{Me}^{-Z_N} \tag{255}$$

where h^+ represents an electron hole having an effective charge + e, Z_N is the valence of the cation in layer N, and $V_{Me}^{-Z_N}$ represents a cation vacancy having an effective negative charge of $-Z_N e$. The cation vacancies and electron holes so produced will migrate through layers N, $N-1$, $N-2, \ldots, 1$ in the direction of the metal interface, being annihilated finally at the parent metal interface. Similarly, those new cation vacancies and electron holes generated by the phase-boundary reaction at $x_i = L_i$ in producing new oxide of layer i will migrate through layers i, $i-1$, $i-2, \ldots, 1$, being finally annihilated at the parent metal. These defect species originate in the solid-state reaction in which the oxygen-richer layer $i+1$ undergoes decomposition to form more oxide of layer i at $x_i = L_i$ in accordance with the reaction

$$q_i \, Me_{p_{i+1}} O_{q_{i+1}} \longleftrightarrow q_{i+1} \, Me_{p_i} O_{q_i} + n_i Z_i \, h^+ + n_i \, V_{Me}^{-Z_i}$$

$$(i = 1, 2, 3, \ldots, N-1) \tag{256}$$

where n_i is again defined by eqn. (214) and $V_{Me}^{-Z_i}$ represents a cation vacancy having an effective negative charge of $-Z_i e$ in layer i. That is, n_i cation vacancies $V_{Me}^{-Z_i}$, each having an effective negative charge of $-Z_i e$, together with $n_i Z_i$ electron holes h^+ (each having charge $+e$), are produced by the solid-state transformation of q_i molecules of layer $i+1$ to form q_{i+1} new molecules for increasing the thickness of layer i. For example, if the oxygen-richer layer is CuO and the oxygen-poorer layer is Cu_2O, then $p_i = 2$ while $q_i = q_{i+1} = p_{i+1} = 1$. Then $n_i = 1$, so one molecule of CuO can react at the phase boundary between the two oxides to form one new molecule of Cu_2O, in addition to one cation vacancy having effective charge $-e$ in the Cu_2O and a positive electron hole in the Cu_2O. In this particular example, the Cu_2O layer grows at the expense of the CuO layer.

The electron holes generated in the reaction described by eqn. (256) result in an increase in the electron-hole current through layer i. In addition, the electron-hole current through layer i must be sufficient to include the electron holes generated in the corresponding growth reactions at layers $i+1$, $i+2, \ldots, N$ (see Fig. 18). An electron-hole charge transport equivalent to the cation-vacancy charge transport, but necessarily of opposite sign, is required for each such reaction. This can be assured by imposing the condition of coupled currents for growth of each oxide

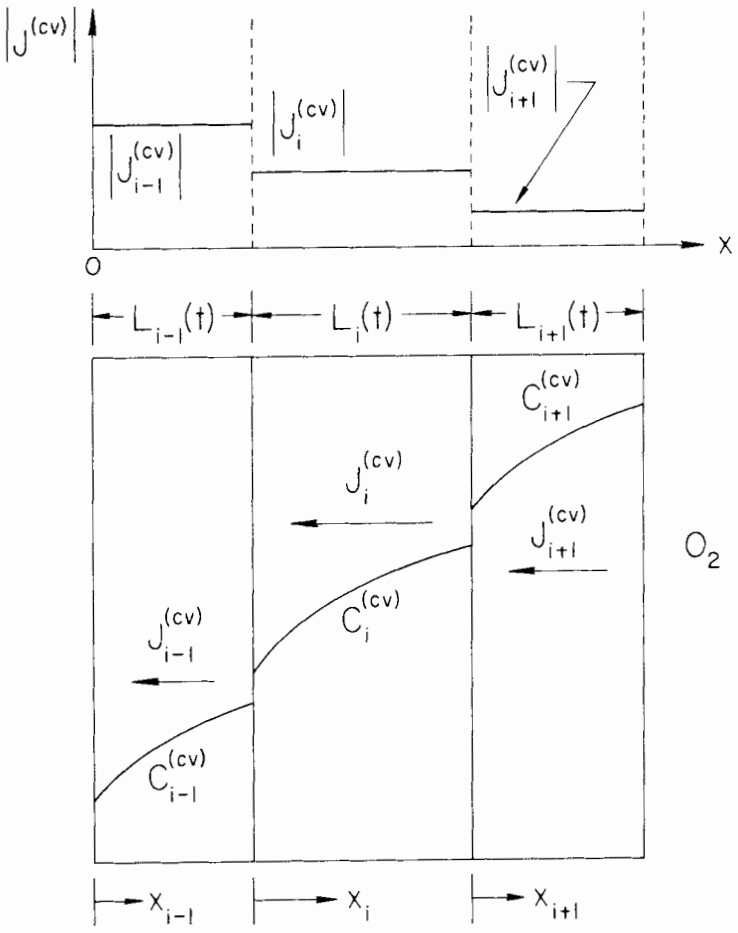

Fig. 20. One of the interior oxide layers labeled i in a sandwich array of multilayered oxides growing by cation vacancy (cv) diffusion illustrated with the relative magnitudes of the negatively directed particle currents through layer i and the adjacent layers $i-1$ and $i+1$.

layer. The rate coefficient appropriate for single-phase growth of each oxide layer can therefore be used to obtain the current J_i through that layer. The set of such currents J_i ($i = 1, 2, 3, \ldots, N$) then can be employed in the set of linked equations for this case of multilayer oxide growth.

Layer 1 in direct contact with the parent metal grows in accordance with the balanced reaction given by eqn. (256). The cation vacancies and electron holes required by that reaction at $x_1 = L_1$ flow through layer 1 and are annihilated at the parent metal interface.

The cation vacancy currents are illustrated in Fig. 20. It should be

noted that the coordinate system used is the same as that used in the previous case, namely that illustrated in Fig. 18. The cation vacancy currents indicated in Fig. 20 are negative in sign but increase in magnitude in the order $i+1$, i, $i-1$, as noted in Fig. 20. All cation vacancies eventually flow to the parent metal for annihilation. Layer i grows by the solid-state transformation of layer $i+1$ at $x_i = L_i$ in accordance with the solid-state defect reaction equation given by (256), with the simultaneous creation of the required number of cation vacancies (and electron holes) in layer i. These mobile defects flow through layer i towards the metal interface. Thus the cation vacancy difference current $J_i^{(cv)} - J_{i+1}^{(cv)}$ yields one contribution $R_i^{(cv)}(J_i^{(cv)} - J_{i+1}^{(cv)})$ to the growth rate of layer i. (Both $R_i^{(cv)}$ and the difference current must be negative in sign to obtain a positive growth rate). We confine attention in the present section to the situation where the various oxide layers i are impermeable to the oxygen species. The growth of layer i then requires a decomposition of the oxygen-richer layer $i+1$ to obtain the necessary oxygen. The picture at the $x_i = L_i$ phase boundary is thus one in which layer $i+1$ is decomposing to yield some cations and oxygen anions which combine with the cations provided by the difference cation vacancy current $J_i^{(cv)} - J_{i+1}^{(cv)}$ to form more of the less-oxygen-rich layer i.

First, let us examine the growth of any interior layer L_i ($i = 2, 3, \ldots, N-1$) and afterwards consider the extreme layers (layers 1 and N). The growth of layer i will involve a simultaneous solid-state decomposition of layer $i+1$ to provide the necessary oxygen. In providing the necessary oxygen to react with the cations provided by the cation vacancy difference current at $x_i = L_i$, the cations simultaneously freed by the decomposition of layer $i+1$ become immediately available for growth of layer i. This leads to an additional equivalent cation vacancy current for growth of layer i given by

$$J_i^{(Mev)} = \left(\frac{1}{R_{i+1}^{(cv)}}\right)\left(\frac{dL_{i+1}}{dt}\right)_- \qquad (i = 1, 2, 3, \ldots, N-1) \tag{257}$$

where the subscript "minus" denotes decomposition. The rate $(dL_{i+1}/dt)_-$ is defined to be positive whenever decomposition is indeed actively occurring. An analogous decomposition of layer i at the interface $x_i = 0$ will likewise be required, leading to a negative contribution to the growth kinetics of layer i. Therefore, the time dependence of the cation balance at the interfaces of layer i leads to the expression

$$\frac{dL_i}{dt} = \left(\frac{dL_i}{dt}\right)_+ - \left(\frac{dL_i}{dt}\right)_- \qquad (i = 2, 3, \ldots, N-1) \tag{258}$$

for the net growth rate of layer i where

$$\left(\frac{dL_i}{dt}\right)_+ = R_i^{(cv)} \left[(J_i^{(cv)} - J_{i+1}^{(cv)}) + J_i^{(Mev)}\right]$$

$$(i = 1, 2, 3, \ldots, N-1) \tag{259}$$

with $J_i^{(Mev)}$ given by eqn. (257). The superscript (Mev) is an abbreviation for metal vacancy and therefore $J_i^{(Mev)}$ represents the equivalent metal vacancy current through layer i.

Next, we must consider the time-dependence of the oxygen atom balance at the interface $x_i = L_i$. Because, by hypothesis, there can be no oxygen transport through any individual layer, the oxygen anions consumed at $x_i = L_i$ by the growth rate $(dL_i/dt)_+$ of layer i must be derived entirely from the equivalent anion current $(1/R_{i+1}^{(Oxy)})\ (dL_{i+1}/dt)_-$ for $i = 2, 3, \ldots, N-1$ obtained from the decomposition of layer $i+1$ at $x_i = L_i$. The volume of oxide $R_i^{(Oxy)}$ associated with each oxygen atom in layer i is given by

$$R_i^{(Oxy)} = \frac{R_i}{q_i} \qquad (i = 1, 2, 3, \ldots, N) \tag{260}$$

The oxygen atom balance then leads to the requirement

$$\left(\frac{dL_i}{dt}\right)_+ = R_i^{(Oxy)} \left(\frac{1}{R_{i+1}^{(Oxy)}}\right) \left(\frac{dL_{i+1}}{dt}\right)_- \qquad (i = 1, 2, 3, \ldots, N-1) \tag{261}$$

Since a molecule of $Me_{p_i}O_{q_i}$ of volume R_i consists of p_i cations and q_i anions

$$R_i = q_i R_i^{(Oxy)} = -p_i R_i^{(cv)} \qquad (i = 1, 2, 3, \ldots, N) \tag{262}$$

where the negative sign arises since $R_i^{(cv)}$ is defined by convention to be a negative quantity because it is associated with a negatively directed species current. Substituting this relation into the previous expression (261) and then equating the result to the rate expression (259) for $(dL_i/dt)_+$ obtained from the cation balance gives

$$\begin{aligned}(dL_i/dt)_+ &= \left[-(p_i/q_i)R_i^{(cv)}\right] \left[-(q_{i+1}/p_{i+1})\,(1/R_{i+1}^{(cv)})\right] \times \\ &\quad (dL_{i+1}/dt)_- \\ &= R_i^{(cv)}(J_i^{(cv)} - J_{i+1}^{(cv)}) + (R_i^{(cv)}/R_{i+1}^{(cv)})\,(dL_{i+1}/dt)_- \\ &\quad (i = 1, 2, 3, \ldots, N-1)\end{aligned} \tag{263}$$

Solving for the decomposition rate of layer $i+1$ then yields

$$\begin{aligned}(dL_{i+1}/dt)_- &= \beta'_{i+1} R_i^{(cv)}\,(J_i^{(cv)} - J_{i+1}^{(cv)}) \\ &\quad (i = 1, 2, 3, \ldots, N-1)\end{aligned} \tag{264}$$

where

$$1/\beta'_{i+1} = [(q_{i+1}/p_{i+1})(p_i/q_i) - 1](R_i^{(cv)}/R_{i+1}^{(cv)}) \tag{265}$$

or, equivalently

$$\beta'_{i+1} = \frac{\lambda_{i+1} R_{i+1}^{(cv)}}{R_i^{(cv)}} \qquad (i = 1, 2, 3, \ldots, N-1) \tag{266}$$

with λ_{i+1} defined in accordance with eqn. (229). This result for the decomposition of layer $i+1$, together with its equivalent for layer i obtained by replacing i by $i-1$, can be substituted into eqns. (257)–(259) to obtain the net growth rate for any inner layer i

$$\frac{dL_i}{dt} = A'_{i,i-1} J_{i-1}^{(cv)} + A'_{ii} J_i^{(cv)} + A'_{i,i+1} J_{i+1}^{(cv)}$$

$$(i = 2, 3, \ldots, N-1) \tag{267}$$

where, for any specific value of i

$$A'_{i,i-1} = -\beta'_i R_{i-1}^{(cv)} = -\lambda_i R_i^{(cv)} \tag{268}$$

$$A'_{ii} = R_i^{(cv)}(1 + \lambda_i + \lambda_{i+1}) \tag{269}$$

and

$$A'_{i,i+1} = -R_i^{(cv)}(1 + \lambda_{i+1}) \tag{270}$$

with eqn. (229) again defining λ_i and λ_{i+1}. A comparison of the result (267) just derived with the corresponding result [eqn. (225)] for growth by cation interstitial diffusion shows that they are essentially the same, the coefficients $A'_{i,i-1}$, A'_{ii}, $A'_{i,i+1}$ differing from the set $A_{i,i-1}$, A_{ii}, $A_{i,i+1}$ only by the replacement of $R^{(cv)}$ by $R^{(ci)}$ for the corresponding layer. Note also the relation

$$A'_{i,i-1} + A'_{ii} + A'_{i,i+1} = 0$$

for the present case, with $A'_{ii} < 0$ but with $A'_{i,i-1} > 0$ and $A'_{i,i+1} > 0$.

Next, we must develop growth equations for the two oxide layers L_1 and L_N. A decomposition of layer N is required in forming layer $N-1$, as required by eqn. (261), and so in this respect layer N does not differ from the inner layers. On the other hand, there is no decomposition of a layer $N+1$ required to obtain the requisite oxygen, since layer N is already in contact with the gaseous oxygen phase. Thus, there is no equivalent cation vacancy current to be considered, in contrast to the other layers. Neither is there an actual cation vacancy current $J_{N+1}^{(cv)}$ to be considered. However, there may be oxide evaporation which must be compensated for by the net growth rate of layer N. Thus we obtain

$$\frac{dL_N}{dt} = R_N^{(cv)} J_N^{(cv)} - \left(\frac{dL_N}{dt}\right)_- - \left(\frac{dL_N}{dt}\right)_{evap} \tag{271}$$

where, from eqns. (264)—(266), we can write

$$\left(\frac{dL_N}{dt}\right)_- = \beta'_N R_{N-1}^{(cv)} (J_{N-1}^{(cv)} - J_N^{(cv)})$$

$$= \lambda_N R_N^{(cv)} (J_{N-1}^{(cv)} - J_N^{(cv)}) \quad (272)$$

The rate equation [eqn. (271)] can then be written in the form

$$\frac{dL_N}{dt} = A'_{N,N-1} J_{N-1}^{(cv)} + A'_{NN} J_N^{(cv)} + A'_{N,N+1} J_{N+1}^{(cv)} \quad (273)$$

by defining

$$A'_{N,N-1} = -R_N^{(cv)} \lambda_N \quad (274)$$

$$A'_{NN} = R_N^{(cv)} (1 + \lambda_N) \quad (275)$$

and

$$A'_{N,N+1} J_{N+1}^{(cv)} = -\left(\frac{dL_N}{dt}\right)_{evap} \quad (276)$$

These definitions of $A'_{N,N-1}$ and A'_{NN} are in accord with the general definitions (268) and (269), provided λ_{N+1} is chosen to be zero.

Considering now oxide layer 1, there will be no decomposition of that layer required since it is in contact with the parent metal. Thus $(dL_1/dt)_- = 0$. Also, we neglect the possibility of a cation vacancy current $J_0^{(cv)}$ due to unannihilated vacancies which diffuse into the parent metal instead of annihilating with metal atoms in the parent metal at the metal—oxide interface. Such would constitute a loss of potential oxide formation for layer 1. Another consideration is the positive contribution to the growth rate of layer 1 due to the decomposition of layer 2, so that we can write

$$\frac{dL_1}{dt} = R_1^{(cv)} [(J_1^{(cv)} - J_2^{(cv)}) + J_1^{(Mev)}] \quad (277)$$

where $J_1^{(Mev)}$ evaluated from eqn. (257) and eqns. (264)—(266) is given by

$$R_1^{(cv)} J_1^{(Mev)} = (R_1^{(cv)}/R_2^{(cv)}) (dL_2/dt)_-$$

$$= (R_1^{(cv)}/R_2^{(cv)}) \beta'_2 R_1^{(cv)} (J_1^{(cv)} - J_2^{(cv)})$$

$$= \lambda_2 R_1^{(cv)} (J_1^{(cv)} - J_2^{(cv)}) \quad (278)$$

with λ_2 defined by eqn. (229). Substituting this result into the growth relation (277) then gives

$$\frac{dL_1}{dt} = A'_{10} J_0^{(cv)} + A'_{11} J_1^{(cv)} + A'_{12} J_2^{(cv)} \quad (279)$$

where we have defined the quantities

$$A'_{10} = 0 \tag{280}$$

$$A'_{11} = R_1^{(cv)} (1 + \lambda_2) \tag{281}$$

and

$$A'_{12} = -R_1^{(cv)} (1 + \lambda_2) \tag{282}$$

These definitions for A'_{10}, A'_{11}, and A'_{12} are consistent with the general definitions (268)—(270) provided we adopt the convention that $\lambda_1 = 0$.

To summarize the case of cation vacancy diffusion, the coupled growth equations for the oxide layers can be written in the form

$$\frac{dL_i}{dt} = A'_{i,i-1} J_{i-1}^{(cv)} + A'_{ii} J_i^{(cv)} + A'_{i,i+1} J_{i+1}^{(cv)}$$

$$(i = 1, 2, 3, \ldots, N) \tag{283}$$

where for any specific value of i

$$A'_{i,i-1} = -\lambda_i R_i^{(cv)} \tag{284}$$

$$A'_{ii} = R_i^{(cv)} (1 + \lambda_i + \lambda_{i+1}) \tag{285}$$

and

$$A'_{i,i+1} = -R_i^{(cv)} (1 + \lambda_{i+1}) \tag{286}$$

with the λ_i and λ_{i+1} determined from

$$\lambda_j = [(q_j/p_j)(p_{j-1}/q_{j-1}) - 1]^{-1}$$

$$(j = 2, 3, \ldots, N) \tag{287}$$

$$\lambda_1 = 0 \tag{288}$$

$$\lambda_{N+1} = 0 \tag{289}$$

and with

$$J_0^{(cv)} = 0 \tag{290}$$

and

$$J_{N+1}^{(cv)} = (1/R_N^{(cv)}) (dL_N/dt)_{evap} \tag{291}$$

Assuming known values for the p_i, q_i, and $R_i^{(cv)}$ and assuming a known evaporation rate for the oxide, we have a set of N equations for the growth rates dL_i/dt of the N layers. This formulation for cation vacancy growth is general from the standpoint that no specific coupled-currents oxidation theory has yet been invoked to evaluate the currents $J_i^{(cv)}$ through the individual layers.

2.4 THE CASE OF OXIDE GROWTH BY DIFFUSION OF ANION INTERSTITIALS AND ELECTRON HOLES

Oxygen atoms can enter oxide layer N as oxygen anion interstitials and electron holes at the oxygen interface (see Fig. 18). The anion interstitials migrate through layers N, $N-1$, $N-2$, . . . , 1 towards the metal interface, being steadily consumed by the phase boundary reactions at the interfaces. Those moving through layer i are available for chemical reaction with the metal-richer layer $i-1$ to form more oxide of layer i at $x = 0$, in accordance with the reaction

$$n_{i-1}\,O^{Z_i} + n_{i-1}\,|Z_i|\,h^+ + p_i\,Me_{p_{i-1}}\,O_{q_{i-1}} \longleftrightarrow p_{i-1}\,Me_{p_i}O_{q_i} \qquad (i = 2, 3, \ldots, N) \tag{292}$$

where

$$n_{i-1} = p_{i-1}q_i - p_i q_{i-1} \tag{293}$$

and h^+ represents an electron hole having an effective positive charge $+e$. That is, n_{i-1} oxygen anions O^{Z_i}, each having a negative charge of $Z_i e$, react with $n_{i-1}\,|Z_i|$ electron holes h^+ (each having charge $+e$) and p_i molecules of layer $i-1$ to form p_{i-1} new molecules for increasing the thickness of layer i. Thus, an anion interstitial current through layer i can lead to decomposition of layer $i-1$, with the attendant growth of layer i. Therefore, layer i grows at the expense of layer $i-1$.

The electron holes required for the reaction given by eqn. (292) must be provided by an electron-hole current through layer i. In addition, this electron-hole current must be sufficient for the corresponding reactions at layers $i-1$, $i-2$, . . . , 1. Because a charge-equivalent number (relative to the charge transported by the mobile reacting anion interstitials) is required for each reaction, the requirements of the coupled-currents condition for single-phase growth are sufficient to ensure the correct electronic current through layer i. In this way, the passage of electronic charge through layer i equivalent to the anion interstitial charge current through layer i utilized in the growth of layers $i-1$, $i-2$, . . . is assured.

Layer 1 is in direct contact with the parent metal Me, so the chemical reaction governing its formation at $x_1 = 0$ is

$$q_1\,O^{Z_1} + q_1\,|Z_1|\,h^+ + p_1\,Me \longleftrightarrow Me_{p_1}\,O_{q_1} \tag{294}$$

The $q_1\,|Z_1|$ positive electron holes required for this reaction are provided by the electron-hole current through layer 1, again in accord with the coupled-currents condition for single-phase growth.

Figure 21 indicates the anion interstitial currents through the layers. The coordinate system is chosen to be the same as that already utilized for cation interstitial diffusion, namely that illustrated in Fig. 18. Because all anion interstitials originate at the oxygen interface, the anion interstitial currents decrease in magnitude in the order $i+1$, i, $i-1$, . . . , as noted in Fig. 21. The difference current $J_i^{(ai)} - J_{i-1}^{(ai)}$ serves to increase the thickness

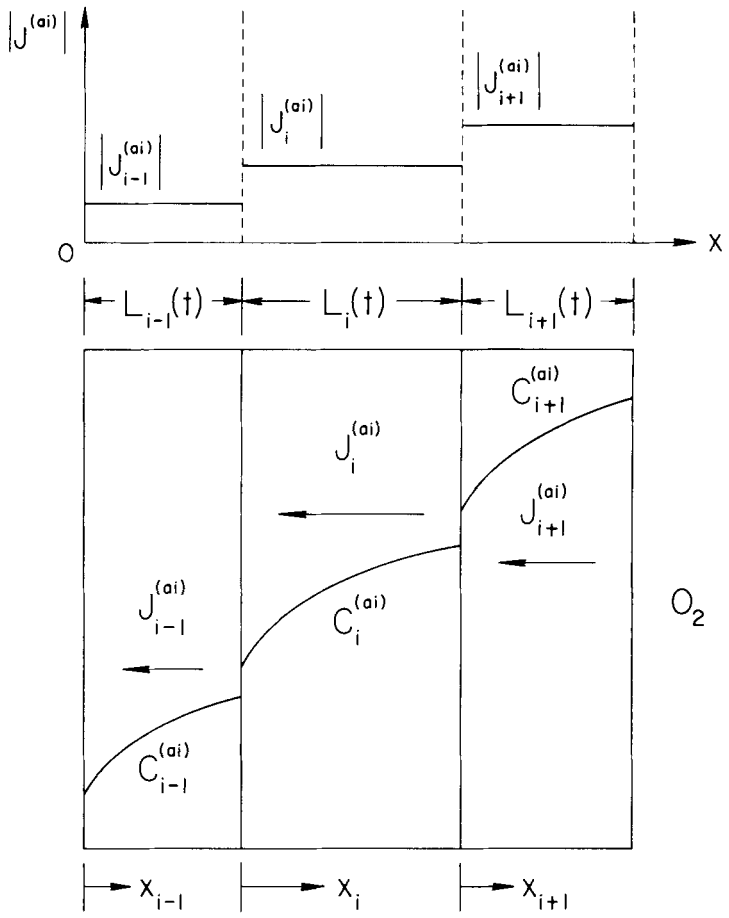

Fig. 21. One of the interior oxide layers labeled i in a sandwich array of multilayered oxides growing by anion interstitial (ai) diffusion illustrated with the relative magnitudes of the negatively directed particle currents through layer i and the adjacent layers $i-1$ and $i+1$.

of layer i in accordance with the relation $R_i^{(ai)}$ $(J_i^{(ai)} - J_{i-1}^{(ai)})$. (The $J_{i-1}^{(ai)}$ are ordinarily negative in sign since the flow is in the negative x direction. The $R_i^{(ai)}$ are therefore chosen to be negative in sign to yield the usually expected positive rates of growth). In this section, we confine our attention to the situation where the various layers i are impermeable to the metal species, so that all layers not in direct contact with the parent metal can grow only by decomposition of the adjoining metal-richer layer. First we examine the growth of any interior layer L_i $(i \neq 1, i \neq N)$ and later consider the oxide layers at the interfaces. The growth of layer i will require a simultaneous solid-state decomposition of layer $i-1$ to provide the necessary metal, in accordance with the solid-state defect reaction

equation given by eqn. (292). In providing the necessary metal to react with the difference current $J_i^{(ai)} - J_{i-1}^{(ai)}$ at $x_i = 0$, the oxygen anions simultaneously freed by the decomposition of layer $i-1$ become immediately available for the growth of layer i. This leads to an additional equivalent anion current for growth of layer i given by

$$J_i^{(Oxy)} = \left(\frac{1}{R_{i-1}^{(ai)}}\right)\left(\frac{dL_{i-1}}{dt}\right)_- \qquad (i = 2, 3, 4, \ldots, N) \tag{295}$$

where the subscript "minus" indicates decomposition. The rate $(dL_{i-1}/dt)_-$ is considered positive whenever decomposition is indeed taking place. Of course, an analogous decomposition of layer i is required by the growth of layer $i+1$, leading to a negative contribution to the growth kinetics of layer i. Thus, the time dependence of the anion current balance at the interfaces of layer i leads to the expression

$$\frac{dL_i}{dt} = \left(\frac{dL_i}{dt}\right)_+ - \left(\frac{dL_i}{dt}\right)_- \qquad (i = 2, 3, \ldots, N-1) \tag{296}$$

for the net growth rate of layer i where

$$\left(\frac{dL_i}{dt}\right)_+ = R_i^{(ai)}\left[(J_i^{(ai)} - J_{i-1}^{(ai)}) + J_i^{(Oxy)}\right]$$

$$(i = 2, 3, \ldots, N) \tag{297}$$

with $J_i^{(Oxy)}$ given by eqn. (295).

Next, we consider the time-dependence of the metal atom balance at the interface $x_i = 0$. Since, by hypothesis, there can be no cation transport through any individual layer, the cations consumed at $x_i = 0$ by the growth rate $(dL_i/dt)_+$ of layer i must be derived entirely from the equivalent cation current, $(1/R_{i-1}^{(Met)})\,(dL_{i-1}/dt)_-$ for $i = 2, 3, \ldots, N$, obtained from the decomposition of layer $i-1$ at $x_i = 0$. The volume of oxide, $R_i^{(Met)}$, associated with each metal atom in any layer i is given by

$$R_i^{(Met)} = \frac{R_i}{p_i} \qquad (i = 1, 2, 3, \ldots, N) \tag{298}$$

The metal atom balance then leads to the requirement

$$\left(\frac{dL_i}{dt}\right)_+ = R_i^{(Met)}\left[\left(\frac{1}{R_{i-1}^{(Met)}}\right)\left(\frac{dL_{i-1}}{dt}\right)_-\right] \qquad (i = 2, 3, \ldots, N) \tag{299}$$

Since a molecule of $Me_{p_i}O_{q_i}$ of volume R_i consists of p_i cations and q_i anions

$$R_i = p_i R_i^{(Met)} = -q_i R_i^{(ai)} \qquad (i = 1, 2, 3, \ldots, N) \tag{300}$$

where the negative sign arises because $R_i^{(ai)}$ is defined by convention to be a negative quantity because it is associated with a negatively directed species current. Substituting into eqn. (299) and then equating the result to the corresponding rate $(dL_i/dt)_+$ obtained from the oxygen balance, namely eqn. (297) [with eqn. (295)], gives

$$\begin{aligned}(dL_i/dt)_+ &= [(-q_i/p_i)R_i^{(ai)}]\,[(-p_{i-1}/q_{i-1})\,(1/R_{i-1}^{(ai)})]\,(dL_{i-1}/dt)_- \\ &= R_i^{(ai)}\,(J_i^{(ai)} - J_{i-1}^{(ai)}) + (R_i^{(ai)}/R_{i-1}^{(ai)})\,(dL_{i-1}/dt)_- \\ &\qquad (i = 2, 3, \ldots, N) \end{aligned} \tag{301}$$

Solving this equation for the decomposition rate of layer $i-1$ then yields

$$\left(\frac{dL_{i-1}}{dt}\right)_- = \alpha_{i-1} R_i^{(ai)}\,(J_i^{(ai)} - J_{i-1}^{(ai)}) \qquad (i = 2, 3, \ldots, N) \tag{302}$$

where

$$\frac{1}{\alpha_{i-1}} = \left[\left(\frac{q_i}{p_i}\right)\left(\frac{p_{i-1}}{q_{i-1}}\right) - 1\right]\left(\frac{R_i^{(ai)}}{R_{i-1}^{(ai)}}\right) \qquad (i = 2, 3, \ldots, N) \tag{303}$$

This result for the decomposition of layer $i-1$, together with its equivalent for layer i obtained by replacing i by $i+1$, can be substituted into eqns. (295)—(297) to obtain the net growth rate of any inner layer i, viz.

$$\frac{dL_i}{dt} = B_{i,i-1} J_{i-1}^{(ai)} + B_{ii} J_i^{(ai)} + B_{i,i+1} J_{i+1}^{(ai)}$$

$$(i = 2, 3, \ldots, N-1) \tag{304}$$

where, for any specific value of i

$$B_{i,i-1} = -R_i^{(ai)}\,(1 + \lambda_i) \tag{305}$$

$$B_{ii} = R_i^{(ai)}(1 + \lambda_i + \lambda_{i+1}) \tag{306}$$

and

$$B_{i,i+1} = -R_i^{(ai)}\lambda_{i+1} \tag{307}$$

with the λ_i and λ_{i+1} defined in exactly the same way as for the cation interstitial case, namely, by eqn. (229). It can be noted from a comparison of these results for $B_{i,i-1}$, B_{ii}, and $B_{i,i+1}$ with the corresponding results given by eqns. (226), (227), and (228) for $A_{i,i-1}$, A_{ii}, and $A_{i,i+1}$ for the cation interstitial diffusion case that the coefficients differ somewhat for the two cases. (Analogously, however,

$$B_{i,i-1} + B_{ii} + B_{i,i+1} = 0$$

but with $B_{ii} < 0$ and $B_{i,i-1} > 0, B_{i,i+1} > 0$).

Next we must develop growth equations for the two layers L_1 and L_N. The layer L_N in contact with the oxygen requires decomposition of layer L_{N-1} to obtain the necessary metal atoms, so the condition given by eqn. (299) imposed by the metal atom balance still holds. Likewise, eqns. (301)—(303) still hold. However, no decomposition of layer N is required to form a layer $N+1$ and, in this respect, layer N differs from the inner layers. Nevertheless, there could possibly be oxide evaporation, in which case

$$\frac{dL_N}{dt} = \left(\frac{dL_N}{dt}\right)_+ - \left(\frac{dL_N}{dt}\right)_{evap} \tag{308}$$

The rate $(dL_N/dt)_{evap}$ is considered to be positive in sign if evaporation is indeed occurring. Utilizing eqn. (302) in eqn. (301), with $i = N$, and then substituting into the net growth rate given by eqn. (308) leads to the result

$$\frac{dL_N}{dt} = B_{N,N-1}\, J^{(ai)}_{N-1} + B_{NN}\, J^{(ai)}_N + B_{N,N+1}\, J^{(ai)}_{N+1} \tag{309}$$

where

$$B_{N,N-1} = -R^{(ai)}_N\,(1+\lambda_N) \tag{310}$$

$$B_{NN} = R^{(ai)}_N\,(1+\lambda_N) \tag{311}$$

and $B_{N,N+1}\,J^{(ai)}_{N+1}$ is defined by

$$B_{N,N+1}\,J^{(ai)}_{N+1} = -\left(\frac{dL_N}{dt}\right)_{evap} \tag{312}$$

The $J^{(ai)}_{N+1}$ is thus not an oxygen anion interstitial current, but is introduced merely to cast the growth equation for layer N into a form analogous to that for the inner layer growth. The λ_N is determined by eqn. (229).

Consider now the layer L_1 in contact with the metal. This layer will have a decomposition rate as required for the formation of the new oxide in layer 2 so, in this respect, it does not differ from the inner layers. However, its growth does not require the decomposition of any underlying layer to obtain metal atoms since it is already in contact with the parent metal. There is, therefore, no equivalent oxygen current to be considered as is the case for the other layers. In the absence of oxygen solution in the parent metal, all of the oxygen current through layer 1 will lead to the formation of new oxide of layer 1 and we could write

$$\left(\frac{dL_1}{dt}\right)_+ = R^{(ai)}_1 J^{(ai)}_1 \tag{313}$$

If, however, there is an oxygen current $J_0^{(ai)}$ into the parent metal due to oxygen solution, we must instead write

$$\left(\frac{dL_1}{dt}\right)_+ = R_1^{(ai)} (J_1^{(ai)} - J_0^{(ai)}) \tag{314}$$

Then

$$\frac{dL_1}{dt} = \left(\frac{dL_1}{dt}\right)_+ - \left(\frac{dL_1}{dt}\right)_- \tag{315}$$

Substituting eqn. (302), with $i = 2$, into eqns. (314) and (315) then leads to the result,

$$\begin{aligned}\frac{dL_1}{dt} &= R_1^{(ai)} (J_1^{(ai)} - J_0^{(ai)}) - \alpha_1 R_2^{(ai)} (J_2^{(ai)} - J_1^{(ai)}) \\ &= B_{10} J_0^{(ai)} + B_{11} J_1^{(ai)} + B_{12} J_2^{(ai)}\end{aligned} \tag{316}$$

where

$$B_{10} = -R_1^{(ai)} \tag{317}$$

$$B_{11} = R_1^{(ai)} (1 + \lambda_2) \tag{318}$$

and

$$B_{12} = -R_1^{(ai)} \lambda_2 \tag{319}$$

with λ_2 defined by eqn. (229).

To summarize the case of anion interstitial diffusion, the growth equations for the N layers can be written in the form

$$\frac{dL_i}{dt} = B_{i,i-1} J_{i-1}^{(ai)} + B_{ii} J_i^{(ai)} + B_{i,i+1} J_{i+1}^{(ai)}$$

$$(i = 1, 2, 3, \ldots, N) \tag{320}$$

where for any specific value of i (except $i = N$)

$$B_{i,i-1} = -R_i^{(ai)} (1 + \lambda_i) \tag{321}$$

$$B_{ii} = R_i^{(ai)} (1 + \lambda_i + \lambda_{i+1}) \tag{322}$$

and

$$B_{i,i+1} = -R_i^{(ai)} \lambda_{i+1} \tag{323}$$

with the λ_i and λ_{i+1} determined from

$$\lambda_j = [(q_j/p_j)(p_{j-1}/q_{j-1}) - 1]^{-1} \quad (j = 2, 3, \ldots, N) \tag{324}$$

$$\lambda_1 = 0 \tag{325}$$

and with

$$J_0^{(ai)} = \text{oxygen solution current into parent metal} \tag{326}$$

For $i = N$, we can utilize the convention

$$\lambda_{N+1} = 0 \tag{327}$$

in which case the coefficients $B_{N,N-1}$ and B_{NN} are given by eqns. (321) and (322), but $B_{N,N+1}$ is still defined only by

$$B_{N,N+1}\, J_{N+1}^{(ai)} = -(\mathrm{d}L_N/\mathrm{d}t)_{evap} \tag{328}$$

instead of by eqn. (323).

Assuming known values for the p_i, q_i, and $R_i^{(ai)}$, and also assuming that the evaporation and oxygen solution rates are known or can be evaluated from experimental data, we have a set of N equations for the growth rates $\mathrm{d}L_i/\mathrm{d}t$ of the N layers. This formalism for anion diffusion growth is general in the sense that no specific oxidation theory has yet been invoked for the rate coefficient of the individual layers to evaluate the currents $J_i^{(ai)}$. Each anion interstitial current J_i ($i = 1, 2, 3, \ldots, N$) can therefore be evaluated by using the appropriate rate coefficient for single-phase growth of that layer and the use of the set of such currents allows us to solve the corresponding set of linked equations [see eqn. (320)] for multiphase growth.

2.5 THE CASE OF OXIDE GROWTH BY DIFFUSION OF ANION VACANCIES AND ELECTRONS

Anion vacancies may be created at the metal interface if metal atoms in the parent metal utilize oxygen ions from the oxide lattice of layer 1 to form new oxide molecules in accordance with the reaction

$$p_1\ \mathrm{Me} \longleftrightarrow \mathrm{Me}_{p_1}\mathrm{O}_{q_1} + q_1 |Z_1|\ \mathrm{e}^- + q_1\, \mathrm{V}_0^{-Z_1} \tag{329}$$

where Z_1 is the oxygen valence (usually -2) in layer 1 and $-Z_1 e$ is the effective positive charge of the oxygen vacancy represented by $\mathrm{V}_0^{-Z_1}$ in layer 1. The anion vacancies so produced and the electrons simultaneously released can migrate through layers $1, 2, 3, \ldots, N$ to the oxygen interface, being supplemented continually by new oxygen vacancies and electrons created by the phase boundary reactions at $x_2 = 0$, $x_3 = 0, \ldots, x_N = 0$. All such anion vacancies and electrons will finally be annihilated at the oxygen interface ($x_N = L_N$) by reaction with the gaseous oxygen. Those new anion vacancies and electrons generated at the phase boundary $x_i = 0$ in producing new oxide of layer i will move through layer i towards the oxygen interface. These defect species are produced by solid-state reaction of the metal-richer layer $i-1$ to form more oxide of layer i at $x_i = 0$ in accordance with the reaction

$$p_i\ \mathrm{Me}_{p_{i-1}}\mathrm{O}_{q_{i-1}} \longleftrightarrow p_{i-1}\ \mathrm{Me}_{p_i}\mathrm{O}_{q_i} + n_{i-1} |Z_i|\ \mathrm{e}^- + n_{i-1}\ \mathrm{V}_0^{-Z_i}$$
$$(i = 2, 3, \ldots, N) \tag{330}$$

where n_{i-1} is defined by eqn. (293) and $V_0^{-Z_i}$ represents the oxygen vacancy having an effective positive charge of $-Z_i e$ in layer i. That is, an integer number n_{i-1} of oxygen vacancies $V_0^{-Z_i}$, each having an effective positive charge $-Z_i e = |Z_i|e$, together with $n_{i-1}|Z_i|$ electrons e^-, are produced by the solid-state reaction of p_i molecules of layer $i-1$ to form p_{i-1} new molecules of layer i. Thus layer i grows at the expense of layer $i-1$.

The electrons generated in the reaction described by eqn. (330) are responsible for one component of the electron current through layer i. The electron current through layer i contains additional components from the electron currents generated by the corresponding solid-state reactions for growth of layers $i-1$, $i-2, \ldots, 1$. An electron charge transport equivalent to the anion vacancy charge transport (but of opposite sign) is required for each of these solid-state reactions. This condition is consistent with the coupled-currents condition for single-phase oxide growth.

The anion vacancy currents are illustrated in Fig. 22. The coordinate system used for this case is again the one illustrated in Fig. 18. The anion vacancy current and corresponding electron particle current through each oxide layer are positive in sign and increase in the order $i-1$, i, $i+1, \ldots$, as noted in Fig. 22. All anion vacancies and electrons eventually flow to the oxygen interface for annihilation with the gaseous oxygen which contacts the interface $x_N = L_N$. Layer i grows by the solid-state transformation of layer $i-1$ at $x_i = 0$ in accordance with the solid-state defect reaction given by eqn. (330), with the simultaneous creation of the requisite number of anion vacancies (and released electrons) in layer i. These flow through layer i toward the oxygen interface. Thus the anion vacancy difference current $J_i^{(av)} - J_{i-1}^{(av)}$ yields one contribution $R_i^{(av)}$ $(J_i^{(av)} - J_{i-1}^{(av)})$ to the growth rate of layer i. The oxide volume $R_i^{(av)}$ is chosen to be positive since a positive anion vacancy current from $x = 0$ to $x = L$ yields a positive contribution to the growth rate of the oxide. Generally, the difference current is also positive in sign, thus yielding a positive contribution to the growth rate of layer i. Let us now confine our attention to specific cases where the various oxide layers i are impermeable to the cation species. Then the growth of layer i requires a decomposition of the metal-richer layer $i-1$ to obtain the requisite metal atoms for reaction. The "reaction zone" for growth of layer i is therefore at the phase boundary $x_i = 0$ separating the i and $i-1$ layers. This zone is a very active place, with a solid-state reaction taking place which results in a transformation of the metal-richer phase $Me_{p_{i-1}}O_{q_{i-1}}$ into the metal-poorer phase $Me_{p_i}O_{q_i}$ with attendant creation of anion vacancies and electrons in layer i. (Alternatively, we can view the $Me_{p_{i-1}}O_{q_{i-1}}$ as decomposing to yield the necessary metal ions for the growth of layer i by new $Me_{p_i}O_{q_i}$ formation, with the additional oxygen required over that released by the decomposition reaction being supplied by the difference oxygen vacancy current $J_i^{(av)} - J_{i-1}^{(av)}$ created to sustain the chemical reaction).

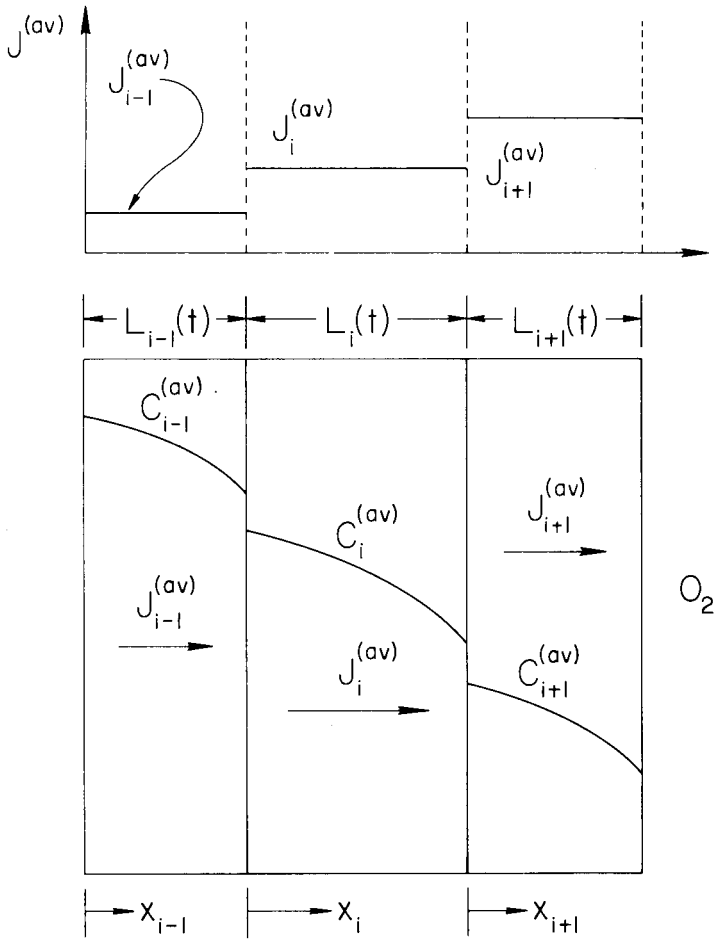

Fig. 22. One of the interior oxide layers labeled i in a sandwich array of multilayered oxides growing by anion vacancy (av) diffusion illustrated with the relative magnitudes of the positively directed particle currents through layer i and the adjacent layers $i-1$ and $i+1$.

The growth of the inner layers L_i ($i = 2, 3, \ldots, N-1$) are first considered. By hypothesis, the cations are immobile for the present case, so the solid-state decomposition of layer $i-1$ denoted by $(\mathrm{d}L_{i-1}/\mathrm{d}t)_-$ yields cations for layer i formation equivalent to an effective cation current of $(1/R_{i-1}^{(\mathrm{Met})})\,(\mathrm{d}L_{i-1}/\mathrm{d}t)_-$. The product of this quantity with the new oxide volume $R_i^{(\mathrm{Met})}$ of layer i which results from each cation provided by the solid-state decomposition of layer $i-1$ then gives the growth

rate of layer i due to the phase boundary reactions occurring in the reaction zone at $x_i = 0$, namely

$$\left(\frac{dL_i}{dt}\right)_+ = \left(\frac{R_i^{(Met)}}{R_{i-1}^{(Met)}}\right)\left(\frac{dL_{i-1}}{dt}\right)_- \qquad (i = 2, 3, \ldots, N) \tag{331}$$

It is helpful to transform into anion vacancy volumes $R_i^{(av)}$ by means of the general relation

$$R_i = p_i R_i^{(Met)} = q_i R_i^{(av)} \qquad (i = 1, 2, 3, \ldots, N) \tag{332}$$

Thus $R_i^{(Met)}/R_{i-1}^{(Met)}$ can be replaced by $(q_i/p_i)\ (p_{i-1}/q_{i-1})R_i^{(av)}/R_{i-1}^{(av)}$ in eqn. (331) to give

$$\left(\frac{dL_i}{dt}\right)_+ = \left(\frac{q_i}{p_i}\right)\left(\frac{p_{i-1}}{q_{i-1}}\right)\left(\frac{R_i^{(av)}}{R_{i-1}^{(av)}}\right)\left(\frac{dL_{i-1}}{dt}\right)_-$$

$$(i = 2, 3, \ldots, N) \tag{333}$$

Next, we must consider the anion balance at this reaction zone located at $x_i = 0$. The decomposition rate $(dL_{i-1}/dt)_-$ of oxide molecules of layer $i-1$ makes available anions for formation of layer i equivalent to those which would be supplied by an anion vacancy current equal to

$$J_i^{(Oxv)} = (1/R_{i-1}^{(av)})\ (dL_{i-1}/dt)_- \qquad (i = 2, 3, \ldots, N) \tag{334}$$

The superscript (Oxv) is an abbreviation for oxygen vacancy. Because the newly forming layer i is oxygen-rich relative to the decomposing layer $i-1$, an additional number of oxygen anions are required in order to utilize all of the cations released in the solid-state decomposition of layer $i-1$ at $x_i = 0$ and in the presently considered case, these are provided by a new component of the anion vacancy current generated in layer i by this phase boundary reaction. Since layer i must carry, in addition, the anion vacancy currents generated by the phase boundary reactions at $x_1 = 0, x_2 = 0, \ldots, x_{i-1} = 0$, we have the identity

$$J_i^{(av)} = J_1^{(av)} + (J_2^{(av)} - J_1^{(av)}) + (J_3^{(av)} - J_2^{(av)}) + \ldots + (J_i^{(av)} - J_{i-1}^{(av)}) \tag{335}$$

Thus, the phase boundary reaction at $x_i = 0$ utilizes the anion vacancy difference current $(J_i^{(av)} - J_{i-1}^{(av)})$ in order to be sustained. This consideration of the anion balance at $x_i = 0$ leads us to the alternative expression

$$\left(\frac{dL_i}{dt}\right)_+ = R_i^{(av)}\ [(J_i^{(av)} - J_{i-1}^{(av)}) + J_i^{(Oxv)}] \qquad (i = 2, 3, \ldots, N)$$

(336)

for the formation rate of layer i at $x_i = 0$. Substituting eqn. (334) for $J_i^{(Oxv)}$ gives

$$\left(\frac{dL_i}{dt}\right)_+ = R_i^{(av)} (J_i^{(av)} - J_{i-1}^{(av)}) + \left(\frac{R_i^{(av)}}{R_{i-1}^{(av)}}\right) \left(\frac{dL_{i-1}}{dt}\right)_- \quad (i = 2, 3, \ldots, N) \tag{337}$$

Consider, also, that layer i will likewise undergo solid-state decomposition at the interface $x_i = L_i$ in the formation of layer $i + 1$, yielding a negative contribution $(dL_i/dt)_-$ to the growth of layer i. The net growth rate of layer i will be given by the difference in the formation rate of layer i at $x_i = 0$ and the decomposition rate of layer i at $x_i = L_i$

$$\frac{dL_i}{dt} = \left(\frac{dL_i}{dt}\right)_+ - \left(\frac{dL_i}{dt}\right)_-$$

$$= R_i^{(av)} (J_i^{(av)} - J_{i-1}^{(av)}) + \left(\frac{R_i^{(av)}}{R_{i-1}^{(av)}}\right) \left(\frac{dL_{i-1}}{dt}\right)_- - \left(\frac{dL_i}{dt}\right)_-$$

$$(i = 2, 3, \ldots, N-1) \tag{338}$$

To obtain the decomposition rate expressions $(dL_i/dt)_-$ and $(dL_{i-1}/dt)_-$ required in this equation for the net growth rate of any interior layer i, we equate the two expressions (333) and (337) which were obtained for $(dL_i/dt)_+$ by means of the cation and the anion balances at the phase boundary $x_i = 0$. This gives

$$\left(\frac{q_i}{p_i}\right)\left(\frac{p_{i-1}}{q_{i-1}}\right)\left(\frac{R_i^{(av)}}{R_{i-1}^{(av)}}\right) \left(\frac{dL_{i-1}}{dt}\right)_- = R_i^{(av)}(J_i^{(av)} - J_{i-1}^{(av)})$$

$$+ \left(\frac{R_i^{(av)}}{R_{i-1}^{(av)}}\right) \left(\frac{dL_{i-1}}{dt}\right)_- \qquad (i = 2, 3, \ldots, N) \tag{339}$$

Solving this expression for $(dL_{i-1}/dt)_-$ yields

$$\left(\frac{dL_{i-1}}{dt}\right)_- = \alpha'_{i-1} R_i^{(av)} (J_i^{(av)} - J_{i-1}^{(av)}) \qquad (i = 2, 3, \ldots, N) \tag{340}$$

where

$$\frac{1}{\alpha'_{i-1}} = \left[\left(\frac{q_i}{p_i}\right)\left(\frac{p_{i-1}}{q_{i-1}}\right) - 1\right] \left(\frac{R_i^{(av)}}{R_{i-1}^{(av)}}\right) \tag{341}$$

In terms of λ_i defined by eqn. (229)

$$\alpha'_{i-1} = \frac{\lambda_i R_{i-1}^{(av)}}{R_i^{(av)}} \tag{342}$$

so that the decomposition rates given by eqn. (340) can be written as

$$\left(\frac{dL_{i-1}}{dt}\right)_- = \lambda_i R_{i-1}^{(av)} (J_i^{(av)} - J_{i-1}^{(av)}) \quad (i = 2, 3, \ldots, N) \tag{343}$$

We note in passing that this result holds for one of the extreme layers (namely, oxide layer 1 in contact with the parent metal) in addition to the inner layers; this will be needed in developing the expression for the net growth rate of layer 1.

The net growth rate for the inner layers now follows by substituting eqn. (343), together with its equivalent obtained by replacing i by $i + 1$, into eqn. (338). This gives

$$\begin{aligned}\frac{dL_i}{dt} &= R_i^{(av)} (J_i^{(av)} - J_{i-1}^{(av)}) + R_i^{(av)} \lambda_i (J_i^{(av)} - J_{i-1}^{(av)}) \\ &\quad - R_i^{(av)} \lambda_{i+1} (J_{i+1}^{(av)} - J_i^{(av)}) \quad (i = 2, 3, 4, \ldots, N-1)\end{aligned} \tag{344}$$

Equivalently

$$\begin{aligned}\frac{dL_i}{dt} &= B'_{i,i-1} J_{i-1}^{(av)} + B'_{ii} J_i^{(av)} + B'_{i,i+1} J_{i+1}^{(av)} \\ &\quad (i = 2, 3, \ldots, N-1)\end{aligned} \tag{345}$$

where, for each value of i

$$B'_{i,i-1} = -R_i^{(av)} (1 + \lambda_i) \tag{346}$$

$$B'_{ii} = R_i^{(av)} (1 + \lambda_i + \lambda_{i+1}) \tag{347}$$

and

$$B'_{i,i+1} = -R_i^{(av)} \lambda_{i+1} \tag{348}$$

Note that

$$B'_{i,i-1} + B'_{ii} + B'_{i,i+1} = 0$$

with the $B'_{i,i-1}$ and $B'_{i,i+1}$ being negative in sign, but with B'_{ii} being positive. (Recall that the λ_i are always positive).

Now we examine separately the growth of the extreme layers L_1 and L_N. Already we have expression (343) which gives us the decomposition rate for layer 1 at $x_1 = L_1$, namely

$$\left(\frac{dL_1}{dt}\right)_- = \lambda_2 R_1^{(av)} (J_2^{(av)} - J_1^{(av)}) \tag{349}$$

The growth rate for layer 1 at $x_1 = 0$ requires an anion vacancy current $J_1^{(av)}$ through layer 1. There are no growing oxide layers i for $i < 1$, so $J_1^{(av)}$ contributes entirely to the growth of layer 1. In addition, there is no oxide decomposition reaction at the phase boundary $x_1 = 0$ since this represents the metal interface: thus, there is no equivalent current $J_1^{(Oxv)}$ to be considered. Therefore, we can write $(dL_1/dt)_+ = R_1^{(av)} J_1^{(av)}$, so the net growth rate of layer 1 is given by

$$\frac{dL_1}{dt} = R_1^{(av)} J_1^{(av)} - \lambda_2 R_1^{(av)} (J_2^{(av)} - J_1^{(av)}) \tag{350}$$

This ignores the possibility of any oxygen solution current $|J_0^{(Oxy)}|$ into the parent metal, which, in terms of the equivalent anion vacancy current, $J_0^{(Oxv)}$, would constitute a loss

$$\left(\frac{dL_1}{dt}\right)_{soln} = R_1^{(av)} J_0^{(Oxv)} \tag{351}$$

to the growth rate of layer 1. If we include this possibility, we obtain eqn. (350) again but with dL_1/dt replaced by $[(dL_1/dt) + R_1^{(av)} J_0^{(Oxv)}]$.

Equivalently, denoting $J_0^{(Oxv)}$ by $J_0^{(av)}$, we obtain

$$\frac{dL_1}{dt} = B'_{10} J_0^{(av)} + B'_{11} J_1^{(av)} + B'_{12} J_2^{(av)} \tag{352}$$

with

$J_0^{(av)}$ = anion vacancy current through L_1 required to supply the oxygen solution current into the metal (353)

$$B'_{10} = -R_1^{(av)} \tag{354}$$

$$B'_{11} = R_1^{(av)} (1 + \lambda_2) \tag{355}$$

and

$$B'_{12} = -R_1^{(av)} \lambda_2 \tag{356}$$

These coefficients B'_{10}, B'_{11}, and B'_{12} are consistent with the general definitions (346)—(348) if we make the choice

$$\lambda_1 = 0 \tag{357}$$

which is allowable since λ_1 is not defined by eqn. (229).

The other extreme layer, viz. L_N, undergoes no decomposition at $x_N = L_N$, since there is no layer $N + 1$; therefore $(dL_N/dt)_- = 0$. The formation rate $(dL_N/dt)_+$ at $x_N = 0$ requires the usual anion vacancy difference current $(J_N^{(av)} - J_{N-1}^{(av)})$ in addition to the equivalent current

$J_N^{(\mathrm{Oxv})}$ [see eqn. (334)] which is provided by the decomposition of layer $N-1$. Thus, we can write

$$\frac{dL_N}{dt} = R_N^{(\mathrm{av})} \left[(J_N^{(\mathrm{av})} - J_{N-1}^{(\mathrm{av})}) + J_N^{(\mathrm{Oxv})} \right] \tag{358}$$

Utilizing eqns. (334) and (343), we obtain

$$\begin{aligned} \frac{dL_N}{dt} &= R_N^{(\mathrm{av})} (J_N^{(\mathrm{av})} - J_{N-1}^{(\mathrm{av})}) + \lambda_N R_N^{(\mathrm{av})} (J_N^{(\mathrm{av})} - J_{N-1}^{(\mathrm{av})}) \\ &= R_N^{(\mathrm{av})} (1 + \lambda_N) (J_N^{(\mathrm{av})} - J_{N-1}^{(\mathrm{av})}) \end{aligned} \tag{359}$$

This ignores any evaporation of oxide at the gas interface ($x_N = L_N$). If such occurs, the evaporation rate $(dL_N/dt)_{\mathrm{evap}}$, considered to have a positive sign if evaporation is indeed occurring, will decrease the net growth rate of layer N, so that (dL_N/dt) in eqn. (359) should then be replaced by $[(dL_N/dt) + (dL_N/dt)_{\mathrm{evap}}]$. Equivalently, we can write

$$\frac{dL_N}{dt} = B'_{N,N-1} J_{N-1}^{(\mathrm{av})} + B'_{NN} J_N^{(\mathrm{av})} + B'_{N,N+1} J_{N+1}^{(\mathrm{av})} \tag{360}$$

where

$$B'_{N,N-1} = -R_N^{(\mathrm{av})} (1 + \lambda_N) \tag{361}$$

$$B'_{NN} = R_N^{(\mathrm{av})} (1 + \lambda_N) \tag{362}$$

and

$$B'_{N,N+1} J_{N+1}^{(\mathrm{av})} = -\left(\frac{dL_N}{dt} \right)_{\mathrm{evap}} \tag{363}$$

These definitions for $B'_{N,N-1}$ and B'_{NN} are consistent with the general definitions (346) and (347) if we make the choice

$$\lambda_{N+1} = 0 \tag{364}$$

which is allowable because λ_{N+1} is not defined by eqn. (229).

Let us now summarize our results for the anion vacancy case. The growth equations for the N layers can be written in the form

$$\frac{dL_i}{dt} = B'_{i,i-1} J_{i-1}^{(\mathrm{av})} + B'_{ii} J_i^{(\mathrm{av})} + B'_{i,i+1} J_{i+1}^{(\mathrm{av})}$$

$$(i = 1, 2, 3, \ldots, N) \tag{365}$$

where, for any specific value of i (except $i = N$)

$$B'_{i,i-1} = -R_i^{(\mathrm{av})} (1 + \lambda_i) \tag{366}$$

$$B'_{ii} = R_i^{(\mathrm{av})} (1 + \lambda_i + \lambda_{i+1}) \tag{367}$$

and

$$B'_{i,i+1} = -R_i^{(av)} \lambda_{i+1} \tag{368}$$

with the λ_i and λ_{i+1} determined from

$$\lambda_j = [(q_j/p_j)(p_{j-1}/q_{j-1}) - 1]^{-1} \quad (j = 2, 3, \ldots, N) \tag{369}$$

$$\lambda_1 = 0 \tag{370}$$

and

$$\lambda_{N+1} = 0 \tag{371}$$

and with

$$J_0^{(av)} = \text{magnitude of oxygen solution current into the parent metal} \tag{372}$$

For $i = N$, we utilize the convention

$$\lambda_{N+1} = 0 \tag{373}$$

stated by eqn. (371), in which case the coefficients $B'_{N,N-1}$ and B'_{NN} are given by eqns. (366) and (367), but $B'_{N,N+1}$ is still defined by

$$B'_{N,N+1} J_{N+1}^{(av)} = -\left(\frac{dL_N}{dt}\right)_{evap} \tag{374}$$

instead of by eqn. (368).

Thus a set of N coupled equations has been derived for growth of the N oxide layers. The rate coefficient appropriate for single-phase growth of each layer can be used to obtain the current $J_i^{(av)}$ through that layer. The set of such currents ($i = 1, 2, 3, \ldots, N$) then enables one to solve the set of linked equations [see eqn. (365)] for multilayer oxide growth. This set is sufficient to predict the growth kinetics for the N layers, assuming the evaporation and oxygen solution rates are known.

2.6 COMPARISON OF THE SETS OF FINAL EQUATIONS DEDUCED ABOVE FOR THE FOUR CASES

It is very informative to compare the set of equations for the anion vacancy case with the corresponding set for anion interstitial diffusion. There is a one-to-one correspondence, with the slight differences being due to the appearance of $R_i^{(av)}$ in place of $R_i^{(ai)}$ in the coefficients. This can be noted most easily by referring to Table 1. Our conclusion is that the growth equations based on anion diffusion are essentially independent of whether the anion diffusion occurs by an interstitial or a vacancy mechanism.

It is likewise informative to compare the set of equations developed for oxide growth by cation interstitial diffusion with the set developed for

TABLE 1

Coefficients H_{ij} for growth of inner layer i[a] for various mobile species

Subscript	Cation motion[b]		Anion motion[b]	
	Interstitial (ci)	Vacancy (cv)	Interstitial (ai)	Vacancy (av)
	A	A'	B	B'
$i, i-1$	$-R_i^{(ci)}\lambda_i$	$-R_i^{(cv)}\lambda_i$	$-R_i^{(ai)}(1+\lambda_i)$	$-R_i^{(av)}(1+\lambda_i)$
ii	$R_i^{(ci)}(1+\lambda_i+\lambda_{i+1})$	$R_i^{(cv)}(1+\lambda_i+\lambda_{i+1})$	$R_i^{(ai)}(1+\lambda_i+\lambda_{i+1})$	$R_i^{(av)}(1+\lambda_i+\lambda_{i+1})$
$i, i+1$	$-R_i^{(ci)}(1+\lambda_{i+1})$	$-R_i^{(cv)}(1+\lambda_{i+1})$	$-R_i^{(ai)}\lambda_{i+1}$	$-R_i^{(av)}\lambda_{i+1}$

[a]Growth of layer i is in accordance with eqn. (375). For the two outer layers, refer to the development in question for the coefficients.
[b]In all cases, $\lambda_1 = \lambda_{N+1} = 0$, whereas $\lambda_j = [(q_j/p_j)(p_{j-1}/q_{j-1}) - 1]^{-1}$ for other values of j.

oxide growth by cation vacancy diffusion. In both sets, the possibility of oxygen solution in the parent metal has been ignored. Again, we find a one-to-one correspondence with the slight differences being due to the set of volume parameters $R_i^{(cv)}$ appearing in the coefficients A'_{ij} for the cation vacancy case, whereas the corresponding set $R_i^{(ci)}$ appear in the coefficients A_{ij} for the cation interstitial case (see Table 1). Thus the growth equations based on cation diffusion are essentially independent of whether cation diffusion occurs by an interstitial or a vacancy mechanism. These conclusions are remarkable in view of the vast difference in the mental pictures we used above in evaluating the solid-state transformations involved in the individual layer growth for the interstitial and the vacancy mechanisms.

A comparison of the set of equations deduced for the cases of anion and cation diffusion is also quite informative. Except for the omission of a term for oxygen solution in the parent metal in the case of growth by cation diffusion, the appearance of the growth equations is the same [compare eqn. (247) with the analogous set given by eqn. (320), for example]. However, an examination of Table 1 shows that the coefficients are somewhat different. Compare, for example, the A_{ij} given by eqns. (248)–(250) for the cation interstitial case with the B_{ij} given by eqns. (321)–(323) for the anion interstitial case. The origin of the differences is not due to the direction of the defect currents, since we have already noted above the close parallel between the equations for the cation vacancy and the cation interstitial cases where the defect currents are in opposite directions. Instead, the difference has its origin in the type of species (metal or oxygen) which is mobile. If the metal species is mobile, then the oxygen balance will demand that the growth of layer i involves the decomposition of an adjacent oxygen-richer layer, namely, layer $i + 1$. The growth zone for layer i occurs at $x_i = L_i$ in both cases of cation motion. On the other hand, if it is the oxygen which is mobile, the metal balance will demand that the growth of layer i involves the decomposition of an adjacent metal-richer layer, namely, layer $i - 1$. The growth zone for layer i occurs at $x_i = 0$ in both cases of anion motion.

In summary, the initially surprising conclusion of the present development is that the coefficients in the equations for growth by either anion species (anion interstitials or anion vacancies) have a somewhat different structure from the corresponding coefficients in the equations for growth by transport of a cation species. On the other hand, the coefficients in the equations for growth by a vacancy species were found to be closely analogous to the corresponding coefficients in the equations for growth by the interstitial species of the same type. That is, the coefficients in the equations for growth by cation vacancies are closely related to the coefficients in the equations for growth by cation interstitials; the coefficients in the equations for growth by anion vacancies are closely related to the coefficients in the equations for growth by anion interstitials.

References pp. 116–117

2.7 GENERAL MATRIX FORM FOR THE GROWTH EQUATIONS VALID FOR ANY SPECIFIC MOBILE DEFECT SPECIES

In the four separate developments given above in Sects. 2.2—2.5, the growth equations for the first and the last layers were found to differ somewhat from the set of growth equations for the intermediate layers. Nevertheless, it was shown how the kinetic equations for the first and last layers could be rewritten so that they had the same formal appearance as the equations for the intermediate layers. This leads to a more compact form, though the content is, of course, unchanged by this device. Now, in the preceding section, some differences were noted between the cation and the anion cases regarding the physical interpretation of the coefficients appearing in the respective sets of equations. Nevertheless, if one does not examine the specific nature of the coefficients, but instead simply examines the equations for overall form, then it can be noted by comparing the four sets given by eqns. (247), (283), (320), and (365), that the general form is the same. Thus we may write the coupled growth equations in the generalized form

$$\frac{dL_i}{dt} = H_{i,i-1} J_{i-1} + H_{ii} J_i + H_{i,i+1} J_{i+1}$$

$$(i = 1, 2, \ldots, N) \tag{375}$$

with the H_{ij} depending specifically on which of the four cases we are dealing with in a particular application.

This generalized form is susceptible to an even more compact notation by employing matrix equations. Suppose that we define additional coefficients H_{ij} for $j \neq i-1$, i, or $i+1$. These coefficients are not directly involved in the coupled growth equations, so we assign their value to be zero. That is

$$H_{ij} = 0 \qquad (j \neq i-1, i, i+1) \tag{376}$$

The generalized form (375) of the growth equations can then be written as

$$\frac{dL_i}{dt} = \sum_{j=0}^{N+1} H_{ij} J_j \qquad (i = 1, 2, 3, \ldots, N) \tag{377}$$

We may change the lower limit from 0 to 1 and the upper limit from $N+1$ to N if we redefine dL_1/dt and dL_N/dt to be the growth rates for layers 1 and N excluding any effects of oxygen solution into the parent metal and excluding any oxide evaporation, respectively. Alternatively, we can simply write the growth equations [eqn. (377)] in the matrix form

$$\begin{pmatrix} dL_1/dt + (dL_1/dt)_{soln} \\ dL_2/dt \\ \cdot \\ \cdot \\ \cdot \\ (dL_N/dt) + (dL_N/dt)_{evap} \end{pmatrix} = \begin{pmatrix} H_{11} & H_{12} & H_{13} & \cdots & H_{1N} \\ H_{21} & H_{22} & H_{23} & \cdots & H_{2N} \\ \cdot & \cdot & \cdot & \cdots & \cdot \\ \cdot & \cdot & \cdot & \cdots & \cdot \\ \cdot & \cdot & \cdot & \cdots & \cdot \\ H_{N1} & H_{N2} & H_{N3} & \cdots & H_{NN} \end{pmatrix} \begin{pmatrix} J_1 \\ J_2 \\ \cdot \\ \cdot \\ \cdot \\ J_N \end{pmatrix} \tag{378}$$

This can be abbreviated as

$$\dot{\mathbf{L}} = \mathbf{HJ} \tag{379}$$

with the obvious identification of the boldface operators in eqn. (379) with the corresponding matrices in eqn. (378). This constitutes a very compact notation for the four sets of growth kinetics equations.

Conclusion

Thus we conclude our presentation of some of the most fundamental aspects of the chemical reactions leading to oxide film formation and growth on metals. The growth of oxide layers on metals involves surface and interfacial reactions which drive ion and electron transport through already-formed oxide layers. Various aspects of these interesting phenomena were surveyed, with especial attention paid to the role of built-in surface-charge and space-charge fields in determining the kinetics of growth of the oxide layers. Emphasis has been placed throughout on the fundamentals of electric-field effects since this aspect of metal oxidation is little understood by most people at the present time. It is sincerely hoped that this review will prove to be helpful to students and researchers in fields other than metal oxidation, as well as to those working in the field.

Acknowledgements

This review summarizes the content of a series of lectures given by one of the authors (A.T.F.) at Hokkaido University in Sapporo, Japan, in July, 1979. Abbreviated versions were presented in lectures given at the Research Institute for Iron, Steel, and other Metals at Tohoku University in Sendai, Nippon Steel Corporation Fundamental Research Institute in Kawasaki, and before the Faculty of Engineering at Kyoto University. Fincancial support by the Japanese Society for the Promotion of Science (J.S.P.S.) and the creative stimulus provided by the Faculty of Engineering

of Hokkaido University are most gratefully acknowledged. The authors wish to thank their son, Thomas William Fromhold, for drawing the figures.

References

1 F.S. Stone, Chemistry of the Solid State, Butterworths, London, 1955, p. 370.
2 P.H. Emmett, in R. Gomer and C.S. Smith (Eds.), Structure and Properties of Solid Surfaces, University of Chicago Press, Chicago, IL, 1953, p. 430.
3 H.H. Uhlig, in Metal Interfaces, American Society for Metals, Cleveland, OH, 1952, p. 317.
4 J.W. May, Adv. Catal., 21 (1970) 151.
5 A.T. Fromhold, Jr. and E.L. Cook, J. Appl. Phys., 38 (1967) 1546.
6 A.T. Fromhold, Jr., J. Electrochem. Soc., 127 (1980) 411.
7 A.T. Fromhold, Jr. and A.-B. Chen. Phys. Status Solidi B, 90 (1973) K21.
8 A.T. Fromhold, Jr., J. Chem. Phys., 69 (1978) 5192.
9 A.T. Fromhold, Jr. and E.L. Cook, Phys. Rev. Lett., 17 (1966) 1212.
10 A.T. Fromhold, Jr., Theory of Metal Oxidation, Vol. I, North-Holland, Amsterdam, 1976.
11 A.T. Fromhold, Jr., Theory of Metal Oxidation, Vol. II, North-Holland, Amsterdam, 1980.
12 S.R. Weart (Ed.), Selected Papers of Great American Physicists, American Institute of Physics, NY, 1976, p. 10.
13 C. Kittel, W.D. Knight and M.A. Ruderman, Mechanics, McGraw-Hill, New York, 1965, p. 356.
14 E.M. Purcell, Electricity and Magnetism, McGraw-Hill, New York, 1965, p. 174.
15 A.T. Fromhold, Jr., in J.V. Cathcart (Ed.), Stress Effects and the Oxidation of Metals, The Metallurgical Society of AIME, New York, 1975, pp. 36—39.
16 A.T. Fromhold, Jr., Theory of Metal Oxidation, Vol. I, North-Holland, Amsterdam, 1976, Appendix C.
17 A.T. Fromhold, Jr., S.R. Coriell and J. Kruger, J. Phys. Soc. Jpn., 34 (1973) 1452.
18 A.T. Fromhold, Jr., Quantum Mechanics for Applied Physics and Engineering, Academic Press, New York, 1981, pp. 108, 250.
19 A.T. Fromhold, Jr., Theory of Metal Oxidation, Vol. I, North-Holland, Amsterdam, 1976, pp. 74—81.
20 W.H. Butler and A.T. Fromhold, Jr., J. Phys. Chem. Solids, 35 (1974) 1099.
21 A.T. Fromhold, Jr., Oxid. Met., 13 (1979) 475.
22 A.T. Fromhold, Jr., Theory of Metal Oxidation, Vol. I, North-Holland, Amsterdam, 1976, pp. 157—159.
23 A.T. Fromhold, Jr., Theory of Metal Oxidation, Vol. II, North-Holland, Amsterdam, 1980, Chaps. 16, 17.
24 A.T. Fromhold, Jr. and E.L. Cook, Phys. Rev., 175 (1968) 877.
25 A.T. Fromhold, Jr., in J.W. Diggle and A.K. Vijh (Eds.), Oxides and Oxide Films, Vol. 3, Marcel Dekker, New York, 1976.
26 A.T. Fromhold, Jr., Theory of Metal Oxidation, Vol. II, North-Holland, Amsterdam, 1980, Chap. 13.
27 B.E. Deal and A.S. Grove, J. Appl. Phys., 36 (1965) 3770.
28 A.T. Fromhold, Jr., J. Phys. Soc. Jpn., 48 (1980) 2022.
29 A.T. Fromhold, Jr., Theory of Metal Oxidation, Vol. II, North-Holland, Amsterdam, 1980, Chap. 15.

30 N. Cabrera and N.F. Mott, Rep. Prog. Phys. 12 (1949) 163.
31 A.T. Fromhold, Jr., J. Phys. Chem. Solids, 33 (1972) 95.
32 N.F. Mott, Trans. Faraday Soc., 35 (1939) 1175.
33 N.F. Mott, Trans. Faraday Soc., 36 (1940) 472.
34 N.F. Mott, Trans. Faraday Soc., 43 (1947) 429.
35 R. Ghez, J. Chem. Phys., 58 (1973) 1838.
36 F.P. Fehlner and N.F. Mott, Oxid. Met., 2 (1970) 59.
37 A.T. Fromhold, Jr. and E.L. Cook, J. Chem. Phys., 44 (1966) 4564.
38 A.T. Fromhold, Jr. and E.L. Cook, Phys. Rev., 158 (1967) 600.
39 A.T. Fromhold, Jr. and E.L Cook, Phys. Rev., 163 (1967) 650.
40 R.B. Mosley and A.T. Fromhold, Jr., Oxid. Met., 8 (1974) 19.
41 R.B. Mosley and A.T. Fromhold, Jr., Oxid. Met., 8 (1974) 47.
42 A.T. Fromhold, Jr. and J. Kruger, J. Electrochem. Soc., 120 (1973) 722.
43 A.T. Fromhold, Jr., J. Electrochem. Soc., 124 (1977) 538.
44 A.T. Fromhold, Jr., J. Phys. Chem. Solids, 24 (1963) 1081.
45 A.T. Fromhold, Jr., Theory of Metal Oxidation, Vol. I, North-Holland, Amsterdam, 1976, pp. 104, 105.
46 A.T. Fromhold, Jr., Phys. Lett. A, 58 (1976) 118.
47 A.T. Fromhold, Jr., Theory of Metal Oxidation, Vol. I, North-Holland, Amsterdam, 1976, p. 135.
48 A.T. Fromhold, Jr., Theory of Metal Oxidation, Vol. I, North-Holland, Amsterdam, 1976, Chap. 7.
49 A.T. Fromhold, Jr., Theory of Metal Oxidation, Vol. I, North-Holland, Amsterdam, 1976, Chap. 12.
50 C.D. Hodgman, R.C. Weast, C.W. Wallace and S.M. Selby (Eds.), Handbook of Physics and Chemistry, Chemical Rubber Publishing Co., Cleveland, OH, 36th edn., 1954, pp. 506, 512, 528.
51 E.G. Clark, Jr. and A.W. Czanderna, Surf. Sci., 49 (1975), 529.
52 O. Kubaschewski and B.E. Hopkins, Oxidation of Metals and Alloys, Butterworths, London, 1962, pp. 2, 103, 113.
53 G.J. Yurek, J.P. Hirth and R.A. Rapp, Oxid. Met., 8 (1974) 265.
54 G. Garnaud and R.A. Rapp, Oxid. Met., 11 (1977) 193.
55 G. Garnaud, Oxid. Met., 11 (1977) 127.
56 J. Paidassi, M.G. Vallee and P. Pepin, Mem. Sci. Rev. Metall., 62 (1965) 789.
57 F. Gesmundo and F. Viani, Corros. Sci., 18 (1978) 217.
58 G.J. Yurek, J.V. Cathcart and R.E. Pawel, Oxid. Met., 10 (1976) 255.
59 R.E. Pawel, J.V. Cathcart and R.A. McKee, J. Electrochem. Soc., 126 (1979) 1105.
60 A.T. Fromhold, Jr., J. Chem. Phys., 76 (1982) 4260.
61 A.T. Fromhold, Jr. and N. Sato, Phys. Lett. A, 84 (1981) 219.
62 A.T. Fromhold, Jr. and N. Sato, Oxid. Met., 16 (1981) 203.
63 F.A. Kröger, The Chemistry of Imperfect Crystals, North-Holland, Amsterdam, 1964.
64 H. Schmalzried, Reaction Kinetics in Heterogeneous Chemical Systems, Elsevier, New York, 1975, p. 558.
65 P. Mark and S.C. Chang, Oxides and Oxide Films, Vol. 3, Dekker, New York, 1976, p. 273.

This Page Intentionally Left Blank

Chapter 2

Reactions of Solids with Gases other than Oxygen

Y. KOGA and L.G. HARRISON

1. Introduction

The general theme of this chapter could be taken to cover a wide variety of rather disparate topics, in most of which either application is far ahead of fundamental knowledge or vice versa. In these not very satisfactory circumstances, we have chosen, despite the general title of this series, to make this account more selective than comprehensive.

The gas other than oxygen which has been most extensively studied as a reactant with solids is, of course, hydrogen and the first and longest section of this chapter is therefore devoted to gaseous reduction. The theory of this topic, especially in relation to iron oxides [1, 2], well exemplifies much of the general theory of solid state kinetics as reviewed by one of us [3] in an earlier volume of this series. For the present purpose, therefore, we have reworked the necessary discussion of kinetic equations into the specific topic of Sect. 2.

Hydrogen, besides reducing oxides to the metal, has important interactions with the fully reduced elemental metals; it dissolves in a variety of metals to very variable extent and it affects the mechanical properties of some metals. Steel more readily undergoes brittle fracture when it is contaminated with hydrogen. From the viewpoint of application, this is important in relation to the nature of the product of a hydrogen reduction; fundamentally, the phenomenon is of interest in that its mechanism seems to involve an interaction between mechanical strain and diffusion of hydrogen.

Reaction of solids with halogens has been much less widely studied because it has less application. Studies have tended to be mostly in the realm of pure chemistry and have turned up some curiosities in the behaviour of defects, especially electronic defects. The role of such species as reaction intermediates, especially in transport to and from reaction interfaces, is not very well understood and, in our opinion, is probably generally rather underestimated. Two major obstacles to the study of these species are their transient nature at high temperatures and the absence of detailed information about them in the oxides, because the lack of nuclear spin on ^{16}O greatly limits the information obtained from the technique, electron spin resonance, which has been most valuable for the halides.

The rate of a gas—solid reaction may be controlled primarily by rates of transport to the reaction interface or by rates of reaction at the

References pp. 146—149

interface. In the latter case, it is important to try to determine the actual activities or concentrations of species in the reaction interface. Various ways in which one may attempt to do this are indicated in Sect. 5.

In the past seventy years, the rate of deterioration of ancient stonework in industrial areas has markedly increased as a result of increased atmospheric pollution, especially by sulphur oxides. The reactions causing this trouble are obviously of interest in relation to the preservation of ancient sculpture and buildings. This topic also, however, raises a question as to the limits of the term "gaseous reactant". The reactions causing damage almost invariably involve water molecules, but not necessarily water supplied in the liquid form as rain. Water adsorbed from atmospheres from 50 to 100% relative humidity is very important; and the principal carriers of the destructive sulphate ion appear to be aerosol droplets ranging in size from a little above molecular dimensions to about 0.01 μm, i.e. on the very borderline between gaseous mixture and separation of a condensed liquid phase.

2. Gaseous reduction of solids

2.1 KINETICS

A voluminous literature exists on the kinetics of gaseous reduction of solids in connection with industrial applications. In particular, that of iron oxides has been comprehensively reviewed by Manning and Philbrook [1]. As these authors evaluate the situation: "Although the science of iron ore reduction is nearly a hundred years old, it is still best characterized by uncertainty, by inconsistent experimental data and by conflicting theories". This evaluation seems to us quite adequate (except, perhaps, that a case could be made for replacing "a hundred years" by "three thousand years"), and the statement is applicable to reductions of other solids.

As is common to general topochemical reactions involving solids, the observed rate of reduction, R, can usually be expressed in terms of a rate r per unit area of reaction interface, multiplied by a surface area, S, which may evolve in many possible ways in time, t, viz.

$$R(T, C_i, t) = r(T, C_i) \cdot S(t) \tag{1}$$

Here, T is temperature and C_is are concentrations of reactants, intermediates and products. Very occasionally, in the entire field of solid—gas reactions, intermediates are formed in such a way that reaction rate is not proportional to surface area and eqn. (1) is violated. This has been observed in halide—halogen reactions (Sect. 4) but not in reductions. The specific rate, r, may be controlled by chemical reaction at the reaction interface, or by diffusion of reactants and products through either the gas phase or the solid reacted zone. Therefore, numerous expressions for r are

possible [1—3]. Generally, factors influencing the mechanisms in heterogeneous systems are many and difficult to control. They include both microscopic (diffusivities, defects, reaction mechanisms) and macroscopic systems (particle size distribution, particle shape, and, for pellets, pore shape and size distribution). Thus, totally different rate expressions may arise for different experiments with the same chemical system. This is a principal reason for the unsatisfactory experimental picture referred to above in the quotation from Manning and Philbrook.

The behaviour of S as a function of time t can be crudely classified into two cases. The first corresponds to formation of nuclei of the product and their growth. As shown schematically in Fig. 1, the reaction interface increases until growing nuclei overlap extensively and then decreases, resulting in a sigmoidal dependence of the extent of reaction, α, on time t. When diffusion is not significant, the early stage of the nucleation is described by a "power law" dependence of α on t

$$\alpha = kt^n \tag{2}$$

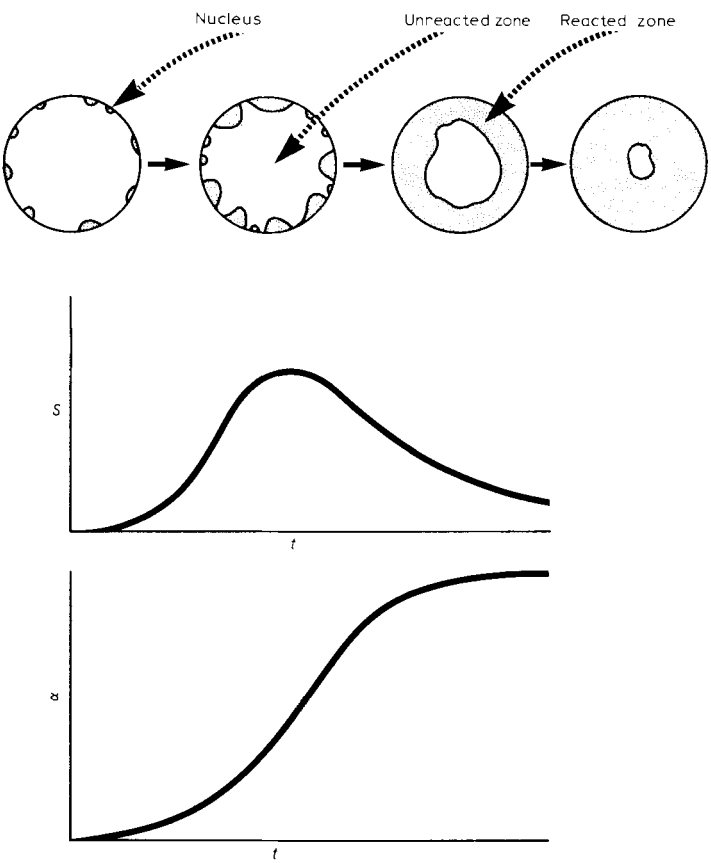

Fig. 1. Nucleation and growth model.

Usually, $n \geqslant 3$. When nuclei start to overlap, the extent of reaction depends on time via the Avrami—Erofeev—Mampel expression

$$\alpha = 1 - \exp(kt^m) \tag{3}$$

The detailed theoretical treatment of these rate equations, as well as others for the second case discussed below, was reviewed extensively by Harrison [3]. Examples of recent studies showing this type of behaviour are the reduction of NiO with H_2 [36] and the reduction of MoO_3, MoO_3—Al_2O_3 and Co_3O_4—MoO_3—Al_2O_3, which are commonly used as hydrosulfurization catalysts [37]. In both these cases, reduction kinetics were fitted to eqn. (3).

The work on NiO/H_2 [36, 38] has indicated an unexpected correlation of reactivity with magnetic properties. The rate of reduction was observed to decrease above the Néel point (265°C) of NiO. Delmon and Roman [36] studied the reaction of a well-crystallized NiO powder with a narrow particle size distribution. By a novel experimental procedure, they separated the dependences on S and r in eqn. (1) and found that the effect of the Néel transition is solely on S and not on r; i.e. the effect is upon the rate of formation of nuclei, not on the rate of advance of their surfaces once formed. By applying Mampel's treatment, they extracted the activation energy of nucleation from the dependence of S on T, and found it to be 142 kJ mole^{-1} below the Néel temperature and 188 kJ mole^{-1} above. As these authors indicate, it is indeed surprising that a change in a bulk property should affect a surface phenomenon. (Strong magnetic fields, of the order of 1000 Oe, have been observed to influence the rate of reduction of Fe_2O_3, Fe_3O_4 and FeO by H_2 [39, 41, 43]. Various explanations have been given and disputed, but none as yet is satisfactory [39—43].)

Another example of an effect of magnetic properties on reactivity was found in the oxidation of Fe_3O_4 to Fe_2O_3 [127]. The Arrhenius plot of the rate data showed no significant change in slope well below and well above the Curie temperature (578°C). In the temperature range from 560 to 640°C, however, an anomalous deviation (a maximum and a minimum on log k), known as the Hedvall effect [128], was observed. No satisfactory explanation has yet been given.

In the second case, as shown in Fig. 2, the entire surface of the reactant particle is covered with a thin layer of the solid product very soon after contacting the reactant gas and the reaction boundary advances inward as reaction proceeds. This model has been known as the "shrinking core" model [2, 3] and has been used by many investigators. Since the functional dependence of S on t behaves well in this model, provided that the assumption of smooth advancement of the reaction boundary without changing its shape is valid, consideration of a variety of forms of r can conveniently be included and the kinetics can be described up to the completion of reaction. Moreover, even in the first case, in which the

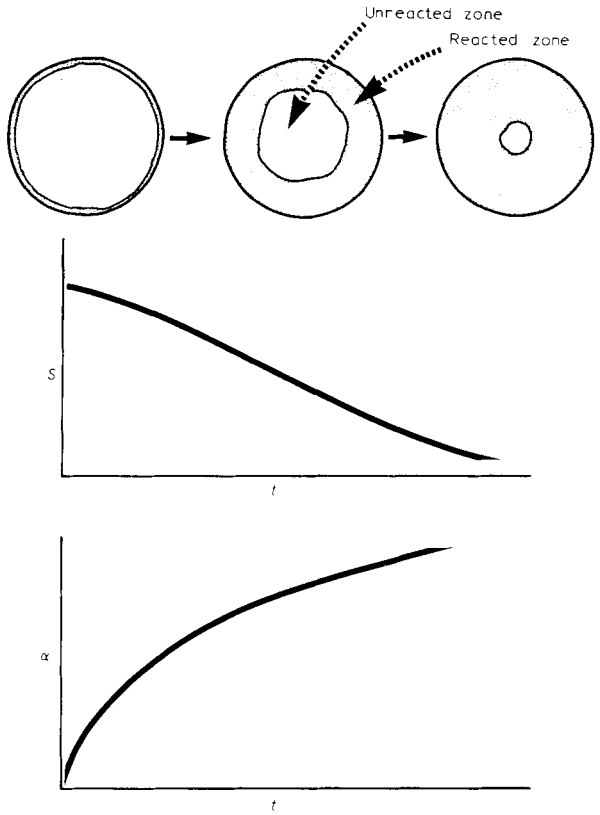

Fig. 2. Shrinking unreacted core model.

initial stage is governed by nucleation and growth of nuclei, the later stage, after nuclei overlap completely, can be well approximated with this model. Most work reported in engineering journals has dealt with this model [1, 2].

In contrast, work published in journals of pure chemistry is usually concerned with reaction at the boundaries and commonly only initial rates are measured so that complications due to diffusion can be neglected. The results and conclusions in such studies are naturally different from case to case and will be enumerated later. First, however the "shrinking core" model will be reviewed.

As shown in Fig. 3, the overall resistance to the reaction is considered to consist of three steps: (i) gas phase mass transfer; (ii) diffusion through the porous reacted zone (in reduction the solid products are generally smaller in volume than the reactants), and (iii) chemical reaction at the boundary. Additional assumptions usually made are

(a) the boundary between the reacted and the unreacted zones is sharp;

(b) the above three resistances are additive (quasi-steady state assumption);

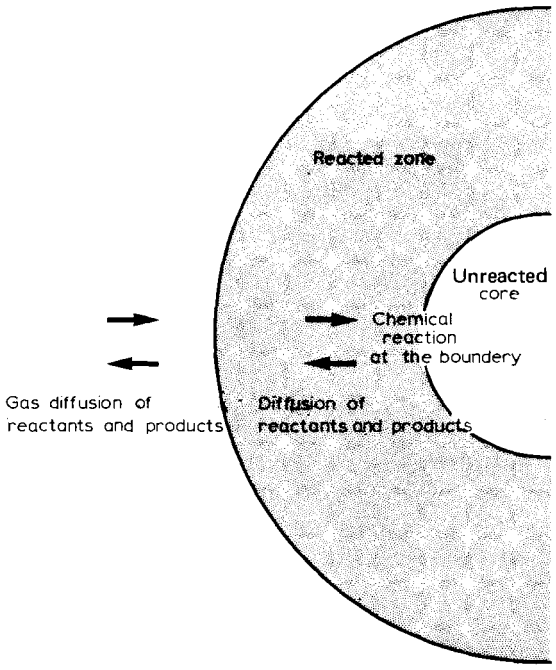

Fig. 3. Detail of shrinking unreacted core model.

(c) the chemical reaction is of first order with respect to the reactant;

(d) the shape of particles does not change during the course of reaction; and

(e) reaction is isothermal.

When one of the above three resistances is predominant and the other two are negligible, the basic mass balance differential equation can be integrated and gives expressions for the relation between the extent of reaction and time, both being experimentally observable. Typical results are given below. For detailed derivation see ref. 1—3.

(i) Gas phase mass transfer is the rate-determining step.

$$t = k_1 \alpha \tag{4}$$

(ii) Diffusion through the reacted zone is the rate-determining step.

$$\text{(a) } t = k_{2a}\alpha^2 \quad \text{plate} \tag{5}$$

$$\text{(b) } t = k_{2b}[\alpha + (1-\alpha)\ln(1-\alpha)] \quad \text{cylinder} \tag{6}$$

$$\text{(c) } t = k_{2c}[1 - 3(1-\alpha)^{2/3} + 2(1-\alpha)] \quad \text{sphere} \tag{7}$$

$$\text{(d) } t = k_{2d}[1 - (1-\alpha)^{2/3} - [1/(\beta-1)][\{1 + (\beta-1)\alpha\}^{2/3} - 1]] \tag{8}$$

Equations (7) and (8) both apply to a sphere. β is the ratio of product volume to reactant volume in the layer of product through which diffusion takes place. When $\beta = 1$, (8) reduces to eqn. (7). This should be the case if reduced material retains its gross geometry, with pores produced in it to account for the entire decrease in volume upon reaction. Equation (7) is known as the Ginstling—Brounshtein equation; eqn. (8) is Carter's modification of it [88] and must be used if there is a volume increase on reaction. This does not often happen in reductions, but can occur in other types of reaction [89].

(iii) Chemical reaction at the sharp boundary is the rate-determining step.

$$t = k_3[1 - (1 - \alpha)^{1/F}] \tag{9}$$

where F is a shape factor and takes the value 1, 2 and 3 for plate, cylinder and sphere, respectively. There have been some experimental results which fit to the above cases (see refs. 1 and 3 and the references therein). Recent examples are the reduction of Ni_3S_2 by H_2 [4], Fe_2O_3 to Fe_3O_4 by $CO—CO_2$ gas mixtures [135] [case (iii) with $F = 3$] and the reduction of PbO by CO/CO_2 gas mixtures [5] [case (iia)]. Also, there are many cases [1] where the diffusion through the reacted zone and the chemical reaction at the boundary contribute comparably to the kinetics; in other cases, even the gas phase diffusion should be taken into account. When an attempt is made to fit experimental results to the theoretical equations, reasonable estimates are made for the diffusion coefficients through the reacted zone and the gas phase, but the rate coefficient for the chemical reaction can be adjusted freely, resulting in a fictitiously good fit. Attempts are usually made to circumvent the complication due to gas phase diffusion. The standard practice is to check that overall rate is independent of the flow rate of the reactant gas. This common presumption has been criticized and disputed [139—141].

Often, the same expressions from this model are applied to the reductions of pellets, in which cases such structural factors as particle size distribution, porosity and pore shape, its size distribution, etc. should really affect the whole kinetics. Thus, the application of this model to such systems has been criticised as an oversimplification and a more realistic model has been proposed [6—12, 136] in which the structure of pellets is explicitly considered to consist of pores and grains and the boundary is admitted to be diffusive due to some partly reduced grains, as shown in Fig. 4. Inevitably, the mathematics becomes very complicated and the matching with experimental results is not straightforward. To cope with this difficulty, Sohn and Szekely [11] employed dimensional analysis and introduced a dimensionless number, σ, given by

$$\sigma = \frac{F_p V_p}{A_p} \sqrt{\frac{(1 - \epsilon) k C_{Ao}^{n-1}}{D_e} \frac{A_g}{V_g}} \tag{10}$$

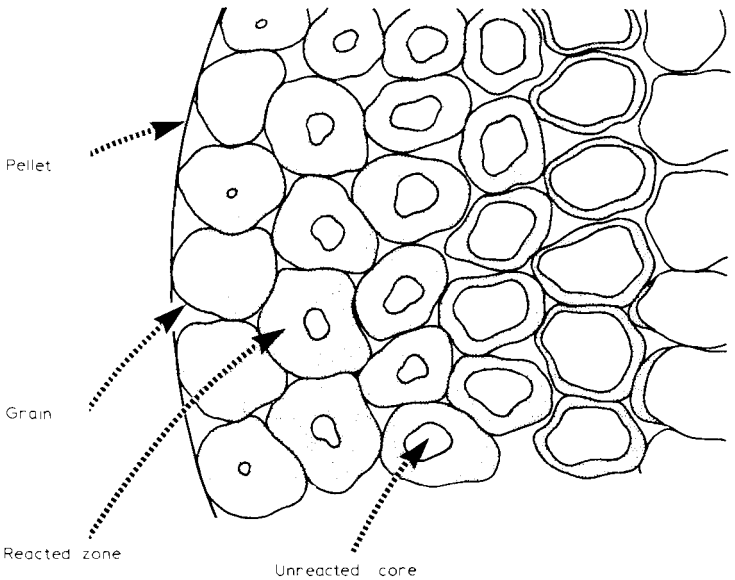

Fig. 4. Detail of partly reacted pellet.

where F is the shape factor (1, 2 and 3 for flat plates, cylinder and sphere, respectively), V is the volume, A is the external surface area, subscripts g and p denote grain and pellet, respectively, ϵ is the porosity of the pellet, k is the reaction rate coefficient, C_{Ao} is the gaseous reactant concentration in the bulk, n is the order of reaction with respect to the gaseous reactant concentration and D_e is the effective diffusivity in the porous pellet. When $\sigma \to 0$, chemical reaction is rate determining and the same expression as eqn. (9) results, k_3 and F being parameters pertinent to grains. When $\sigma \to \infty$, the overall rate is solely controlled by the diffusion of the gaseous reactant within the pellet and the same solutions as eqns. (5)—(7) will result. By controlling experiments so that the two asymptotic regimes ($\sigma \to 0$ and $\sigma \to \infty$) can be realized, e.g. by changing the value of V_p/A_p by varying the size of pellet, the parameters for chemical kinetics and for diffusion can be obtained separately. Then, by using these parameters, the behaviour of the system can be predicted in the intermediate region according to this theory. Attempts to apply this principle were made for the reduction of NiO pellets by H_2 (after an induction period) in the temperature range 224—412°C [12], the hydrogen reduction of cobalt ferrite [137] and the reduction of wüstite discs with CO [138]. The matching, however, is not necessarily a perfect one. Moreover, an inevitable assumption had to be made that the chemical reaction is of the first order with respect to the reactant gas. Hence no insight can be gained as to the reaction mechanism at the molecular level.

Nabi and Lu [13] have cast doubt on this general assumption that chemical reaction is first order with respect to the reactant and have studied the reduction $Fe_2O_3 \to Fe_3O_4$ by H_2 in the temperature range 650—800°C. They measured the initial rate of reaction of a perfectly

spherical and well-sintered sample of hematite. The reduction was allowed to proceed only up to 6% conversion so that the mass transfer process was negligible. They then analysed data in the following manner: reasonable reaction mechanisms were assumed and a rate expression for every possible rate-determining step for each mechanism was written down; then each rate equation with multiple parameters was fitted to the experimental results. In this way, the rate equation

$$\text{rate} = A + Bp_{H_2}^{1/2} + Cp_{H_2O} \tag{11}$$

was decided to be the best approximation, since the parameters A, B and C obtained happened to be thermodynamically quite reasonable. A compatible mechanism is

$$\begin{aligned} &H_2(g) + O_s{-}O_s \longrightarrow \overset{*}{H}O{-}\overset{*}{O}H && \text{(adsorption)} \\ &\overset{*}{H}O{-}OH + H_2(g) \longrightarrow H_2\overset{*}{O}{-}\overset{*}{O}H_2 && \text{(surface reaction)} \\ &H_2\overset{*}{O} \longrightarrow H_2O(g) + s && \text{(desorption)} \end{aligned} \tag{12}$$

where * indicates adsorbed species, and $O_s{-}O_s$ and s are the adjacent oxygen sites and the site on the hematite surface, respectively.

For the reduction of NiO by CO in the temperature range 566—796°C, the kinetics were determined by the initial rate method and the rate expression was found to be of the first order with respect to CO [14].

Evidence that reaction with hydrogen may sometimes be autocatalytic arises in the so-called "hydrogen spillover" effect [44]. For the reduction of oxides, a minute amount of metal (Pt, Pd, Au, Cu, Ag, Co, Ti, Fe, etc.) added (even mechanically mixed) speeds up the reaction considerably. This effect is understood as the activation of hydrogen on the added metal and the subsequent migration of the activated hydrogen towards the oxide surface. One of the recent studies [45] on the effect of added Pt on the reduction of Co_3O_4, Fe_2O_3, UO_3, Ni_3O_4, MnO_2 and V_2O_5 showed that the activation energies are all the same as that of the desorption of hydrogen from Pt, $96 \pm 8\,\text{kJ mole}^{-1}$. The reduction of V_2O_5 with hydrocarbons, C_3H_6, C_2H_4, C_3H_8, C_2H_6, etc., showed the same effect of added noble metals and it was interpreted as due to the same hydrogen activation mechanism [46]. In this connection, it was suggested [32, 47] that the sigmoidal nature of α vs. t curves in the reduction of MoO_3 and WO_3, which is commonly interpreted as due to nucleation, could well be explained by the autocatalytic effect of the small amounts of low-valent Mo and W formed at the surfaces via the hydrogen spillover effect.

Grunze and Hirschwald [15] developed a vacuum microthermobalance with cold fingers and studied the reduction of ZnO by H_2 and CO in the temperature range 450—1000°C. By making sure that the reaction products, Zn and CO_2 or H_2O, were removed to cold traps as fast as they formed, they were able to measure the intrinsic surface reaction rates. The reaction order, n, depended on temperature and pressure; for $T > 700$°C and $p < 1$ torr, $n \leq 1$ and for $T < 500$°C and $p > 1$ torr, $n \simeq 0.2$ [16].

Imoto et al. [79—81] followed the reduction by monitoring the hydrogen pressure (60—20 torr) in an enclosed system at 690—738°C and concluded that the reaction is not really a gas—solid reaction but proceeds via the two steps

$$ZnO\ (solid) \longrightarrow Zn_{(vapor)} + O_{(vapour)}$$

$$O + H_2 \longrightarrow H_2O$$

When the amount of the sample was small, it was found that the first step controlled the overall rate. Upon increasing the amount of ZnO and hence the availability of O, the second process became rate-determining. This conclusion was supported by a separate study of the decomposition of ZnO [82].

Imoto et al. [83] also determined the rate equation using a flow reactor at low pressures of H_2 (3×10^{-4} to 10^{-3} torr) and at 660—780°C as

$$1 - (1 - \alpha)^{1/3} = kt\left\{\frac{P_{H_2}}{(1 + K_H P_{H_2} + K_N P_{N_2})^2}\right\} \tag{13}$$

where K_H and K_N are the equilibrium constants for adsorption of H_2 and N_2 respectively. This rate equation is not incompatible with the results of Gruntz et al., mentioned above, that the order of the reaction is ≤ 1 for $P_{H_2} < 1$ torr.

The reduction of UO_3 to UO_2 has drawn much attention in connection with the preparation of fuels for nuclear reactors. Above 400°C, in which temperature range most of the reductions have been studied, the oxides of uranium take the forms, UO_{2+x}, U_4O_9, $U_3O_{8-x}(UO_{2.6})$ and UO_3, as in Fig. 5 [65]. In common with other gas—solid reactions, the details of the kinetics vary depending on the origin of the sample [69], the surface area [68], etc. Some authors claim that the reduction by hydrogen proceeds stepwise; $UO_3 \rightarrow U_3O_8 \rightarrow UO_2$ [66—69], but there is a report [70] that no evidence for the existence of the intermediate oxides was found by X-ray diffraction at the reaction boundary of UO_3 and UO_2.

In spite of diversity in details, however, it is striking that almost all the studies agree over two observations; for a certain range of the extent of reaction, α, corresponding roughly from $UO_{2.6}$ to $UO_{2.2}$, the rate $d\alpha/dt$ is constant [66—70] and the order of reaction with respect to hydrogen is between 0.6 and 0.9 [66—69]. Thus, the common conclusion is that for this range of α, the rate-determining step is the adsorption of hydrogen on the surface and both nucleation and diffusion are very rapid. From the fact that the order of the reaction with respect to hydrogen is from 0.6 to 0.9, the dissociation of H_2 at the surfaces seems to be involved. The rapid diffusion of oxygen ions in uranium oxides has also been observed in studies of the oxidation of UO_2 [72, 73] and the exchange reaction between H_2O and a variety of uranium oxides [71]. The reduction by

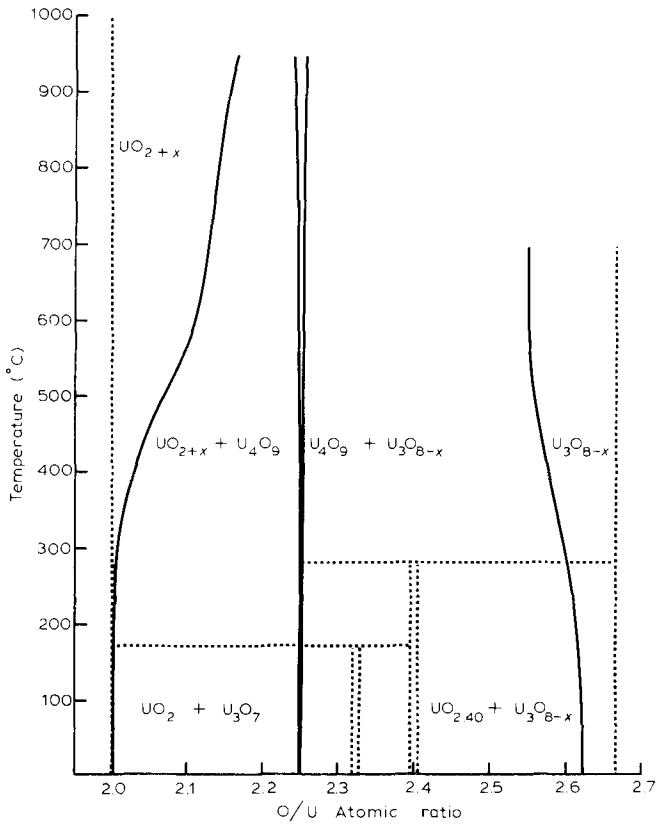

Fig. 5. Phase diagram for uranium oxides in the UO_2—U_3O_8 region [65].

CH_4 [75, 76] yielded the same result, i.e. that the rate was constant for the range from $UO_{2.6}$ to $UO_{2.2}$ and 0.7th order in methane. For the reduction by ethylbenzene [77], the rate was also constant for the range from $UO_{2.6}$ to $UO_{2.25}$, though the order of reaction with respect to ethylbenzene was zero.

While the general conclusion that the rate-determining step is the dissociative adsorption of reducing gas on the surfaces is compatible with the results mentioned above, the fact that the constant rate region ($UO_{2.6} \sim UO_{2.2}$) is independent of the nature of the gas and coincides with the two-phase region ($U_3O_{8-x} + U_4O_9$) in the phase diagram of the U—O system (Fig. 5 [65]) suggests an alternative explanation [77], viz. the constant rate is due to a constant oxygen pressure which is in equilibrium with the two solid phases, U_4O_9 and U_3O_{8-x}. This point of view will be extended further in Sect. 5.

The rate of reduction of U_4O_9 [74] by hydrogen was also found to be from 0.5 to 0.9th order in hydrogen and the kinetics was between two

possible cases; the linear regime $t = k\alpha$ and the interface reaction regime, $t = k[1 - (1 - \alpha)^{1/3}]$.

The reductions with hydrogen of the oxides and the oxysalts of W and Mo have been actively studied, mainly in Europe, and reviewed by Haber [32]. Hence, only a brief summary is given here.

For the reductions of WO_3, MoO_3, $MnMoO_4$, $MgMoO_4$, a-$CoMoO_4$ and b-$CoMoO_4$, induction periods or sigmoidal dependence of the conversion, α, on the time, t, have been observed and interpreted as the formation and the growth of nuclei, although an alternative explanation as an autocatalytic activation of hydrogen due to a product metal (the hydrogen spillover effect, see above) has also been given. For the reductions of a-$CoMoO_4$ and b-$CoMoO_4$, the dependences of the maximum rate (the rate when S reaches a maximum) on the hydrogen pressure were measured and it was concluded that the rate-determining step is the reaction

$$2\,H(ads) + O(surf) \longrightarrow H_2O(ads)$$

at the interface. On the other hand, in the reduction of Bi_2MoO_6, $Bi_2Mo_2O_9$ and $Bi_2(MoO_4)_3$, neither induction periods nor sigmoidal dependence were observed. Therefore, it was considered that the product layer covered the entire surface of the particle at the very beginning of the reduction. At low hydrogen pressure ($\sim$ 20 torr), α was linear with t up to several percent conversion and the rate was proportional to the pressure. It was concluded that the adsorption of hydrogen is the rate-determining step. At somewhat higher pressure ($\sim$ 250 torr), the kinetics follow the parabolic law, eqn. (5), and it was concluded that the diffusion of oxygen ions through a thin product layer was the rate-determining step. This conclusion was supported by the fact that the activation energy measured for this reduction agreed well with that for oxygen diffusion in MoO_3.

The reducibility of catalysts has been used as one of the means to characterize their surfaces. For hydrodesulfurization catalysts (MoO_3–Co_3O_4–Al_2O_3 system), the catalytic activity shows a volcanic dependence on the reducibility [37], i.e. passes through a maximum. The effect of supports (SiO_2, Al_2O_3, and SiO_2–Al_2O_3) on the polymerization catalyst Cr_2O_3 was studied by following the reduction rate by H_2 and CO at a constant rate of temperature rise [48]. The reduction rate profile as a function of temperature can show thermal stabilities towards the reducing atmosphere. It was found that the thermal stability of the catalyst was in the order of $SiO_2 > SiO_2$–$Al_2O_3 > Al_2O_3$, which was in the same order of efficiency as for catalysis of polymerization. The oxides of Mo–Bi–P are known to be very effective catalysts for the selective oxidation of propene to acrolein. Miura et al. [49], following the idea of the temperature-programmed desorption technique [50], reduced the catalysts and reoxidized them at a constant rate of temperature rise. They found that the peak at 320°C in the profile of the rate of reoxidation as a

function of temperature correlated well with the catalytic activity. All of these studies on the surfaces of catalyst by reduction, however, remain quite phenomenological and cannot give any insight at a molecular level.

2.2 STRUCTURAL CHANGE ON REDUCTION. ORDERING OF DEFECTS

Due to the intrinsic complications involved in the study of gas—solid reactions, kinetic investigation alone does not give a full understanding of the reduction process at a molecular level. Instead, structural investigation of both products and reactants may help to elucidate the reduction processes. As the knowledge about the structure of Fe_xO (wüstite) accumulates [17—20], the reduction process from Fe_3O_4 (magnetite) to Fe_xO (wüstite) may become better understood. Both structures are based on cubic close packed oxygen ions, hence the change from magnetite to wüstite can be looked upon as the loss of the particular order of magnetite in which iron ions occupy octahedral and tetrahedral holes [21], as oxygens are removed and irons diffuse inward via vacant octahedral and tetrahedral holes. No doubt the wüstite structure must have certain types of order. In order to accomodate gross non-stoichiometry, there should be some stabilizing cooperative interactions among defects, which would lead to the formation of a variety of clusters of these defects. The structures of such clusters have been suggested as shown in Fig. 6 [18, 20].

Although they differ in detail, it may be accepted that the basic unit of the cluster is a tetrahedron with one interstitial iron (most likely Fe^{3+} [52, 53] surrounded by four vacancies on the nearest octahedral site, which is found locally in the magnetite structure. The wüstite structure is then understood to have these unit tetrahedra arranged in some ordered manner. From this point of view, the measurements suggesting three phases separated by second- or higher-order transitions within the wüstite phase [22, 22a, 78] can be interpreted as successive loss of different types of order as the temperature is raised or the number of the unit tetrahedra decreases (the reduction proceeds). However, no definite conclusions have yet been drawn and indeed, the existence of these three subphases is still disputed [19, 20, 23, 24, 28].

The reduction process from α-Fe_2O_3 (hematite) to Fe_3O_4 (magnetite) needs a major change in the oxygen lattice from h.c.p. to f.c.c., and seems difficult to depict. However, it is interesting to note that in the reverse reaction (i.e. the oxidation of magnetite to hematite), the reaction product is γ-Fe_2O_3 (based on an f.c.c. lattice) when the particle size is less than 3000 Å, while otherwise α-Fe_2O_3 is formed [25—27]. Feitknecht and Gallagher [26] concluded that the reaction path was

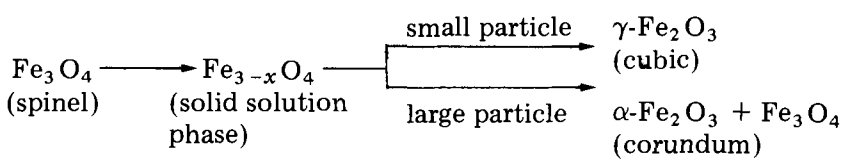

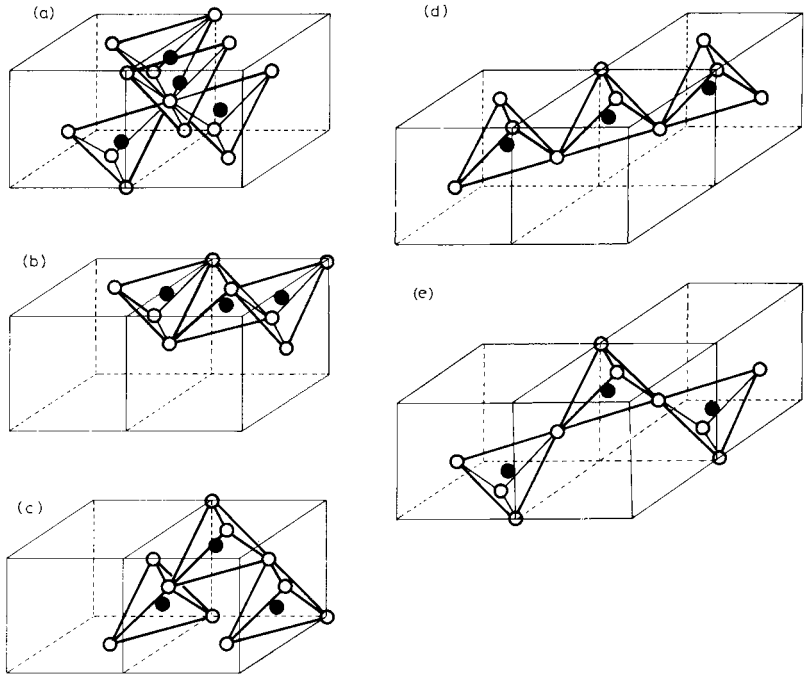

Fig. 6. (a) The Koch cluster in Fe_xO [18, 51]. (b), (c), (d) and (e) Other possible clusters in Fe_xO [20]. Oxygen ions and octahedral iron ions are omitted for clarity. ○, Cation vacancy; ●, tetrahedral iron ion.

Namely, the reaction proceeds topotactically and γ-Fe_2O_3 results when the particle size is small, but in large particles accumulated strain causes the nucleation of α-Fe_2O_3 before the completion of the reaction.

The mechanism for the transformation from γ-Fe_2O_3 to α-Fe_2O_3 has been proposed [29] to involve associated movements of the oxygen close packed planes in the $(11\bar{2})$ direction of the f.c.c. lattice and of Fe^{3+} ions so that the tetrahedral ions in γ-Fe_2O_3 move into vacant octahedral sites.

The similar mechanism involving the structural change of the oxygen lattice from f.c.c. to h.c.p. has been proposed for the reduction of the spinel $CoCr_2O_4$ [30] and for the final stage of the reduction of $CoCr_2O_4$—Co_2O_4 solid solution [31] according to the equation

$$\underset{\text{(spinel)}}{Co^{2+}[Cr_2^{3+}]_B O_4^{2-}} + H_2 \longrightarrow \underset{(\gamma\text{-}Cr_2O_3)}{\tfrac{3}{4}\, Cr^{3+}[Cr_{5/3}^{3+}\square_{1/3}]_B O_4^{2-}} + Co + H_2O$$

and

$$\underset{\text{(cubic)}}{\gamma\text{-}Cr_2O_3} \longrightarrow \underset{\text{(corundum)}}{\alpha\text{-}Cr_2O_3}$$

where $[\ ]_B$ signifies an octahedral cation site of the spinel structure and

□ means a vacancy. As oxygen ions are removed, the unreducible Cr^{3+} ions rearrange by a short-range inward migration to form γ-Cr_2O_3 with a few atomic layers, while Co^{2+} ions counter diffuse towards the reaction boundary where they are reduced to metal. This latter diffusion could be the rate-determining step characterized by the experimental activation energy for the reaction $E_a = 167\,kJ\,mole^{-1}$. From this temporary arrangement of γ-Cr_2O_3 with a few atomic layers, the stable α-Cr_2O_3 precipitates by the same shear mechanism as for γ-Fe_2O_3 to α-Fe_2O_3 mentioned above, before γ-Cr_2O_3 extends to the entire bulk of particle. This process of formation of Co metal and α-Cr_2O_3 is considered [30] to take place repeatedly in discontinuous layers a few atomic planes thick.

The process of reduction of the oxides and the oxysalts of W and Mo can be understood [32] in terms of crystallographic shear [33]. Namely, these oxides and oxysalts are built with the unit oxygen octahedron with a Mo or W cation in the center. These units stack together by sharing vertices and/or edges. As the reduction proceeds and oxygen ions are removed, the oxygen vacancies thus formed apparently arrange themselves in ordered arrays along particular crystal planes. When the concentration of vacancies reaches a certain value, they are eliminated by rearrangement of the original vertex-sharing octahedra into an edge-sharing arrangement, resulting in the formation of a shear plane.

For example, WO_3 takes the ReO_3 structure, in which the unit octahedron shares six vertices with six nearest neighbour octahedra. When vacancies are introduced, they tend to arrange as shown in Fig. 7(a), for example, and they are annihilated by crystallographic shear movement indicated by arrows resulting in Fig. 7(b).

This view of the process of reduction of the oxides and the oxysalts of W and Mo has been supported by an electron microscopy study [34] and by electron spectroscopy [32, 35]. However, the actual mechanism by which vacancies arrange cooperatively in ordered manners to give rise to crystal shear is yet to be elucidated.

3. Effects of hydrogen on metals

3.1 SOLUTION OF HYDROGEN IN METALS

Metals of the s- and p-blocks of the periodic table react with hydrogen to form stoichiometric compounds either of the ionic, "salt-like" type, or of the gaseous covalent type, such as arsine. Among the transition metals, however, there are many examples of hydrogen uptake in which no precisely stoichiometric compound is formed and the structure and metallic properties of the solid are essentially maintained during hydrogen uptake. This type of uptake has long been known as occlusion and the metals concerned are classified into endothermic occluders, such as iron, which take up hydrogen only to a very small extent (solubility of hydrogen in Fe, 0.002 at. % at 400°C and 0.064 at. % at 1500°C), and

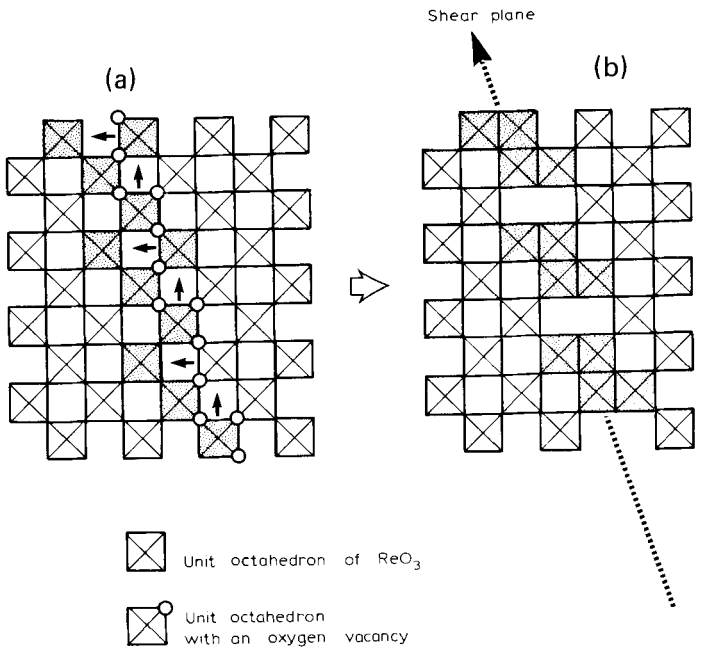

Fig. 7. Defect elimination by crystallographic shear in ReO_3 structure [33, 51].

exothermic occluders, of which the best known is palladium, which take up hydrogen to very much greater extent, up to an atomic ratio H/Pd ~ 0.6 close to room temperature. The general nature of the occlusion phenomenon was comprehensively reviewed by Smith [117] and by Cotterill [118] in connection with the topic of Sect. 3.2 below and by Mueller et al. [129]. In both endothermic and exothermic occlusion, solution of hydrogen takes place in atomic form, as deduced from Sievert's law that the solubility is proportional to the square root of the gas-phase pressure; e.g. for the solubility of hydrogen in Fe, see Armbruster [119]. More recently, attempts have been made to gain a more detailed understanding about structures and properties based on statistical thermodynamics [130—133].

Endothermic occlusion takes place by diffusion of hydrogen into a metal lattice which is very little changed by the process. In exothermic occlusion by palladium, however, the face-centred cubic lattice (α phase) of palladium, with lattice constant 3.88 Å, will accomodate, below 100°C, no more than about 5 at. % hydrogen, and then undergoes a transition to an expanded phase (β phase), with lattice constant 4.02 Å and H/Pd = 0.5—0.6. The H—Pd system thus splits into α and β phases in the manner familiar for two partially miscible liquids. The consolute temperature (rarely observable for solid phases) is about 310°C at H/Pd = 0.22. The phase diagram is, however, not well established because formation of the

system is by diffusion in which a true equilibrium is rarely reached and the final state is governed by kinetic factors. It will be evident from the above account that, as diffusion of hydrogen into palladium proceeds, the outer regions, of high hydrogen content, undergo the transition to the β-phase while inner regions are still in the α-phase. Thus, a moving boundary is established between the two phases and each phase contains within it a diffusion gradient of hydrogen concentration. The nucleation process of the reverse transformation, from β- to α-phase, has been recently observed by electron microscopy and diffraction [134].

Although the passage of hydrogen through palladium is a well-known and important process for the purification of hydrogen and for the separation of hydrogen isotopes, its kinetics are rather complicated and not well understood. For reasons which are obvious from the above account, simple diffusion rate laws are not obeyed. At low temperatures, from room temperature to about 400°C, the permeability of palladium to hydrogen often decreases irreversibly with time [120]. This is not well understood and has been attributed to poisoning by hydrocarbons or by oxygen and to decrease of external surface area for hydrogen uptake by smoothing of an initially rough surface.

3.2 HYDROGEN EMBRITTLEMENT OF METALS

Pfeil [121] observed in 1926 that hydrogen in steel caused a considerable decrease in room temperature ductility. Later detailed studies of this effect have produced evidence suggesting that a diffusion-controlled mechanism is involved. In particular, the degree of embrittlement decreases with increasing strain rate and with decreasing temperature below room temperature [118]. It also decreases, however, with increase of temperature above room temperature and the effect disappears above 100°C. This evidence has been taken to indicate that gaseous hydrogen in cracks or voids in the metal is involved, since its equilibrium pressure will decrease rapidly close to 100°C. Theories based on simple hydrostatic pressure of H_2 aiding the propagation of cracks have not found general favour, however, largely because they fail to explain why the embrittling effect is observed commonly in extension but never in compression.

Most theories of embrittlement involve some kind of defect in the metal, dislocations, microcracks or voids; diffusion of hydrogen to these defects while they are growing or moving in the deformation and cracking of the metal; and finally an effect produced by hydrogen either in gaseous form in the defect, or adsorbed on the surface of the defect if it is a crack or void, or in solution in regions of high stress concentration very near to the defect. Only a very brief indication of the possible nature of such effects is given here, in terms of the simplest theories of brittle fracture.

Brittle fracture mechanisms of the type first proposed by Griffiths [122] are based on the concept of competition between a decrease of

energy (strictly, free energy) when a stress is relieved by crack formation and an increase of energy corresponding to the surface energy of the crack. When the former exceeds the latter, the crack will propagate. For a crack of width c, extending right across the sample, it may thus be calculated that propagation leading to fracture will occur whenever the stress, σ, exceeds a value determined by c, Young's modulus, E, and the surface tension (surface excess free energy), S, on the surfaces of the crack

$$\sigma > \left(\frac{2ES}{c}\right)^{1/2} \tag{21}$$

Orowan [123] proposed a modification in which a plastic deformation energy, P, replaces the surface tension, S. This arose because X-ray back reflection showed a thin layer of plastic deformation at brittle fractures. Orowan's condition is

$$\sigma > \left(\frac{2EP}{\pi c}\right)^{1/2} \tag{22}$$

The relationship of brittle fracture to plastic deformation has, of course, been elaborated in various ways with the aid of dislocation theory, e.g. nucleation of microcracks has been discussed in terms of piling-up of dislocations [124]. Davies [145] has shown that embrittlement requires the presence of islands of martensite (about 1 μm in size) and has suggested that cracks are initiated in the martensite or at the martensite–ferrite interface.

Some basic ways in which hydrogen may act to facilitate brittle fracture may be considered, in very general terms, in relation to eqns. (21) and (22) and the concepts underlying them. Adsorbed hydrogen at the surface of a crack could decrease S, as the Gibbs adsorption equation requires. If the important effect around a crack, on the other hand, involves stress concentrations producing plastic deformation, rather than surface tension, then hydrogen may act principally in dissolved form in the region of stress concentrations near to, but not actually at, microcracks. This seems to be, in very general terms, the basic concept of the theories of Morlet et al. [125, 126] who have found that hydrogen tends to concentrate in highly stressed regions of the lattice. There is then a complicated relation between diffusion of hydrogen and stress-induced concentration gradients as the regions of stress move. Ransom and Ficalora [144] studied H_2 adsorption isotherm, adsorption rate, magnetization changes and crack growth rate. They concluded that adsorption takes place in two stages, first as H_2^+ and then as H^-. They identify the latter as the embrittling species and its formation as rate-controlling for embrittlement.

This phenomenon therefore appears to involve most of the concepts of interest to the kineticist of gas–solid reactions.

4. Reactions of solids with halogens

4.1 ISOTOPIC EXCHANGE REACTIONS

Alkali halides will exchange halogen atoms with the corresponding halogen gas or hydrogen halide [90]. At room temperature, this process often involves only the outermost layer of the solid, with equilibrium times of the order of one hour. But for some vacuum-sublimed high surface area samples of NaCl, the reaction with Cl_2 involves a greater fraction of the solid phase and appears to be controlled by bulk defects rather than surface area [91]. The nature of the difference in defect structure between different preparations of alkali halides has not been resolved. Formation of electronic defects of the trapped-hole (or "V-centre") type, involving halogen atoms, molecules or molecule-ions in some form, was proposed to account for low-temperature bulk exchange activity [92]. No such defect was detected by electron spin resonance, however, in Cl_2-treated samples; but F_2 treatment or X-irradiation produced ESR-detectable defects and, at the same time, profoundly influenced the exchange kinetics [93] in a manner generally compatible with the type of defect mechanism proposed earlier for the Cl_2 exchange in the absence of previous F_2 treatment [92].

When strictly surface-layer exchange occurs, it discloses a marked contrast in properties, both kinetic and thermodynamic, between surface and bulk. The remarkably rapid reaction rate would not be expected on a smooth (100)-type surface without a high concentration of defects and the nature of the defects responsible for the reaction rate has never been clearly resolved. Suggestions have ranged [99—101] from equilibrium surface disorder, via the Verwey distortion (which is believed to involve the anions of an alkali halide surface projecting out beyond the plane of the cations [94, 95] to processes related to crystal growth mechanisms and growth spirals [100]. There has been some indication [99] that the surface layer is composed of two domains of differing reactivity for exchange, but this is by no means clearly established for all samples.

The exchange of NaBr and KBr with HCl reaches an equilibrium in which, near to room temperature, a mixed Cl^-/Br^- surface is at equilibrium with a gaseous HCl/HBr mixture whose composition depends on the surface anion ratio, but which is typically about 1 mole % HBr. This equilibrium was discovered in the laboratory of one of us (LGH) about eighteen years ago [96], but the topic proved difficult to pursue because of the difficulty of quantitative analysis of the gas mixture. Eventually, a temperamental but workable gas chromatographic technique [97] having provided the key to this analysis, we were able to show that the equilibrium is highly non-ideal [98]. The bromide surface apparently undergoes a two-dimensional phase transition, induced by HCl or HBr adsorption, close to room temperature, in which the halide ions become mobile,

as indicated by a very large entropy of transition: $\Delta S = 62.8\,\mathrm{kJ\,mole^{-1}\,K^{-1}}$ and $\Delta H = 18.4\,\mathrm{kJ\,mole^{-1}}$. These values were found by extrapolation of exchange data to zero mole fraction of surface Cl^-. For finite fractions of surface Cl^- in the surface, evidence was obtained for depression of the transition temperature and for phase separation in the partly exchanged surface, involving a "two-dimensional compound" K_4Br_3Cl. This contrasts very strongly with the complete and essentially ideal miscibility of KBr and KCl in the bulk. Further studies on this subject have been under way intermittently in our laboratory. In the most recent of these [143], study of the adsorption of HBr on KBr has shown that the geometry of adsorption may be a determining factor in the K_4Br_3Cl stoichiometry found for exchange with HCl. There is also a remarkably large repulsion between adsorbate molecules (mean field repulsion constant about $40\,\mathrm{kJ\,mole^{-1}}$). This is also discussed in relation to the geometry of adsorption.

At elevated temperatures, and with single crystal samples, halogen exchange can be used to study halide diffusion in the solid. In these conditions, surface exchange is effectively instantaneous and involves a negligible amount of material and diffusion through the bulk is rate-controlling. It is then possible, by doping an alkali chloride with radioactive ^{36}Cl and exposing it to circulating Cl_2 gas, to follow diffusion continuously from the appearance of radioactivity in the gas phase. In one such experiment, diffusion can be followed as a function of time at several different temperatures, without touching the sample. This procedure is comparable, for convenience, with an electrical conductivity experiment and much less cumbersome than a series of sectioning experiments on several samples, which would be needed to obtain the same data by conventional techniques. In this way, it was shown [102] that anion diffusion behaviour closely parallels the better-known transport behaviour of cations as observed by electrical conductivity. In both cases, the concentration of mobile vacancies is controlled at high temperatures by the intrinsic formation of Schottky defects of both signs in equal numbers from the pure host lattice. At lower temperatures, where the concentration of defects thus formed would be much lower than the concentrations of multiply charged defects, the latter control the vacancy concentrations.

In the temperature range between room temperature and 250°C, and with high surface area samples, behaviour intermediate between surface exchange and bulk diffusion has been observed by two sets of workers [90, 99] who obtained essentially similar results. As the temperature is raised, the second, third and fourth layers can be observed to exchange separately with activation energies of about 0.56—0.78 eV for the second layer, 1.17 for the third layer, and for the fourth layer either a similar value to the third [90] or a value close to the bulk diffusion activation energy of 1.61 eV [99]. The depth to which the solid behaves significantly differently from bulk properties correlates quite well with the

depth to which Verwey-type displacements from ideal lattice sites should be significant as calaulated by Benson et al. [95].

Secco et al. studied the exchange reaction between Zn vapour and polycrystalline Zn [84], ZnS [85], ZnSe [86] and ZnTe [87] in the temperature range 700—900°C. It was found that for ZnO and ZnS, which take hexagonal wurzite structures, the exchange was controlled by two processes, an initial first-order reaction followed by a diffusion process. The clear switch over from the first process to the second occurred when the exchange amounted to a depth of 25 atomic layers for ZnO and 15—18 for ZnS. It was then postulated that exchange reaction and zinc mobility via interstices occurred simultaneously and, at the beginning, the exchange reaction was rate-determining while later, after the effectively available interstices became filled, a coupled interstitial-lattice motion, i.e. interstitial diffusion, became rate-determining.

On the other hand, for ZnSe, and ZnTe, both being of cubic zinc blende structure, the exchange was found to be controlled solely by diffusion. For the ZnTe case, the diffusion process could be interpreted in terms of a vacancy mechanism.

No further elucidation has been attempted, however, as to the relations between the structures of zinc compounds and the exchange mechanisms.

4.2 CHEMICAL REACTIONS. ELECTRON TRANSFER AND ELECTRONIC DEFECTS

Reactions of KI with Cl_2 and of NaCl and KCl with F_2 have been studied [92, 93, 103, 104] and a variety of properties have been measured as a function of the extent of reaction in the conversion of CuCl to $CuCl_2$ by reaction with Cl_2 [89, 105, 106]. A consistent feature of all these studies is that, together with or sometimes preceding nucleation and growth of new solid phases, the solid reactant is damaged by electron withdrawal, leading to the formation of various types of electronic defect of the trapped-hole or "V-centre" type. Studies of electrical conductivity, electron spin resonance spectra and UV absorption are useful in elucidating the behaviour of these defects.

In the KI/Cl_2 reaction, an interesting effect of high defect concentration in preventing growth of nuclei of a new solid phase was disclosed [103]. Solid samples differed widely in their initial ionic conductivity and hence in their initial concentration of cation vacancies. The ones with high vacancy concentration reacted very slowly with chlorine and the colour of iodine was seen uniformly as a pale coloration of the whole solid, which had reacted to the extent of only a few percent after several days. Samples with a low vacancy concentration reacted more rapidly and a sharp boundary developed between an outer, iodine-blackened completely reacted region and a pale-coloured inner region. In the unreactive samples, electronic (presumably positive hole) conductivity appeared transiently for a few hours and then decayed. In the reactive

samples, conductivity increased along a sigmoid curve; in the initial portion, conductivity increased with the square of the time. This is to be expected for a reaction intermediate formed in proportion to the area of reaction interface, $S(t)$, when that interface is the combined surfaces of numerous nuclei, each growing at a constant linear rate, and hence with surface proportional to t^2. For the type of behaviour of the unreactive samples, it was suggested that cation vacancies were competing with the reaction interface as trapping sites for the charge carriers and preventing growth of nuclei. It was indicated that a drop in Fermi level of as much as 2 eV, representing a very great increase in the resistance of KI to further oxidation, could readily occur in this way.

Trapped-hole centres have been definitely identified in this type of reaction only when the reactant gas was fluorine. UV absorption bands were seen in the reaction of F_2 with NaCl single crystals [104]. ESR spectra were seen after partial reaction of NaCl, KCl and $SrCl_2$ with F_2 and were interpreted as forms of Cl atom or Cl_2^- ion (H centre) occupying a single anion site or a position somewhat displaced from it [93, 107]. Kinetic evidence was used to deduce models for the trapped holes in $NaCl/F_2$ [92] and in $CuCl/Cl_2$ [106]. In the latter case, various electrical studies disclosed the existence of two acceptor levels, or types of trapping site, which were tentatively assigned as cation vacancies and anion interstitials. For $NaCl/F_2$, a complete interpretation of the rather unusual kinetic evidence was devised involving a molecular (neutral Cl_2 in two anion sites) type of defect in the surface interacting with a bulk-mobile Cl atom defect.

In the $CuCl/Cl_2$ reaction, the "parabolic law" for diffusion through the zone of solid product, eqn. (5), has been observed right from the start of reaction [108]. In another study [89, 105], however, the reaction at first proceeded linearly, suggesting recrystallization of the product into separate crystals, leaving new CuCl surface continuously exposed, and that the parabolic behaviour, as represented for large extents of reaction by Carter's modification of the Ginstling–Brounshtein equation, eqn. (8), was established at a later stage. Various studies, including X-ray diffraction and magnetic studies, suggested that, in the $CuCl_2$ layer through which diffusion takes place, there is a spinel-like displacement of some Cu^{2+} ions into normally vacant layers of octahedral holes, opening up diffusion paths which are not present in the perfect $CuCl_2$ lattice.

5. Direct determination of the activities of reacting species at the interface

One of the most serious drawbacks in studies of gas–solid reactions is that, in general, the activities or concentrations of the reacting species at the interfaces cannot be measured directly and hence the rate equation (if successfully determined) is usually expressed in terms of gaseous

reactants and products only. This imposes a serious limitation on kinetic studies in elucidating the reaction mechanisms.

In the studies of gaseous reactions on solid catalysts, experimental work to determine the concentration of reacting species on the surfaces is undoubtedly important and has been reviewed comprehensively by Wagner [63]. In this section, a brief summary is attempted, emphasizing this aspect of gas—solid reaction.

Kobayashi and Wagner [54] studied the reaction

$$S\,(\text{in } M_2S) + H_2(g) = H_2S(g)$$

at 300 and 385°C where M_2S means Ag_xS ($x = 2.000 \sim 2.0025$) and Cu_yS ($y = 1.93 \sim 1.999$); Taking advantage of solid electrolytes MI, the iodides of the metal, they constructed cells of the type shown in Fig. 8. By using the coulometric titration method [55], the values of x and y were fixed under an applied voltage, E, which is proportional to the activity of the metal in the bulk. Then the sample M_2S was exposed to H_2 gas and the reduction was allowed to proceed sufficiently slowly, by choosing appropriate conditions, so that the diffusion or the migration of cations and electrons is fast in comparison. Under these conditions, the activity of the metal at the surface is considered approximately equal to that in the bulk, which is determined by the applied voltage, E. The reaction rate is proportional to the electric current through the cell and it was measured with a galvanometer of high sensitivity. The results showed that for Ag_xS the logarithm of the rate was proportional to the voltage E, and for Cu_yS it was constant. By applying the Gibbs—Duhem equation to metal ions, sulfur ions and excess electrons as the constituent particles and taking advantage of the fact that the metal ions are distributed at random, the activities of S^{2-} and the excess electrons (i.e. conduction electrons, whose chemical potential is the Fermi level) were calculated. These bulk activities were regarded as equal to the surface activities. Furthermore, by considering the equilibria

$$S^{2-}(\text{surf}) = S^{-}(\text{surf}) + e^{-}$$

$$S^{2-}(\text{surf}) = S(\text{surf}) + 2e^{-}$$

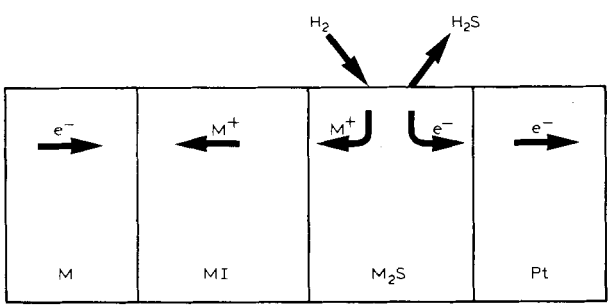

Fig. 8. Cell with solid electrolyte MI.

at the surface, the activities of S^-(surf) and S(surf) were also evaluated as a function of the applied voltage, E. A comparison was then made between the expression thus obtained and the observed dependence of the rate on the applied voltage, E. It was thus concluded that for Ag_xS, the reaction

$$S(surf) + H_2 \longrightarrow H_2S$$

and for Cu_yS, the reaction

$$S^{2-}(surf) + H_2 \longrightarrow H_2S + 2e^-$$

are predominant.

An example of the direct application of this method of measuring activities electrochemically during the course of reactions is the nucleation of Ag during the reduction of Ag_2S with H_2 [56].

The extension of this Kobayashi—Wagner method to studies of heterogeneous catalysis is straightforward as suggested [54], since catalytic redox reactions can be regarded as repetitive cycles of reduction and oxidation of the surface species [64]. Examples are the studies of $H_2 + \frac{1}{2}S_2 \rightarrow H_2S$ and $COS + H_2 \rightarrow CO + H_2S$ on Ag_2S [57], and of $CO + H_2O \rightarrow CO_2 + H_2$ on Fe_xO [58]. This method, however, is based on the very special premise that the bulk activity is equal to the surface activity, which is hardly realized in general kinetic studies.

Another method has been suggested to measure the activity of the surface oxygens on NiO catalysts as a quantity proportional to the ratio P_{CO_2}/P_{CO} of the gas mixture of CO_2 and CO which, on contacting the surface of NiO, does not change in its composition [59]. The contact time allowed should be short so as not to oxidize or reduce the bulk oxygen, but long enough so that the local equilibrium between the gas phase and the surface is established. Thus the use of a differential reactor is most effective. In this way, the activities of the surface species alone can in principle, be determined.

In the oxidation of graphite by a gas mixture of CO_2 and CO at 900—110°C [60], it was found that the rate is proportional to the ratio P_{CO_2}/P_{CO} when the latter is low. It was then concluded that reaction (15) below is the rate-determining step and reaction (14) is in equilibrium.

$$CO_2 = CO + O(ads) \tag{14}$$

$$O(ads) + C \longrightarrow CO \tag{15}$$

Therefore, the activity of the absorbed oxygen and hence the rate is proportional to the ratio P_{CO_2}/P_{CO}. When the ratio becomes higher, the rate of reaction (15) becomes comparable with that of (14) and reaction (14) is no longer in equilibrium, hence the activity of the absorbed oxygen cannot be determined by the ratio P_{CO_2}/P_{CO}. A similar analysis was employed for the water gas shift reaction on an FeO surface between 700 and 1000°C [142]. From the previous studies, the step $H_2 + O(ads) \rightleftharpoons$

H_2O was known to proceed fast and to be in equilibrium. Hence the activity of O(ads) is proportional to P_{H_2O}/P_{H_2}. The overall reaction is then controlled by the step $CO_2(g) \rightarrow CO(g) + O(ads)$. The rate law was found to be first order with respect to P_{CO_2} as expected, but the order with respect to O(ads) (i.e. P_{H_2O}/P_{H_2}) was about $-2/3$ instead of -1. The latter fact was argued to be consistent with the sequences of partial reaction steps involving the transfer of two electrons to an oxygen atom on incorporation to the wüstite lattice [61].

For catalytic isotope exchange reactions on solids, however, the activity of the surface species can be rigorously determined by the ratio of the partial pressures of oxidant and reductant. This idea was used in the study of the exchange reaction

$$^{14}CO_2 + {}^{12}CO \rightleftharpoons {}^{14}CO + {}^{12}CO_2$$

on Fe_xO, Fe_3O_4, CoO, ZnO and MgO [61]. For the exchange reaction

$$H_2S + D_2 \longrightarrow D_2S + H_2$$

on Cu_2S [62], the dependence of the exchange rate coefficient in the surface activity of sulfur ion (proportional to the ratio $P_{H_2S+D_2S}/P_{H_2+D_2}$) was determined and it was concluded that the predominant reaction on the surface of Cu_2S is

$$H_2S + 2e^- \longrightarrow H_2 + S^{2-}$$

In this last example, the catalytic exchange reaction can be regarded as a probe to study the oxidation of the surface of Cu_2S by H_2S.

As mentioned in Sect. 2.1, the reduction rate of uranium trioxide by H_2 was found to be $0.6 \sim 0.9$th order in hydrogen and to stay constant under a constant hydrogen pressure in the region from $UO_{2.6}$ to $UO_{2.2}$, where two phases, U_4O_9 and $U_3O_{8-x}(UO_{2.6})$ coexist about 400°C [65] (see Fig. 5). If the diffusion of oxygen ions in uranium oxides is rapid enough so that reaction (16) reaches equilibrium, then the following mechanism could be probable.

Bulk, with rapid diffusion of O

$$\frac{1}{0.35}UO_{2.60}(U_3O_{8-x}) = \frac{1}{0.35}UO_{2.25}(U_4O_9) + O \qquad (16)$$

Surface

$$H_2 = 2H(ads) \qquad (17)$$

$$2H + O \xrightarrow{k_1} H_2O \qquad (18)$$

$$H + O \xrightarrow{k_2} HO \qquad (19)$$

Then the rate is expressed as

$$\text{rate} = (k_1 p_{H_2} + k_2 p_{H_2}^{0.5}) a_O \qquad (20)$$

where a_O is the activity of oxygen and is fixed by the two-phase equilibrium (16). In other words, the activity of oxygen is controlled and measured indirectly by taking advantage of the existence of two phases and of the rapid diffusion of oxygen. There is another two-phase region from $UO_{2.25}$ to UO_{2+x} and it was found that the kinetics of the reduction of U_4O_9 by H_2 [74] were in between *the constant rate regime* and the interface reaction regime. More extensive studies on the reduction of U_4O_9 may be fruitful to resolve this.

6. Reaction of atmospheric pollutants with calcite and marble

Deterioration of ancient stonework appears to have accelerated very markedly in many places in the present century. Winkler [109], whose treatise on the durability of stone is the major source for the material in this section, shows photographs of early eighteenth century sandstone statues in places close to the Rhine–Ruhr industrial region. After two hundred years, at the beginning of the present century, these statues had clearly delineated features of faces, hands, etc. Sixty years later, they appeared rough outlines, faceless and handless. If this deterioration indeed owes nothing to the military activities of two world wars, it is a remarkable illustration of the effects of industrial pollution of the atmosphere.

The atmospheric pollutants concerned are SO_2, SO_3, nitrogen oxides and Cl_2, and they produce their effects on stone when they are associated in some way with water. The dominant destructive process is conversion of $CaCO_3$ and $MgCO_3$ to gypsum and $MgSO_4$. The latter process is particularly destructive because of the high solubility of $MgSO_4$ in water. The two carbonates are very widespread constituents of sedimentary and metamorphic rocks. Marble, limestone, magnesian limestone and dolomite consist of $CaCO_3$, in the case of the first two, or mixtures of it with $MgCO_3$. Sandstones, however, although consisting principally of SiO_2 particles, have these particles cemented together by a variety of substances, among which calcite is the commonest. Thus processes which attack calcite will destroy most sandstones. The porous Baumberg sandstone from Westphalia, used for the statues referred to above, is an Upper Cretaceous deposit containing more calcite than quartz. Serpentine is a magnesium silicate. Veins of calcite and magnesite improve its appearance for decorative purposes, but make it susceptible to attack as described above.

Since the deterioration of stone generally requires water, it might be thought to be essentially a solid–liquid reaction and hence outside the scope of this article. There are, however, many indications that the water for these processes is picked up by the solid from the gas phase, at relative humidities often well below 100%, so that the water is itself a gaseous reactant.

The most direct indication of this is that a dry climate does not prevent conversion of $CaCO_3$ to gypsum, but merely prevents removal of the gypsum. Sculptures in the Erechtheum at Athens have about a centimetre depth of gypsum on their surfaces [110]. Rocks commonly contain cracks and pores of a very wide size range [112, 113], down to sub-micron diameters at which capillary condensation can occur well below 100% relative humidity. In cellular concrete, water content has been found to rise from 1.5% at 50% R.H., via 3% at 70% R.H. and 8% at 90% R.H., to as much as 15% at 95% R.H. [111]. So-called "ordered-water" or "non-freezable water" on surfaces (2—3 nm thickness at 50% R.H.) has been indicated as instrumental in damage by alternate wetting and drying [109], though the mechanism of such damage seems rather obscure.

Between molecular water vapour in the atmosphere and macroscopic liquid raindrops lies a wide range of aerosol particles, which contain water molecules and ions such as SO_4^{2-}, Cl^- and NO_3^-. These are generally classified into three size ranges [114]: "Aitken" aerosols, 10^{-4} to 10^{-2} μm, i.e. 10^{-1} to 10^{1} nm; large aerosols, 10^{-2} to 10^{-1} μm, i.e. 10^{1} to 10^{2} nm; and giant aerosols, 10^{-1} to 10^{0} μm, i.e. 10^{2} to 10^{3} nm. The Aitken aerosols or "large ions" cover the size range from a single small molecule up to an assemblage of some tens of thousands of ions and water molecules and certainly pose a challenge to the definition of the gas phase. These aerosol particles, which are found in concentrations of the order of 10^{5} m^{-3} in the air of towns, going down to 10^{3} in mountainous areas over 2000 m and over oceans, have been indicated as the most important in stone decay [109]. The lifetimes, structure and chemistry of aerosol particles in the atmosphere have been comprehensively reviewed by Graedel and Weschler [146]. Particles of 10^{-1}—1 μm size are the longest-lived (10 days), but the smaller ones have lifetimes of 15 min to 1 day. For solid-cored aerosol particles, these authors conclude that something like an inverted micelle model may be applicable. (Organic molecules arrayed with polar ends inwards, towards an aqueous layer surrounding a solid core.) This structure is in itself a fascinating gas—solid interaction. They write: "It is premature to apply the results of micelle research to atmospheric problems, but we consider the prospect a promising one."

Quantitative data on stone decay seem rather scarce. Winkler [109] indicates that measurements of the rate of decay were made in Scotland by Sir Archibald Geikie [115] and in New York by Julien [116] in the 1880s and that work of this type was not resumed until after the Second World War. Fundamental knowledge of the kinetics and mechanisms is equally scarce: a single paragraph in Winkler's book speculates about possibilities ranging from autocatalytic acceleration to retardation by transport across a product layer, i.e. the usual general topics of solid—gas kinetics, with no detail at all. There seems to be an important field for future work here; and another in the matter of gas—solid interaction in the aerosol particles themselves.

References pp. 146—149

References

1 F.S. Manning and W.O. Philbrook in J.H. Strassburger (Ed.), Blast Furnace, Theory and Practice, Gordon-Breach, New York, 1969, Chap. XVII.
2 O. Levelspiel, Chemical Reaction Engineering, Wiley, New York, 1962, Chap.12.
3 L.G. Harrison, in C.H. Bamford and C.F.H. Tipper (Eds.), Comprehensive Chemical Kinetics, Vol. 2, Elsevier, Amsterdam, 1969, Chap. 5.
4 T. Chida and J.D. Ford, Can. J. Chem. Eng., 55 (1977) 313.
5 Y.K. Rao and I.J. Lin, Can. Metall. Q., 12 (1973) 125.
6 R.H. Tien and E.T. Turkdogan, Metall. Trans., 3 (1972) 2639.
7 J. Szekely and J.W. Evans, Chem. Eng. Sci., 25 (1970) 1091.
8 J. Szekely and J.W. Evans, Chem. Eng. Sci., 26 (1971) 1901.
9 J. Szekely and J.W. Evans, Metall. Trans., 2 (1971) 1691.
10 J. Szekely and J.W. Evans, Metall. Trans., 2 (1971) 1699.
11 H.Y. Sohn and J. Szekely, Chem. Eng. Sci., 27 (1972) 763.
12 J. Szekely, C.I. Lin and H.Y. Sohn, Chem. Eng. Sci., 28 (1973) 1975.
13 G. Nabi and W.K. Lu, Ind. Eng. Chem. Fundam., 13 (1974) 311.
14 J.H. Krasak and J.M. Smith, AIChE J., 18 (1972) 506.
15 M. Grunza and W. Hirschwald, J. Vac. Sci. Technol., 11 (1974) 424.
16 M. Grunze, W. Hirschwald and S. Krebs, Z. Phys. Chem. N.F., 102 (1976) 73.
17 P. Kofstad and A.Z. Hed, J. Electrochem. Soc., 115 (1968) 102.
18 F. Koch and J.B. Cohen, Acta Crystallogr. Sect. B, 25 (1969) 275.
19 M. Hayakawa, M. Moringa and J.B. Cohen, in M.S. Seltzer and R.I. Jaffe (Eds.), Defects and Transport in Oxides, Plenum Press, New York, 1974, pp. 117—204.
20 B. Andersoon and J.O. Sletnes, Acta Crystallogr. Sect. A, 33 (1977) 268.
21 Y. Koga, Chem. Phys. Lett., 16 (1972) 598.
22 B.E.F. Fender and F.D. Riley, J. Phys. Chem. Solids, 30 (1969) 793.
22a P. Vallet and P. Raccah, Mem. Sci. Rev. Metall, 62 (1966) 1.
23 R.A. Giddings and R.S. Gordon, J. Am. Ceram. Soc., 56 (1973) 111.
24 M. Hayakawa and J.B. Cohen, J. Am. Ceram. Soc., 55 (1972) 160.
25 K.J. Gallagher, W. Fertknecht and U. Mannweiler, Nature (London), 217 (1968) 1118.
26 W. Feitknecht and K.J. Gallagher, Nature (London), 228 (1970) 548.
27 B. Gillot, A. Rousset and G. Dupre, J. Solid State Chem., 25 (1978) 263.
28 C. Carel, C. R. Acad. Sci. Ser. C, 277 (1973) 69.
29 A. Deschanvres and B. Raveau, Rev. Chim. Miner., 5 (1958) 201.
30 P. Bracconi and L.-C. Dufour, J. Phys. Chem., 22, (1975) 2395.
31 P. Bracconi and L.-C. Dufour, J. Phys. Chem., 22 (1975) 2400.
32 J. Haber, J. Less-Common Met., 54 (1977) 243.
33 A.D. Wadsley, Non-Stoichiometric Compunds, Academic Press, New York, 1964, Chap. 3.
34 J.G. Allpress, R.J.D. Tilley and M.J. Sienko, J. Solid State Chem., 3 (1971) 440.
35 J. Haber, J. Stoch and L. Ungier, J. Solid State Chem., 19 (1976) 113.
36 B. Delmon and A. Roman, J. Chem. Soc. Faraday Trans. 1, 69 (1973) 941.
37 P. Ratnasamy, A.V. Ramaswamy, K. Banerjee, D.K. Sharma and N. Ray, J. Catal., 38 (1975) 19.
38 F. Chiesa and M. Rigaud, Can. J. Chem. Eng., 49 (1971) 617.
39 R. Skorski, Nature (London), 240 (1972) 15.
40 I. Svare, Nature (London) 244 (1973) 78.
41 C.T. Peters, Nature (London), 244 (1973) 79.
42 M.W. Rowe, R. Fanick, D. Jewett and J.D. Rowe, Nature (London), 263 (1976) 756.
43 M.W. Rowe, S.M. Lake and R. Fanick, Nature (London), 266 (1977) 612.

44 P.A. Sermon and G.C. Bond, Catal. Rev. 8 (1979) 211.
45 G.E. Batley, A. Ekstrom and D.A. Johnson, J. Catal., 34 (1974) 368.
46 A.W. Naumann and A.S. Behan Jr., J. Catal., 39 (1975) 432.
47 J.M. Zembala, P. Grange and B. Delmon, C.R. Acad. Sci. Ser. C, 279 (1974) 561.
48 J.M. Finch, J. Catal., 43 (1976) 111.
49 H. Miura, Y. Morikawa and T. Skirasaki, J. Catal., 39 (1975) 22.
50 R.J. Cvetanovic and Y. Amenomiya, Adv. Catal., 17 (1967) 103.
51 D.M. Adams, Inorganic Solids, London, 1974.
52 D.S. McClure, J.Phys. Chem. Solids, 3 (1957) 311.
53 J.D. Dunitz and L.E. Orgel, J. Phys. Chem. Solids, 3 (1957) 318.
54 H. Kobayashi and C. Wagner, J. Chem. Phys., 26 (1957) 1609.
55 C. Wagner, J. Chem. Phys., 21 (1953) 1819.
56 H. Schmalzried and C. Wagner, Trans. AIME, 227 (1963) 539.
57 E. Bechtold, Ber. Bunsenges, Phys. Chem., 69 (1965) 328.
58 S. Stotz, Ber. Bunsenges. Phys. Chem., 70 (1966) 37.
59 Y. Koga, M.Sc. Thesis, Tokyo University, 1962, Part 2, Chap. 3.
60 H.J. Grabke, Ber. Bunsenges. Phys. Chem., 70 (1966) 664.
61 H.J. Grabke, Ber. Bunsenges. Phys. Chem., 69 (1965) 48.
62 K. Fueki, H. Inaba and T. Mukaibo, Bull. Chem. Soc. Jpn. 43 (1970) 23.
63 C. Wagner, Adv. Catal., 21 (1970) 323.
64 S. Makishima, Y. Yoneda and Y. Saito, Actes du Deuxième Congres International de Catalyse, Technip., Paris, 1960, p. 617.
65 F. Gronvold, J. Inorg. Nucl. Chem., 1 (1955) 357.
66 R.E. DeMarco and M.G. Mendel, J. Phys. Chem., 64 (1960) 132.
67 K.J. Notz and M.G. Mendel, J. Inorg. Nucl. Chem., 14 (1960) 55.
68 S.A. Morrow, S. Graves and L. Tomlinson, Trans. Faraday Soc., 57 (1961) 1400.
69 A.H. LePage and A.G. Fane, J. Inorg. Nucl. Chem., 36 (1974) 87.
70 V.H. Heiskala, J. Phys. Chem., 69 (1965) 2012.
71 F.J. Johnson, D.A. Hutchinson and J.J. Katz, J. Inorg. Nucl. Chem., 7 (1958) 392.
72 J.S. Anderson, L.E.J. Roberts and E.A. Harper, J. Chem. Soc., (1955) 3496.
73 S. Aronson, R.B. Roof and J. Belle, J. Chem. Phys., 27 (1957) 137.
74 S. Aronson and J.C. Clayton, J. Inorg. Nucl. Chem., 7 (1958) 384.
75 V.G. Vlasov and Yu N. Semavin, J. Appl. Chem. U.S.S.R., 40 (1967) 374.
76 V.G. Vlasov and Yu N. Semavin, J. Appl. Chem. U.S.S.R., 40 (1967) 1169.
77 H.W.G. Heyman, C.G.M.M. Camp-van Berkel and H.S. can der Baan, J. Catal., 48 (1977) 386.
78 C. Carel, C. R. Acad. Sci. Ser. C, 265 (1967) 533.
79 T. Imoto, Y. Harano and Y. Nishi, Nippon Kagaku Zasshi, 84 (1963) 115.
80 T. Imoto, Y. Harano, Y. Nishi and S. Masuda, Nippon Kagaku Zasshi, 85 (1964) 106.
81 T. Imoto, Y. Harano, Y. Nishi and S. Masuda, Bull. Chem. Soc. Jpn., 37 (1964) 441.
82 T. Imoto, Y. Harano and Y. Nishi, Bull. Chem. Soc. Jpn., 37 (1964) 1181.
83 T. Imoto, Y. Harano and Y. Nichi, Nippon Kagaku Zasshi, 86 (1965) 485.
84 E.A. Secco, Can. J. Chem., 39 (1961) 1544.
85 E.A. Secco, Can. J. Chem., 42 (1964) 1396.
86 E.A. Secco, and Chien-Huo Su, Can. J. Chem., 46 (1968) 1621.
87 E.A. Secco and R. Swee-Chye Yeo, Can. J. Chem., 49 (1971) 1953.
88 R.E. Carter, J. Chem. Phys., 34 (1961) 2010.
89 L.G. Harrison and C.F. Ng, Trans. Faraday Soc., 67 (1971) 1787.
90 L.G. Harrison, J.A. Morrison and G.S. Rose, J. Phys. Chem., 61 (1957) 1314.

91 L.G. Harrison, I.M. Hoodless and J.A. Morrison, Discuss. Faraday Soc., 28 (1959) 103.
92 R.J. Adams and L.G. Harrison, Trans. Faraday Soc., 60 (1964) 1792.
93 L.G. Harrison, R.J. Adams and R.C. Catton, J. Chem. Phys., 45 (1966) 4023.
94 E.J.W. Verwey, Rec. Trav. Chim. Pays-Bas, 65 (1946) 521.
95 G.C. Benson, P.I. Freeman and E. Dempsey, J. Chem. Phys., 39 (1963) 302.
96 L.G. Harrison and R.A. Siddiqui, Trans. Faraday Soc., 58 (1962) 982.
97 J.G. Bergman and R.L. Martin, Anal. Chem., 34 (1962) 911.
98 L.G. Harrison and Y. Koga, Proc. Soc. London Ser. A, 327 (1972) 97.
99 K. Takaishi and Y. Sensui, Surf. Sci., 19 (1970) 339.
100 W.J. Dunning, Discuss. Faraday Soc., 28 (1959) 131.
101 L.G. Harrison, J.A. Morrison and G.S. Rose, Proc. 2nd Int. Congr. Surf. Activity, Butterworths, London, 1957, p. 287.
102 L.G. Harrison, J.A. Morrison and R. Rudham, Trans. Faraday Soc., 54 (1958) 106.
103 L.G. Harrison, M.D. Baijal and D.J. Bird, Trans. Faraday Soc., 60 (1964) 1099.
104 L.G. Harrison, R.J. Adams, M.D. Baijal and D.J. Bird in G.-M. Schwab (Ed.), Proceedings of the 5th International Symposium on the Reactivity of Solids, Munich, 1964, Elsevier, 1965, p. 279.
105 L.G. Harrison and C.F. Ng, Trans. Faraday Soc., 67 (1971) 1801, 1810.
106 L.G. Harrison and M. Prasad, J. Chem. Soc. Faraday Trans. 1, 70 (1974) 471.
107 R.C. Catton and L.G. Harrison, J. Chem. Phys., 47 (1967) 3810.
108 R. Cini, G. Guarini and E. Ferroni, Ann. Chim. (Rome), 51 (1961) 1113; R. Cini, G. Guarini, E. Ferroni and G. Taddei, Ann. Chim. (Rome), 51 (1961) 1129.
109 E.M. Winkler, Stone: Properties, Durability in Man's Environment, Springer-Verlag, New York, 2nd edn., 1975.
110 K. Lal Gauri, Sci. Am., 238 (1978) 126.
111 B.H. Vos and E. Tammes, Rep. B 1-96-96, TNO for Building Materials and Building Structures, Delft, The Netherlands, 1969.
112 P.W. Choquette and L.C. Pray, Bull. Am. Assoc. Pet. Geol., 54 (1970) 207.
113 B.H. Vos, unpublished Rep. TNO for Building Materials and Building Structures, Delft, The Netherlands, 1970, quoted by Winkler in ref. 109.
114 C.E. Junge, Adv. Geophys., 4 (1958) 1.
115 A. Geikie, Proc. R. Soc. Edinburgh, (1880) 518.
116 A.A. Julien, U.S. 10th Census 1880, Vol. X, Spec. Rep. Pet., Coke, Bldg. Stone, (1884) 364.
117 D.P. Smith, Hydrogen in Metals, University of Chicago Press, Chicago, 1948.
118 P. Cotterill, Prog. Mater. Sci. 9 (1961) 205.
119 M. Armbruster, J. Am. Chem. Soc., 65 (1943) 1043.
120 A.S. Darling, Platinum Met. Rev., 2 (1958) 16.
121 L.B. Pfeil, Proc. R. Soc. London Ser. A, (1926) 182.
122 A.A. Griffiths, Philos. Trans. R. Soc. London Ser. A, 221 (1920) 163.
123 E. Orowan, Weld. Res. Suppl., March (1955) 1575.
124 C. Zener, Fracturing of Metals, American Society of Metals, Cleveland, 1948, p. 3.
125 J.G. Morlet, H.H. Johnson and A.R. Troiano, J. Iron Steal Inst. London, (1958) 37.
126 H.H. Johnson, J.G. Morlet and A.R. Troiano, Trans. Metall. Soc. AIME, (1958) 528.
127 P.K. Gallagher, E.M. Gyorgy and H.E. Bair, J. Chem. Phys., 71 (1979) 830.
128 J.A. Hedvall, Reactionfäigkeit fester stoffe, reprinted by Edwards Brothers, Ann Arbor, Michigan, 1943.
129 W. Mueller, J.P. Blackledge and G.G. Libowitz, Metal Hydrides, Academic Press, New York, 1968.

130 A.D. McQuillan, J. Chem. Phys., 53 (1970) 156.
131 W.A. Oates, Scr. Metall., 10 (1976) 797.
132 V.B. Vykhodets, A. Ya. Fishman and V.B. Demin, Phys. Status Solidi B, 82 (1977) K59.
133 W.A. Oates and T.B. Flanagan, J. Chem. Soc. Faraday Trans. 1, 73 (1977) 407.
134 H;C. Jamieson, G.C. Weatherly and F.D. Manchester, J. Less Common Met., 50 (1976) 85.
135 P.C. Hayes and P. Grievson, Metall. Trans., 12B (1981) 319.
136 J. Szekely, J.W. Evans and H.Y. Sohn, Gas—Solid Reactions, Academic Press, New York, 1976.
137 J.R. Porter and L.C. De Jonghe, Metall. Trans., 12B (1981) 299.
138 J. Szekely and C. Karatas, Metall. Trans., 9B (1978) 147.
139 A.W.D. Hills, Metall. Trans., 9B (1978) 121.
140 H.Y. Sohn, Metall. Trans., 9B (1978) 723.
141 A.W.D. Hills, Metall. Trans., 9B (1978) 725.
142 P.J. Meschter and H.J. Grabke, Metall. Trans., 10B (1979) 323.
143 L.G. Harrison, Y. Koga, R.T. Lassau, M. Nagao and J.C.S. Scott, J. Chem. Soc. Faraday Trans. 1, 77 (1981) 1393.
144 C.M. Ransom and P.J. Ficalora, Metall. Trans., 11A (1980) 801.
145 R.G. Davies, Metall. Trans., 12A (1981) 1667.
146 T.E. Graedel and C.J. Weschler, Rev. Geophys. Space Phys., 19 (1981) 505.

This Page Intentionally Left Blank

Chapter 3

Heterogeneous Atomisation and Recombination

D. BRENNAN

1. Introduction

Heterogeneous atomisation and recombination are amongst the simplest surface processes with chemical content and, as such, they have been much investigated in the hope that their kinetic behaviour would be experimentally definable and capable of being represented by models which, while simple enough to be theoretically tractable, would still be realistic enough to be useful. Studies of these reactions have also been motivated by the belief that they could serve to formulate some of the basic vocabulary with which to describe more complex catalytic reactions. The object of this article will be to examine to what extent these aspirations have been realised and to what extent optimism must remain a substitute for achievement. In addition to this fundamental work, heterogeneous atomisation and recombination reactions have recently attracted applied interest in connection with space exploration and the chemistry of the upper atmosphere. It can be anticipated that this new stimulus will result in further progress, particularly in the field of recombination.

Greatest progress has been made with heterogeneous atomisation. There is now a substantial body of agreed kinetic data for atomisation reactions obtained by several workers using different experimental techniques. There is also a large measure of agreement on how these data should be interpreted in fundamental terms. Unfortunately, the same cannot be said of recombination, although, for these reactions also, there is much that is understood. The unusual degree of accord prevailing in the atomisation field is owed to two experimental details. Firstly, the reaction takes place at high temperatures with low surface concentrations. The result is that many of the complexities and subtleties associated with overlayers at high concentration and relatively low temperature are avoided and the approximation of uniformity becomes quite good. Secondly, there is only one reactant species, viz. the molecule, and it is stable until it meets the experimental surface. This is because the equilibrium concentration of atoms in the molecular gas at ambient temperature is entirely negligible and, if care is taken, the atoms produced at the catalyst surface can be prevented from returning there. Recombination studies do not benefit from such simplifications. Usually, surface coverages can be high and temperatures low enough for the overlayer to become complex (and heterogeneous). Considerable experimental difficulties arise because the reactant atoms must be formed in the presence of molecules and are

References pp. 231—234

liable to recombine before they reach the experimental surface. However, recombination as well as atomisation kinetics have been described in terms of primary surface parameters, like energy of adsorption, surface mobility, collision frequency, etc., in a way which is more meaningful than has yet been achieved with other catalytic systems.

2. General theory of atomisation and recombination

2.1 DESORPTION MECHANISMS

2.1.1 A model for the adsorbed state

In order to discuss the factors which relate rates of desorption of atoms and molecules to concentrations of adsorbed species, we require a fairly detailed description of the adsorbed state. We do not possess the knowledge necessary for a truly quantitative account, but will adopt a simple model of the overlayer which will permit us to develop the discussion in a semi-quantitative way. In this manner, we will be able to discover the important ingredients of the problem and even at times to obtain results which are in fair agreement with experiment. However, we ought to recognise at the outset that the simplicity of our model will severely limit its value and, indeed, there will be occasions when we will find it difficult even to maintain self-consistency.

We assume that the chemisorption of hydrogen, oxygen and nitrogen entails dissociation into atoms according to the equation

$$X_2(g) + S = 2X{-}S \qquad \Delta U_{2,1} \tag{Ia}$$

where $\Delta U_{2,1}$ is the change in internal energy for the adsorption at 0 K. In its most general sense, S denotes the surface without implying anything as to its structure or the nature of the surface bond, although for most of our discussion S will signify a surface site. It is possible that chemisorption occurs via a weakly held precursor state, thus

$$X_2(g) + S = X_2{-}S \tag{II}$$

$$X_2{-}S = 2X{-}S \tag{III}$$

We make the further assumption that the surface is crystallographically perfect and isotropic, so that no matter in which direction the adatom moves parallel to the surface, it experiences the same variation in potential (see Fig. 1).

When the temperature is sufficiently low, the probability of an adatom's surmounting the potential energy barrier between adjacent sites will be negligible and then each adatom occupies an adsorption-site, of which there are N_S per unit area. When RT is large relative to the barrier height, adatoms are free to translate over the surface without sensing its atomic

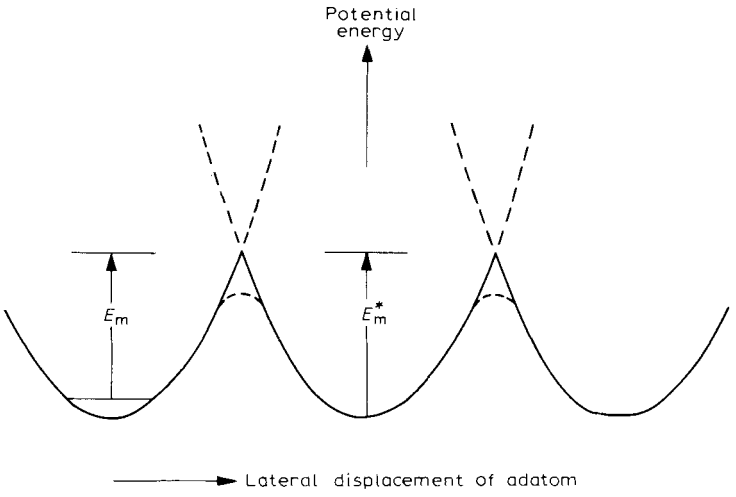

Fig. 1. The variation of the potential energy of an adatom moving parallel to the surface. E_m is the barrier height measured from the zero point energy of the two degenerate modes of vibration parallel to the surface, i.e. $E_m = E_m^* - h\nu_p$, where ν_p is the frequency of vibration of a localised adatom parallel to the surface.

structure. At intermediate temperatures, the adatoms spend most of their time in a localised state but make frequent hops to neighbouring sites. Adatoms moving parallel to the surface are able to collide with other adatoms and thereby provide a route for molecular desorption by the reverse of reaction (Ia), viz.

$$2\,X{-}S \;=\; X_2(g) + S \qquad -\Delta U_{2,1} \qquad \text{(Ib)}$$

This is the Langmuir—Hinshelwood recombination mechanism.

We adopt the discussion of Holland [1, 2] whose treatment of surface mobility in terms of a simple quantum mechanical model provides explicit relations for the frequency of collision between adatoms at temperatures ranging from $RT \gg E_m$ to $RT \ll E_m$. According to this model, adatoms experience only two kinds of interaction, other than chemical reaction. Firstly, an adatom occupying a site excludes others from that site. Secondly, an adatom experiences a collision if a second adatom approaches so their centres are separated by a distance σ_1, regardless of whether the adatom is in an adsorption site or in transit. The frequency of such collisions per unit area (ζ) and the probability ($\kappa_{1,2}$) that a collision results in the formation of a molecule, determine the rate at which molecules leave the surface by reaction (Ib). When the surface coverage is very low, the chance of two adatoms colliding is correspondingly low. If the temperature is high enough, the rate of direct desorption of adatoms, i.e.

$$X{-}S \;=\; X(g) + S \qquad -\Delta U_{1,1} \qquad \text{(IVa)}$$

becomes significant relative to the rate of surface recombination; $\Delta U_{1,1}$ again relates to the process occurring at 0 K. We will see later that the sole mechanism of atomisation is the desorption of adatoms derived from the adsorption of molecules. Hence, the rate of reaction (IVa) is of key importance to our discussion.

2.1.2 Desorption of atoms

The rate of desorption of atoms per unit area is proportional to the concentration $(N_a)_1$ of adatoms, and the constant of proportionality is the rate coefficient d_1, i.e.

$$D_1 = d_1(N_a)_1 \tag{1}$$

The dependence of d_1 on temperature is given by the Arrhenius-type relation

$$d_1 = A_1 \exp\left(\frac{\Delta U_{1,1}}{RT}\right) \tag{2}$$

since the activation energy for the desorption of atoms is simply the energy of the formation of the surface bond (see Fig. 2), there being no energy of activation for the adsorption of atoms. A_1 will be the order of kT/h, which at 1000 K has the value 2×10^{13} s^{-1}.

2.1.3 Frequency of collision between adatoms

Following Holland [1, 2], a localised atom is assigned to one of the localised quantum states, with energy less than E_m^*, associated with an adsorption site (see Fig. 1). Quantum states, whose energies are in excess of E_m^*, embrace the whole surface and are approximated to be the states of a particle in a two-dimensional box of uniform potential. An adatom in one of these quantum states is able to move about the surface and encounter other adatoms, both localised and mobile, the effective collision diameter always being σ_1.

Let us focus our attention on one such *mobile* adatom. In unit time, it will travel on average a distance $\bar{c}_1$ and it will collide with *all* the adatoms whose centres are within a distance σ_1 of the line defining its path. Since there is a total of $(N_a)_1$ adatoms per unit area, each mobile adatom will have a collision frequency of $2\sigma_1\bar{c}_1(N_a)_1$. Further, since it takes two adatoms to make a collision and there are $({}^mN_a)_1$ mobile adatoms eligible per unit area, the total collision frequency per unit area is $\frac{1}{2}[2\sigma_1\bar{c}_1(N_a)_1]({}^mN_a)_1$, viz.

$$\zeta = \sigma_1\bar{c}_1(N_a)_1({}^mN_a)_1 \tag{3}$$

To estimate $({}^mN_a)_1$, Holland supposes that the same vibrational motion

perpendicular to the surface is experienced by both localised and mobile adatoms, but that the frequency (ν_p) of the oscillations parallel to the surface of a localised adatom are characteristic of the harmonic potential of a site cut off at E_m^*, and of the mass (m_1) of the adatom. Holland's expression for $({}^mN_a)_1$ is

$$({}^mN_a)_1 = \frac{1}{2} N_S (1 - a\theta) \times \left[\left\{\left(\beta + \frac{1-\theta}{1-a\theta}\right)^2 + \frac{4\beta\theta}{1-a\theta}\right\}^{1/2} - \left(\beta + \frac{1-\theta}{1-a\theta}\right)\right] \quad (4)$$

where

$$\theta = \frac{(N_a)_1}{N_S} \quad (5)$$

$$a = \tfrac{1}{4}\pi\sigma_1^2 N_S \quad (6)$$

$$\beta = \frac{2m_1 kT}{N_S h^2} \left(\frac{1 - \exp(-\Theta_p/T)}{1 - \exp(-E_m^*/RT)}\right)^2 \exp\left(-\frac{E_m}{RT}\right) \quad (7)$$

$$\Theta_p = \frac{h\nu_p}{k} \quad (8)$$

The frequency (ν_p) of the two degenerate vibrational modes parallel to the surface of an adatom confined to an adsorption site is given to a first approximation by the relation

$$\nu_p = \left(\frac{2N_S}{\pi^2} \cdot \frac{E_m^*}{m_1 N_A}\right)^{1/2} \quad (9)$$

Substitution of eqn. (4) in eqn. (3) shows that the general expression for the collision frequency per unit area depends on coverage in a complex manner. The occupation of translatory states is determined not only by the availability of the thermal energy required for excitation to states with energies in excess of E_m^*, but also by the degree to which lattice sites are occupied. A temperature which is low enough for a high degree of localisation at small coverages could result in substantial mobility at high coverages because the adatom has now a much reduced probability of finding an unoccupied site. The model gives a limiting value for θ not of unity but of a^{-1}, a being the fraction of the area of an adsorption site actually occupied by the adatom. We now consider the low and high temperature limits of eqn. (3).

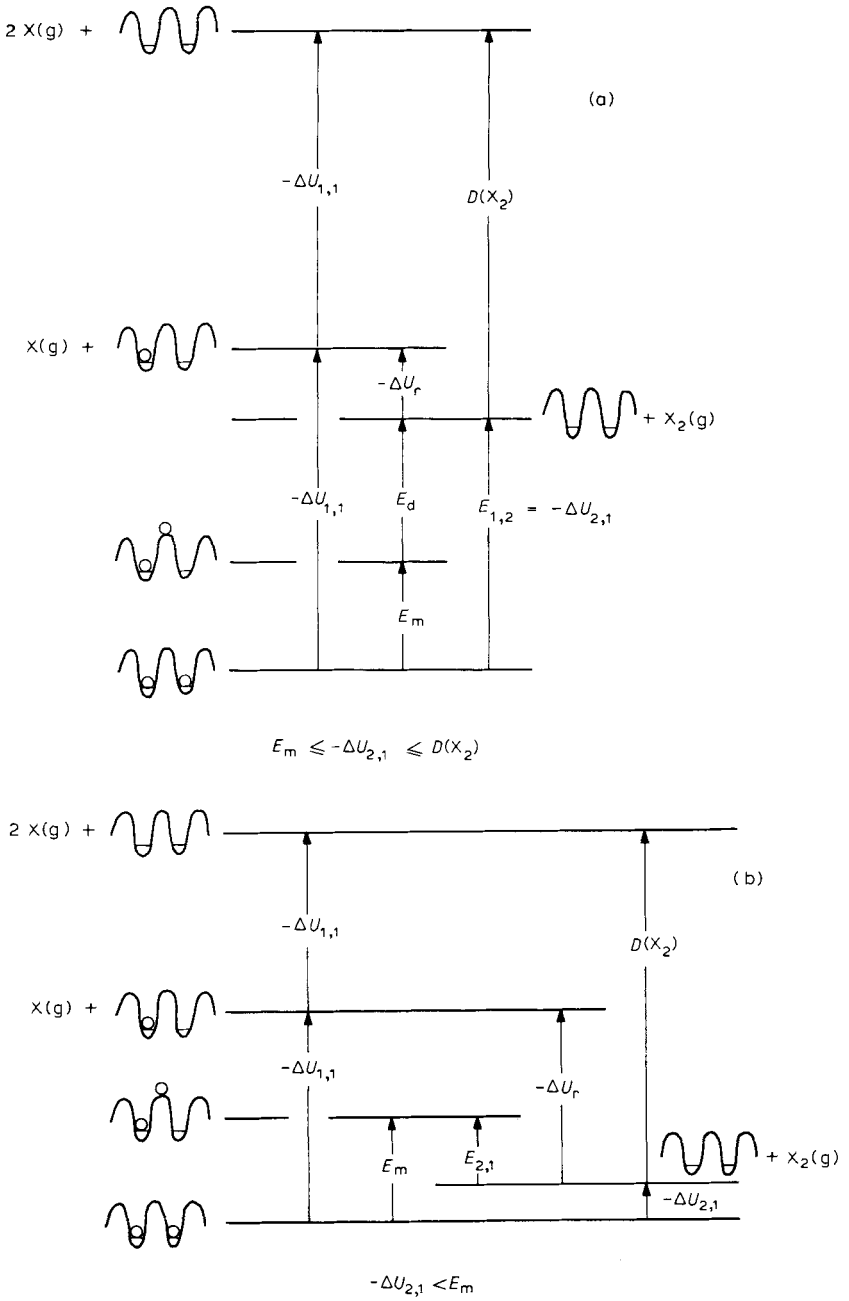

Fig. 2. Potential energy relationships. The energies are measured from the zero point levels of the appropriate species. (a) Unactivated molecular adsorption and Rideal–Eley recombination; (b) activated exothermic molecular adsorption; (c) endothermic molecular adsorption; (d) very strong adsorption resulting in activated Rideal–Eley recombination.

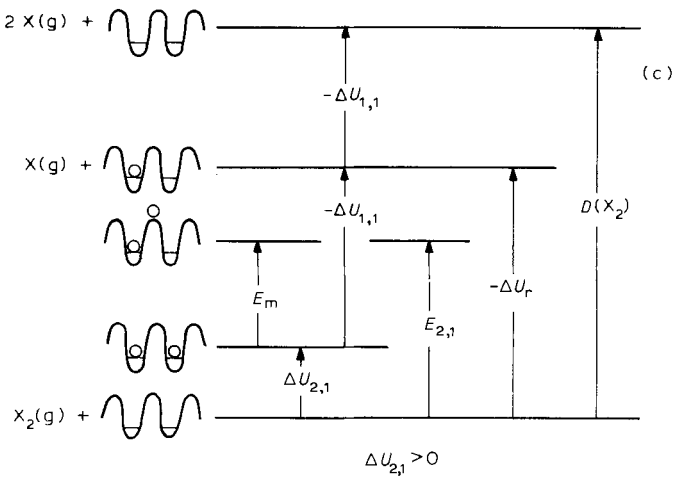
2 X(g) +
(c)
$-\Delta U_{1,1}$
X(g) +
$-\Delta U_{1,1}$
$D(X_2)$
E_m
$-\Delta U_r$
$E_{2,1}$
$\Delta U_{2,1}$
$X_2(g)$ +
$\Delta U_{2,1} > 0$

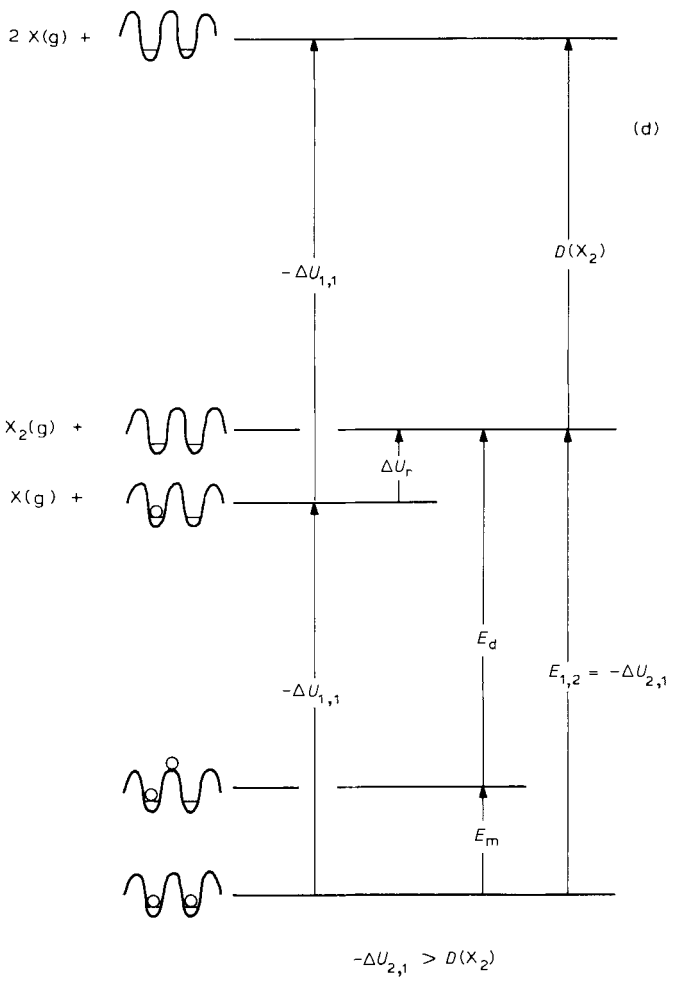
2 X(g) +
(d)
$-\Delta U_{1,1}$
$D(X_2)$
$X_2(g)$ +
ΔU_r
X(g) +
E_d
$E_{1,2} = -\Delta U_{2,1}$
$-\Delta U_{1,1}$
E_m
$-\Delta U_{2,1} > D(X_2)$

(*i*) *Case* $RT \ll E_m$. In the low temperature limit, provided also that θ is small

$$\zeta = (N_a)_1^2 \sigma_1 (\pi kT)^{3/2} \times$$

$$\frac{\sqrt{2m_1}}{N_S h^2} \left(\frac{1 - \exp(-\Theta_p/T)}{1 - \exp(-E_m^*/RT)} \right)^2 \exp\left(-\frac{E_m}{RT}\right) \tag{10}$$

A similar expression has been given by Ehrlich [3] who said that the frequency of hopping for each adatom would be proportional to $\exp(-E_m/RT)$ and the chance that an adjacent site was already occupied would be $(N_a)_1/N_S$, so

$$\zeta \propto (N_a)_1 \frac{(N_a)_1}{N_S} \exp\left(-\frac{E_m}{RT}\right)$$

The merit of eqn. (10) is that it is explicit about the constant of proportionality. It should be noted that the final expression given by Holland for ζ is too small by a factor of 2.

We will make considerable use of eqn. (10) in developing kinetic relationships, but we will not always satisfy the restriction that θ should be small. This point will be discussed when we come to consider molecular adsorption

(*ii*) *Case* $RT \gg E_m$. In this limit, $({}^m N_a)_1 = (N_a)_1$ because, in effect, the average energy of *all* the adatoms is in excess of E_m and eqn. (3) becomes

$$\zeta = (N_a)_1^2 \bar{c}_1 \sigma_1 \tag{11}$$

with

$$\bar{c}_1 = \left(\frac{\pi kT}{2m_1}\right)^{1/2} \tag{12}$$

This is the customary relation [3] for the collision frequency in an ideal two-dimensional gas moving freely in a constant potential field provided by the surface, except for the absence of a $\sqrt{2}$ factor. The kinetic theory derivation of the collision frequency involves the *relative* velocity, which is the origin of the $\sqrt{2}$ factor. In the present model, there are two types of collisions, firstly with the localised adatoms, when the $\sqrt{2}$ factor would not be appropriate, and secondly with mobile adatoms, when it would. However, the degree of approximation in the treatment is such that the refinement of a $\sqrt{2}$ factor is unwarranted; it is mentioned merely to clarify its presence in expressions found in the literature.

2.1.4 Desorption of molecules

If $\kappa_{1,2}$ is the probability that a collision between adatoms will result in molecular desorption, we have

$$D_2 = \kappa_{1,2}\zeta \tag{13}$$

or

$$D_2 = d_2(N_a)_1^2 \tag{14}$$

where d_2 is the second-order rate coefficient.

We suppose that the temperature dependence of $\kappa_{1,2}$ can be represented by an Arrhenius-type expression, i.e.

$$\kappa_{1,2} = (\kappa_0)_{1,2} \exp(-E_d/RT) \tag{15}$$

where E_d is the activation energy for the desorption of the collision complex (see Fig. 2); hence

$$d_2 = \frac{(\kappa_0)_{1,2}\zeta}{(N_a)_1^2} \exp\left(-\frac{E_d}{RT}\right) \tag{16}$$

In the manner of Section 2.1.3, we now again consider limiting cases.

(*i*) *Case* $RT \ll E_m$. From eqns. (10), and (16), we obtain

$$d_2 = (\kappa_0)_{1,2}\sigma_1(\pi kT)^{3/2} \times \frac{\sqrt{2m_1}}{N_S h^2}\left(\frac{1-\exp(-\Theta_p/T)}{1-\exp(-E_m^*/RT)}\right)^2 \exp\left(-\frac{E_{1,2}}{RT}\right) \tag{17}$$

where

$$E_{1,2} = E_d + E_m \tag{18}$$

Highly exothermic adsorption of molecular hydrogen, oxygen and nitrogen into the atomic state on clean metals is virtually unactivated [Fig. 2(a) and (d)], so we can write for such systems $E_{1,2} = -\Delta U_{2,1}$. When $-\Delta U_{2,1}$ is less than E_m, molecular adsorption is activated and, in such cases, we suppose that E_d is zero and then $E_{1,2} = E_m$ [see Fig. 2(b) and (c)].

(*ii*) *Case* $RT \gg E_m$. For this condition, the adatoms are freely translating on the surface and are unaware that there is a fluctuating potential below them. From eqns. (11), (12) and (16), we obtain

$$d_2 = (\kappa_0)_{1,2}\sigma_1\left(\frac{\pi kT}{2m_1}\right)^{1/2} \exp\left(-\frac{E_{1,2}}{RT}\right) \tag{19}$$

with $E_{1,2}$ taking the values $-\Delta U_{2,1}$ for exothermic adsorption and zero for endothermic adsorption.

Numerical values for eqns. (17) and (19), written in the form

$$d_2 = A_2 \exp(-E_{1,2}/RT) \tag{20}$$

are given in Table 1 for localised and mobile adsorption at low coverage. The values of A_2 for the two states are not very different, although experimental evidence [107] concerning the values of E_m for the systems considered indicates that localised adsorption is the more appropriate description, even up to the highest temperatures of interest.

2.1.5 *Conditions for a negligible rate of molecular desorption relative to the rate of atomic desorption*

When we come to consider experimental results, we will find (in Sect. 3.3) that the interaction of oxygen with tungsten or rhenium at high temperatures produces atoms or oxides, but not molecules. The reason for this has been given by Ehrlich [4]. The effect is associated with the case $-\Delta U_{2,1} > D(X_2)$, when the desorption of molecules requires more activation than the desorption of adatoms [see Fig. 2(d)]. The relative rate of desorption of molecules compared with atoms is obtained by combining eqns. (1) and (14), viz.

$$\frac{D_2}{D_1} = \frac{d_2}{d_1}(N_a)_1 \tag{21}$$

Substituting eqns. (2) and (20), we have

$$\frac{d_2}{d_1} = \frac{A_2}{A_1} \exp\left(-\frac{E_{1,2} + \Delta U_{1,1}}{RT}\right) \tag{22}$$

TABLE 1

Values at 1000 K of the pre-exponential factor A_2 [eqn. (20)] for localised and mobile adsorption. The parameters for the localised state relate to tungsten, and Θ_p has been calculated assuming that the activation energy for surface diffusion (E_m) is one-fifth the energy of desorption of atoms ($-\Delta U_{1,1}$) [107]; $(\kappa_0)_{1,2}$ has been assigned the value 0.5 and N_S the value 10^{15} cm^{-2}.

	Hydrogen	Oxygen	Nitrogen
$-\Delta U_{2,1}$/kJ mole^{-1}	146 [108]	812 [109]	335 [110]
E_m/kJ mole^{-1}	58	131	128
Θ_p/K	537	196	208
σ_1/nm	0.24	0.28	0.30
A_2(localised)/10^{-3} cm^2 s^{-1}	25	21	23
A_2(mobile)/10^{-3} cm^2 s^{-1}	4.3	1.3	1.4

For oxygen, A_2 is unlikely to exceed about 0.02 (see Table 1) and with A_1 set at about $2 \times 10^{13}\,s^{-1}$ (see Sect. 2.1.2), we have

$$\frac{D_2}{D_1} \sim 10^{-15} \left(\frac{(N_a)_1}{cm^{-2}}\right) \exp\left[\frac{\frac{1}{2}\{D(X_2) + \Delta U_{2,1}\}}{RT}\right] \qquad (23)$$

making our usual assumption for highly exothermic adsorption that molecular adsorption is unactivated. When $-\Delta U_{2,1} > D(X_2)$, the index of the exponential term will be negative, and we expect the rate of atomic adsorption to exceed that of molecular adsorption by a substantial factor. In the example of the oxygen—tungsten system at 2000 K, $\Delta U_{2,1} = -812\,kJ\,mole^{-1}$ [109] and $D(O_2) = 494\,kJ\,mole^{-1}$, and with $(N_a)_1$ set at $10^{-14}\,cm^{-2}$ (which is an over-estimate), we obtain $D_2/D_1 \sim 7 \times 10^{-6}$. The value of D_2/D_1 is sensitive to the value of $\Delta U_{2,1}$, but this calculation, approximate as it is, is quite sufficient to demonstrate that $D_1 \gg D_2$. The circumstances which give rise to this result are also those which result in a very strong surface bond, so the desorption of oxides rather than atoms is readily understood. Any attempt to increase the value of D_2/D_1 by raising the temperature will enhance the probability of oxide desorption as well as adversely affect the value of $(N_a)_1$.

2.2 ATOMISATION KINETICS

2.2.1 Significant processes at the surface

In the atomisation reaction, we have a flux of molecules impinging on the surface, generally at a temperature (T') very much lower than the temperature (T) of the surface, and a flux of atoms and molecules departing from the surface. Before we consider the kinetics for these practical conditions, we will examine the situation for an equilibrium system.

Imagine an isothermal system, at temperature T, consisting of gaseous molecules and gaseous atoms in equilibrium with one another according to the equation

$$X_2(g) = 2X(g) \qquad D(X_2) \qquad (V)$$

and with the surface overlayer, which may include adsorbed molecules as well as adatoms. As usual, we will assume that the surface is uniform. We begin by deciding which are the important processes. They are: (i) the chemisorption of molecules directly as atoms according to reaction (Ia) [3, 5, 7] [or via the molecular precursor state, according to reactions (II) and (III) [8]], (ii) the surface recombination of adatoms according to reaction (Ib), (iii) the adsorption of atoms, i.e.

$$X(g) + S = X{-}S \qquad \Delta U_{1,1} \qquad (IVb)$$

and (iv) the desorption of atoms according to reaction (IVa).

For many years, the various workers interested in the atomisation reaction (Roberts and Bryce [9], Miller [10], Laidler [11]) favoured the mechanism

$$X_2(g) + S = S{-}X + X(g) \qquad -\Delta U_r \qquad \text{(VIa)}$$

which provides for the simultaneous removal of gaseous molecules and the production of gaseous atoms. Brennan and Fletcher [5] have given a detailed analysis of the kinetics of the atomisation reaction for the conditions used in these workers' experiments and their own. They showed that the observed pressure dependence of the atomisation process was incompatible with a significant contribution from reaction (VIa). Further experimental evidence that this reaction is unimportant comes from the work of Smith and Fite [12], who showed that the distribution of the departing flux of H atoms from a tungsten surface was uncorrelated with the angle of incidence of the impinging flux of H_2 molecules (see Fig. 14, p. 197). More recently, however, Cochran, et al. [13] have suggested a contribution from reaction (VIa) in an attempt to account for observations in an electron spin resonance (ESR) study of the atomisation of hydrogen over tungsten at pressures between 0.1 and 100 torr in the temperature range 1000—2000 K. A combination of high pressure and low temperature will favour reaction (VIa) and, if conditions are moved sufficiently in these directions, reaction (VIa) will undoubtedly assume a significant role. Cochran et al. were unable to account quantitatively for the fate of the atoms produced by their hot filament, so their study lacks kinetic definition. An additional difficulty attaching to their experiments is the problem of surface cleanliness. It is evident from the design of the ESR cavity used, that their vacuum conditions must have been poor. The use of high pressures without special precautions to remove surface active contaminants casts further doubt on the state of their surface, especially at the lower temperatures. Because of these difficulties, Cochran et al. were unable to isolate a contribution from reaction (VIa) in useful kinetic terms, even though their conditions were sometimes such that a contribution from it might have been anticipated.

A description of the atomisation process in which both reactions (Ia) and (VIa) compete has not yet been given. It is a difficult problem, requiring for its proper treatment a description of the overlayer in terms of lattice statistics. When $-\Delta U_{2,1}$ is comparable to or greater than $D(X_2)$, making the activation energy for reaction (VIa) small or zero (see Fig. 2), then reaction (VIa) must be regarded as a serious contender. Metals which adsorb oxygen very strongly have to be considered with this possibility in mind, although we have already seen that we may also expect the additional complication of oxide formation. Such a complication arises in the case of the atomisation of oxygen by rhenium (see Sect. 3.3), but the system O_2/Pt, which has been thoroughly investigated (see Sects. 3.2.1 and 3.2.3), seems to be largely free of it. It is

possible to show, using theoretical arguments similar to those to be developed in Sect. 3.2.2, that reaction (VIa) would not be expected to be significant at pressures below 10^{-3} torr for any of the systems for which the atomisation kinetics have been determined. Accordingly, we will not give further consideration to reaction (VIa) as an atomisation process, but will adopt the treatment of Brennan and Fletcher [5] and suppose that atomisation occurs by direct desorption of adatoms. As final justification for this course, we will rely on the excellence of the fit of the kinetic consequences of the model with the experimental results.

2.2.2 Application of the principle of microscopic reversibility

The principle of microscopic reversibility enables us to say that, at equilibrium, the rates of adsorption and desorption of molecules are equal, and independently that the rates of adsorption and desorption of atoms are also equal. In the first case, we will not attempt to apply the discussion of Sect. 2.1, but will simply make use of the molecular and atomic sticking coefficients (s_2 and s_1, respectively). This procedure is useful when s_2 and s_1 are constants, as in the case when the coverage is low and molecular and atomic adsorption are unactivated. The resulting kinetic description contains only the sticking coefficients as adjustable parameters.

The rate of collision of gaseous atoms (Z_1) with unit area of the surface is given by

$$Z_1 = z_1 P_1 \tag{24}$$

where

$$z_1 = (2\pi m_1 \mathrm{k}T)^{-1/2} \tag{25}$$

Here, P_1 is the *equilibrium* pressure of gaseous atoms. Similarly, for the molecules, we have

$$Z_2 = z_2 P_2 \tag{26}$$

and

$$z_2 = \frac{z_1}{\sqrt{2}} \tag{27}$$

The relations for z_1 and z_2 require that the gas phase behaves ideally (an excellent approximation for the conditions of interest), and that the dimensions of the catalytic surface be small relative to the mean free path; we also require that the distribution of velocities be Maxwellian. The rate of adsorption of molecules per unit area of surface is $s_2 Z_2$. We recall that

the rate of desorption of molecules per unit area is D_2. Then the principle of microscopic reversibility enables us to write

$$D_2 = s_2 Z_2 \tag{28}$$

and similarly for atoms

$$D_1 = s_1 Z_1 \tag{29}$$

The value of Z_1 in terms of P_2 can be obtained from the equilibrium constant (K_p) of reaction (V), i.e.

$$K_p = \frac{P_1^2}{P_2} \frac{1}{P^\ominus} \tag{30}$$

or

$$P_1 = (P^\ominus K_p P_2)^{1/2} \tag{31}$$

$P^\ominus$ defines the standard state to which K_p is referred. Substituting eqn. (31) in eqn. (24), we obtain

$$Z_1 = z_1 (P^\ominus K_p)^{1/2} \sqrt{P_2} \tag{32}$$

Hence, the total rate of loss of material (atoms plus molecules) from unit area of the surface, measured as *atoms*, will be

$$\begin{aligned} D_1 + 2D_2 &= s_1 Z_1 + 2 s_2 Z_2 \\ &= z_1 [s_1 (P^\ominus K_p)^{1/2} \sqrt{P_2} + \sqrt{2}\, s_2 P_2] \end{aligned} \tag{33}$$

At a given temperature, the values of D_1 and D_2 will be uniquely determined by the concentrations of adsorbed atoms and molecules, viz. $(N_a)_1$ and $(N_a)_2$, respectively. The values of $(N_a)_1$ and $(N_a)_2$ can be altered (but not independently) by changing P_2.

The equilibrium state we have just described has to be contrasted with the non-equilibrium conditions which prevail in practice. The general experimental condition is a stationary state in which the gaseous molecules, at a pressure P_2', are not in equilibrium with the surface. The extent of adsorption remains constant for a given pressure, by reason of a mass balance between incident and desorbing material, but may be substantially greater than the thermodynamic coverage.

2.2.3 Kinetics of atomisation under stationary conditions when molecular adsorption is unactivated

We have already seen that atomisation experiments are designed to prevent the atoms produced by the surface ever returning there. This is done either by trapping the atoms at the walls of the apparatus, or by pumping them away, having tried to eliminate the possibility of their prior

collision with the internal surfaces of the apparatus. Under these conditions, the equation analogous to eqn. (26) is

$$Z_2' = z_2' P_2' \tag{34}$$

where

$$z_2' = \left(\frac{T}{T'}\right)^{1/2} z_2 \tag{35}$$

and the condition for mass balance is

$$2s_2' Z_2' = D_1 + 2D_2 \tag{36}$$

The constant surface coverage characteristic of any particular stationary condition can be identified with a corresponding equilibrium state in an isothermal system with partial pressures P_1 and P_2 as discussed in the previous paragraph. Accordingly, we substitute eqn. (33) into eqn. (36) to obtain

$$\frac{s_2}{s_1}\left(\frac{2}{P^{\ominus}K_p}\right)^{1/2} P_2 + \sqrt{P_2} - \frac{s_2'}{s_1}\left(\frac{T}{T'}\right)^{1/2}\left(\frac{2}{P^{\ominus}K_p}\right)^{1/2} P_2' = 0 \tag{37}$$

which can be solved for $\sqrt{P_2}$, i.e.

$$\sqrt{P_2} = \left[2\frac{s_2}{s_1}\left(\frac{2}{P^{\ominus}K_p}\right)^{1/2}\right]^{-1} \times \left[-1 \pm \left\{1 + \frac{s_2 s_2'}{s_1^2}\left(\frac{T}{T'}\right)^{1/2}\frac{8}{P^{\ominus}K_p} P_2'\right\}^{1/2}\right] \tag{38}$$

This equation relates the equilibrium pressure (P_2) of molecular gas in the hypothetical isothermal system which is necessary to achieve the same surface concentration of adsorbate as prevails during the practical atomisation experiment with an observable pressure P_2', but it contains nothing which would enable that concentration to be calculated.

Rather than consider the absolute rate of atomisation, it is sometimes more convenient to employ a parameter which expresses the efficiency of the process in terms of the probability that a molecular collision with the surface results in the atomisation of the molecule involved. Such a parameter is $\mathscr{P}_a$, defined by the relation

$$\mathscr{P}_a = \frac{\text{Rate of production of atoms}}{2(\text{Rate of collision of molecules with the surface})} = \frac{D_1}{2Z_2'} \tag{39}$$

From eqns. (28) and (36)

$$D_1 = 2(s_2' Z_2' - s_2 Z_2) \tag{40}$$

and from eqn. (35)

$$\frac{Z_2}{Z_2'} = \left(\frac{T'}{T}\right)^{1/2} \frac{P_2}{P_2'} \tag{41}$$

Hence, eqn. (39) becomes

$$\mathscr{P}_a = s_2' - s_2 \left(\frac{T'}{T}\right)^{1/2} \frac{P_2}{P_2'} \tag{42}$$

Using eqn. (38), we can eliminate the experimentally inaccessible P_2 from this equation and obtain $\mathscr{P}_a$ in terms of measurable quantities, i.e.

$$\mathscr{P}_a = \frac{s_1^2}{s_2} \left(\frac{T'}{T}\right)^{1/2} \frac{P^{\ominus} K_p}{4} \frac{1}{P_2'} \times$$

$$\left[\left\{1 + \frac{s_2 s_2'}{s_1^2} \left(\frac{T}{T'}\right)^{1/2} \frac{8}{P^{\ominus} K_p} P_2'\right\}^{1/2} - 1\right] \tag{43}$$

We can see now that the negative sign associated with the square root in eqn. (38) is inadmissible, because it would lead to negative $\mathscr{P}_a$. Equation (43) covers the entire pressure range of practical interest and its form is illustrated graphically in Fig. 3 for the case of hydrogen.

It is evident that two distinct types of behaviour can occur depending on the conditions. When the rate of atomisation is slow relative to the collision rate, $\mathscr{P}_a$ is proportional to $(P_2')^{-1/2}$ (half-order kinetics) and when the rate of atomisation is comparable to the collision rate, $\mathscr{P}_a$ approaches a limiting upper value (first-order kinetics). The circumstances in which these two kinds of behaviour are to be expected will now be examined.

(*a*) *Half-order kinetics.* Equation (43) may be greatly simplified when the experimental conditions are such that

$$\frac{s_2 s_2'}{s_1^2} \left(\frac{T}{T'}\right)^{1/2} \frac{8}{P^{\ominus} K_p} P_2' \gg 1 \tag{44}$$

It becomes

$$\mathscr{P}_a = s_1 \left(\frac{s_2'}{s_1}\right)^{1/2} \left(\frac{T'}{T}\right)^{1/4} \left(\frac{P^{\ominus} K_p}{2}\right)^{1/2} (P_2')^{-1/2} \tag{45}$$

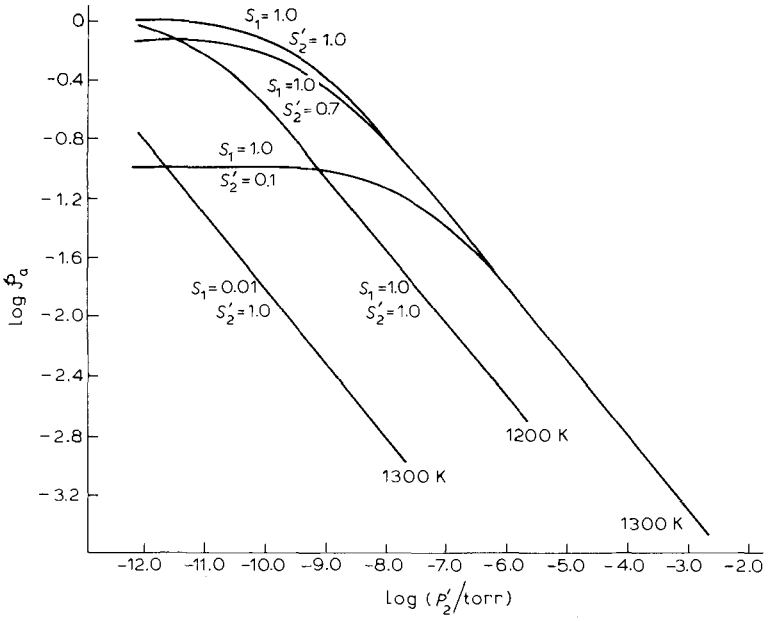

Fig. 3. The transition from half-order to first-order kinetics calculated by means of eqn. (43) for the atomisation of hydrogen at 1200 K and 1300 K (courtesy Brennan [6]).

This result can be transformed into an expression relating the absolute rate of production of *atoms* per unit area of surface to the pressure of gas. Thus

$$D_1 = 2Z_2' \mathscr{P}_a$$

$$= s_1 \left(\frac{s_2'}{s_2}\right)^{1/2} \left(\frac{T'}{T}\right)^{1/4} (P^{\ominus} K_p)^{1/2} z_1' \sqrt{P_2'} \qquad (46)$$

and the order of reaction is one half with respect to the pressure of gas, assuming the sticking coefficients are virtually independent of pressure, which we may do because coverages are always very low. When we consider experimental results, we will see that, under appropriate conditions, eqn. (46) gives an excellent representation of the atomisation process.

Examination of eqn. (46) shows that the temperature coefficient of D_1, in the region of half-order kinetics, is dominated by the temperature coefficient of K_p. If we write

$$K_p = A \exp\left(-\frac{2B}{RT}\right) \qquad (47)$$

TABLE 2

Values of the constants A, B and C [defined in eqns. (47) and (49)] for the atomisation of hydrogen, oxygen and nitrogen, calculated from the data of Stull and Sinke [13a], with $P^{\ominus} = 1$ atm

System	$\frac{T}{\mathrm{K}}$	$10^{-6} A$	$\frac{B}{\mathrm{kJ\,mole^{-1}}}$	$\frac{10^{-25} C}{\mathrm{cm^{-2}\,s^{-1}\,torr^{-1/2}}}$
Hydrogen	1250	1.07	223	4.04
Oxygen	1250	7.01	253	5.18
Nitrogen	2100	9.77	480	5.55

eqn. (46) assumes the form

$$D_1 = s_1 \left(\frac{s_2'}{s_2}\right)^{1/2} C\sqrt{P_2'} \exp\left(-\frac{B}{RT}\right) \tag{48}$$

with

$$C = z_1' A \left(\frac{T'}{T}\right)^{1/4} (P^{\ominus})^{1/2} \tag{49}$$

The pre-exponential factor can be regarded as being virtually constant over normal temperature ranges in comparison with the temperature dependence of the exponential factor. Values of A, B and C are given in Table 2. Note especially that $2B$ is the enthalpy change of reaction (V) at the temperature of the surface, viz. approximately $\frac{1}{2}D(\mathrm{X_2})$. We can see from eqn. (48) that the entire specificity of the surface in bringing about atomisation under these conditions is contained in the factor $s_1(s_2'/s_2)^{1/2}$. We can expect, therefore, that clean metals will give very similar values for D_1, because atoms adsorb with sticking coefficients of near unity, and s_2'/s_2 will depart from unity by virtue of only second-order effects. This expectation is well borne out by the experimental results.

The physical interpretation of the conditions defined by eqn. (44) is that there will be many molecules adsorbed and desorbed for every atom which leaves the surface. This means that the stationary concentration of the adsorbed layer is negligibly different from the *equilibrium* value. In the region of half-order kinetics, the mechanism of atomisation is

$$\mathrm{X_2(g) + S \rightleftharpoons 2\,X{-}S} \tag{VII}$$

$$\mathrm{X{-}S = X(g) + S} \tag{IVa}$$

with D_1 being determined by the thermodynamic equilibrium coverage.

(*b*) *First-order kinetics.* Equation (43) again assumes a simple form in the limit when

$$\left\{\frac{s_2 s_2'}{s_1^2}\left(\frac{T}{T'}\right)^{1/2} \frac{8}{P^{\ominus} K_p} P_2'\right\}^{-1} \gg 1 \tag{50}$$

Under this restriction, the square root factor of eqn. (43) can be expanded into a rapidly converging series, of which we will neglect second and higher order terms. Equation (43) now becomes

$$\mathscr{P}_a = \frac{s_1^2}{s_2}\left(\frac{T'}{T}\right)^{1/2}\frac{P^{\ominus}K_p}{4}\frac{1}{P_2'} \times$$

$$\left[1 + \frac{1}{2}\frac{s_2 s_2'}{s_1^2}\left(\frac{T}{T'}\right)^{1/2}\frac{8}{P^{\ominus}K_p}P_2' - 1\right] = s_2' \qquad (51)$$

In this limit, the rate of atomisation is determined solely by the sticking coefficient of the molecules at temperature T' on the surface at temperature T. That is, all the molecules which become adsorbed are atomised, so the rate of atomisation is determined by the rate at which material is supplied to the surface, and the properties of the surface in determining s_2', viz.

$$D_1 = 2s_2' z_2' P_2' \qquad (52)$$

This is why the transition from half-order to first-order behaviour moves to higher pressures as the temperature of the surface increases (see Fig. 3), or, at a given temperature, to a pressure sufficiently low to restrict the rate of supply of molecules to the surface.

2.2.4 Atomisation kinetics when molecular adsorption is activated

So that we will be able to consider the controversy concerning the atomisation of hydrogen by gold [111], we now develop relations for the kinetics of atomisation when s_2 is not constant, but depends on temperature. The discussion will also be relevant to our later development of the kinetics of recombination. We assume that the adsorption of a molecule requires the presence of two adjacent vacant surface sites and that the probability that adsorption occurs when a molecule strikes such a pair of sites is $\kappa_{2,1}$; so we write

$$s_2 = \kappa_{2,1}(1-\theta)^2 \qquad (53)$$

Again, we suppose that activated processes at the surface are controlled by the temperature of the surface, so that

$$\kappa_{2,1} = (\kappa_0)_{2,1}\exp(-E_{2,1}/RT) \qquad (54)$$

with $(\kappa_0)_{2,1}$ virtually independent of temperature. The implication of eqn. (53) is that the overlayer is localised. The dependence of s_2 on $(1-\theta)^2$ will be a good approximation only for small θ, but no difficulties will arise from this limitation in our atomisation calculations. However, we will later apply eqn. (53) to recombination kinetics at coverages too high for it to remain a satisfactory representation of molecular adsorption. Quite apart from the requirements of lattice statistics,

it has to be recognised that the procedure of using eqn. (53), regardless of how large θ may be, is not even consistent with our commitment to the Holland model of the overlayer. We are obliged to adopt this course for the want of a practical alternative, but it will serve to illustrate certain kinds of limiting kinetic behaviour. As a step towards self-consistency, we will use a value of $(\kappa_0)_{2,1}/(\kappa_0)_{1,2}$ which satisfies the requirements of the Holland model.

Reference to Fig. 2(b) and (c) enables us to write a relation for $E_{2,1}$, i.e.

$$E_{2,1} = E_m + \Delta U_{2,1} \tag{55}$$

and we express E_m as a fraction (ρ) of the adsorption energy, thus

$$E_m = -\rho \Delta U_{1,1} \tag{56a}$$

$$= -\tfrac{1}{2}\rho [D(X_2) - \Delta U_{2,1}] \tag{56b}$$

The condition for a stationary surface concentration [cf. eqn. (36)] is now

$$2\kappa_{2,1}(1-\theta)^2 Z_2' = d_1 N_S \theta + 2d_2 N_S^2 \theta^2 \tag{57}$$

which, on rearranging, becomes

$$2(\kappa_{2,1} - d_2 N_S^2 Z_2'^{-1})\theta^2 - (4\kappa_{2,1} + d_1 N_S Z_2'^{-1})\theta + 2\kappa_{2,1} = 0 \tag{58}$$

Solution of this equation for θ enables the calculation of the probability of atomisation by means of eqn. (39) written in the form $\mathscr{P}_a = \frac{1}{2} d_1 N_S Z_2'^{-1} \theta$.

2.3 RECOMBINATION REACTIONS

2.3.1 Mechanisms of recombination

In our discussion of recombination, we will again suppose that there is only one state of adsorption and that it is homogeneous. For atomisation, these suppositions were not too restrictive, because there we were dealing with low coverages at high temperatures. In the present situation, these simplifications are more likely to prove too crude because now we may have high coverages and relatively low temperatures, when additional adsorption states are possible.

For recombination, two processes have to be considered: (i) the combination of adatoms according to reaction (Ib) and (ii) the reverse of reaction (VIa), viz.

$$S{-}X + X(g) = X_2(g) + S \qquad \Delta U_r \tag{VIb}$$

often called the Rideal—Eley mechanism. Reaction (VIb) was not appropriate to our consideration of atomisation because there we arranged that virtually no atoms impinged on the surface. Now, however, there is a

significant flux of gaseous atoms to the surface and we express it in terms of the molecular flux through the parameter α, i.e.

$$\alpha = \frac{Z_2}{Z_1} \tag{59}$$

Accordingly, the Rideal—Eley mechanism is significant and we assume it is unactivated so long as $-\Delta U_{2,1} < D(X_2)$ (see Fig. 2). Reaction (VIa), being activated for this condition, can be omitted from consideration without serious error. However, when $-\Delta U_{2,1} > D(X_2)$, it is reaction (VIb) which is activated and reaction (VIa), now being unactivated or nearly so, requires careful consideration. The need for a proper description of the simultaneous occurrence of reactions (Ia) and (VIa) is more pressing for recombination than for atomisation. Unfortunately, such a description is not available in the literature and one will not be attempted here. We are already familiar with the rate of reaction (Ib), viz, D_2 [see eqn. (14)]. The rate of production of molecules per unit area by reaction (VIb) is denoted by R, and its activation energy by E_r. We write (Ehrlich [4], Dickens, et al. [14])

$$R = r(N_a)_1(N_g)_1 \tag{60}$$

where r is the rate coefficient. We will also find it convenient to express R in terms of the probability (κ_r) that a collision between a gaseous atom and an adatom results in recombination, i.e.

$$R = \kappa_r \theta Z_1 \tag{61}$$

with κ_r virtually independent of temperature, since we are confining ourselves to the case for which reaction (VIb) requires zero or negligible activation. Substitution of eqn. (24) gives

$$R = \kappa_r z_1 \theta P_1 \tag{62}$$

and

$$r = \kappa_r(z_1/N_S)\mathbf{k}T \tag{63}$$

Gaseous atoms, which collide with adatoms, but fail to recombine, are all assumed to be reflected back into the gas phase. This is a simplification, since it is very probable that some of these gaseous atoms will end up on the surface. However, to this degree of approximation, the rate of reflection of gaseous atoms per unit area is $(1-\kappa_r)\theta Z_1$. We make a similar assumption that a gaseous atom which strikes a vacant site, but fails to be adsorbed, is reflected back into the gas phase. Thus, if $\kappa_{1,1}$ is the probability of adsorption when a gaseous atom strikes a vacant site, we write for the atomic sticking coefficient

$$s_1 = \kappa_{1,1}(1-\theta) \tag{64}$$

and the rate of reflection of atoms from vacant sites per unit area is $(1-\kappa_{1,1})(1-\theta)Z_1$. We again suppose that atom adsorption is unactivated.

The efficiency of the overall recombination reaction is generally expressed in terms of the *recombination coefficient* (γ), defined as the probability that a collision of a gaseous atom with the catalyst will result in recombination, i.e. the absolute rate of recombination is given by γZ_1 and

$$\gamma = \frac{\left(\begin{matrix}\text{Rate of collision of}\\ \text{atoms with surface}\end{matrix}\right) - \left(\begin{matrix}\text{Overall rate of departure}\\ \text{of atoms from surface}\end{matrix}\right)}{\text{Rate of collision of atoms with surface}} \tag{65}$$

Hence

$$\begin{aligned}\gamma &= \frac{[Z_1 - D_1 - (1-\kappa_{1,1})(1-\theta)Z_1 - (1-\kappa_r)\theta Z_1]}{Z_1} \\ &= \kappa_{1,1} - (\kappa_{1,1} - \kappa_r + d_1 N_S Z_1^{-1})\theta\end{aligned} \tag{66}$$

We see that to evaluate γ and determine its dependence on P_1, we have to elucidate the factors that control the magnitude of θ.

The condition for a stationary surface concentration is

$$s_1 Z_1 + 2s_2 Z_2 = D_1 + 2D_2 + R \tag{67}$$

Substitution of primary parameters into this equation gives an expression of the form

$$b_2\theta^2 + b_1\theta + b_0 = 0 \tag{68a}$$

where

$$b_0 = \kappa_{1,1} + \kappa_{2,1}\alpha \tag{68b}$$

$$b_1 = -(\kappa_{1,1} + \kappa_r + 4\kappa_{2,1}\alpha + d_1 N_S Z_1^{-1}) \tag{68c}$$

$$b_2 = 2(\kappa_{2,1}\alpha - d_2 N_S^2 Z_1^{-1}) \tag{68d}$$

and, of course

$$\theta = \frac{-[b_1 + (b_1^2 - 4b_0 b_2)^{1/2}]}{2b_2} \tag{69}$$

the sign of the square root being chosen to ensure θ is less than one, as the model requires.

To illustrate the way the recombination coefficient is affected by the conditions [see eqn. (66)], we will use the model of a localised overlayer

expounded in Sect. 2.1. For clarity, we give the expressions for $d_1 N_S Z_1^{-1}$, and $d_2 N_S^2 Z_1^{-1}$, using $N_S = 10^{19}$ m^{-2}, viz.
where

$$d_1 N_S Z_1^{-1} = 839\alpha \left(\frac{M}{\text{g mole}^{-1}}\right)^{1/2} \left(\frac{T}{\text{K}}\right)^{3/2} \left(\frac{P_2}{\text{torr}}\right)^{-1} \exp\left(\frac{\Delta U_{1,1}}{RT}\right) \tag{70}$$

$$d_2 N_S^2 Z_1^{-1} = 1511\alpha(\kappa_0)_{1,2} \left(\frac{\sigma_1}{\text{nm}}\right) \left(\frac{M_1}{\text{g mole}^{-1}}\right) \left(\frac{T}{K}\right)^2 \left(\frac{P_2}{\text{torr}}\right)^{-1} \times \left(\frac{1 - \exp(-\Theta_p/T)}{1 - \exp(-E_m^*/RT)}\right)^2 \exp\left(-\frac{E_{1,2}}{RT}\right) \tag{71}$$

where M_1 is the mass of a mole of atoms. The exemplification will be quantitative, but the numerical values quoted will not, in general, be deserving of direct comparison with experimental result except, possibly, in certain instances when the coverage is low. However, consideration of numerical values will help us to put the discussion on a firm foundation and provide a context within which experimental measurements may be considered.

2.3.2 Recombination in the absence of atomic desorption

In this section, the temperature is never allowed to rise so high that direct desorption of adatoms plays a significant role. Because their recombination behaviours are so different, we consider separately the cases of (a) moderately strong molecular chemisorption, (b) weak or endothermic molecular adsorption and (c) exceptionally strong chemisorption.

(a) Recombination characteristics for the case $E_m \leqslant -\Delta U_{2,1} \ll D(X_2)$

The energetics of this situation are represented in Fig. 2(a). Molecular adsorption is unactivated, so $\kappa_{2,1}$ is temperature-independent, as is κ_r. From eqn. (66), remembering that D_1 is zero for this case, we see that γ varies linearly with coverage, the temperature dependence of γ being determined solely by the temperature dependence of the stationary concentration of adatoms. In Fig. 4 is shown the unique straight line relating γ to θ for the hydrogen—tungsten system; also shown is the dependence of θ on P_2 at three selected temperatures. Essentially the same information is given in Fig. 5, but with a different emphasis. The restriction that D_1 should be negligible restricts the temperature to less than 1400 K in this example.

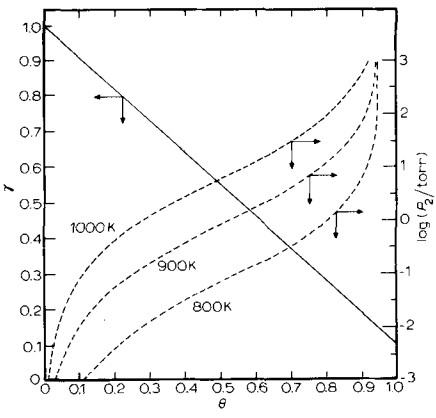

Fig. 4. The dependence of the recombination coefficient on the stationary concentration of adatoms and on the pressure for the hydrogen—tungsten system. The curves are derived from eqns. (66) and (69) using the following values for the various parameters: $\alpha = 50$, $D(H_2) = 432\,\mathrm{kJ\,mole^{-1}}$, $\Delta U_{2,1} = -146\,\mathrm{kJ\,mole^{-1}}$, $\sigma_1 = 0.24\,\mathrm{nm}$, $\kappa_{1,1} = 1$, $(\kappa_0)_{2,1}/(\kappa_0)_{1,2} = 0.2$, $(\kappa_0)_{1,2} = 0.5$, $\kappa_r = 0.1$, $\rho = 0.2$.

(*i*) *Low coverage.* Our model applied to the hydrogen—tungsten system, with $P_2 = 1$ torr and $\alpha = 50$, gives $\theta = 0.0456$ at 1300 K and, because $\kappa_{1,1}$ is so large (unity here), nearly all the atoms arriving strike a vacant site and are adsorbed; in fact, $s_1 = 1 - \theta = 0.954$. Because the coverage is so low, the Rideal—Eley process accounts for only a small fraction of the impinging atoms ($RZ_1^{-1} = 7.9 \times 10^{-3}$), so recombination occurs almost entirely through the Langmuir—Hinshelwood mechanism. Since every gaseous atom which is adsorbed is eventually recombined and since so few of the gaseous atoms which reach the surface fail to be adsorbed, recombination is very efficient ($\gamma = 0.959$). The stationary concentration is only about 4% higher than the equilibrium coverage and correspondingly insensitive to α. Hence, the controlling factor in the recombination process is the supply of atoms to the surface and the order with respect to atoms is consequently very close to unity.

(*ii*) *High coverage.* At about 600 K, the recombination coefficient for the hydrogen—tungsten system, under the conditions of this example, reaches a lower limit of 0.153, corresponding to an upper limit to θ of 0.941. At this limit, the temperature is too low for significant desorption of molecules and the Langmuir—Hinshelwood route to recombination is no longer of consequence. Because θ is now close to unity, a high proportion of atoms reaching the surface is reflected, but the Rideal—Eley process, depending as it does on θ, is no longer unimportant. In fact, the removal of adatoms by the Rideal—Eley process provides virtually the entire means of balancing the flux of material onto the surface by adsorption of atoms and molecules. For this reason, this lower limit to γ is

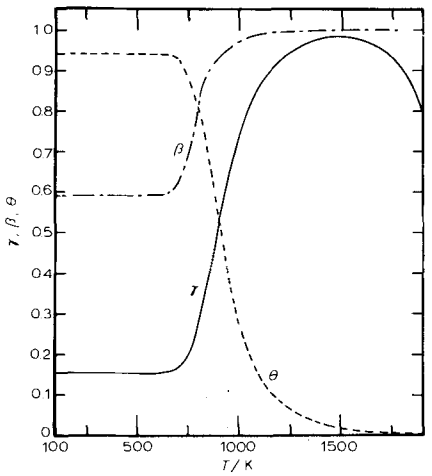

Fig. 5. The dependence of the recombination coefficient, the energy accommodation coefficient and the stationary concentration of adatoms on temperature for the hydrogen—tungsten system when $P_2 = 1$ torr and the other parameters have the values specified in Fig. 4.

independent of $\Delta U_{2,1}$. Reliance on the Rideal—Eley mechanism means that recombination is inefficient, since κ_r will be appreciably less than unity (for $\kappa_r = 0.1$ in this example, $\gamma = 0.153$). An additional feature is that the adsorption of atoms is now sensitive to coverage, since it depends on $1 - \theta$, so the order of recombination with respect to atoms can be noticeably different from unity (1.09 in this example).

(b) Recombination characteristics for the case $-\Delta U_{2,1} < E_m$

The energetics of this case are illustrated in Fig. 2(b) when molecular adsorption is still exothermic and in Fig. 2(c) when the adsorption is endothermic.

(i) Low coverage. Provided rapid adsorption and desorption are still able to occur, the coverage will be low, even at quite low temperatures, because of the smallness of $-\Delta U_{2,1}$. Consider, for example, molecular hydrogen ($P_2 = 1$ torr, $\alpha = 50$) adsorbing with an energy $\Delta U_{2,1} = -40\,\mathrm{kJ\,mole^{-1}}$, corresponding to $E_m = 47.2\,\mathrm{kJ\,mole^{-1}}$. At 400 K, θ is still only 0.0448. Consequently, the efficiency of adsorption of atoms and their subsequent recombination is high ($\gamma = 0.960$) and the Rideal—Eley process will be unimportant. The stationary surface coverage will also be significantly greater than the equilibrium coverage. Thus, for this example, 47.7% of the adatoms appearing on the surface at 400 K derive from gaseous atoms despite their partial pressure being only 1/70th that of molecular hydrogen. Even so, the smallness of θ, and the corresponding insensitivity of θ to Z_1, ensures that the order of recombination with respect to atoms is close to unity.

(*ii*) *High coverage.* As the temperature is reduced, the mobility of the adatoms is also reduced until eventually D_2 has declined to insignificance. The fact that molecular adsorption is also activated and that $-\Delta U_{2,1}$ is small does not prevent θ becoming large, since direct adsorption of gaseous atoms is a powerful influence, even for large values of α (small Z_1). Eventually, the temperature will have fallen to a value at which the stationary coverage is determined by a simple balance between direct atom adsorption and adatom removal by the Rideal—Eley process. Each of these processes is unactivated under the present conditions and so is independent of temperature. Consequently, the only experimental parameter to which the limiting values of θ (and of γ) are sensitive is α and the only system parameters of consequence are $\kappa_{1,1}$ and κ_r. The larger $\Delta U_{2,1}$, the lower the temperature at which the transition from high to low γ occurs (see Fig. 6).

(*iii*) *The transition region.* As the movement of adatoms is frozen by lowering temperature and the coverage driven up by the flux of gaseous atoms to the surface, γ falls. If κ_r were zero, then the only recombination which could occur would be via the residual desorption of molecules and θ would be very close to unity. Since in our model the desorption of molecules depends on θ^2, recombination with $\kappa_r = 0$ would be insensitive to Z_1 and the order of recombination with respect to atoms

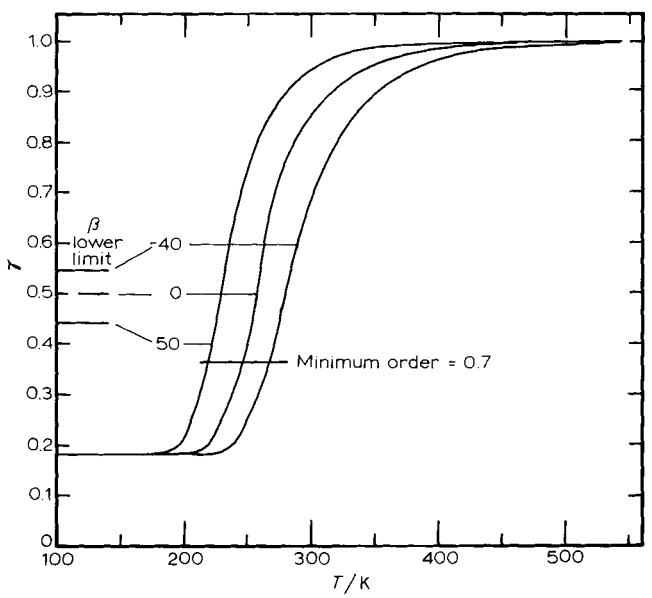

Fig. 6. The dependence of the recombination coefficient on temperature or hydrogen when $-\Delta U_{2,1} < E_m$. The numbers designating the curves refer to the values of $-\Delta U_{2,1}$/kJ mole^{-1}. The other parameters are as specified in Fig. 4 and $P_2 = 1$ torr.

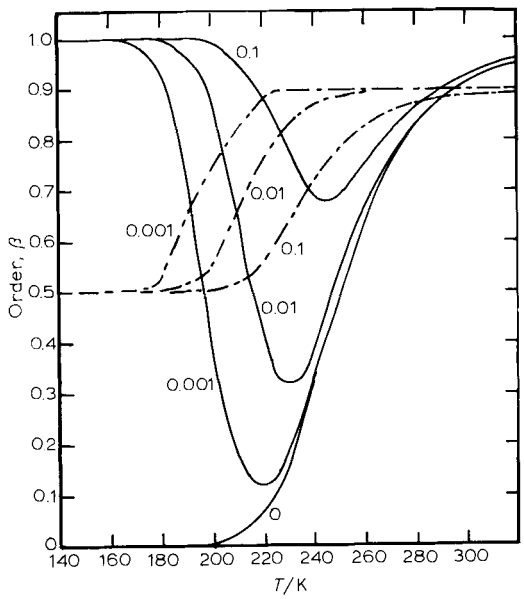

Fig. 7. The dependency of the order of recombination with respect to atoms and of the energy accommodation coefficient on temperature for hydrogen when $\Delta U_{2,1} = 0$, $P_2 = 1$ torr. The numbers designating the curves refer to values of κ_r; the other parameters have the values specified in Fig. 4. ———, Order; — – —, β.

would be virtually zero, as shown in Fig. 7. However, with non-zero values of κ_r, the Rideal—Eley process must eventually dominate as the temperature is lowered. When this happens, the recombination becomes first order. The result of these competing factors is that the order with respect to atoms passes through a minimum (see Fig. 7) whose depth and position depend on κ_r, other parameters being held constant. This result is of special significance for those experimental techniques for the determining of γ which rely on the assumption that the recombination is first order. We see also that, when a low energy of molecular adsorption is associated with a sustained low value of γ and first-order recombination kinetics, the recombination must be occurring via the Rideal—Eley mechanism.

(c) *Recombination when* $-\Delta U_{2,1} > D(X_2)$

In the case of very strong chemisorption [see Fig. 2(d)], the desorption of molecules is even more activated than the desorption of adatoms. At temperatures not high enough for appreciable desorption of adatoms, the very large value of $-\Delta U_{2,1}$ ensures values of θ close to unity. The virtual absence of molecular desorption rules out the Langmuir—Hinshelwood process, so that recombination is restricted to the Rideal—Eley mechanism, which is now activated, causing recombination to be

very inefficient. A complicating feature, which has been omitted from the present model, is that reaction (VIa) is now unactivated (or nearly so). However, as this reaction depends on $(1-\theta)$, its contribution at high θ will be small, but such effect as it does have will be to make γ even smaller since it is a source of gaseous atoms. The recombination will be first order with respect to atoms. To illustrate the inefficiency of the recombination process for these conditions, we write

$$\kappa_r = (\kappa_0)_r \exp(-\Delta U_r/RT) \tag{72}$$

where $\Delta U_r = -\frac{1}{2}[D(X_2) + \Delta U_{2,1}]$, and use our present model to obtain an upper limit for γ. For hydrogen, with $\Delta U_{2,1} = -600\,\text{kJ mole}^{-1}$, $(\kappa_0)_r = 0.1$, $P_2 = 1$ torr, $\alpha = 50$ and the other parameters as specified in Fig. 4, we find γ has the value 2.4×10^{-4} at 1500 K and 8.2×10^{-6} at 1000 K.

(d) Recombination when $\Delta U_{2,1}$ depends on coverage

The assumption of a constant energy of adsorption is rather restrictive, it being frequently the case that the energy of adsorption decreases with increasing coverage. To simulate this behaviour, we assume an empirical dependence of $\Delta U_{2,1}$ on θ (see Fig. 8) and calculate the consequences for an initial energy of adsorption appropriate to the hydrogen—tungsten system. When the coverage is low, the behaviour is similar to that when $\Delta U_{2,1}$ is constant. However, as the temperature decreases, θ increases less rapidly when $\Delta U_{2,1}$ decreases with θ and this is reflected in the higher values of γ. An additional feature is that when $\Delta U_{2,1}$ declines with increasing θ, the molecular adsorption may eventually become activated, whereas for constant $\Delta U_{2,1}$ this does not happen and molecular adsorption decreases then only by reason of its $(1-\theta)^2$ dependence. In this particular example, the two lower limits for the recombination coefficients are very similar, but this is fortuitous. Indeed, when $\Delta U_{2,1}$ is a function of θ, the low value of γ (see Fig. 8) is not a true limit at all. This is because molecular adsorption, which at 200 K still accounts for 28.1% of adatoms appearing on the surface, would decrease if the temperature were reduced further. In contrast, for $\Delta U_{2,1}$ having a constant value of $-146\,\text{kJ mole}^{-1}$, molecular adsorption has already reached its limiting value of 37.2% (of adatoms) at 600 K.

2.3.3 Recombination in the presence of atomic desorption

At sufficiently high temperature, the desorption of adatoms becomes appreciable. This is not only because the high temperature reduces the contrast in the exponential factors of D_1 and D_2, but because the sparse coverage increases the relative significance of D_1 by virtue of its dependence on θ (as opposed to θ^2). Any factor (e.g. low pressure) which favours very low values of θ will contribute to the relative importance of D_1.

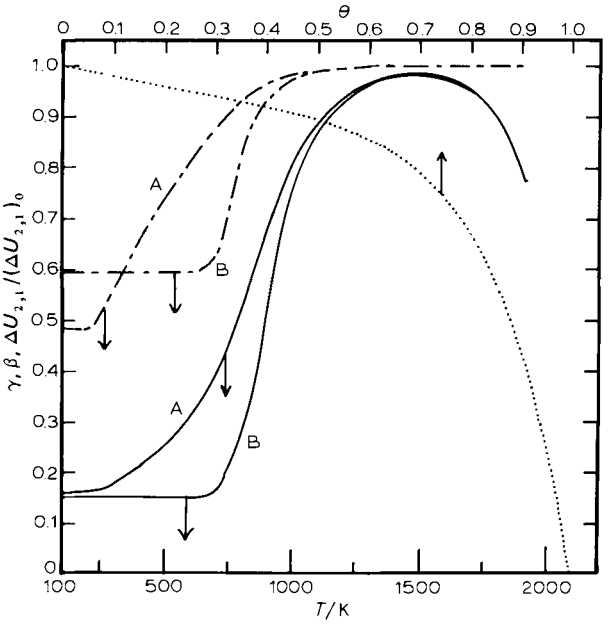

Fig. 8. The effect on recombination and energy accommodation efficiencies (γ_A, β_A) of the energy of adsorption decreasing with coverage according to the empirical relation $\Delta U_{2,1} = (\Delta U_{2,1})_0(1-0.2\theta - 0.8\theta^7)$, with $(\Delta U_{2,1})_0 = -146\,\mathrm{kJ\,mole^{-1}}$ as for the hydrogen—tungsten system. γ_B and β_B refer to a constant value for $\Delta U_{2,1}$ of $-146\,\mathrm{kJ\,mole^{-1}}$; $P_2 = 1$ torr, $\alpha = 50$ and the other parameters are as specified in Fig. 4. ———, γ; — — —, β; · · · · ·, $\Delta U_{2,1}/(\Delta U_{2,1})_0$.

Reference to eqn. (66) shows that the growth in the $d_1 N_S Z_1^{-1}$ term with continued increase in temperature will reduce γ and this effect is illustrated in Fig. 5 for the hydrogen—tungsten system ($T > 1500$ K). Eventually, γ will become negative and when this happens, the parameter is no longer a convenient way of accounting for the processes occurring.

It is commonly held that the growth in importance of adatom desorption with increasing temperature is accompanied by a transition from first- to a limit of second-order kinetics. This is a mistaken belief, because a limit of second-order kientics would require $\theta \sim 1$, and so high a coverage is not attainable with practical values of P_2 and α. In practice, the high temperature necessary for significant adatom desorption causes θ to become much less than unity and γ becomes very sensitive to Z_1 both through its influence on θ and on $d_1 N_S Z_1^{-1}$. Consequently, we must expect the recombination to proceed eventually with an order in excess of two. Indeed, when conditions become critical, the order will rise very rapidly and this parameter also ceases to be useful in characterising the kinetic behaviour.

3. Experimental methods and results. Atomisation

3.1 ENERGY LOSS METHOD

When an incandescent filament is surrounded by a stable gas, heat is lost by gaseous conduction, by convention (if the pressure is high enough) and, of course, by radiation. There will also be end effects due to cooling by the electrodes on which the filament is mounted. As with so much of the early work in this field, the technological needs of electric lamp manufacture were the main stimulus to the investigation of these factors. Langmuir [15] by 1912 had developed a general theory of heat loss from filaments and this was the foundation for his measurement of the additional energy loss which occurs when some of the gas dissociates. When the pressure of the gas is sufficiently low for the mean free path to be comparable to the dimensions of the containing vessel, the temperature of the gas is effectively uniform, being the same as that of the walls of the vessel. This is because the area of the filament is negligible relative to the area of the walls and there are no gas phase collisions in which energy could be transferred. At higher pressures, there is a gradient of temperature from wall to filament and there is a temperature discontinuity at the filament. Measurements at high pressures are more likely to be free of the difficulties due to contamination which can bedevil low pressure work, but the analysis of the temperature gradient problem at high pressures is formidable. Langmuir [16—19] gave a number of discussions of this method. His first was in 1912, but the definitive statement of his findings for the hydrogen—tungsten system was not given until 1926 [19]; the core of the experimental work upon which his conclusions rest was published with Mackay, in 1914 [17]. The method has also been applied to the hydrogen—tungsten system by Farber and Darnell [20], but they restricted their measurements to a pressure of 0.05 torr to avoid the complications of temperature gradients in the gas phase. The values derived by this method for the equilibrium constant of reaction (I) are compared with the spectroscopic value [13a] in Table 3. Considering the difficulties, the agreement is remarkably good.

A knowledge of the additional energy loss due to dissociation enables the rate of atomisation to be calculated. Langmuir's expression [19, 21] for the rate of production of *atoms* (v_a) is

$$v_a = 2.8 \times 10^{25} \times P_2'^{1/2} \exp\left(-\frac{211\ \text{kJ mole}^{-1}}{RT}\right) \text{torr}^{-1/2}\,\text{cm}^{-2}\,\text{s}^{-1} \qquad (73)$$

In keeping with the fact that the method gives values of K_p which are about ten times too large, Langmuir's rates of atomisation are correspondingly rather too fast. However, their closeness to later values [5, 22],

TABLE 3

The equilibrium constant for the reaction $H_2(g) = 2H(g)$, at 1200 K, referred to $P^{\ominus} = 1$ atm, determined by the energy loss method, and spectroscopically

$\Delta H^{\ominus}$ / kJ mole^{-1}	$\Delta S^{\ominus}$ / J mole^{-1} K^{-1}	K_{atm} / 10^{-13}	Ref.
421	109	2.48	19
423	113	3.20	20
446.6	115.4	0.387	13a

as shown in Table 4 (p. 186), is a triumph for experimental technique and theoretical analysis. For many years, it was believed that Langmuir's rates of atomisation were substantially too low, a criticism which originated with Bryce [23] and was not corrected until 1970 [24].

Farber and Darnell [20] attempted to extend the method to the study of the atomisation of nitrogen over tungsten. Despite their use of temperatures up to 3000 K, they failed to detect any energy loss which could be attributed to dissociation. This is very much what Langmuir [16] found; he went up to 3500 K. Gregory and Hayward [25] have pointed out that the sensitivity of the energy loss measurements was inadequate for the detection of the small degree of dissociation occurring. However, it is not clear why Farber and Darnell did not report a fall in the pressure of nitrogen as observed by Langmuir [26] and used by Nornes and Donaldson [8] to determine the rate of atomisation of nitrogen (see Sect. 3.2.1); possibly their pressure was too high for adequate sensitivity.

3.2 METHODS BASED ON THE TRAPPING OF ATOMS

The atomisation reaction was discovered by Langmuir in 1912 [27]. He explained the clean up action observed in aged electric lamps in terms of the atomisation of residual gas by the filament followed by the trapping of the resulting atoms at the wall of the lamp [28]. The editor of the *General Electric Review* for 1913, announcing his company's introduction of the nitrogen-filled lamp, explained that a great deal of empirical searching for the causes of lamp failure had been unsuccessful and that it had been decided to "take the bull by the horns" and investigate the matter scientifically. Langmuir was 28 years old when he joined the General Electric Research Laboratory in 1909 and soon demonstrated the wisdom of that decision. Langmuir combined his successful pursuit of an improved electric lamp with the laying of the foundations of surface studies. In the words of the editor of the *General Electric Review*, referring to a forthcoming paper by Langmuir [29] ". . . .these improvements were the result of several years work on the part of a corps of efficiently trained men in the research laboratory". This is a classic success

story of scientific technology, but it is worth recalling again, because there is ever a danger that we may forget the way technology and science can profit mutually when allowed to flourish together.

3.2.1 Experiments with static systems

(a) Experimental procedures

In this method, an electrically heated filament is suspended in a closed vessel containing the gas to be atomised. The method relies on *all* the atoms produced in the reaction being trapped at the wall of the containing vessel or elsewhere. A further essential requirement is that no molecules, including those which have been thermally excited by collision with the hot filament, should be removed by the atom trap (see Sect. 3.2.3). The electrical resistance of the filament, and hence its temperature, are maintained constant throughout the reaction, the progress of which is most directly followed by observing the decrease in pressure in the system. Langmuir [27] and Zaitsev [30], in their studies of the atomisation of hydrogen over tungsten, simply used the glass wall of the reaction vessel cooled in liquid air as the H atom trap. Hickmott [22, 31] has shown that, under the conditions of their experiments, the capacity of the glass to trap atoms without any recombination would soon be exceeded. Langmuir [27] was aware of fatigue effects but, in his 1915 paper [21], he singles out two of his fastest rates of atomisation and these are included in Table 4 (p. 186). Bryce's use of molybdenum oxide as a much more efficient H atom trapping agent marked a substantial improvement in this technique [23]. He evaporated the oxide on to the wall of the glass reaction vessel by heating a molybdenum filament in about 1 torr of oxygen and then baked the deposited oxide in oxygen. In this form, the oxide has excellent trapping properties and is superior in this respect to more bulky forms, e.g. as when deposited from a slurry [32, 33]. Unfortunately, the data of Bryce are inaccurate due to the limitations of his vacuum technique. In the work of Brennan and Fletcher [5, 7], careful attention was given to achieving sufficiently clean vacuum conditions, as well as to the state of the oxide, which was used to trap both H atoms and, in a specially reduced form, O atoms also. More recently, Kislyuk and Tret'yakov [111] have used a sputtered silver film cooled in liquid nitrogen to study the atomisation of hydrogen by gold.

Nornes and Donaldson [8] have studied the atomisation of nitrogen by tungsten in the temperature range 2025—2210 K using an aluminosilicate system. They relied on the walls at 300 K to trap all the N atoms produced, very much as Langmuir had done for hydrogen fifty years earlier. However, their vacuum technique was of a high standard (10^{-10} torr, with filament and ion gauge hot) and the amount of atomisation was kept small (typically of the order of 10^{16} atoms). The atom-trapping

efficiency might have been helped by the gettering action of the W atoms evaporated from the filament at the very high temperatures involved. Indeed, Nornes and Donaldson were anxious that some N_2 molecules might also have been gettered, but present convincing arguments that this did not, in fact, happen. In this connection, it has been found [34] that a tungsten filament operated at 2300 K in nitrogen at a pressure of 10^{-3} torr for periods up to 30 min deposits fewer W atoms on a surface 3 cm away than can be detected by Auger spectrometry (sensitivity limit $3 \times 10^{13}\,cm^{-2}$). It would appear, therefore, that the evaporation of tungsten does not have an adverse effect on these measurements, although the reason for this welcome simplification is not understood. A difficulty in the measurements of Nornes and Donaldson arose from slow solubility effects. It took several hours for the tungsten filament to become saturated, which was an essential condition for defined rates of atomisation. Moore and Unterwald [35] had warned of the danger of changes in the amount of dissolved hydrogen influencing rates of atomisation determined under transitory conditions, as in flash filament procedures, but they found no evidence of *slow* solubility effects for hydrogen in tungsten.

Gregory and Hayward [25] studied the atomisation of nitrogen over tungsten in a static system, not by following the fall in pressure, but by collecting a proportion of the atom flux on a separate nickel filament, which was then flashed to obtain a measure of the number of atoms captured. The nickel is inert towards N_2 molecules (Gregory and Hayward [36]). The essence of the procedure is that the nickel filament should trap a *constant* fraction of the atoms produced by the tungsten filament and that the remainder should be trapped at the walls and elsewhere. This requirement seems to be met, provided the extent of the atomisation is kept sufficiently low. There appears to be no trouble from the slow solution effects which necessitated prolonged pre-conditioning in the work of Nornes and Donaldson [8]. This might be because Gregory and Hayward used much higher temperatures (2275—2617 K), allowing higher rates of diffusion. The use of very high temperatures introduces a further possibility for systematic error due to the substantial rate of evaporation of W atoms, which has become comparable with the rate of production of N atoms. Once again, there is no evidence that this has affected their rates of atomisation, but clearly caution is necessary. A disadvantage of this method is that it would require difficult calibration procedures for it to give absolute rates.

(*b*) *Atomisation rates in the region of half-order kinetics*

Brennan and Fletcher [5] found, for the atomisation of hydrogen over tungsten at about 1200 K, that $dP^{1/2}/dt$ is constant over the pressure range 9.3×10^{-3} to 1.52×10^{-6} torr, as shown in Fig. 9. Similar behaviour was observed for H_2—Pt, H_2—Au and O_2—Pt [5, 7, 37]. Kislyuk and

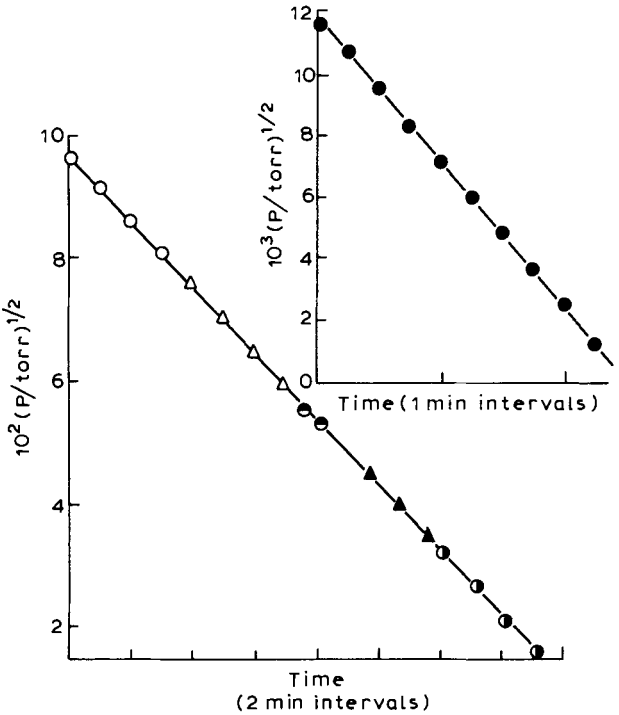

Fig. 9. The dependence on pressure of the rate of atomisation of hydrogen over tungsten at about 1200 K. The differently styled points denote separate experiments made over a period of a few days. (Courtesy Brennan and Fletcher [6].)

Tret'yakov [111] did not find half-order kinetics for the atomisation of hydrogen by gold under these conditions. On the contrary, they reported first-order kinetics. They attributed the observation of half-order kinetics by Brennan and Fletcher for this system to the presence of surface impurities capable of rapidly dissociating molecular hydrogen, whereas molecular adsorption on the clean surface, being activated, was considered by them to be rate-determining. We will return to the H_2—Au system in Sect. 3.2.1(d). Nornes and Donaldson [8] have demonstrated half-order behaviour for the N_2—W system, but over a narrower pressure range.

The effect of varying the temperature is exemplified in Fig. 10 using data for the O_2—Pt and N_2—W systems. Similar plots were obtained for the other systems studied and all can be accommodated in a relation of the form

$$v_a = bP_2'^{1/2} \exp(-E_a/RT) \tag{74}$$

where v_a is the rate of production of atoms per unit area of surface. In calculating v_a, the geometrical areas of the filaments have been assumed. Values for the parameters in eqn. (74) are given in Table 4.

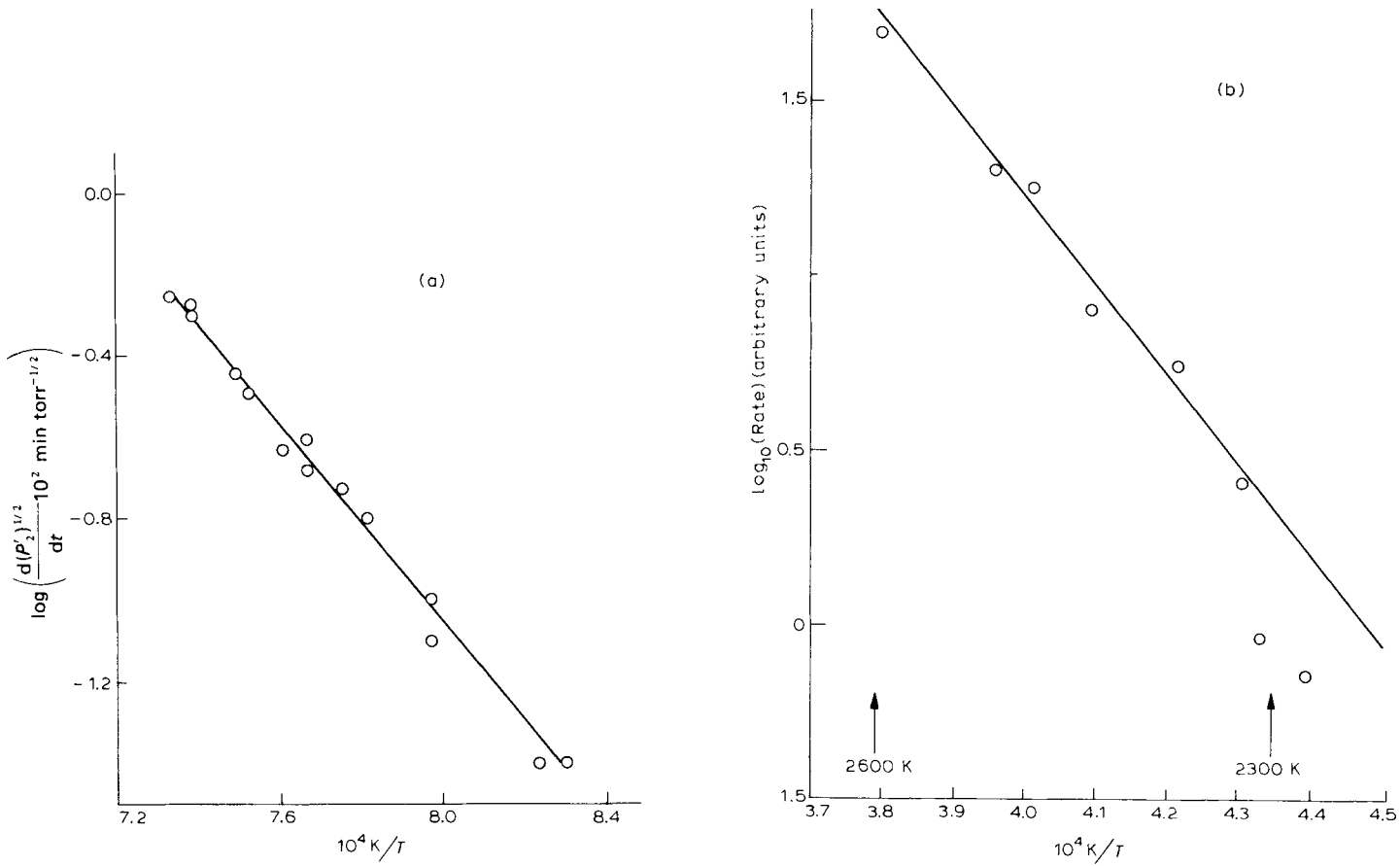

Fig. 10. The dependence on temperature of rates of atomisation, uncorrected for end cooling. The lines are the least squares fit to the experimental points. (a) System O_2—Pt (Brennan and Fletcher [7]); the parameters in the text are corrected for end cooling. (b) System N_2—W (Gregory and Hayward [25]); the first two low temperature points have been excluded.

TABLE 4

Experimental rates of formation (v_a) of *atoms* per unit area of surface in the region of half-order kinetics at 1200 K, expressed in the form $v_a = b(P_2')^{1/2} \exp(-E_a/RT)$. Values of $s_1(s_2'/s_2)^{1/2}$ have been calculated from the theoretical equation, eqn. (48), and the values of its parameters given in Table 2.

System	$\frac{E_a}{\text{kJ mole}^{-1}}$	$\frac{10^{-25}b}{\text{cm}^{-2}\,\text{s}^{-1}\,\text{torr}^{-1/2}}$	$s_1\left(\frac{s_2'}{s_2}\right)^{1/2}$	Ref.
H_2—W	217	1.5	0.68	5
	218	0.57	0.23	22
	211	2.8	2.3	19, 21
H_2—Au	212	0.23	0.17	7
H_2—Pt	214	1.3	0.79	7
O_2—Pt	257	16	2.1	7
	251	16	3.8	47

Brennan and Fletcher [5] were able to reproduce the higher rates of atomisation of hydrogen over tungsten obtained by Bryce [23] when they dispensed with the protection of a cold trap; Bryce had no cold trap. They also obtained a lower activation energy just as he had done. Anderson et al. [24] have calculated rates at 1800 and 2100 K from Bryce's values of b and E_a and obtained good agreement with Langmuir's data, with the implication that Bruce's data are reliable. This kind of result is to be expected for rates which are too high at 1200 K, but have a temperature coefficient which is too low. As an experimental fact, the reason for Bryce's low value of E_a is well established; however, the fundamental cause is by no means clear.

(c) *Transition to first-order kinetics*

We have seen in Sect. 2.2.3(b) that, when the rate of adsorption of molecules becomes comparable with the rate of desorption of atoms, we expect failure of the half-order rate law and, eventually, first-order behaviour will be observed. All the metals investigated by Brennan and Fletcher [5, 7] exhibited this transition. Figure 11(a) illustrates the behaviour using the example of the H_2—Pt system at 1750 K. According to eqn. (51), the limiting probability of atomisation is the molecular sticking coefficient, s_2', values of which are listed in Table 5.

(d) *The atomisation of hydrogen by gold*

Kislyuk and Tret'yakov [111] have reported that the atomisation of hydrogen (and deuterium) over gold is first-order in the temperature range 950—1250 K at pressures in the range 10^{-3} to 10^{-5} torr. Their result for

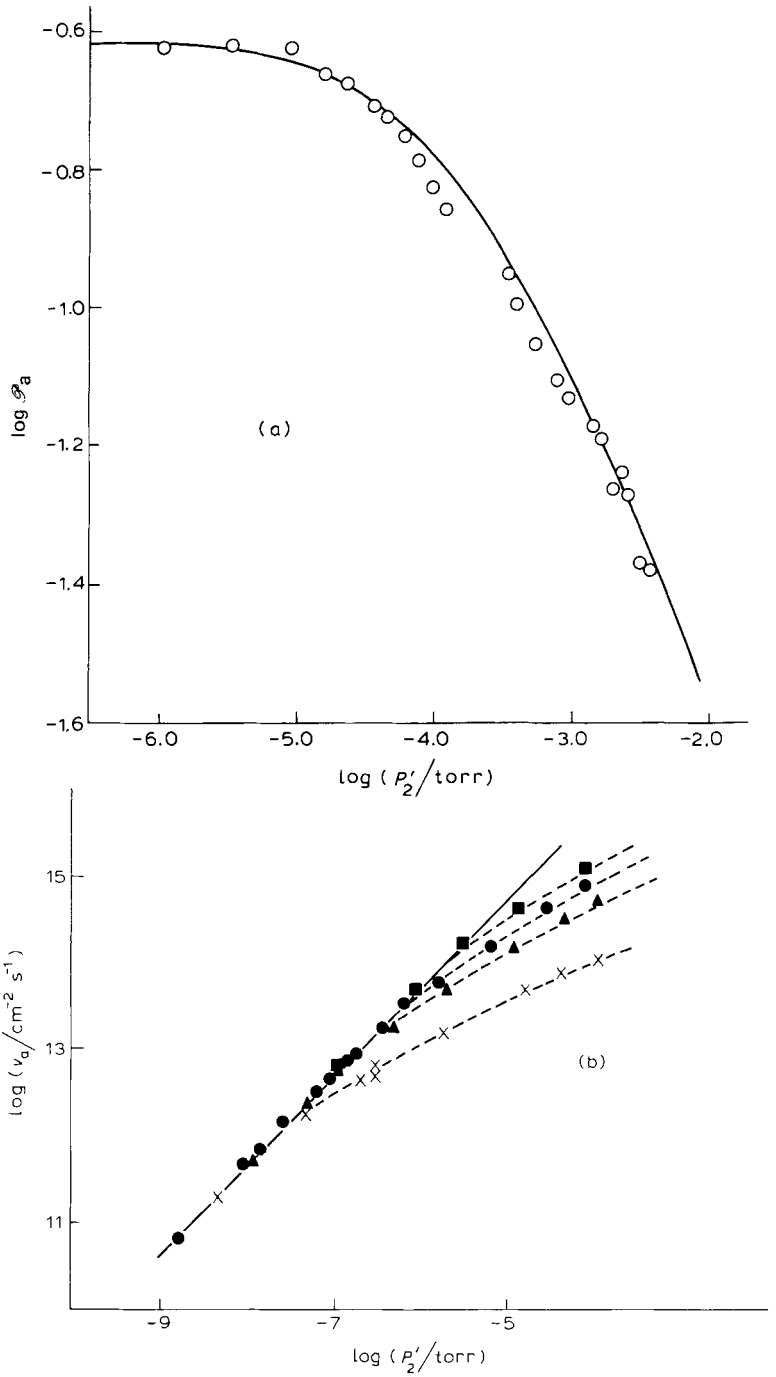

Fig. 11. The transition from half-order to first-order kinetics. (a) H_2—Pt at 1750 K (Brennan and Fletcher [7]); the points represent experimental data and the curve has been drawn using eqn. (20). (b) O_2—Pt (courtesy Weber et al. [47]). X, 1370 K; ▲, 1480 K; ●, 1570 K; ■, 1640 K.

TABLE 5

Sticking coefficients for the adsorption of molecules, derived from the probability of atomisation in the region of first-order kinetics

System	T/K	s_2'	Ref.
H_2—W	1830	0.30	5
	1458, 1975	(0.05), 0.1	22
	2500	0.3	12
	1500—1800	0.54	38
H_2—Pt	1750	0.24	7
H_2—Re	1400—1700	0.46	38
H_2—Ir	1400—1800	0.35	38
O_2—Pt	1750	0.058	7
	1770	0.068	42
	1370—1640	0.12	47
O_2—Re	2200	0.64	39

both hydrogen and deuterium, in the terminology of this article, can be expressed as

$$\mathscr{P}_a = 0.03 \exp\left(-\frac{75\ \text{kJ mole}^{-1}}{RT}\right)$$

Their gold filament was initially heated in oxygen at 900 K, then in hydrogen at 1000 K and finally in vacuo at 1200 K. The purpose of this pre-treatment was to remove traces of carbon and oxygen, and the origin of the difference between their results and those obtained for the H_2—Au system by Brennan and Fletcher [7] was attributed to the successful attainment of this objective. Kislyuk and Tret'yakov interpret their result in the same terms as used by Brennan and Fletcher to explain the first-order atomisation kinetics obtained for the H_2—C system, and the limit of first-order kinetics for systems also exhibiting half-order kinetics, as explained in the previous paragraphs. In support of their view, Kislyuk and Tret'yakov point to their finding that the rates of atomisation of hydrogen and deuterium were in the ratio of $\sqrt{2}$ or, as we have expressed it, that hydrogen and deuterium have the same probability of atomisation. Unfortunately, there are several features of this explanation which are unsatisfactory. If we suppose that $E_m/\Delta U_{1,1}$ has the same value (viz. 0.2) as for other metals [107] and utilize an earlier postulate that $E_{2,1} = E_m + \Delta U_{2,1}$, then we can calculate the consequences for the H_2—Au system of our model of atomisation as embodied in eqns. (39) and (58). For this purpose, we assign to $E_{2,1}$ the value 75 kJ mole^{-1} and to $(\kappa_0)_{2,1}$ the value 0.03 as obtained by the Russian workers. In order to calculate $\mathscr{P}_a(D_2)$, we must take into account not only the effect of the change in atomic mass on the collision rate with the surface, but also on the zero

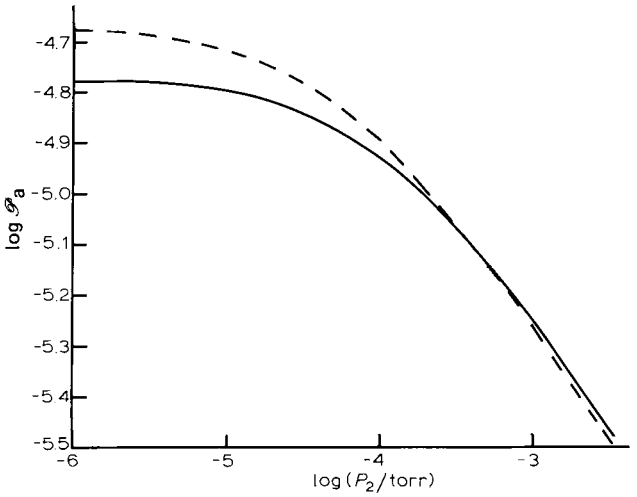

Fig. 12. The dependence on pressure of the probability of atomisation of hydrogen by gold at 1200 K using the model embodied in eqns. (39) and (58). In the following specification of parameters, the first of a pair of values refers to protium and the second to deuterium: $\Delta U_{2,1} = 35.00,\ 31.66\,\mathrm{kJ\,mole^{-1}}$; $D(H_2,\ D_2) = 432,\ 439.56\,\mathrm{kJ\,mole^{-1}}$; $\rho = 0.2$; $\kappa_{1,1} = 1$; $(\kappa_0)_{2,1} = 0.03$; $(\kappa_0)_{1,2} = 0.15$; $\sigma_1 = 0.24\,\mathrm{nm}$; $T' = 77\,\mathrm{K}$. ———, H_2; — — —, D_2.

point energies of the gaseous molecule and the adatom. Kislyuk and Tret'yakov have neglected the energetics of the isotope effect and from Fig. 12 it is apparent that this is a significant factor. Indeed, seen from the point of view of the atomisation rates, the energetics of the isotope effect have the result of almost balancing the effect due to differences in collision rates; thus in the first-order region at 1200 K

$$\frac{v_a(H_2)}{v_a(D_2)} = \left(\frac{M_D}{M_H}\right)^{1/2} \exp\left(-\frac{E_{2,1}(H_2) - D_{2,1}(D_2)}{RT}\right)$$

$$= 1.414 \times 0.7979$$

$$= 1.128$$

However, the really important point of Fig. 12 is to demonstrate that an activation energy of only $75\,\mathrm{kJ\,mole^{-1}}$ is not sufficient to make the supply of molecules to the surface rate determining under the conditions used by Kislyuk and Tret'yakov. At their highest pressures for 1200 K, the kinetics have almost completed the transition to half-order. Clearly, more work is required to resolve these inconsistencies.

(e) *A catalytic vacuum pump*

Murakami et al. [38, 39] have developed a pump with a very high speed for hydrogen ($5000\,\mathrm{l\,s^{-1}}$ at hydrogen pressures between 10^{-7} and

10^{-5} torr) using the atomisation reaction as the pumping mechanism. Atomisation takes place on an array of rhenium wire grids and the atoms formed are trapped by baffles of cuprous oxide. Any water produced by the atom traps is condensed by liquid nitrogen-cooled surfaces. Successful development of the prototype pump would fill a gap left by cryogenic and sputter-ion pumps which are inefficient for the pumping of hydrogen. In the course of the development of this pump, measurements were made with it of atomisation rates over a wide range of pressures and in the presence of contaminants. The data in the region of half-order kinetics are likely to be unreliable [40], but the data for the first-order region should be accurate and are included in Table 5.

3.2.2 Flow system experiments

(a) Principle of the method

Hickmott [22] adapted the procedures of the flash filament method to the study of the H_2—W system. He was the first to apply genuine UHV technology to the study of the atomisation reaction. Molecular hydrogen was leaked at a constant rate (F_{leak}) from a constant pressure reservoir into the reaction vessel containing the tungsten filament and pumped away through a port which could be closed when desired. Pressures were measured by means of a ionisation gauge employing a lanthanum boride-coated tantalum filament to achieve adequate electron emission at temperatures too low for significant atomisation of hydrogen. An omegatron mass spectrometer served to identify the composition of the background (which was typically about 10^{-10} torr) and the species involved in the reaction. The combined pumping speed of the port, the ionisation gauge and of the system walls is denoted by S and is required to be constant. Thus, the rate of flow of molecular hydrogen from the system (F_{system}) is given by

$$F_{\text{system}} = \frac{S}{\mathbf{k}T'} P_2' \tag{75}$$

It is assumed that the pressure at the pumps side of the orifice is zero.

The rate of addition of *molecules* to the system due to the desorption of H_2 molecules by the filament is denoted by F_2; in the event of molecules being removed from the gas phase by adsorption at the filament, F_2 will have a negative value. When the filament is sufficiently hot, it will produce atoms at a rate F_1 (expressed as *atoms* per unit time and always positive), and these are then adsorbed irreversibly on the glass walls of the reaction vessel (at 77 K) with an assumed sticking coefficient of unity. The rate of change of pressure in the reaction vessel will then be determined

by the difference in the rates of processes adding molecules to the system and the rates of processes removing them, according to the relation

$$\frac{V}{\mathbf{k}T} \cdot \frac{\mathrm{d}P_2'}{\mathrm{d}t} = F_{\text{leak}} + F_2 - F_{\text{system}} - \frac{1}{2} F_1 \tag{76}$$

where V is the volume of the system. Under stationary conditions, $\mathrm{d}P_2'/\mathrm{d}t = 0$ and $F_2 = 0$, so if P_0 is the steady value of P_2' in the absence of atomisation and P_a the value when the filament is hot enough to cause atomisation, then

$$F_1 = \frac{2S}{\mathbf{k}T}(P_0 - P_a) \tag{77}$$

Hickmott found that the value of P_a started to rise after about 30 s from the commencement of atomisation due to recombination of atoms at the walls; however, during the true stationary condition, the assumption that *all* the H atoms were being trapped was taken to be valid. Procedures were also available for determining F_2, either by establishing a steady state or by flash desorption. Hickmott applied a correction factor (ϵ) for end cooling and assumed that the surface area of the filament was the same as its geometric area ($\mathscr{A}$) i.e.

$$D_1 = \frac{\epsilon F_1}{\mathscr{A}} \tag{78}$$

(*b*) *Desorption of molecules*

Hickmott measured the rate of desorption of H_2 molecules from tungsten in the temperature range 600—800 K, when the desorption of atoms was negligible, and demonstrated that it was second order with respect to the concentration of adatoms. This result confirms that the overlayer at these temperatures exists in the form of atoms. The experimental relation for the rate coefficient, d_2, (cf. eqn. (20) and Table 1) is

$$d_2 = 1.25 \times 10^{-3} \exp(-130\ \text{kJ mole}^{-1}/RT)\ \text{cm}^2\ \text{s}^{-1} \tag{79}$$

(*c*) *Rate of formation of atomic hydrogen*

We have seen how D_1 can be obtained from the experimental value of F_1, determined under steady state conditions [eqns. (77) and (78)]. From eqn. (1)

$$d_1 = \frac{D_1}{(N_a)_1} \tag{80}$$

so knowledge of the stationary value of $(N_a)_1$ would provide d_1.

The stationary condition of constant $(N_a)_1$ requires mass balance at the surface, i.e.

$$s_2' z_2' P_2' = \tfrac{1}{2} D_1 + d_2 (N_a)_1^2 \tag{81}$$

or

$$(N_a)_1 = \left(\frac{s_2' z_2' P_2' - \tfrac{1}{2} D_1}{d_2} \right)^{1/2} \tag{82}$$

The value of s_2' is determined by a separate experiment in which it is arranged that $(N_a)_1$ is so small that $(N_a)_1^2 \ll (N_a)_1$, corresponding to the first-order behaviour. Then

$$s_2' = \frac{D_1}{2 z_2' P_2'} \tag{83}$$

From measurements of D_1 at 1458 and 1975 K, in the pressure range 1×10^{-8} to 6×10^{-8} torr, the value of s_2' was found to be 0.05.

In a determination of s_2' involving the adsorption of hydrogen at 77 K, a value of 0.07 was obtained. The more accurate method of flash desorption gave $s_2' = 0.1$. These experiments establish that s_2' is virtually temperature independent. For reasons of self-consistency, the value $s_2' = 0.05$ was used in implementing eqns. (80) and (82).

Figure 13(a) shows a typical set of plots for the rate of desorption of atoms at different temperatures and pressures. Although straight lines have been drawn through the points, it should not be concluded that F_1 depends linearly on the pressure in these reactions. On the contrary, as we have seen, F_1 will depend on the rate of desorption of atoms as compared with the rate of adsorption of molecules. For all the conditions represented in Fig. 13(a), the rate of atomisation is only an extremely small fraction of the rate of adsorption of molecules, so the kinetics will be half-order with respect to P_2'. However, the range of pressure over which the measurements have been made is insufficient to reveal the $\sqrt{P_2'}$ dependence. The variation of d_1 with temperature is shown in Fig. 13(b) and the equation of the least squares straight line gives the relation

$$d_1 = 2.4 \times 10^{13} \exp(-283\ \mathrm{kJ\,mole^{-1}}/RT)\ \mathrm{s^{-1}} \tag{84}$$

which is a little different from the expression given by Hickmott, who estimated the best fit visually.

(d) Rate expression for half-order kinetics

From eqn. (81) taking the positive square root, we obtain

$$(N_a)_1 = \frac{1}{2d_2} \left[-\frac{d_1}{2} + \left(\frac{d_1^2}{4} + 4 d_2 s_2' z_2' P_2' \right)^{1/2} \right] \tag{85}$$

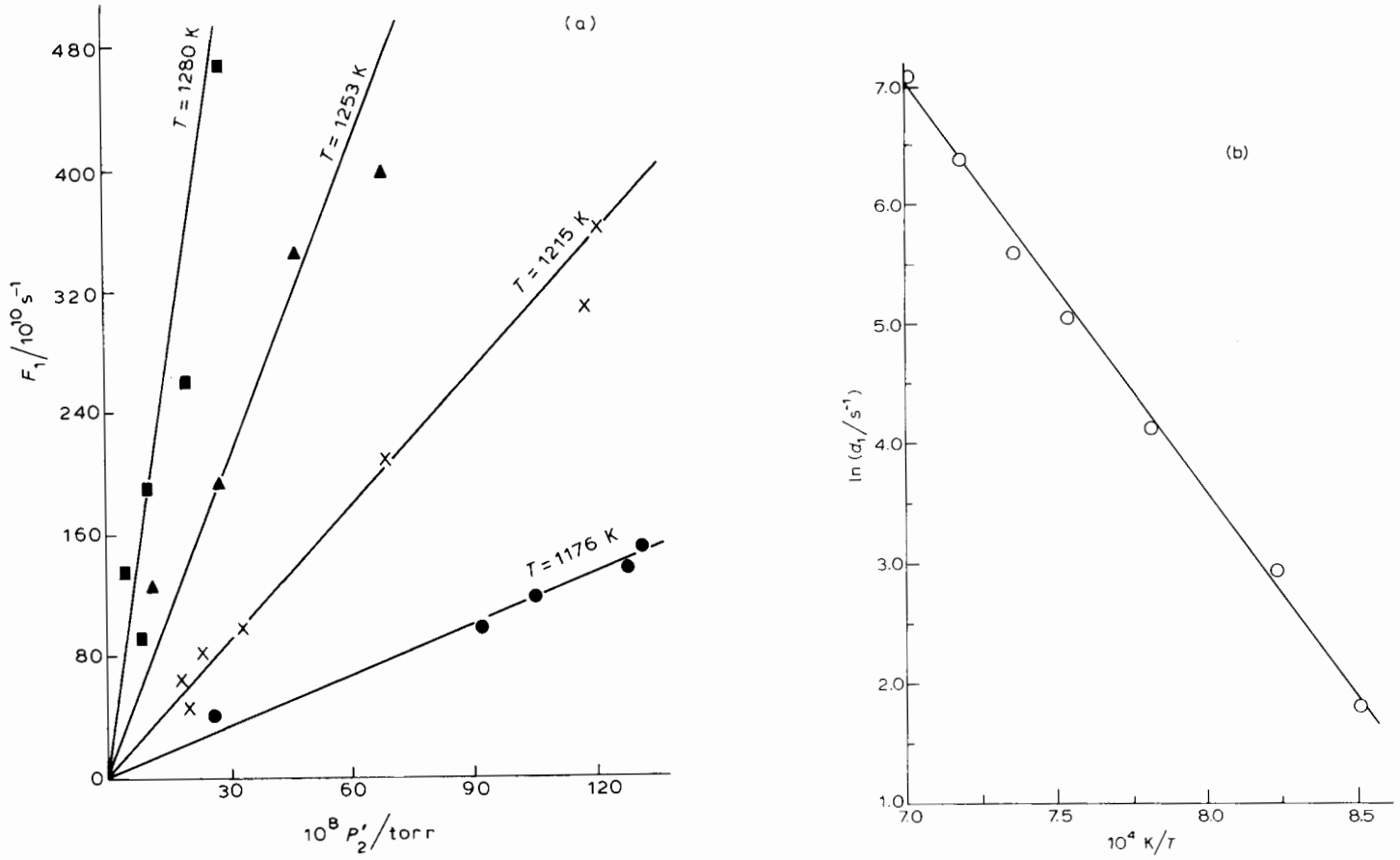

Fig. 13. Rates of desorption of H atoms from a tungsten filament (Hickmott [22]). (a) The dependence of the rate of removal of H atoms by glass (assuming perfect trapping) on temperature, in the range 1176—1280 K, at pressures less than 1.3×10^{-6} torr. (b) The dependence on temperature of the rate coefficient, d, for the desorption of H atoms. The points are those of Hickmott [22]; the straight line is the least squares fit.

Typical conditions for half-order kinetics are $T = 1200$ K and $P_2' = 10^{-3}$ torr, for which it is readily verified that the expression in the square brackets is dominated by the term in P_2'. Hence

$$D_1 = d_1(N_a)_1$$
$$= \frac{d_1}{\sqrt{d_2}}(s_2' z_2')\sqrt{P_2'} \tag{86}$$

and substituting experimental values

$$v_a = 5.7 \times 10^{24}(P_2')^{1/2} \times$$
$$\exp(-218\,\text{kJ mole}^{-1}/RT)\,\text{cm}^{-2}\,\text{s}^{-1}\,\text{torr}^{-1/2} \tag{87}$$

which is in excellent agreement with the relation obtained by Brennan and Fletcher (Table 4), especially remembering the large temperature coefficient of the reaction and the very different conditions employed in the rate measurements.

3.2.3 The absence of trapping of thermally excited molecules

Anderson and Ritchie [45], as the result of a study of the sorption by sodium films of hydrogen activated at a hot filament, suggest that the rate-determining step in their experiments and those of Brennan and Fletcher, and of Hickmott is not atomisation at the filament, but incorporation of H atoms in the atom trap. They base this conclusion mainly on their observation that the rate of hydrogen sorption *falls* when the pressure rises to as high as about 0.1 torr. This effect, they believe, is due to the increase in the deactivation by gas phase collisions of molecules thermally excited by the filament and otherwise destined to combine with the trap surface. A more likely reason for the fall in their apparent sorption rate is the fact that their filament was operated at a constant current (not constant resistance). The filament temperature is reported as 1700 ± 20 K, but the actual temperature for the higher hydrogen pressures would be much lower than this because of the increasing thermal conduction of the gas. The cooling of the reaction vessel would further lower the filament temperature. An additional complication is the shortness of the filament used (only 5 cm) and the neglect of the very substantial end cooling. In essence, Anderson and Ritchie represent the process occurring in these kinds of systems as

$$\tfrac{1}{2}H_2\,(\text{filament}) \rightleftharpoons \tfrac{1}{2}H_2\,(\text{trap surface}) \rightleftharpoons H(\text{trap surface})$$
$$\downarrow \text{ slow}$$
$$H(\text{incorporation})$$

They claim, in an entirely qualitative way, that this scheme is compatible with half-order kinetics and an activation energy of $\frac{1}{2}D(H_2)$, assuming

that the slow process is unactivated. In arriving at these conclusions, they appear to take no account of the difference in the temperatures of the filament and the trap surfaces in representing the "equilibria", nor do they consider the energetics of the system in relation to concentrations and rates; to do so would be to arrive at very contrary conclusions. Roberts and Young [46] give a similar description of the sorption by lead films of hydrogen activated at a hot filament and their view is subject to the same criticisms. In the writer's opinion, therefore, there is nothing of substance in these studies, lacking as they do any quantitative definition, to call into question the impressive agreement achieved by workers using carefully controlled atom trapping methods applied to different methods of determining atomisation rates, different trapping agents and widely different reaction conditions. However, perhaps the clearest evidence that adsorption of thermally activated molecules is not a factor in the atom trapping experiments comes from the pressure dependence of the atomisation rate observed by Brennan and Fletcher.

Over the pressure range 10^{-2} to 10^{-6} torr, $dP_2'^{1/2}/dt$ is constant to within at least 1% when the temperature of the filament is low enough for the restrictions of Sect. 2.2.3(a) to apply [5]. Let us determine the upper limit this result sets on the fraction of hydrogen which could disappear from the gas phase in consequence of direct adsorption of thermally excited molecules. We will take the most pessimistic view and suppose that none of the molecules which might be so removed are returned to the gas phase; we also assume that the probability that the collision of a thermally excited molecule results in adsorption remains undiminished throughout the reaction. The absolute rate (v_m) of trapping molecules would then be directly proportional to the pressure, thus

$$v_m = k_m P_2' \tag{88}$$

The rate coefficient k_m would contain factors for the thermal accommodation of a molecule in collision with the filament, the geometry of the filament and the trap, and the efficiency of capture of thermally excited molecules by the trap. The observed fall in pressure in a static atomisation reaction, occurring at the rate $v_a = k_a P_2'^{1/2}$ for a given filament temperature, would then be

$$\frac{dP_2'}{dt} = f_{app}\left(\frac{1}{2}v_a + v_m\right)$$

$$= f_{app}\left(\frac{1}{2}k_a P_2'^{1/2} + k_m P_2'\right) \tag{89}$$

where f_{app} is a factor determined by the dimensions of the apparatus, and

$$\frac{dP_2'^{1/2}}{dt} = \frac{1}{2} f_{app} \left(\frac{1}{2} k_a + k_m P_2'^{1/2} \right) \tag{90}$$

Let us consider two values of pressure, viz. $(P_2')_a = 10^{-2}$ torr and $(P_2')_b = 10^{-6}$ torr; then, utilising the result of Brennan and Fletcher, we can write as a limiting relation

$$\frac{(dP_2'^{1/2}/dt)_a}{(dP_2'^{1/2}/dt)_b} < 1.01 \tag{91}$$

and hence

$$2k_m < 0.101\, k_a \text{ torr}^{-1/2} \tag{92}$$

So, at the high pressure limit of $P_2' = 10^{-2}$ torr

$$\frac{v_m}{\frac{1}{2} v_a} < \frac{2k_m}{k_a} P_2'^{1/2}$$
$$< 10^{-2} \tag{93}$$

which means that, at most, only one in a hundred of the molecules disappearing from the gas phase could do so as the result of thermal activation; at $P_2' = 10^{-6}$ torr, the maximum proportion is 1 in 10^4. Clearly, the adsorption of thermally activated molecules is not a significant factor in the atomisation measurements of Brennan and Fletcher, nor, by association, in similar measurements by other workers.

3.3 MASS SPECTROMETRIC METHODS

The use of mass spectrometry for the measurement of the fluxes of reactants and products has the very great advantage of directness. In this application, it is essential that the ioniser of the mass spectrometer allow unobstructed passage of the neutral beam to avoid surface recombination of atoms. A further requirement [41] is that the electron-emitting filament should be at a temperature below that at which atomisation can occur, but this condition has not always been met.

Fabian and Robertson [42], as part of a larger investigation of the dehydrogenation of ethane, studied the atomisation of oxygen by platinum at 1770 K. They obtained the limiting value $\mathscr{P}_a = 0.068$, in good agreement with Brennan and Fletcher (see Table 5). However, Smith and Fite [12] were the first to undertake mass spectrometric measurements devoted exclusively to the study of the reflection and atomisation of hydrogen and tungsten.

Smith and Fite used modulation techniques to differentiate material which had interacted with the tungsten surface from background material

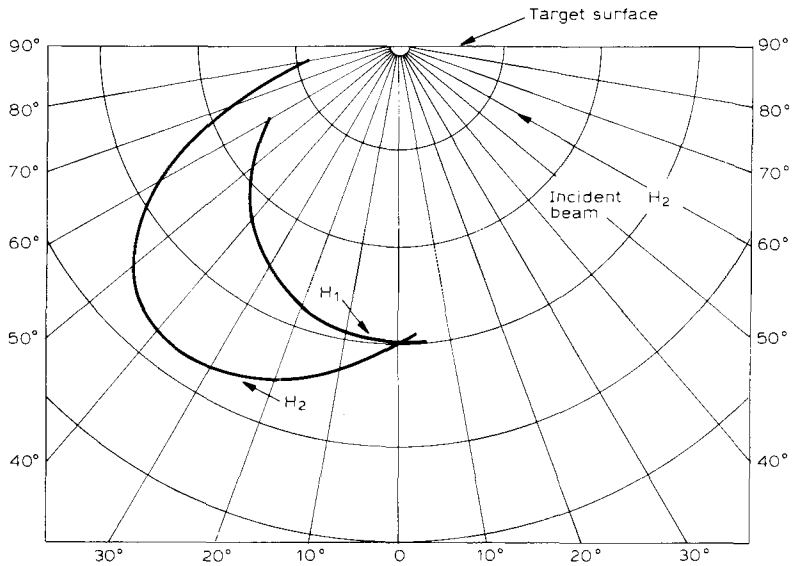

Fig. 14. Angular distribution of H atoms and H_2 molecules evaporating from tungsten surface at 2500 K. The curve for H_2 molecules corresponds to a much lower sensitivity than that for H atoms. (Courtesy Smith and Fite [12].)

by observing phase differences; they were also able to determine the lag between adsorption and desorption. In one configuration of their apparatus, a beam of H_2 molecules was directed at the tungsten surface and the angular distribution of material leaving the surface was observed. It was found (Fig. 14) that a substantial porportion of the H_2 molecules leaving the surface at 2500 K was in the specular direction, indicating that it had experienced only a very short localised contact with the surface. However, it is clear that, even at 2500 K, a significant fraction of the molecular hydrogen leaving the surface is distributed according to the cosine law, meaning that it had been on the surface long enough to loose all memory of how it came to be there. Very significantly, *all* the atomic hydrogen leaving the surface was distributed according to the cosine law. These observations lend weight to the view that atomisation occurs by desorption of adatoms equilibrated with the surface. In a second configuration of the apparatus, the tungsten surface was exposed to hydrogen incident from all directions, but the mass spectrometer "saw" only material which had desorbed from the experimental surface. With this arrangement, it was possible to measure the limiting value of $\mathscr{P}_a$, which was found to become constant only above 2500 K. Smith and Fite attributed this to the presence of contamination on the tungsten surface at lower temperatures because of the poor vacuum conditions (background pressure approximately 7×10^{-7} torr). However, at temperatures sufficiently high for the desorption of contamination, the probability was

found to be constant at 0.3, identical to the value obtained by Brennan and Fletcher (see Table 5).

Moore and Unterwald [35, 43] have made an extensive mass spectrometric study of the atomisation of hydrogen by molybdenum in a dynamic system. They held that their measurements supported the findings of Langmuir, whose rates, it will be recalled, were believed at that time to be about 200 times too slow, and they criticised the experiments of Brennan and Fletcher [5, 7] and of Hickmott [22]. Now that Langmuir's results have been given their rightful place, we have no need to examine the contemporary discussion of the results of Moore and Unterwald. However, we do need to understand why Moore and Unterwald could believe their results were at variance with those obtained by the atom trapping method; the basic reason is they never quoted an *absolute* rate of atomisation. Although Moore and Unterwald do not give either explicit information about the sensitivity of their mass spectrometer or sufficient detail to enable this to be derived from the constants of the apparatus, the demands of self-consistency enable the evaluation of the mass spectrometric sensitivity actually used by these workers in the calculation of their results. The absolute rates of atomisation (v_a) obtained in this way from the data of Moore and Unterwald [43] are, for the pressure $P_2' = 2.60 \times 10^{-4}$ torr, 5.8×10^{14} cm^{-2} s^{-1} at 1200 K and 3.3×10^{15} cm^{-2} s^{-2} at 1300 K. The corresponding rates calculated from the kinetic data of Brennan and Fletcher [eqn. (74) and Table 4] are 0.87×10^{14} and 0.46×10^{15} cm^{-2} s^{-1}, respectively. So, far from being slower than the rates obtained by the atom trapping method, the results of Moore and Unterwald are approximately 7 times faster. However, having in mind the experimental difficulties inherent in the work of Moore and Unterwald, their absolute rates are in satisfactory agreement with those of Brennan and Fletcher and of Hickmott. The problems of ab initio mass spectrometric calibration can be by-passed by using the theoretical equation, eqn. (46), with s_2'/s_2 and s_1 both set to unity, to standardise the mass spectrometer. When this is done for the reaction at 1200 K and the resulting sensitivity factor applied to the measurements at all the other temperatures used, up to the maximum of 2000 K, excellent agreement is obtained over the entire range between the observed rates and those calculated from eqn. (43), with $s_2' = 0.30$. This value of s_2' is exactly that found by Brennan and Fletcher for the hydrogen—tungsten system. Unfortunately, these agreements are marred by an unresolved anomaly concerning the emission currents used in the mass spectrometer. Internal consistency appears to require that emission currents of 11.6, 6.27 and 6.60 μA should have been used in the three experiments for which complete ion current data are given, but these currents are much lower than the 20 μA minimum thought to be set by the limitations of the apparatus ratus [44]. This reappraisal of the measurements of Moore and Unterwald shows that they are no longer to

be regarded [45] as disturbing the general accord existing on atomisation rates and that any difficulties remaining are internal to that particular set of measurements.

Cassuto and co-workers [47] have studied the atomisation of oxygen over polycrystalline platinum by the method of mass spectrometry applied to stationary conditions. They demonstrated that the desorption of O_2 molecules was second order with an activation energy which decreased with increasing coverage. At zero coverage, their relation for the rate coefficient is

$$d_2 = 6 \exp(-243\,\mathrm{kJ\,mole^{-1}}/RT)\,\mathrm{cm^{-2}\,s^{-1}} \quad (94)$$

(see Table 1). However, there is evidence [48] of considerable crystallographic specificity in the parameters of the second-order rate coefficient. Despite this, the evidence points to a single adsorbed state of O atoms under the conditions of atomisation. Atomisation rates were measured over the full range of conditions necessary to observe the transition from half-order to first-order kinetics. The results of Cassuto and his co-workers are shown in Fig. 11(b). In the first-order region, they found the limiting value of $\mathscr{P}_a$ to be 0.12, which is rather higher than obtained by Brennan and Fletcher [7], and by Fabian and Robertson [42] (see Table 5). In the region of half-order kinetics, their results are in very good agreement with those of Brennan and Fletcher [7] (see Table 4). Some of the oxygen desorbed from platinum may be in the form of oxide. In the case of oxygen over tungsten and rhenium, the desorption of oxides assumes a dominant role to the exclusion of molecular desorption.

Schissel and Trulson [49] showed that the interaction of oxygen with tungsten at a pressure of about 2×10^{-4} torr produced W_3O_9, W_2O_6, WO_3 and WO_2, in that order as the temperature was increased from 1400 K, the rate of production of each species declining as that of the next increased. At about 2000 K, O atoms begin to appear and by 2800 K every O_2 molecule which strikes the surface is atomised. Under none of the conditions employed were O_2 molecules detected desorbing from the surface, in accordance with the discussion given in Sect. 2.1.5. McCarrol [50] studied the adsorption of oxygen on tungsten at room temperature by the flash desorption method. He detected only the mono-tungstic oxides WO, WO_2 and WO_3, but confirmed the formation of the poly-tungstic oxides above 1400 K. Again, no molecular desorption was observed when the filament was flashed within a limit of detection $D_2/D_1 < 0.05$. Schissel and Trulson invoked two states of adsorbed oxygen to account for their atomisation results. In contrast, the atomisation rate of oxygen over rhenium can be accounted for by a single atomic state of adsorption.

Cassuto and co-workers [51—53] investigated the interaction of oxygen with rhenium in a manner which combined the methods used by Schissel

and Trulson and by McCarrol for tungsten. They found that ReO_3 was desorbed as the primary oxide product with some ReO_2 as a secondary product. The production of O atoms was demonstrated to be first order, the rate coefficient being given by the relation

$$d_1 = 2.8 \times 10^{12} \exp(-531\,\mathrm{kJ\,mole^{-1}}/RT)\,\mathrm{s^{-1}} \quad (95)$$

The activation energy decreases linearly with coverage, viz.

$$\Delta U_1 = (-531 + 79\,\theta)\,\mathrm{kJ\,mole^{-1}} \quad (96)$$

Weber and Cassuto were able to account quantitatively for the rate of production of O atoms with just two assumptions: (i) that the rate of adsorption of O_2 molecules was proportional to $(1-\theta)^2$ and (ii) that there was a single adsorbed state of O atoms for which the energy of the surface bond varied according to eqn. (96).

4. Experimental methods and results. Recombination

4.1 EXPERIMENTAL METHODS

4.1.1 Side arm method. Steady state static system

(*a*) *Theory*

The development of this technique by Smith [54] in 1943 laid the foundation for the majority of recombination studies. A constant concentration of atoms is maintained at one end of a closed cylindrical tube (see Fig. 15). Along the tube, the concentration of atoms decreases because recombination occurs at the walls and at the end plate. Recombination may also occur in the gas phase, but nearly always conditions are chosen so that this does not happen. The essence of the method is to establish a theory of the diffusion and recombination processes occurring which relates the atom concentration profile along the side arm to the recombination coefficients of the wall (γ) and of the end plate (γ'). Then, by arranging for either the wall or the end plate to be the surface of interest and by measuring parameters which define the atom concentration profile, γ or γ' can be determined. The development of the necessary theory requires a knowledge of the kinetics of the recombination, which is usually first-order, but may not be so; in some studies, however, proper allowance has not been given to dependence on order. Before we describe methods of generating atoms and measuring their concentrations, we will first examine more closely, but still rather superficially, the nature of the diffusion problem presented by atom transport in the side arm.

Smith's original treatment was one-dimensional, i.e. it ignored the possibility that radial as well as longitudinal atom concentration gradients

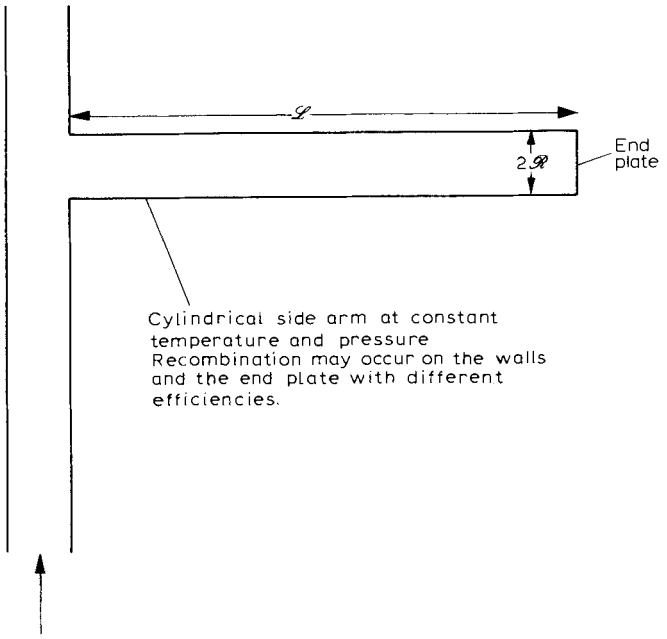

Fig. 15. Schematic representation of the side arm method of Smith [54] for determining recombination coefficients.

may exist. Wise and Ablow [55] extended the treatment to include the radial dimension, but the fact that recombination as well as diffusion of atoms was occurring was still omitted from their models. This deficiency was made good by Greaves and Linnett [56], who recognised that allowance must be made for the fact that reaction reduced the number of atoms; their discussion was for a one-dimensional model. This nonlinearity of the diffusion relations was tested in three dimensions by Dickens et al. [57], who showed that allowance for non-linearity was more important than inclusion of the radial dimension. Their paper, and the review by Wise and Wood [58], provide more detailed summaries of the algebraic consequences of the various models. Fortunately, many experimental studies employ conditions for which some fairly drastic simplifications are possible. The contribution of radial diffusion can be kept negligible by arranging for the pressures to be low enough (typically, a few torr) and for the radius of the tube to be small enough to allow sufficiently rapid diffusion of atoms to the wall. By making the side arm sufficiently long, the axial gradient can be made independent of the recombination efficiency of the end plate. Reflection at the end plate will be unimportant if the atom concentration in its vicinity has fallen to a low level; the presence of an atom probe, which recombines all the atoms passing the cross-section

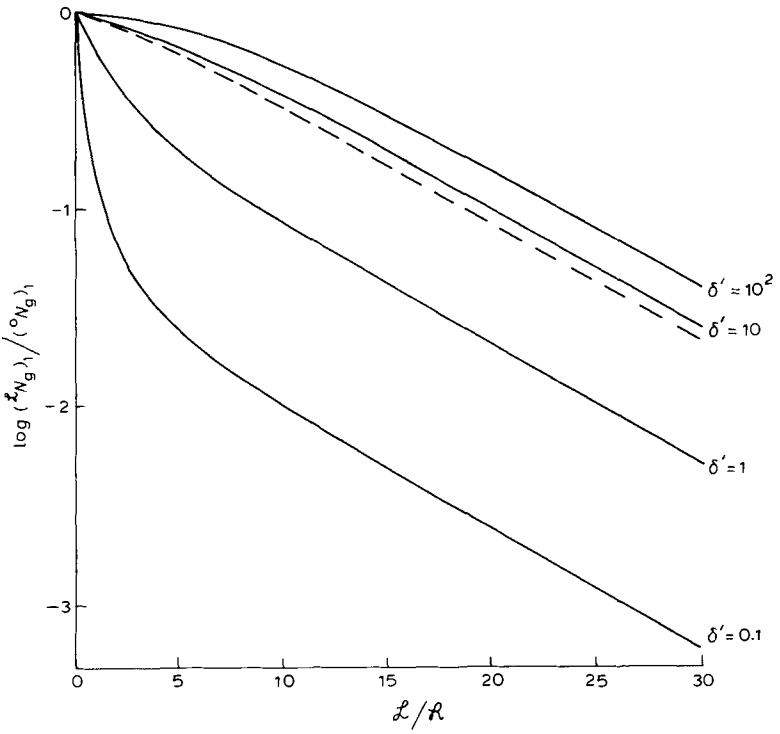

Fig. 16. The concentration of atoms at a probe, which is behaving as an end plate, as a function of the length of the side tube and the activity of the end plate. The recombination efficiency (γ') of the end plate is inversly proportional to δ' [see eqn. (97)]. (Courtesy Dickens et al. [57].)

at which it is located, guarantees the absence of reflection. The attainment of these simplifying conditions is illustrated in Fig. 16; it shows how the atom concentration at a terminal probe, which is simulating an end plate, depends on length. When the effective length is sufficient, the slope of the graph of $\log [(\mathscr{L}N_g)_1/({}^0N_g)_1]$ vs. $\mathscr{L}/\mathscr{R}$ becomes independent of the activity of the probe and equal to $-(2/\delta)^{1/2}$, where the wall parameter δ is defined by the relation

$$\delta = \frac{4\,\mathscr{D}_{1,2}}{\bar{c}\gamma\mathscr{R}} \tag{97}$$

Here, $({}^0N_g)_1$ and $(\mathscr{L}N_g)_1$ are the numbers of atoms per unit volume at the entrance to the side arm and at the end plate, $\bar{c}_1$ is the mean kinetic velocity of the atoms $\mathscr{D}_{1,2}$ is the diffusion coefficient of atoms in the gas, and δ' and γ' relate to the end plate. We see that to obtain δ from the experimental value of δ requires a knowledge of $\mathscr{D}_{1,2}$, and authors do not always agree on the values of $\mathscr{D}_{1,2}$ to be used.

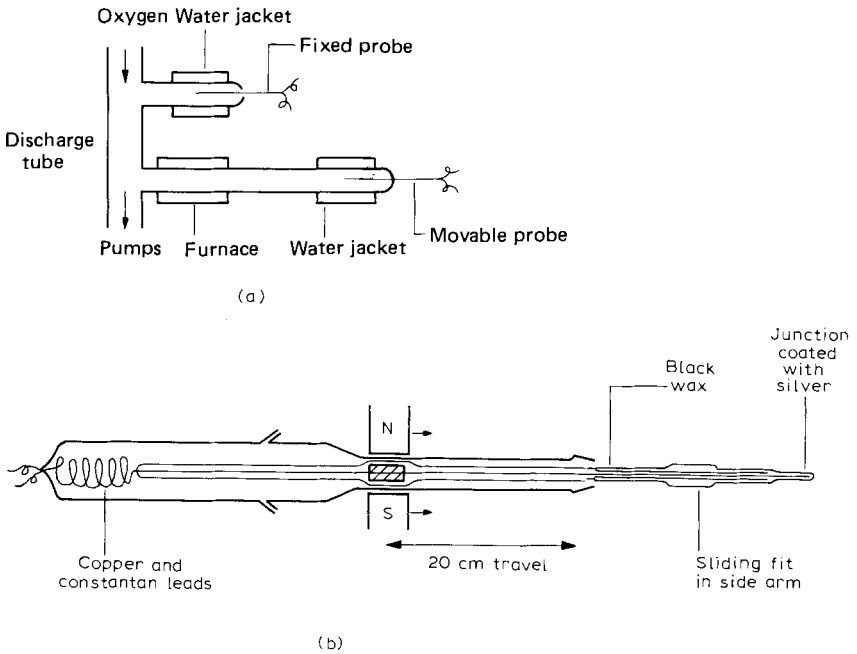

Fig. 17. Apparatus for studying the recombination of O atoms. (a) The discharge tube and side arm showing the fixed and movable thermocouple probes for monitoring $({}^0N_g)_1$ and $(\mathscr{L}N_g)_1$, respectively. (b) Details of the movable thermocouple probe. (Courtesy Linnett and Marsden [59].)

(*b*) *Experimental arrangements*

The apparatus [59] shown in Fig. 17 is typical. Oxygen atoms are generated by electrodeless discharge; electrodes are avoided because sputtering can cause electrode material to be deposited on the experimental surface. Copper—constantan thermocouples in thin glass sleeves coated with an evaporated film of silver serve to monitor the atom concentration. In another design [56], the junction was not sheathed, but simply had a helix of silver wire pressed on to it. The cold junctions of the thermocouples are kept in a thermostat which also supplies the water for the jacket surrounding the probe. The increase in temperature (ΔT) registered by the probe is assumed to be proportional to the atom concentration in its immediate vicinity. Values of ΔT are typically of the order of tens of degrees. The signal from the fixed probe (ΔT_0) should be proportional to $({}^0N_g)_1$ and that from the movable probe ($\Delta T\mathscr{L}$) to $(\mathscr{L}N_g)_1$. Good linear plots of log $[\Delta T\mathscr{L}/\Delta T_0]$ vs. $\mathscr{L}$ were obtained by Linnett and Marsden [59] in a study of the recombination of O atoms. Workers using this method have always been concerned lest the probe used to measure the atom concentration will seriously disturb the concentration gradient along the side arm. Experiments in which the temperature and pressure

conditions are varied provide indirect evidence that this is not happening. However, direct demonstrations of the reliability of the method have been given by Greaves and Linnett [60] and by Pospelova and Myasnikov [61] using Wrede—Harteck gauges to determine atom concentrations absolutely.

The Wrede—Harteck gauge consists of a small chamber in communication with the atom—molecule mixture via a hole whose dimensions are small compared with the mean free path. The chamber is coated with an efficient catalyst so that, ideally, every atom which enters is recombined. Because the atom flux is unidirectional, a pressure difference (ΔP) between the pressure outside and inside the gauge will characterise the stationary condition, such that

$$\psi = \frac{(N_g)_1}{(N_g)_1 + (N_g)_2} = 3.41 \frac{\Delta P}{P} \tag{98}$$

where P is the total pressure of gas outside the gauge. The magnitude of ΔP is typically of the order 10^{-2} torr. While considerable care is needed in the design and operation of Wrede—Harteck gauges if systematic error is to be avoided, they do have the great merit of providing ψ absolutely and they also remove fewer atoms from the system than thermocouple probes. A further advantage of the Wrede—Harteck gauge is that it does not respond to excited species, which might be generated in the discharge, unlike thermal probes upon which such species could be deactivated. Unfortunately, the gauge has poor sensitivity (typically 10^{17} cm^{-3}). Greaves and Linnett [60] used the Wrede—Harteck gauge to show that the thermocouple response, ΔT, was proportional to H atom concentration up to $\Delta T = 150^{\circ}$C. Perhaps even more importantly, this study also demonstrated the soundness of the diffusion model used to describe the transport processes occurring in the side arm. In a similar comparative study, Pospelova and Myasnikov [61] demonstrated excellent agreement between the results for H atom recombination obtained with three different detectors covering a wide range of sensitivities, viz. Wrede—Harteck gauge, calorimetric probe and semiconductor probe (sensitivity typically 10^{6} cm^{-3}).

In contrast to the use of large $\mathscr{L}/\mathscr{R}$ ratios, where attention is focussed on the wall of the tube, Wood and Wise [62, 63] have used short tubes to determine γ' for the material simulating the end plate. They investigated the recombination efficiency of several metals for H atoms. In the later study [63], their terminal probe was in the form of a heated spiral filament of the metal under investigation. The decrease in energy necessary to maintain the filament at constant temperature was measured and assumed to be proportional to the atom concentration at the cross-section occupied by the filament. The method is preferable to the use of thermocouple probes, whose change in temperature might affect the atom decay profiles. Wood and Wise attribute differences in their results obtained

with thermocouples from those using the constant temperature filament to such an effect. In this study, Wood and Wise used a linear representation of diffusion in a short tube with end plate [55], and adjusted δ and δ' so that the theoretical variation of $\psi \mathscr{L}/\psi_0$ with $\mathscr{L}$ fitted the observed variation. The fitting procedure was simplified by a well-characterised value of δ for the glass wall of the side tube. Tsu and Boudart [64] have argued that the presence of an active probe at small values of $\mathscr{L}/\mathscr{R}$ could influence the value of ψ_0. However, Wise and Rosser [65] have confirmed the validity of the Wood and Wise treatment of the short side arm problem by a direct demonstration that the response of the probe nearest the discharge is independent of the position of a very active terminal probe placed at low values of $\mathscr{L}/\mathscr{R}$. This was done by determining the atom concentration profile by ESR spectroscopy in the presence of the probe.

4.1.2 Steady state flow systems

A gas flow techique was successfully used by Hacker et al. [66] in 1961, who studied the recombination of O atoms on quartz and platinum using ESR spectroscopy and isothermal calorimetry with mutually consistent results. However, only in the last few years has the technique been developed for the study of recombination under conditions far removed from those associated with static side arm systems.

Villermaux and co-workers [67—70] have studied H atom recombination in a flow system at pressures between 50 and 760 torr, with atom concentrations kept low (typically 10^{11} cm^{-3}) to ensure that homogeneous recombination is negligible, in part of the pressure range at least. Their method has the advantage of providing both $\mathscr{D}_{1,2}$ and γ independently from the one set of measurements. In one study, Chéry and Villermaux [67] measured the recombination coefficient of H atoms on glass at 285 K using mercury photosensitisation to produce the atoms and the variation of a semiconducting TiO_2 probe to estimate the atom concentration. In a later more comprehensive study, Lédé and Villermaux [68] studied the recombination in the temperature range 278—333 K; an electric discharge between electrodes was used to produce the atoms and a movable yellow HgO probe to estimate them (see Fig. 18). The oxide is inert to H_2 molecules but is reduced by H atoms, the resulting mercury vapour being proportional to the atom concentration for very low concentrations. The atom concentration is monitored continuously by measuring the adsorption at 253.7 nm of the mercury in the effluent hydrogen. The reliability of the HgO probe has been established by comparison with other sensitive H atom measuring devices [70]. Laminar parabolic flow of the hydrogen is assumed and, provided that the recombination is first-order, the mean atom concentration decreases exponentially along

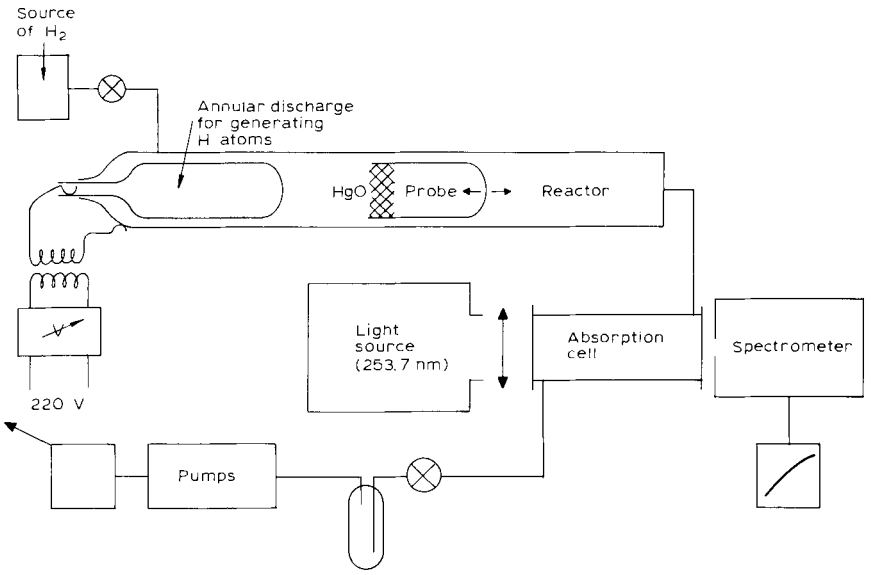

Fig. 18. Apparatus for studying the recombination of H atoms in a flow system. (Courtesy Lédé and Villermaux [69].)

the tube; this decay is characterised by the time constant τ. When the entire recombination is heterogeneous

$$\tau = \phi\tau_0 + \tau_c \tag{99}$$

where

$$\tau_0 = \frac{2\mathscr{R}}{\gamma\bar{c}} \tag{100}$$

$$\tau_c = \frac{P\mathscr{R}^2}{3.66\mathscr{D}^*_{1,2}} \tag{101}$$

and

$$\phi = \frac{1 + 0.4167(\gamma\bar{c}_1\mathscr{R}/4\mathscr{D}_{1,2})}{1 + 0.5053(\gamma\bar{c}_1\mathscr{R}/4\mathscr{D}_{1,2})} \tag{102}$$

As a first approximation, the pressure dependence of ϕ can be neglected, so $\phi\tau_0$ is approximately constant. Consequently, the plot of τ vs. P will be a straight line whose gradient yields $\mathscr{D}^*_{1,2}$, the diffusion coefficient of atoms in the gas at 1 atm. By arranging for conditions which make ϕ significantly different from unity (its lowest value is about 0.8), γ may be obtained from the intercept of the graph. Greater accuracy is achieved by allowing for pressure dependencies through optimisation of ϕ and γ to fit the τ, P data.

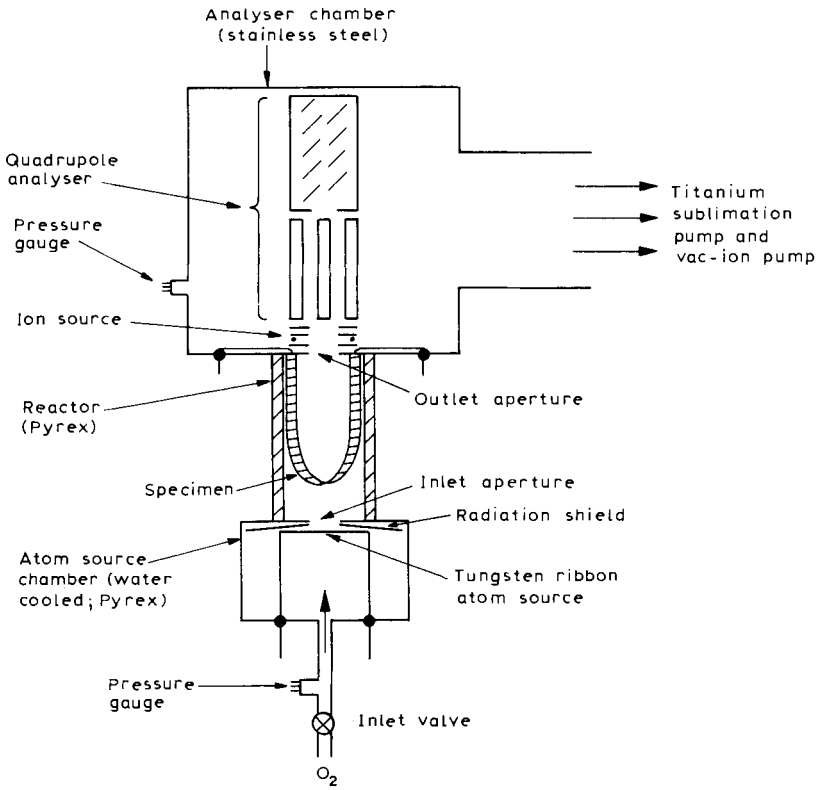

Fig. 19. Apparatus for the study of atom reactions under molecular flow conditions. (Courtesy Wood [72].)

At the other extreme of pressure, Baker and Wood [71] have devised a mathematical model to describe molecular flow of atoms through short cylinders with apertures at either end. Their treatment is designed to accommodate the experimental arrangement (see Fig. 19) used by Wood [72] to study the interaction of O atoms and H atoms with silver and gold. Atoms are generated at a hot tungsten filament and the atom flux which survives to escape through the exit aperture is measured mass spectrometrically. The method does not yield the recombination coefficient directly, but gives instead the atom-loss coefficient, λ, which is defined as the probability that an atom will be removed from the gas phase upon collision with the wall (by recombination or sorption). Flash filament studies were carried out in the same apparatus.

4.1.3 Non-steady state methods

In steady state experiments, time-dependent effects are deliberately elimented by waiting, often for an hour or even longer, until all

parameters are constant. More is involved than merely allowing concentration gradients to establish themselves. Undoubtedly, the recombination catalyst is undergoing changes during this settling down period. The use of pulse methods is directed at elucidating the initial surface changes which must occur.

Hartunian et al. [73] and Myerson [74, 75] have studied the recombination of O atoms by metals during intervals ranging from tens to hundreds of milliseconds. Gas at a pressure of a few torr flows through a tube at high velocity (up to $1.5\,m\,s^{-1}$) and carried with it is a plug of atoms generated by a short pulse of a radio frequency electrodeless discharge with a rise time of a few microseconds. Ideally, the concentration of atoms in this plug would retain the form of a step function, but some diffusion broadening has inevitably occurred by the time the probe is reached. The probe consists of metal foil, or an evaporated metal film, formed on a cylinder and in thermal contact with a film of platinum which acts as a resistance thermometer. The platinum is electrically insulated from the metal catalyst by a very thin layer of TiO_2 or SiO_2. These films are about $0.1\,\mu m$ thick, so the response time of the probe is less than $1\,\mu s$. The atom flux at the probe could be measured by titration with NO_2, the reaction

$$NO_2 + O = NO + O_2$$

being both rapid and quantitative; the end point was detected using the probe itself. The diameter of the flow tube was made large (10 cm) compared with the size of the probe, so that wall recombination could be neglected, and very long (5 m) to ensure the gas temperature was virtually unaffected by the discharge. The diffusion coefficient $\mathscr{D}_{1,2}(=\mathscr{D}^*_{1,2}/P)$ again enters the problem and the method, in principle, provides an independent method of evaluating $\mathscr{D}^*_{1,2}$. However, the recombination reaction is the dominant process and attempts [73] to estimate $\mathscr{D}_{1,2}$ are subject to a 30% error; Myerson used theoretical values of $\mathscr{D}_{1,2}$.

Despite a well-considered rejection in earlier work of the possibility that excited O_2 molecules could reach the probe, Myerson [75] has shown that, if pure oxygen gas is used, thermal effects due to this cause do occur. For this reason, he used argon as a diluent. Elias et al. [76], using an isothermal calorimeter probe, also found evidence for the persistence of excited species, but they found that *fresh* silver oxide would recombine O atoms without significantly deactivating excited molecules. They found cobalt oxide is particularly efficient in deactivating excited molecules. As we have seen, when considering the side arm method, the silver thermocouple probe of Greaves and Linnett gives a reliable measure of the O atom concentration. More specifically, Melin and Madix [77] carefully looked for such an effect, using cobalt as their probe material, without finding any evidence for the survival of excited O_2 molecules so far down the side arm. Clearly, however, caution is

necessary on this point and it is possible, in some cases, that apparent differences in recombination efficiencies measured with thermal probes could, in part at least, be due to specificity for the deactivation of excited molecules.

A different approach to the transient problem is to study the growth and decay of the atom concentration in a Smith-type side tube when the atom source is switched on and off. This was done by Krongelb and Strandberg [78], using ESR spectroscopy for the measurement of O atom concentrations, as part of a larger investigation which also included steady state static and flow measurements. Sancier and Wise [79] have carried out a similar study for hydrogen. The pressures in these workers' experiments were limited to no more than a few torr, but recently Ahumada and Michael [80], using much lower atom concentrations made possible by very sensitive atom detection, have studied the recombination of H atoms on quartz up to a pressure of 700 torr. They generated the atoms photochemically by mercury sensitisation of hydrogen and measured their concentration using time-resolved Lyman α-photometry, which has a detection limit of 5×10^{10} cm^{-3}. Direct spectroscopic techniques such as this and ESR have the very great merit that they cannot be poisoned, they do not disturb the atom concentration profile, they are insensitive to excited states, and they have very fast response times. In this high pressure work, quantitative interpretation of the results was limited to pressures below 350 torr, above which homogeneous recombination becomes troublesome; an independent value of $\mathscr{D}_{1,2}$ was also required for the evaluation of γ. However, Krongelb and Strandberg were able to evaluate both $\mathscr{D}_{1,2}$ and γ from one set of experiments.

4.1.4 Effusion method

In this method, May and Linnett [81] arranged for a mixture of O atoms and O_2 molecules to effuse through a small hole on to the catalyst, in the form of a disc, placed opposite the hole. The disc also served as an isothermal calorimeter; the recombination coefficient was evaluated on the assumption that *all* the energy of recombination was accommodated by the catalyst and that no excited species were present. Isothermal calorimetry is more taxing in this application than when used in side arm experiments because the power differentials involved are a factor of 10^{-4} smaller. The atom concentration on the high pressure side of the hole was calibrated with a Wrede—Harteck gauge. The method has two substantial advantages. It does not require a knowledge of $\mathscr{D}_{1,2}$ and it copes best with high recombination efficiencies, unlike side arm methods. However, the method is limited to low pressures (about 0.01 torr) by the need to maintain Knudsen conditions at the effusion hole, which is about 0.5 nm in diameter.

4.2.1 The diffusion coefficient

Since the majority of determinations of the recombination coefficient depend on the value of $\mathscr{D}_{1,2}$, it is important that we should be aware of the reliability to be placed on experimental values for this parameter.

(*a*) *Hydrogen*

Lédé and Villermaux [68] have reviewed the data available for hydrogen; values of $\mathscr{D}^*_{1,2}$ at different temperatures are given in Fig. 20. The values of Wise and his co-workers while self-consistent if somewhat scattered, lie well removed from the other results, particularly at the higher temperatures. The results of Cheng and Blackshear [84] are derived from measurements of the viscosity of H/H_2 mixtures, without the assumption of an interaction potential, unlike the values of Browning and Fox [83], which depend on the assumption of a potential. These results,

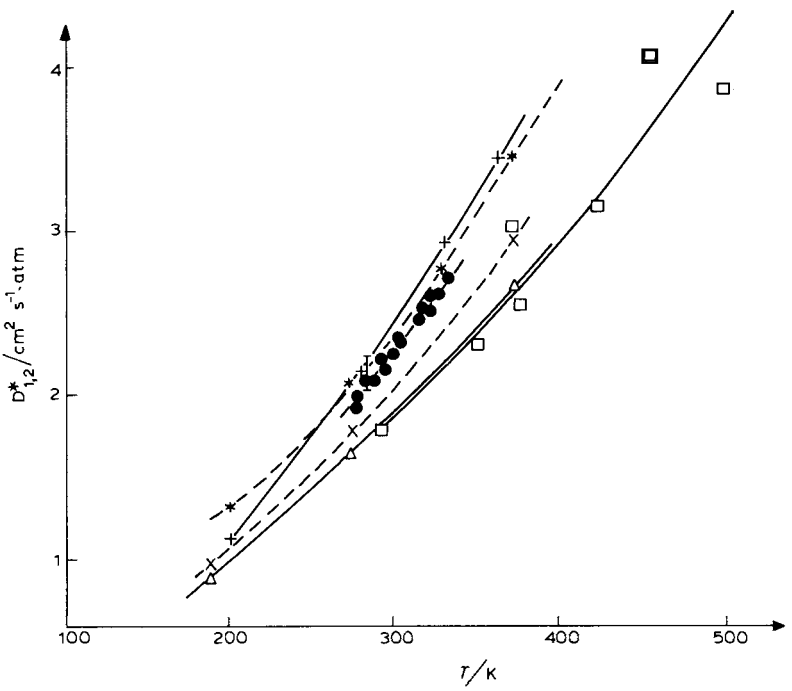

Fig. 20. The dependence on temperature of the coefficient of diffusion of H atoms in H_2 molecules at 1 atm ($\mathscr{D}^*_{1,2}$). □, Sancier and Wise [79]; △, Wise [82]; ×, Browning and Fox [83]; *, Cheng and Blackshear [84]; +, Schiff and co-workers [85]; I, Chéry and Villermaux [67]; ●, Lédé and Villermaux [68]. (Courtesy Lédé and Villermaux [68].)

together with those of Knouw et al. [85] and of Lédé and Villermaux, represent a substantial measure of agreement, which gives confidence in their use for the evaluation of recombination coefficients.

(*b*) *Oxygen*

There is good agreement on the value of $\mathscr{D}^*_{1,2}/\mathrm{cm}^2\ \mathrm{s}^{-1}$ atm at 298 K, viz. 0.27 [86], 0.29 [87], 0.30 [88] and 0.31 [78].

4.2.2 Energy accommodation during heterogeneous recombination

The extent to which the molecules formed by recombination are in thermal equilibrium with the catalyst is of fundamental interest for the light it sheds on the nature of the interaction with the surface at the instant of reaction. It is also of practical interest, particularly in the use of thermal probes for the determination of atom concentrations, where the need to take account of factors influencing energy transfer processes has not always been recognised. Fresh interest in the phenomenon has been stimulated by the demands of space technology for information on surface heating due to recombination during re-entry into the earth's atmosphere.

The parameter used to characterise the energy transfer to the surface is the energy accommodation coefficient (β) which is defined as the fraction of the total energy of recombination adsorbed by the catalyst.

(*a*) *Some theoretical considerations*

To provide a context in which to consider experimental results, we need a simple model to describe the way β can vary depending on the conditions. For this purpose, we adopt in essence the discussion of Halpern and Rosner [112]. We suppose that if molecular adsorption is unactivated, then the molar energy contributed to the catalyst due to adsorption is $-\Delta U_{2,1}$, whereas if it is activated, the energy contributed is only E_m. Conversely, for molecular desorption in the first case, the energy transfer is $\Delta U_{2,1}$ and, in the second case, $-E_\mathrm{m}$. For recombination occurring by the Rideal–Eley mechanism, we deal only with the case for which the process is unactivated, so our present very simple view means that for this reaction no energy is transferred. For atomic adsorption, the molar energy contributed to the surface is $-\Delta U_{1,1}$ and for desorption the energy transfer is $\Delta U_{1,1}$. With these assumptions, and provided $-\Delta U_{2,1} < D(\mathrm{X}_2)$, we can write an expression for the lower limit of the energy coefficient, viz.

$$\beta = \frac{2[s_1 Z_1(-\Delta U_{1,1}) + s_2 Z_2 Q + D_1 \Delta U_{1,1} - D_2 Q]}{\gamma Z_1 D(\mathrm{X}_2)} \qquad (103)$$

with Q taking the value $-\Delta U_{2,1}$ for $-\Delta U_{2,1} \geqslant E_m$ and E_m for $-\Delta U_{2,1} \leqslant E_m$. More conveniently, we write eqn. (103) as

$$\beta = \frac{2[s_1(-\Delta U_{1,1}) + s_2\alpha Q + D_1 Z_1^{-1}\Delta U_{1,1} - D_2 Z_1^{-1} Q]}{\gamma D(X_2)} \tag{104}$$

One of the objectives of the following numerical exemplification of this simple model is to show that a prerequisite of any discussion of energy accommodation in the recombination process is a knowledge of its mechanism.

(*i*) *Limiting cases.* When the coverage is low, and recombination occurs via the Langmuir—Hinshelwood recombination of atoms, each pair of gaseous atoms recombined will have contributed $-2\Delta U_{1,1}$ to the surface and removed $-\Delta U_{2,1}$. In this limit, therefore, the energy accommodation coefficient for unactivated molecular adsorption is given by

$$\beta = \frac{-2\Delta U_{1,1} + \Delta U_{2,1}}{D(X_2)} \tag{105}$$

Substituting $-2\Delta U_{1,1} = D(X_2) - \Delta U_{2,1}$ (see Fig. 2), we obtain $\beta = 1$. When molecular adsorption is activated, the limiting value of β is given by

$$\beta = \frac{-2\Delta U_{1,1} + E_m}{D(X_2)} \tag{106}$$

Substituting $E_m = \rho\Delta U_{1,1}$, we obtain

$$\beta = \frac{2-\rho}{2}\left[1 - \frac{\Delta U_{2,1}}{D(X_2)}\right] \tag{107}$$

When the coverage is high and when, in addition, the Rideal—Eley process predominates, the value of β will depend on the origin of the surface atom participating in the recombination process. We recall that, in the present model, none of the energy associated with reaction (VIb) is transferred to the surface, since we are restricting the discussion to the case when reaction (VIb) is unactivated. If the adatom involved derived from a gaseous atom, then reaction (VIb) has brought about the recombination of two gaseous atoms for an energy contribution to the surface of only $-\Delta U_{1,1}$. Hence

$$\beta = -\frac{\Delta U_{1,1}}{D(X_2)} = \frac{1}{2} - \frac{\Delta U_{2,1}}{2D(X_2)} \tag{108}$$

When the adatom participating in the recombination derives from the adsorption of a molecule, then reaction (VIb) has brought about the

recombination of only one gaseous atom and the energy transfer to the surface has been $-\frac{1}{2}\Delta U_{2,1}$ for the case of unactivated adsorption. Under these circumstances

$$\beta = -\frac{\frac{1}{2}\Delta U_{2,1}}{\frac{1}{2}D(X_2)} = -\frac{\Delta U_{2,1}}{D(X_2)} \quad (109)$$

(*ii*) *Values for β for a range of conditions.* We again use the hydrogen—tungsten system, with the parameter values specified in Fig. 4, to exemplify the way β depends on the conditions. In Fig. 5, for which $\Delta U_{2,1} = -146\,\mathrm{kJ\,mole^{-1}}$, we see that the upper limit of β is unity, as given by eqn. (105) and that this value is maintained as the temperature decreases, even after γ has declined significantly. This is because recombination is still occurring almost entirely by the Langmuir—Hinshelwood mechanism and the fall in γ is due to the increasing reflection of gaseous atoms from occupied sites. In due course, as the temperature is lowered, the Rideal—Eley mechanism becomes significant and β decreases. At the lower temperature limit, when recombination is entirely due to the Rideal—Eley process, only 63% of the adatoms appearing on the surface derive from gaseous atoms, so the lower limit of β will be less than the value 0.669 given by eqn. (108), which caters for the case when all the adatoms derive from gaseous atoms. We see also that the lower limit for β of 0.338 given by eqn. (109) could be reached only by making α very large, since $\kappa_{1,1}$ will always be close to unity. In the present example, with $\alpha = 50$ and $P_2 = 1$ torr, the intermediate lower limit for β is 0.594.

When molecular adsorption is activated (see Fig. 7), the high temperature limit of β is given by eqn. (107). In this example, with $\rho = 0.2$ and $\Delta U_{2,1} = 0$, the upper temperature limit to β is 0.9. For the lower temperature, the only adsorption is atomic, so eqn. (108) applies, corresponding to $\beta = 0.5$ in the present example.

(*iii*) *The value of β when $-\Delta U_{2,1}$ decreases with coverage.* We have already considered the effect on γ of an energy of adsorption which depends on coverage [see Sect. 2.3.2(d)]. Different kinds of consequence for energy accommodation are possible depending on the value of $(\Delta U_{2,1})_0$ and the exact form of the dependence on coverage. An example is given in Fig. 8. The accommodation coefficient declines less rapidly than when $\Delta U_{2,1}$ is constant, because molecular desorption is sustained to lower temperatures and with it the relative importance of the Langmuir—Hishelwood mechanism. When eventually the temperature is low enough for the Rideal—Ely mechanism to be significant if not dominant, molecular adsorption may have become activated and its energy contribution to the surface limited to $\frac{1}{2}E_m$ for every adatom appearing on the surface via this route. In the example illustrated in

Fig. 8, the low value of β at low temperature arises because adatoms derived from gaseous atoms bring an energy of only about 240 kJ mole^{-1} (compared with 289 kJ mole^{-1} for $\Delta U_{2,1}$ constant at -146 kJ mole^{-1}) and adatoms derived from molecular adsorption bring only about 23.5 kJ mole^{-1} (compared with 73 kJ mole^{-1} when $\Delta U_{2,1}$ is constant). We could expect β to pass through a minimum in an example where molecular adsorption was eventually reduced to insignificance by a growing activation energy.

(*b*) *Experimental techniques*

(*i*) *Use of calorimetric probes.* Two studies have been made using steady state flow systems and isothermal calorimetric probes, in which the atom concentration is obtained independently of the probe. Knowing the absolute atom concentration at the probe and having also determined the recombination coefficient of the probe material, the fraction of the energy of recombination adsorbed by the catalyst can be calculated. In the study of Wood et al. [89], ESR spectroscopy was used to determine the concentration of H atoms, molecular oxygen being employed for calibration; Melin and Madix [77, 90] used Wrede—Harteck gauges positioned along the side arm. For their study of O atom recombination, Melin and Madix calibrated the gauges using the NO_2 reaction, the titration being followed by observing the accompanying chemiluminescence; for use with hydrogen, the gauges were assumed to behave ideally.

(*ii*) *The co-axial filament flow reactor.* More recently, Halpern and Rosner [112] have developed a well-conceived design of reactor with which they have successfully studied the recombination of N atoms by a number of metals under a range of conditions, and which holds the promise of further successful applications. The apparatus is shown in Fig. 21. Recombination occurs on only the central 25% of the co-axial filament, the remainder of the filament being shielded from atoms by glass sleeves so that disturbing end effects are virtually eliminated. The proportion of the recombination occurring on the glass surfaces of the apparatus is negligible. The electrical energy necessary to maintain the filament at a given temperature is determined by measuring the current flowing and the potential drop between leads attached to the filament just inside the shields. The energy accommodation measurement consists of determining the change in the energy necessary to maintain the temperature of the filament in the presence of atoms recombining on its surface and in their absence. A microwave discharge is used to generate the atoms and, because of its slow and unreliable equilibrium characteristics, the flux of N atoms to the reactor filament is cut-off by causing them to recombine on a nickel foil cylinder placed in the gas stream. The concentration of N atoms is measured downstream of the filament by titration with NO and automatic monitoring of the resulting chemiluminescence. To

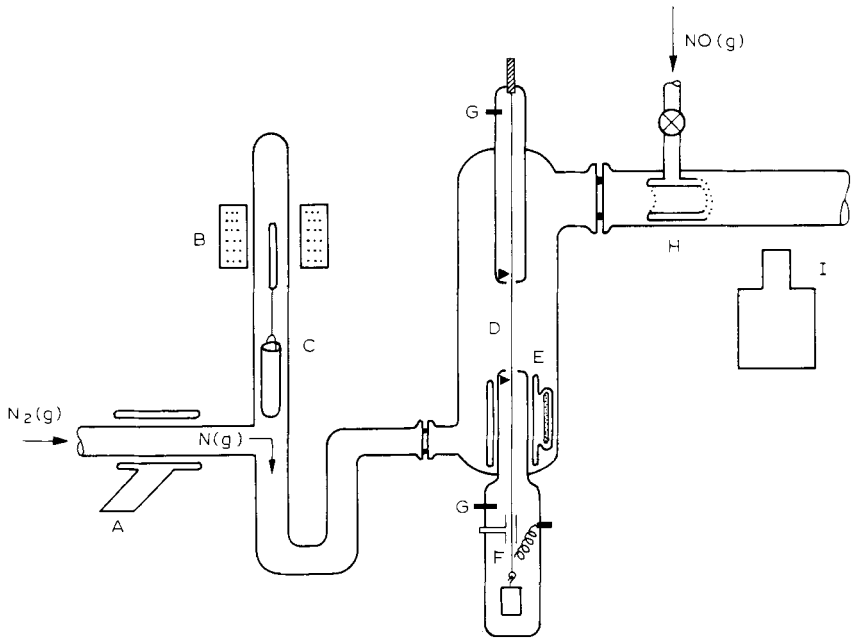

Fig. 21. Schematic diagram of the co-axial filament flow reactor of Halpern and Rosner [112]. A, microwave cavity for generating N atoms; B, electromagnetic for positioning nickel. "atom-gate"; C, nickel foil cylinder for cutting-off supply of N atoms to filament; D, the filament; E, glass shield for screening filament from atom flux; F, weight assembly for tensioning the filament; G, contacts for potential leads whose points of attachment to the filament are denoted by ▶; H, cylindrically symmetric NO diffuser to give virtual step function mixing with main gas stream; I, photomultiplier for monitoring chemiluminescence of NO + N titration. (Courtesy Halpern and Rosner [112].)

determine the recombination efficiency of the filament, N atoms are titrated first with the filament exposed, then with it shrouded by a glass shield. Computation of γ from these measurements is based on the assumption that recombination is first order; it also requires the absence of a transverse concentration gradient. In a detailed analysis of the factors influencing the conversion of experimental parameters to estimates of γ and β, Halpern and Rosner show that the geometry of their reactor is particularly well suited to minimising the influence of potentially complicating factors, some of which we have already discussed in connection with other reactor designs. An important merit of their method is that the determination of β is independent of the evaluation of γ.

(c) *Experimental results and their interpretation*

The dependence of β and γ on temperature for the nitrogen—tungsten system [112] is shown in Fig. 22 and it is seen that it resembles in its

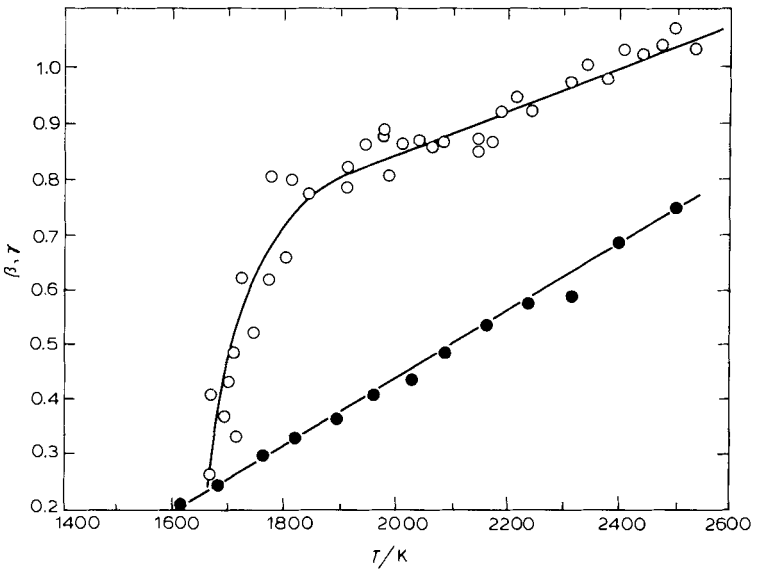

Fig. 22. Temperature dependence of the energy accommodation coefficient and of the recombination coefficient for the nitrogen—tungsten system. $P_2 = 1$ torr, $\alpha = 100$. ○, β; ●, γ. (Courtesy Halpern and Rosner [112].)

qualitative features the consequences of the model expounded in Sect. 4.2.2(a) and illustrated in Fig. 5. The curves for the nitrogen—rhenium system [112] are similar. Halpern and Rosner point out that the lowest value for β of about 0.3 observed by them for the nitrogen—tungsten system is comparable with the value of 0.36 calculated by means of eqn. (109) using the value $\Delta U_{2,1} = -335\,\mathrm{kJ\,mole^{-1}}$ [113]. They also point out that the lowest value for γ for this system is rather lower than for other systems and offer the explanation that a N atom adsorbed on the (100) plane of tungsten is screened by neighbouring W atoms from gas phase atoms other than those approaching at high angles of incidence. A more detailed consideration, however, shows that these conclusions are not compatible with the energy accommodation model being employed, since it is not possible to make molecular adsorption the exclusive source of adatoms except by assigning unreasonable values to the parameters involved [see Sect. 4.2.2(a)]. Further, a low value of γ at high coverage, according to the model, would be expected to be associated with a high lower limit to β. We also notice that the interdependence of γ and β over the entire temperature range is not that required by the model, except in a very broad way. Some of the discrepancy between theory and experiment may have its origin in our inability to represent the model properly at high coverage. It is also very probable that the low values of β at high coverage indicate a decreasing value of $-\Delta U_{2,1}$, possibly due to contamination of the surface at the lower temperatures.

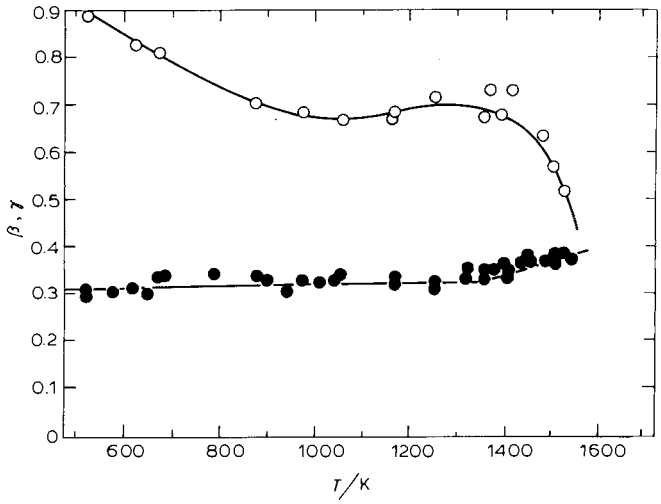

Fig. 23. Temperature dependence of the energy accommodation coefficient and of the recombination coefficient for the nitrogen—platinum system. $P_2 = 1$ torr, $\alpha = 100$. ○, β; ●, γ. Courtesy Halpern and Rosner [112].

From Fig. 23, it is seen that the recombination of nitrogen by platinum [112] behaves quite contrary to the requirements of our simple energy accommodation model. A falling value of β as temperature increases is found [112] also for the nitrogen—cobalt system up to a temperature of about 700 K. Halpern and Rosner discuss this behaviour in terms of energy transfer to the surface from the excited nitrogen molecules (N_2^*) formed as the result of the Rideal—Eley process. Contrary to the zero energy transfer postulated for this process in our simple model, it is quite possible that energy transfer occurs from physically held N_2^*, provided its lifetime on the surface is long enough. Halpern and Rosner discuss some of the details of likely mechanisms for the energy transfer, viz. (a) vibrational deactivation of N_2^* during surface hopping, (b) conversion of vibrational energy of adsorbed N_2^* into translational energy, (c) conversion of vibrational energy of adsorbed N_2^* into electronic energy of the metal, and (d) formation of an azide-type complex as the transition state for the Rideal—Eley step. Energy transfer to the surface through the transition state of the Rideal—Eley step was also the essential feature of the hypothesis advanced by Melin and Madix to account for the results obtained for the recombination of hydrogen by metals, as we will see below.

The values of the energy accommodation coefficient for the recombination of H and O atoms by metals measured by Wood et al. [89] and by Melin and Madix [77] are given in Table 6. The β(H) values of Wood et al. for nickel, platinum and tungsten are substantially higher than those reported by Melin and Madix, but no explanation appears to be forthcoming for this difference. From Table 6, it is seen that a given metal has

TABLE 6

Experimental values of the energy accommodation coefficient for the recombination of H atoms, $\beta(H)$, and O atoms, $\beta(O)$, at 300 K, reported by Melin and Madix [77, 90] θ_D is the Debye temperature of the metal.

Metal	$\beta(H)$	$\beta(O)$	θ_D/K
Ag	0.87 ± 0.3	0.95 ± 0.25	220
Au	0.65 ± 0.2	0.17 ± 0.05	160
Co	0.28 ± 0.1	0.67 ± 0.20	380
Cu	0.43 ± 0.15	0.30 ± 0.08	340
Fe	0.08 ± 0.04	0.07 ± 0.04	420
Ni	0.11 ± 0.05	0.16 ± 0.05	380
	0.82 ± 0.15[a]		
Pt	0.15 ± 0.05	0.10 ± 0.04	230
	0.67 ± 0.10[b]		
W	0.20 ± 0.08	0.09 ± 0.04	320
	1.08 ± 0.11[c]		

[a] 423 K [89].
[b] 376 K [89].
[c] 443 K [89].

similar values for both $\beta(H)$ and $\beta(O)$, gold and cobalt being exceptional in this respect. There is a trend of decreasing values of β with increasing Debye temperatures (θ_D) of the bulk metals, a correlation which embraces even the values of $\beta(H)$ for gold and cobalt, but the correlation is only fair. It must be remembered that all the surfaces used by Melin and Madix for O atom recombination had been converted to oxide by exposure to the O/O_2 flow prior to measurements being made; also, it was thought probable that H atom recombination on tungsten and platinum also occurred on oxide-coated surfaces. We might well wish to be even more cautious and say that in no case was it very probable that the parameters were characteristic of the clean metal surfaces.

Melin and Madix have attempted to interpret $\beta(H)$ values in terms of the mechanical properties of a one-dimensional model of a Rideal—Eley-type recombination complex. According to their model, the controlling influences in determining β are the force constants of the S—X bond and of the metal lattice, and they were able to obtain a moderately good correlation of $\beta(H)$ for the various metals in these terms. The inclusion of copper, silver and gold in this correlation presents difficulties. We have seen that surfaces on which molecular adsorption is very weak should be efficient recombination catalysts, provided the temperature is high enough for adatom mobility, viz. for ordinary atom fluxes, $\gamma \sim \kappa_{1,1} \sim 1$ (see eqn. (66)]. We will discuss the values of $\gamma(H)$ for the group IB metals in Sect. 4.2.4, but we note for the present that the measured recombination efficiencies of these metals (see Table 8, p. 224) are unexpectedly

low. The discussion of Melin and Madix requires a Rideal mechanism for all the metals and makes no distinction between endothermic and exothermic molecular adsorption. The success of their correlation could mean that their measurements do indeed relate to a common mechanism, but for contaminated surfaces.

A further feature of the dependence of β on temperature which cannot be accounted for in terms of our simple model of energy accommodation is the rapid decline of β with increasing temperature at high temperatures as illustrated in Fig. 23 for the nitrogen—platinum system and also reported by Halpern and Rosner for iridium. These workers suggest that this effect is the result of Langmuir—Hinshelwood recombination being so rapid that adatoms are lost to the surface before they have been able to contribute the full amount of their adsorption energy ($\Delta U_{1,1}$) to the surface.

It will be clear from this account of energy accommodation during recombination that, while our simple model is just about adequate as a point of departure, the phenomenon is so diverse and complex that much more experimental evidence and theoretical analysis will be required before we can claim a real understanding of the factors involved.

4.2.3 Recombination of H atoms on glass and silica

(*a*) *Results*

Many more measurements have been made of the recombination efficiencies of glass and silica than of any other materials, for the simple reason that most apparatuses are made of either glass or silica and the wall recombination efficiency is a natural by-product of most investigations. The recombination is predominantly first order and the more systematic measurements, for these recombination kinetics, are shown in Fig. 24; presently, we will see that, under some conditions, the recombination can be second order. Up to a threefold scatter in the values of γ have been found even for the one apparatus (Melin and Madix [90]) depending on the history of the glass, but Fig. 24 demonstrates that there are also substantial systematic differences between the results obtained by different workers.

(*b*) *Theory*

Wood and Wise [91] reported that at sufficiently high and sufficiently low temperatures, the recombination of H atoms on Pyrex and quartz becomes second order (see Fig. 25). Their experimental values of γ were always calculated on the assumption of pure first-order or pure second-order kinetics, whereas, in fact, intermediate orders prevail in the quite broad transition regions. The values of γ obtained for the high temperatures ($T > 500$ K) do not appear to be much affected by this simplification,

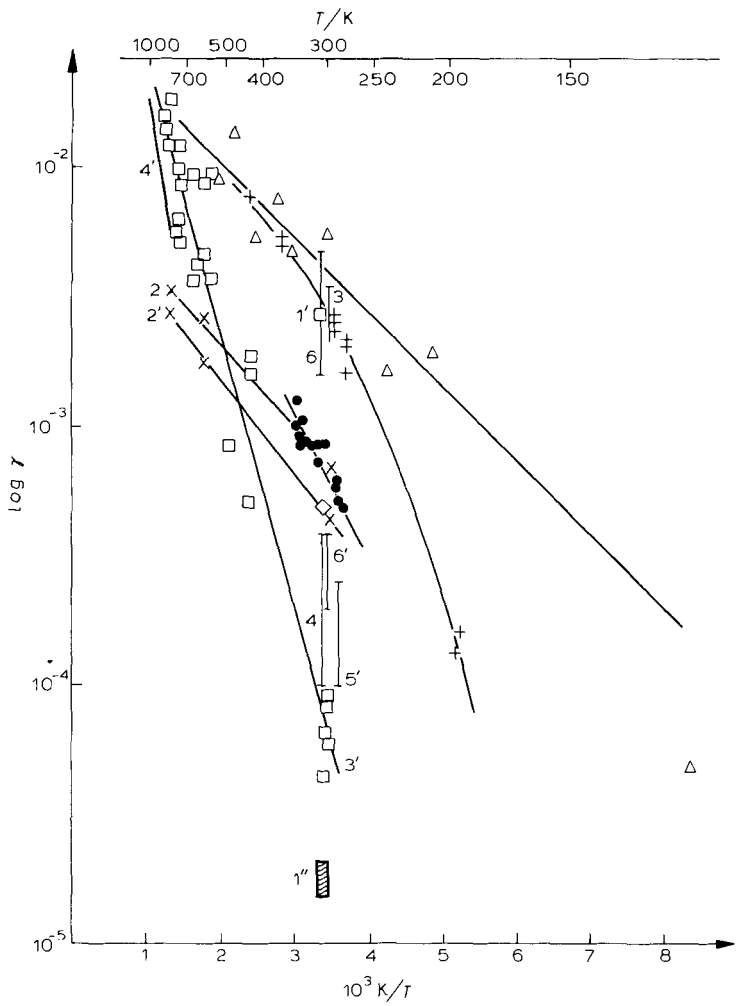

Fig. 24. The efficiency of glass and quartz, at various temperatures, for the recombination of H atoms in the region of first-order kinetics. Pyrex: △, Wood and Wise [91]; +, Tsu and Boudart [64a]; × (2), Smith [54]; ◇, Lédé and Villermaux [69]; (3), Tal'roze and co-workers [92]; (4), Villermaux and co-workers [93]; (5), Pospelova and Myasnikov [61]; ●, Lédé and Villermaux [68]. Silica: ■ (1), Wood and Wise [91]; (1″), Sancier and Wise [79]; × (2′), Smith [54]; □ (3′), Linnett and co-workers [94]; (4′), Kislyuk and Krylov [95]; (5′), Chéry and Villermaux [67]; (6′), Villermaux and co-workers [96]. (Courtesy Lédé and Villermaux [68].)

but values are critically dependent on it at lower temperatures ($50\,\mathrm{K} < T < 120\,\mathrm{K}$) (Wood [97]). For example, in the low temperature kinetic transition region, at $T = 119\,\mathrm{K}$, the value of γ, calculated on the assumption of first-order kinetics, is 5×10^{-5} (see Fig. 25), whereas had second-order behaviour been assumed, the derived value of γ would have been 0.1.

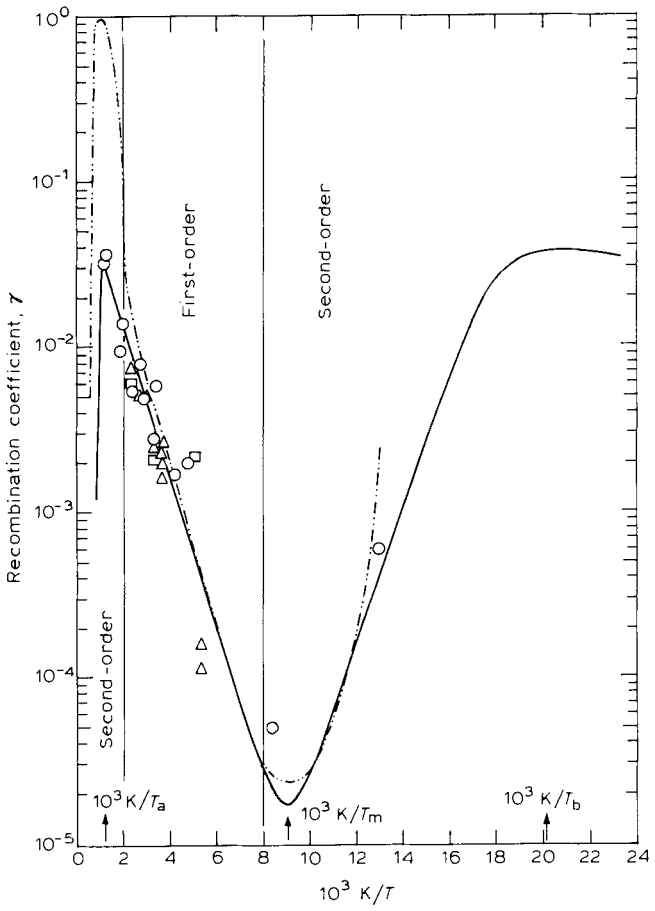

Fig. 25. Kinetics for the recombination of H atoms by Pyrex and quartz. Experimental points: ○, Wood and Wise [91]; △, Tsu and Boudart [64a]; □, Smith [54]. Theoretical lines [$(N_g)_1 = 10^{14}$ cm^{-3}]: —··—, Wood and Wise [91] calculated for the model of de Boer and van Steenis [98] (see Table 8 for values of the energy parameters). ———, Gelb and Kim [100] based on $(\Delta U_1)_a = -176$ kJ mole^{-1}, $(\Delta U_1)_b = -8.8$ kJ mole^{-1}, $(E_r)_a = 8.8$ kJ mole^{-1}, $(E_r)_b = 0.44$ kJ mole^{-1}, the calculated values of T_a, T_b and T_m are indicated by arrows. (Courtesy Gelb and Kim [100].)

Wood and Wise endeavoured to account for the variation in kinetic behaviour shown in Fig. 25, together their absolute values of γ, in terms of the discussion given by de Boer and van Steenis [98]. In keeping with the evidence from adsorption experiments, the overlayer is considered to consist of two states, one strongly held [designated (a)] and the other weakly held [designated (b)]. Recombination is considered to proceed by reaction of adatoms, viz. reaction (Vb) and by the Rideal—Eley mechanism, viz. reaction (VIb), occurring in each of the two adsorption states. Gaseous atoms colliding with an adatom of the first layer [state (a)] are

supposed to recombine via reaction (VIb), or be adsorbed into the second-order layer [state (b)]; gaseous atoms striking state (b) adatoms are supposed to recombine or be reflected back into the gas phase. Adsorption of molecules is taken to be negligible. Indeed, because the energy parameters for the two adsorption states are so different, each state can be considered independently to a fair approximation, using the procedures of Sect. 2.3. Energies of adsorption are estimated from rates of molecular desorption and the Hirschfelder rule, $E_r = -0.05\,\Delta U_1$, is used to estimate the activation energies. Transition state theory is used to calculate the pre-exponential factors of the rate equations for D_2 and R relating to each adsorption state (Shuler and Laidler [99]). For this purpose, adatoms in state (a) are considered to be immobile and those in state (b) to translate freely about the surface. The problem of the value of the partition function of the transition state (less the degree of freedom directly implicated in bond rupture) is dealt with simply by putting it equal to the partition function of the adsorbed state. We have seen, in Sect. 2.3.2(a) that, for a given state of adsorption, a sufficiently low temperature will result in first-order kinetics, with γ increasing with increasing temperature. In Sect. 2.3.3, we also saw that, at higher temperatures, γ decreases and the order with respect to atoms increases. By adjustment of the energy parameters, Wood and Wise obtained a satisfactory fit to their experimental data in the temperature range 77—500 K (see Fig. 25). Over the main part of this temperature interval, the recombination is due to the Rideal mechanism involving state (a) (see Table 7) and the kinetics are first-order, $\theta \sim 1$. By the time 500 K is reached, recombination of adatoms predominates and both the coverage and the order have intermediate values. At temperatures above 500 K, we can expect desorption of adatoms to become increasingly significant; Wood and Wise consider a transition to the limit of second-order kinetics to be the eventual outcome, but we saw in Sect. 2.3.3 that this is much too simple a view. This pattern is repeated at lower temperatures for reactions involving state (a). Unfortunately, the de Boer and van Steenis model fails to account quantitatively for the rate of recombination at the highest temperatures because the effect of the desorption of adatoms does not make itself felt soon enough to counterbalance the highly efficient recombination by reaction (Vb). In an attempt to avoid some of the artificialities of the de Boer and van Steenis treatment, Gelb and Kim [100] dispensed with transition state theory and used instead a simple kinetic theory with an assumed hard sphere cross-section to describe reaction (VIb), which they assigned to be the *sole* route to recombination. They reject altogether surface recombination by reaction (Vb), on the grounds that it gives too high recombination rates at high temperatures; it is unusual, to say the least, to reject a mechanism because it is *too* efficient. Gelb and Kim retain the two states of adsorption; indeed, this postulate, fortunately well founded in experiment, is the very essence of their treatment. The energetics of the two

TABLE 7

Percentage contributions to the overall recombination of H atoms on glass by the reaction of adatoms [$(D_2)_a$ and $(D_2)_b$] and by the Rideal mechanism (R_a and R_b), calculated by Wood and Wise [91] using the model of de Boer and van Steenis [98] $(\Delta U_1)_a = -188.3\,\mathrm{kJ\,mole^{-1}}$, $(\Delta U_1)_b = -6.28\,\mathrm{kJ\,mole^{-1}}$, $(E_{1,2})_a = 94.14\,\mathrm{kJ\,mole^{-1}}$, $(E_{1,2})_b = 3.14\,\mathrm{kJ\,mole^{-1}}$, $(E_r)_a = 9.41\,\mathrm{kJ\,mole^{-1}}$, $(E_r)_b = 0.314\,\mathrm{kJ\,mole^{-1}}$, $N_S = 10^{19}\,\mathrm{m^{-2}}$, four nearest neighbours per adatom in state (a).

$(N_g)_1$ / $\mathrm{cm^{-3}}$	T / K	Percentage contribution to the overall rate of recombination of component			
		$(D_2)_a$	R_a	$(D_2)_b$	R_b
10^{13}	500	98.2	1.8	0	0
	250	0	100	0	0
	120	0	96.0	3.9	0.1
	77	0	0	92.6	7.4
10^{14}	500	89.1	10.9	0	0
	250	0	100	0	0
	120	0	70.3	28.6	1.1
	77	0	0	99.2	0.8
Temperature range of kinetic predominance (K)		500	500—120	120—50	< 50

adsorption states are so different that, again, they can be considered separately. Depending on the temperature, each state is associated with either a high θ (first-order kinetics) or a low θ (second-order kinetics). The transition to second-order kinetics has now quite a different basis from that considered above. In the absence of the Langmuir—Hinshelwood process, recombination at low coverage is second-order merely because its rate will be determined by θ and Z_1, each of which depends directly on P_1. Consequently, the plot of γ vs. T must appear as two contiguous peaks, the first associated with the weakly held state (b) and having its maximum at T_b, and the second associated with state (a) with its maximum at T_a. The trough between the two peaks is located at T_m. This model, with slightly different energy parameters from those used by Wood and Wise, gives a satisfactory fit to the experimental data (see Fig. 25). However, the second-order regions, at both high and low temperatures, are not sufficiently well characterised to provide a critical test of such a theory. The omission of reaction (Vb), without any cogent physical reason, diminishes the significance of this model. It seems unlikely that our understanding of this process will be deepened until there become available reliable experimental values for the energy parameters, which at the moment are little more than adjustable parameters in curve-fitting exercises.

TABLE 8

Recombination of H atoms on metals (after Melin and Madix [90])

Metal	T/K	γ	Ref.
Ag	293	0.05	90
	293	0.1	114
Al	328	0.3	63
Au	293	0.03	90
	299	0.0006	14
	300	0.06[a]	72
Co	293	0.13	90
Cu	293	0.09	90
	333	0.14	63
Fe	293	0.10	90
Ni	293	0.10	90
	423	0.10	63, 89
Pd	294	0.10—0.001	14
	448	0.08	63
Pt	293	0.06	90
	376	0.033	89
	813	0.085	89
Ti	308	0.4	63
W	293	0.08	90
	443—733	0.06	63, 89

[a] Author's calculation.

4.2.4 Recombination of H atoms on metals

The efficiencies of various metals for the recombination of H atoms are given in Table 8. In all cases, the recombination is first-order and the activation energy is less than 5 kJ mole^{-1}. The fact that the state of anneal of the metal can alter γ by a factor of ten [14] suggests that the reaction may occur on minority sites, rather than on a well-defined surface characterised by the intrinsic properties of the metal. This is certainly the explanation for the wide range of values reported for palladium. The extent of diffusion of H atoms into the bulk is also a complicating factor, making γ dependent on the time of exposure to H atoms; for palladium, this effect can be so gross as to result in distortion of the sample.

We consider first the metals on which hydrogen is most weakly held. On gold, molecular hydrogen is adsorbed endothermically. On copper, the adsorption may be weakly exothermic (the isosteric heat of adsorption on films is about -50 kJ mole^{-1} [101]), although the adsorption behaviour is very dependent on the origin of the surface. The situation for silver is confused. Rossington and co-workers [102, 103] give an exothermic value for the heat of adsorption on silver, but their own Langmuir isotherm data imply an endothermic value ($+$ 10.9 kJ mole^{-1});

for aluminium, they obtain a value of about $-33\,\mathrm{kJ\,mole^{-1}}$. While our knowledge of the energetics of the adsorption of H_2 molecules on these metals leaves much to be desired, particularly in respect of the surfaces actually used in the recombination studies, it seems fair to suppose a high degree of surface mobility leading to efficient recombination of adatoms so we expect the adsorption of gaseous atoms to be the rate-determining step ($\gamma \sim \kappa_{1,1}$). However, the experimental values of γ for gold, are not readily accounted for by this model. Further, the difference between the value of γ for gold and those for the other metals is more than expected, since differences in κ_r exert only a weak influence and values of $\kappa_{1,1}$ must be too near to unity to provide much scope for variation. In the view of Linnett and co-workers [14], the recombination on gold occurs by the Rideal mechanism. Their argument is that low values of γ are incompatible with the observed first-order kinetics, but they appear to forget that such a view would require a low rate of surface recombination relative to the rate of supply of gaseous atoms, whereas just the reverse ought to be true under these reaction conditions. We are obliged, therefore, to return to eqn. (66) and to conclude that the state of these gold surfaces was such that the discussion for a homogeneous adsorption state is not applicable.

Wood [72] has studied the adsorption and recombination of H atoms by gold foil, under relatively clean conditions, by determining the total atom-loss rate. From his derived rate coefficients for reactions (IVb), (Ib) and (VIb), it is possible to calculate, respectively, the parameters $\kappa_{1,1} = 0.033$, $\kappa_r = 0.53$ and $d_2 N_S^2 = 4.3 \times 10^{16}\,\mathrm{m^{-2}\,s^{-1}}$. (N.B. The ordinate of Fig. 11, ref. 72 is incorrect.) It is difficult to accept that the probability of the adsorption of a H atom by a vacant site is so low, both absolutely and relative to the probability of reaction of a H atom with an occupied site. Use of eqns. (66) and (69) gives $\gamma = 0.059$, with $R/D_2 \sim 13$ for the experimental conditions employed. Again, the predominance of the Rideal—Eley mechanism over the recombination of adatoms is not consistent with the usual adsorption characteristics of hydrogen on gold. Apart from the question of the state of the gold surface, these measurements are limited by the large uncertainty in measuring the extremely small mass 1 peak [97].

The values of γ for aluminium, copper and perhaps silver seem high enough to be explicable in terms of the discussion of Sect. 2.3.2(b).

The values of the accommodation coefficient β for the recombination over silver and gold (see Table 6) are probably high enough to be compatible with reaction between mobile adatoms, but the low value for copper is not. Once again, we face the same dilemma posed by recombination over the Group IB metals.

For the other metals on which fast chemisorption of H_2 molecules occurs, the discussion of Sect. 2.3.2(a) for the Rideal—Eley mechanism applies. The measured values of γ and first-order kinetics can be accounted for in terms of different values of κ_r (and $\kappa_{1,1}$). Even if here,

too, there is substantial contamination of the surface, there is still likely to be a sufficiently high degree of coverage to make acceptable an explanation of the recombination in terms of the Rideal—Eley mechanism. Undoubtedly, surface contamination and the pysical state of the surface must influence the recombination, but the basic model of Sect. 2.3.2(a) is probably sound, even if some of the values of γ are surprisingly high and there is no rationale with which to correlate them.

4.2.5 Recombination of O atoms on metals and oxides

Values of the recombination efficiencies at 300 K of various oxides and of metals which have been completely oxidised by prolonged exposure to molecular and atomic oxygen, are given in Table 9; first-order kinetics

TABLE 9

Recombination of O atoms on "metals" and oxides at 300 K, except where specified otherwise (after Melin and Madix [77])

Surface	γ	Ref.	Surface	γ	Ref.
Ag	0.24	77	Cr	~ 0.06	81
	0.15	73	Cr_2O_3	0.0002	105
	0.22	81	Fe	0.010	77
	0.12	75		0.036	56
Al	0.007	75		0.017	75
Al_2O_3	0.0021	60a	Fe_2O_3	0.0082	56
Au	0.008	77		0.0052	60a
	0.0052	56		0.0085	105
	0.0040	14	Mg	0.0026	56
	0.0061	81	MgO	0.0035	56
	0.005	75		0.011	105
	0.04[a]	104	Ni	0.017	77
Co	0.075	77		0.028	56
	0.0049	60a		0.0085	75
Co_3O_4	0.0025	105		0.04	73
Cu	0.015	77	NiO	0.0077	56
	0.17	56		0.0089	60a
	0.15	73		0.0015	105
	0.063	81	Pt	0.014	77
	0.03	75		0.01 (200°C)	66
Cu_2O	0.11	105		0.10 (850°C)	66
CuO	0.020	56		0.001 (100°C)	106
	0.043	60a		0.004	73
	0.045	105	W	0.013	77
			Tungsten oxide	0.017	60a

[a] Author's calculation.

apply in all cases. Overall, there is a fair measure of agreement between the results of different workers and between catalysts which started out as metals and those which were always the powdered oxide. Some variation could arise due to differences in the extent of oxidation of the metals. The low values given for cobalt are particularly discordant, the more so when it is recalled that Schiff and co-workers [76] found this oxide was a good recombination catalyst and very effective at deactivating excited molecules.

The adsorption of O_2 molecules on gold is endothermic. We can calculate from the total atom-loss data of Wood et al. [104] for this system the parameters $\kappa_{1,1} = 0.25$, $\kappa_r = 0.017$, and $d_2 N_S^2 = 1.5 \times 10^{15}\ m^{-2}\ s^{-1}$. Under the experimental conditions used, the rate of adsorption of atoms was very high relative to the rate of removal of adatoms by recombination of adatoms ($d_2 N_S^2$ is much smaller than for the H—Au system) and by Rideal—Eley-type abstraction. Consequently, the degree of surface coverage is forced up well above its thermodynamic value; eqn. (69) gives $\theta = 0.90$, which agrees well with the measured value $\theta = 0.91$. Application of eqn. (66) gives the result $\gamma = 0.040$, which is considerably higher than the other values given in Table 9.

Oxygen chemisorption on the other metals is exothermic; indeed, we have already remarked that the effective surface is oxide. If the recombination occurs via a Rideal—Eley mechanism, involving either an adsorbed O atom or possibly an oxide lattice atom, then first-order kinetics, the range of values reported for γ, and the low activation energy (< 10 kJ mole^{-1}) are all understandable in terms of the discussion of Sect. 2.3.2. It is much more difficult to account for the values of β(O) (see Table 6) in these terms. Melin and Madix [77], in attempting to account for $\beta < \frac{1}{2}$ in terms of eqn. (79), suggested that it was weakly bound adatoms ($\Delta U_{2,1}$ positive) which participated in the Rideal—Eley- type recombination. However, we have seen that this is a satisfactory explanation only if the adatoms are relatively immobile. Alternatively, the low values of γ and β could both be explained if the recombination took place by the Rideal—Eley mechanism on isolated sites for which $-\Delta U_1 < \frac{1}{2} D(X_2)$. These special sites, if they occurred singly, would avoid recombination of adatoms. However, it ought not to be forgotten that values of $\beta < \frac{1}{2}$ do not necessarily require endothermic adsorption; eqn. (80) (in conjunction with $\Delta U_{2,1}$ dependent on coverage) is available to explain low values of β, but only more experimental work will provide the basis for a rational quantitative analysis.

Symbols

a fraction of the area of an adsorption site actually occupied by the adatom [see eqn. (6)].

b	pre-exponential constant for the experimental rate of production of *atoms* (v_a) as defined by eqn. (24).
$\bar{c}_1$	average velocity of a freely translating adatom or gaseous atom.
d_1	First-order rate coefficient for the desorption of adatoms [see eqn. (1)].
d_2	Second-order rate coefficient for the desorption of molecules by recombination of adatoms [see eqn. (14)].
f_{app}	constant of proportionality defined by eqn. (89) to give the rate of change of pressure in an atomisation system.
k_a	rate coefficient for the production of atoms per unit are of surface at temperature T and gas pressure P_2'.
k_m	rate coefficient for wall trapping of thermally excited molecules per unit area of filament.
m_1, m_2	masses of atom (X) and molecule (X_2), respectively.
r	rate coefficient for the Rideal recombination mechanism [see equation (60)].
s_1, s_2	sticking coefficients in an isothermal system of atoms and molecules, respectively.
s_1', s_2'	corresponding sticking coefficients in a non-isothermal system.
t	time
v_a	experimental rate of formation of *atoms* per unit area of surface, at temperature T, in the presence of gas at pressure P_2' [see eqn. (73)].
v_m	rate of trapping of thermally excited molecules in a static atomisation apparatus.
z_1, z_2	constants of proportionality relating Z_1, Z_2 to P_1, P_2 for an isothermal system, respectively [see eqns. (25) and (27)].
z_1', z_2'	corresponding constants for a non-isothermal system.
A	pre-exponential factor for the equilibrium constant K_p [see eqn. (47)].
A_1	pre-exponential factor for the rate coefficient d_1 [see eqn. (2)].
A_2	pre-exponential factor for the rate coefficient d_2 [see eqn. (20)].
B	molar enthalpy change for the reaction $\frac{1}{2}\,X_2(g) = X(g)$.
C	non-specific factor in the theoretical expression for the rate of atomisation calculated for half-order kinetics [see eqn. (49)].
$D(X_2)$	change in the internal energy at 0 K accompanying the process $X_2(g) = 2\,X(g)$.
D_1	rate of desorption of adatoms from unit are of surface.
D_2	rate of desorption of molecules from unit area of surface due to the recombination of adatoms.

E_a	*experimental* molar activation energy for the production of atoms [see eqn. (74)].
E_d	activation energy for the desorption of the complex formed by the collision of two adatoms.
E_m, E_m^*	molar potential energy barrier between adjacent adsorption sites, measured from the zero point energy of the two lateral vibrational modes of an adatom and from the bottom of the potential well, respectively.
E_r	molar activation energy for the recombination by the Rideal—Eley mechanism.
$E_{1,2}$	activation energy at 0 K for the process $2\,X{-}S = S + X_2(g)$.
$E_{2,1}$	activation energy at 0 K for the process $X_2(g) + S = 2\,X{-}S$.
F_{leak}	rate of admission of gas into a flow system.
F_{system}	rate of removal of *molecules* from a flow system by the combined pumping action of the port, the ionisation gauge and the walls of the reaction vessel.
F_1	rate of desorption of *atoms* from the experimental surface in a flow system.
F_2	rate of addition of *molecules* to the gas phase of a flow system due to desorption from the experimental surface.
K_p	equilibrium constant for reaction (V).
M_1	atomic weight of the adatom (X).
$(N_a)_1$, $(N_a)_2$	total number of adsorbed atoms or molecules, respectively, per unit area of surface under stationary conditions.
$({}^mN_a)_1$	number of *mobile* adatoms per unit area.
$(N_g)_1$	number of atoms per unit volume.
$({}^0N_g)_1$, $({}^{\mathscr{L}}N_g)_1$	the number of atoms per unit volume at the entrance and at the end plate, respectively, of the side arm of a Smith-type recombination apparatus.
N_S	number of adsorption sites per unit area of surface.
P	total pressure.
P_a	steady state pressure in a flow system when atomisation is taking place.
P_0	steady state pressure in a flow system in the absence of atomisation.
P_1, P_2	pressure of atoms and molecules, respectively, in an isothermal equilibrium system.
P_1', P_2'	pressure of atoms and molecules, respectively, in a non-equilibrium system.
$P^{\ominus}$	standard state to which K_p is referred (1 atm in this chapter).

R	rate of production of molecules per unit area by the Rideal recombination mechanism.
S	combined pumping speed of the port to the pumps, the ionisation gauge and the system walls.
T	temperature of the catalytic surface.
T'	temperature of the gas, if different from that of the surface with which it is interacting.
V	volume of the reaction system.
Z_1, Z_2	number of collisions per unit time with unit area of the surface made by gaseous atoms or molecules, respectively, in an isothermal system.
Z_1', Z_2'	the corresponding quantities for stationary conditions.
$\mathscr{A}$	geometric area of active surface.
$\mathscr{D}_{1,2}$	diffusion coefficient of atoms in the diatomic gas at a pressure P.
$\mathscr{D}^*_{1,2}$	diffusion coefficient of atoms in the diatomic gas at a pressure of 1 atm.
$\mathscr{L}$	length of the Smith side arm.
$\mathscr{P}_a$	probability of atomisation
$\mathscr{R}$	radius of Smith side arm.
α	parameter inversely dependent on the flux of gaseous atoms to the surface [see eqn. (59)].
β	(i) fraction of the energy of recombination accommodated by the catalyst. (ii) a parameter defined by eqn. (7)].
γ	recombination coefficient.
δ	a parameter related inversely to the recombination coefficient [see eqn. (97)].
ϵ	factor to correct for end cooling of a hot filament.
ζ	number of collisions between adatoms in unit time per unit area.
θ_D	Debye temperature
θ_i	the total fractional coverage for the ith adsorption state.
$\kappa_{1,1}$	probability of adsorption when a gaseous atom strikes a surface site.
$\kappa_{1,2}$	probability that the collision of two adatoms results in the desorption of a molecule.
$(\kappa_0)_{1,2}$	corresponding quantity when $RT \gg E_{1,2}$ [see eqn. (15)].
$\kappa_{2,1}$	probability of adsorption when a gaseous molecule strikes a pair of adjacent surface sites.
$(\kappa_0)_{2,1}$	corresponding quantity when $RT \gg E_{2,1}$ [see eqn. (54)].
κ_r	probability that a collision between a gaseous atom and an adatom results in recombination.

$(\kappa_0)_r$	corresponding probability when $RT \gg E_r$ [see eqn. (72)].
λ	atom loss coefficient.
ν_p	frequency of vibration of a localised adatom parallel to the surface.
ρ	the ratio of the activation energy for mobility of an adatom to the desorption energy of an adatom [see eqn. (56)].
σ_1	collision diameter for adatoms.
τ, τ_0, τ_c	time constants characterising the decay of the atom concentration in a flow system [see eqn. (99)].
ϕ	parameter relating time constants of the atom concentration decay in a flow system [see eqns. (99) and (102)].
ψ	ratio of atom density to total gas density [see eqn. (98)].
Θ_p	characteristic temperature of vibration parallel to the surface [see eqn. (8)].
$\Delta U_{1,1}$	change in the molar internal energy for the adsorption of gaseous atoms at 0 K.
$\Delta U_{2,1}$	change in the molar internal energy for the dissociative chemisorption of gaseous molecules at 0 K.
ΔU_r	change in the molar internal energy accompanying Rideal—Eley recombination [see reaction (VIb)] at 0 K.

References

1 B.W. Holland, Trans. Faraday Soc., 61 (1965) 546.
2 B.W. Holland, Trans. Faraday Soc., 61 (1965) 555.
3 G. Ehrlich, J. Chem. Phys., 31 (1959) 1111.
4 G. Ehrlich, Transactions of the 8th Vacuum Symposium and the Second International Congress, Pergamon Press, Oxford, 1962, p. 126.
5 D. Brennan and P.C. Fletcher, Proc. R. Soc. London Ser. A, 250 (1959) 389.
6 D. Brennan, Adv. Catal., 15 (1964) 1.
7 D. Brennan and P.C. Fletcher, Trans. Faraday Soc., 56 (1960) 1662.
8 S.B. Nornes and E.E. Donaldson, J. Chem Phys., 44 (1966) 2968.
9 J.K. Roberts and G. Bryce, Proc. Cambridge Philos. Soc., 32 (1936) 653.
10 A.R. Miller, The Adsorption of Gases on Solids, Cambridge University Press, London 1949.
11 K.J. Laidler, Catalysis, Vol. 1 Reinhold, New York, 1954, p. 75.
12 J.N. Smith Jr. and W.L. Fite, J. Chem. Phys., 37 (1962) 898.
13 E.L. Cochran, V.A. Bowers and F.J. Adrian, J. Chem. Phys., 57 (1972) 2384.
13a D.R. Stull and G.C. Sinke, Thermodynamic Properties of the Elements, The American Chemical Society, Washington, 1956.

14 P.G. Dickens, J.W. Linnett and W. Palczewska, J. Catal., 4 (1965) 140.
15 I. Langmuir, Phys. Rev., 34 (1912) 401.
16 I. Langmuir, J. Am. Chem. Soc., 34 (1912) 860.
17 I. Langmuir and M.J. Mackay, J. Am. Chem. Soc., 36 (1914) 1708.
18 I. Langmuir, J. Am. Chem. Soc., 38 (1916) 1145.
19 I. Langmuir, Gen. Electr. Rev., 29 (1926) 153.
20 M. Farber and A.J. Darnell, J. Chem. Phys., 21 (1953) 172.
21 I. Langmuir, J. Am. Chem. Soc., 37 (1915) 417.
22 T.W. Hickmott, J. Chem. Phys., 32 (1960) 810.
23 G. Bryce, Proc. Cambridge Philos. Soc., 32 (1936) 648.
24 J.R. Anderson, I.M. Ritchie and M.W. Roberts, Nature (London), 227 (1970) 704.
25 J.C. Gregory and D.O. Hayward, private communication, 1975.
26 I. Langmuir, J. Am. Chem. Soc., 35 (1913) 931.
27 I. Langmuir, J. Am. Chem. Soc., 34 (1912) 1310.
28 I. Langmuir, J. Am. Chem. Soc., 37 (1915) 1139.
29 I. Langmuir and J.A. Orange, Gen. Electr. Rev., 16 (1913) 956.
30 N.S. Zaitsev, J. Phys. Chem. USSR, 14 (1940) 644.
31 T.W. Hickmott, J. Appl. Phys., 31 (1960) 128.
32 S.J.B. Corrigan, J. Chem. Phys., 43 (1965) 4381.
33 W.M. Jones and D.F. Dever, J. Chem. Phys., 60 (1974) 2900.
34 R.E. Kirby, C.S. McKee, L.V. Renny and M.W. Roberts, private communication, 1975.
35 G.E. Moore and F.C. Unterwald, J. Chem. Phys., 40 (1964) 2639.
36 J.C. Gregory and D.O. Hayward, in G.A. Somorjai (Ed.), The structure and Chemistry of Solid Surfaces, Wiley, New York, 1969.
37 P.C. Fletcher, Ph.D. Thesis, University of Liverpool, 1959.
38 Y. Murakami, J. Vac. Sci. Technol., 10 (1973) 359.
39 Y. Murakami, T. Kurisaki, Y. Ishibe and K. Okamoto, Jpn. J. Appl. Phys., Suppl. 2, (1) (1974) 89.
40 Y. Murakami, private communication, 1975.
41 T.W. Hickmott, J. Vac. Sci. Technol., 2 (1965) 257.
42 D.J. Fabian and A.J.B. Robertson, Proc. R. Soc. London Ser. A, 237 (1956) 1.
43 G.E. Moore and F.C. Unterwald, J. Chem. Phys., 40 (1964) 2626.
44 G.E. Moore, private communication, 1975.
45 J.R. Anderson and I.M. Ritchie, J. Phys. Chem., 70 (1966) 3681.
46 M.W. Roberts and N.J. Young, Trans. Faraday Soc., 66 (1970) 2636.
47 B. Weber, J. Fusy and A. Cassuto, J. Chim. Phys., 66 (1969) 708.
48 M. Alnot, A. Cassuto, J. Fusy and A. Pentenero, Jpn. J. Appl. Phys., Suppl. 2, (2) (1974) 79.
49 P.O. Schissel and O.C. Trulson, J. Chem. Phys., 43 (1965) 737.
50 B. McCarroll, J. Chem. Phys., (1967) 863.
51 B. Weber, J. Fusy and A. Cassuto, in K. Ogata and T. Hayakawa (Eds.), Recent Developments in Mass Spectroscopy, University Park Press, Tokyo, 1970 p. 1319.
52 B. Weber and A. Cassuto, J. Chim. Phys., 68 (1971) 29.
53 B. Weber and A. Cassuto, Surf. Sci., 36 (1973) 81.
54 W.V. Smith, J. Chem. Phys., 11 (1943) 110.
55 H. Wise and C.M. Ablow, J. Chem. Phys., 29 (1958) 634.
56 J.C. Greaves and J.W. Linnett, Trans. Faraday Soc., 54 (1958) 1323.
57 P.G. Dickens, D. Schofield and J. Walsh, Trans. Faraday Soc., 56 (1960) 225.
58 H. Wise and B.J. Wood, Adv. At. Mol. Phys., 3 (1967) 291.
59 J.W. Linnett and J.W. Marsden, Proc. R. Soc. London Ser. A, 234 (1956) 489.
60 J.C. Greaves and J.W. Linnett, Trans. Faraday Soc., 55 (1959) 1338.

60a J.C. Greaves and J.W. Linnett, Trans. Faraday Soc., 55 (1959) 1346.
61 I.N. Pospelova and I.A. Myasnikov, Kinet. Katal., 7 (1966) 178.
62 B.J. Wood and H. Wise, J. Chem. Phys., 29 (1958) 1416.
63 B.J. Wood and H. Wise, J. Chem. Phys., 65 (1961) 1976.
64 K. Tsu and M. Boudart, Can. J. Chem., 39 (1961) 1239.
64a K. Tsu and M. Boudart, Proc. 2nd Int. Congr. Catalysis, Paris, 1960, Editions Technip, Paris, 1961, p. 593.
65 H. Wise and W.A. Rosser, 9th Symp. Combustion, Cornell University, Ithaca, New York, 1962, Academic Press, New York, 1963, p. 733.
66 D.S. Hacker, S.A. Marshall and M. Steinberg, J. Chem. Phys., 35 (1961) 1788.
67 D. Chéry and J. Villermaux, J. Chim. Phys., 69 (1972) 452.
68 J. Lédé and J. Villermaux, J. Chim. Phys., 71 (1974) 85.
69 J. Lédé and J. Villermaux, J. Chim. Phys., 67 (1970) 847.
70 J. Villermaux, J. Lédé and J. Chéry, J. Chim. Phys., 65 (1968) 1673.
71 B.R. Baker and B.J. Wood, J. Vac. Sci. Technol., 8 (1971) 555.
72 B.J. Wood, J. Phys. Chem., 75 (1971) 2186.
73 R.A. Hartunian, W.P. Thompson and S. Safron, J. Chem. Phys., 43 (1965) 4003.
74 A.L. Myerson, J. Chem. Phys., 42 (1965) 3270.
75 A.L. Myerson, J. Chem. Phys., 50 (1969) 1228.
76 L. Elias, E.A. Ogryzlo and H.I. Schiff, Can. J. Chem., 37 (1959) 1680.
77 G.A. Melin and R.J. Madix, Trans. Faraday Soc., 67 (1971) 198.
78 S. Krongelb and M.W.P. Strandberg, J. Chem. Phys., 31 (1959) 1196.
79 K.M. Sancier and H. Wise, J. Chem. Phys., 51 (1969) 1434.
80 J.J. Ahumada and J.V. Michael, J. Phys. Chem., 78 (1974) 465.
81 J.W. May and J.W. Linnett, J. Catal., 7 (1967) 324.
82 H. Wise, Chem. Phys. Lett., 9 (1971) 133.
83 R. Browning and J.W. Fox, Proc. R. Soc. London Ser. A 278 (1964) 274.
84 D.Y. Cheng and P.L. Blackshear Jr., J. Chem. Phys., 56 (1972) 213.
85 B. Khouw, J.E. Morgan and H.I. Schiff, J. Chem. Phys., 50 (1969) 66.
86 R.S. Yolles and H. Wise, J. Chem. Phys., 48 (1968) 5109.
87 J.E. Morgan and H.I. Schiff, Can. J. Chem., 42 (1964) 2300.
88 R.E. Walker, J. Chem. Phys., 34 (1961) 2196.
89 B.J. Wood, J.S. Mills and H. Wise, J. Phys. Chem., 67 (1963) 1462; 68 (1964) 3911.
90 G.A. Melin and R.J. Madix, Trans. Faraday Soc., 67 (1971) 2711.
91 B.J. Wood and H. Wise, J. Phys. Chem., 66 (1962) 1049.
92 E.B. Gordon, A.N. Ponomarev and V.L. Tal'roze, Kinet. Katal., 7 (1966) 577.
93 J. Lédé, J. Davaine and J. Villermaux, C.R. Acad. Sci., Ser. C, 269 (1969) 541.
94 M. Green, T.R. Jennings, J.W. Linnett and D. Schofield, Trans. Faraday Soc., 55 (1959) 2152.
95 M.V. Kislyuk and O.V. Krylov, Kinet. Katal., 11 (1970) 1200.
96 J.L. Houzelot, D. Chéry and J. Villermaux, C.R. Acad. Sci., Ser. C., 269 (1969) 1339.
97 B.J. Wood, private communication, 1975.
98 J.H. de Boer and J. van Steenis, Proc. K. Ned. Akad. Wet. Ser. B, 55 (1952) 587.
99 K.E. Shuler and K.J. Laidler, J. Chem. Phys., 17 (1949) 1212.
100 A. Gelb and S.K. Kim, J. Chem. Phys., 55 (1971) 4935.
101 C.S. Alexander and J. Pritchard, J. Chem. Soc., Faraday Trans. 1, 68 (1972) 202.
102 S.J. Holden and D.R. Rossington, J. Phys. Chem., 68 (1964) 1061.
103 D.R. Rossington and R.B. Runk, J. Catal., 7 (1967) 365.

104 B.J. Wood, C.M. Ablow and H. Wise, NASA Contract. Rep. No. 2271, 1973.
105 P.G. Dickens and M.B. Sutcliffe, Trans. Faraday Soc., 60 (1964) 1272.
106 B.J. Wood and H. Wise, Rarefied Gas Dyn., Proc. Int. Symp., Suppl. 1, (1961) 51.
107 G. Ehrlich, Br. J. Appl. Phys., 15 (1964) 349.
108 D. Brennan and F.H. Hayes, Trans. Faraday Soc., 60 (1964) 589.
109 D. Brennan, D.O. Hayward and B.M.W. Trapnell, Proc. R. Soc. London, Ser. A, 256 (1960) 81.
110 T.W. Hickmott and G. Ehrlich, J. Phys. Chem. Solids, 5 (1958) 47.
111 M.U. Kislyuk and I.I. Tret'yakov, Kinet. Katal., 17 (1976) 1515: Engl. Transl., Plenum Publications Corp., p. 1302.
112 B. Halpern and D.E. Rosner, J. Chem. Soc., Faraday Trans. 1, 74 (1978) 1883.
113 G. Ehrlich, J. Chem. Phys., 36 (1962) 1171.
114 M.U. Kislyuk and I.I. Tret'yakov, Kinet. Katal., 14 (1973) 1497; Engl. Transl. Plenum Publications Corp., p. 1325.

Index

This Page Intentionally Left Blank